EXPERIMENTAL AND ANALYTICAL INVESTIGATION OF REFRIGERANT AND LUBRICANT MIGRATION

BY

STEFFEN PEUKER

DISSERTATION

Submitted in partial fulfillment of the requirements
for the degree of Doctor of Philosophy in Mechanical Engineering
in the Graduate College of the
University of Illinois at Urbana-Champaign, 2010

Urbana, Illinois

Doctoral Committee:

Research Professor Predrag S. Hrnjak, Chair
Research Professor Clark W. Bullard
Professor Barclay G. Jones
Associate Professor Dimitrios C. Kyritsis
Professor Emeritus Ty A. Newell

Abstract

The off-cycle refrigerant mass migration has a direct influence on the on-cycle performance since compressor energy is necessary to redistribute the refrigerant mass. No studies, as of today, are available in the open literature which experimentally measured the lubricant migration within a refrigeration system during cycling or stop/start transients. Therefore, experimental procedures measuring the refrigerant and lubricant migration through the major components of a refrigeration system during stop/start transients were developed and implemented. Results identifying the underlying physics are presented.

The refrigerant and lubricant migration of an R134a automotive A/C system—utilizing a fixed orifice tube, minichannel condenser, plate and fin evaporator, U-tube type accumulator and fixed displacement compressor—was measured across five sections divided by ball valves. Using the Quick-Closing Valve Technique (QCVT) combined with the Remove and Weigh Technique (RWT) using liquid nitrogen as the condensing agent resulted in a measurement uncertainty of 0.4 percent regarding the total refrigerant mass in the system. The determination of the lubricant mass distribution was achieved by employing three different techniques—Remove and Weigh, Mix and Sample, and Flushing. To employ the Mix and Sample Technique a device—called the Mix and Sample Device—was built. A method to separate the refrigerant and lubricant was developed with an accuracy—after separation—of 0.04 grams of refrigerant left in the lubricant. When applying the three techniques, the total amount of lubricant mass in the system was determined to within two percent. The combi-

nation of measurement results—infrared photography and high speed and real time videography—provide unprecedented insight into the mechanisms of refrigerant and lubricant migration during stop-start operation.

During the compressor stop period, the primary refrigerant mass migration is caused by, and follows, the diminishing pressure difference across the expansion device. The secondary refrigerant migration is caused by a pressure gradient as a result of thermal nonequilibrium within the system and causes only vapor phase refrigerant migration. Lubricant migration is proportional to the refrigerant mass during the primary refrigerant mass migration. During the secondary refrigerant mass migration lubricant is not migrating.

The start-up refrigerant mass migration is caused by an imbalance of the refrigerant mass flow rates across the compressor and expansion device. The higher compressor refrigerant mass flow rate was a result of the entrainment of foam into the U-tube of the accumulator. The lubricant mass migration during the start-up was not proportional to the refrigerant mass migration.

The presence of water condensate on the evaporator affected the refrigerant mass migration during the compressor stop period. Caused by an evaporative cooling effect the evaporator held 56 percent of the total refrigerant mass in the system after three minutes of compressor stop time—compared to 25 percent when no water condensate was present on the evaporator coil. Foam entrainment led to a faster lubricant and refrigerant mass migration out of the accumulator than liquid entrainment through the hole at the bottom of the U-tube. The latter was observed for when water condensate was present on the evaporator coil because—as a result of the higher amount of refrigerant mass in the evaporator before start-up—the entrainment of foam into the U-tube of the accumulator ceased before the steady state refrigerant mass distribution was reached.

To my wife for her endless love and the happiness she brings into my life.

Acknowledgments

This study was funded by the Air Conditioning and Refrigeration Center (ACRC), an industry/university cooperative research center. Without the generous support of the ACRC member companies this research would have not been possible. I want to thank my advisor, Professor Predrag S. Hrnjak, for supporting me throughout my time at the University of Illinois. He gave me the opportunity to learn how to conduct independent research, mentor undergraduate students and explore teaching.

I also want to thank the members of my dissertation committee, Professor Clark W. Bullard for the insightful discussions, Professor Dimitrios C. Kyritsis for his comments and his help in improving my teaching, Professor Barclay G. Jones and Professor Ty A. Newell, for their suggestions, comments and recommendations.

Special thanks goes to the visiting scholars—Michael Peterson, Helena Mai, Matthias Koffler, Sebastian Bellm, and Jascha Ruebeling—for their invaluable help in the laboratory.

Last but not least I want to thank my family and friends, most of all my parents for their love and support—thank you!

Table of Contents

List of Tables

List of Figures

Chapter 1

Introduction and Literature Review

"... a major issue for the future in refrigeration is the time-dependent behavior of systems" [1]. Refrigerant migration, redistribution and oil solubility have been identified as factors affecting the transient and cycling performance of all refrigeration and air conditioning equipment [2]. However, there are few published studies of experimentally measured refrigerant migration in refrigeration systems during off cycle and start-up. No studies, as of today, are available in the open literature which experimentally measured the lubricant migration within a refrigeration system during cycling or stop–start transients. Therefore, the main objective of this doctoral research is to develop and apply experimental procedures measuring the refrigerant and lubricant migration through the major components of a refrigeration system during stop–start transients. Besides the successful implementation of the experimental procedures regarding the refrigerant and lubricant migration, analysis of the experimental results identify the underlying physics.

A detailed literature review was conducted to identify and evaluate publications related to the work presented. The literature review is organized into three parts. The first part looks at the available literature regarding experimental techniques to measure refrigerant mass distribution in refrigerating systems. The second part focuses on literature presenting experimental results of direct measurements of refrigerant charge distribution at steady state and migration during stop-start operation. The third part addresses the literature regarding lubricant migration in refrigeration systems.

1.1 Experimental Techniques to Measure Refrigerant Mass Distribution

The different experimental techniques found in the literature can be divided into two main categories: The Quick-Closing Valve Technique (QCVT) and the On-Line Measurement Technique (OLMT). Both of these experimental techniques can be characterized as global techniques since they can be used to measure the refrigerant mass in each component and/or the whole system. It should be noted that numerous techniques are available to determine the refrigerant mass by locally measuring the void fraction through, e.g., determination of the volumes of the liquid and vapor phase in a channel by optical means, radioactive absorption and scattering, or light scattering [3]. These techniques to determine the total refrigerant mass in a system require knowledge of the void fraction inside each channel of a heat exchanger, making these techniques infeasible for a system-level investigation. Therefore, the focus is on the two global techniques. Figure 1.1 shows an overview of the global techniques and their secondary techniques.

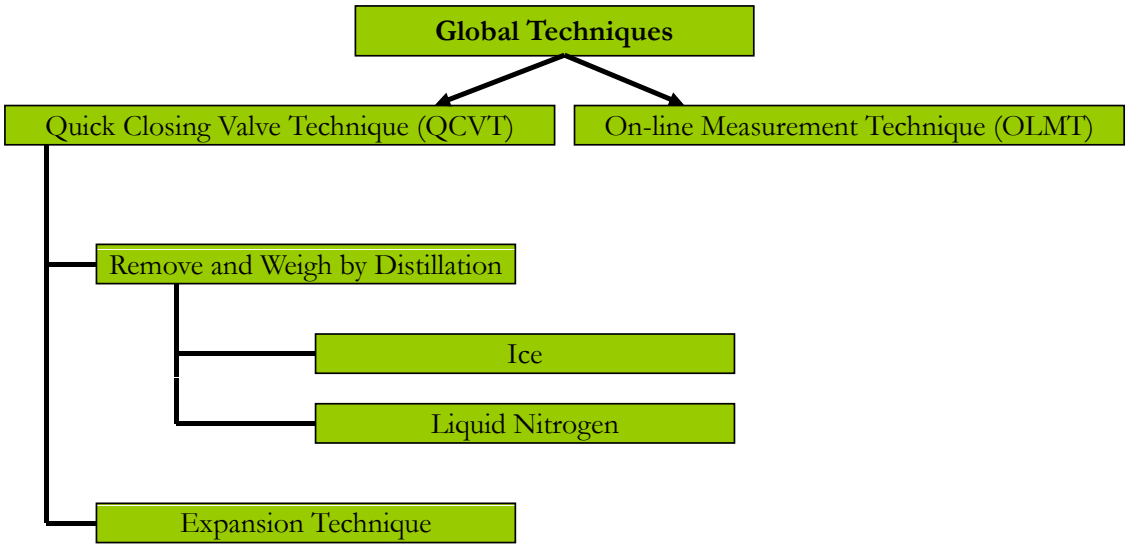

Figure 1.1: Global techniques to measure refrigerant mass distribution

The QCVT involves two (or more) valves which are closed simultaneously, trapping the fluid of interest in a section. A secondary procedure determines the mass of the trapped fluid. One secondary procedure is called the Remove and Weigh Technique (RWT); in which the refrigerant from a system or a section is distilled into a chilled recovery cylinder. As shown in Figure 1.1, the most common method is to use either ice or liquid nitrogen as chilling medium. Another secondary procedure—introduced by Björk [4]—expands the refrigerant from a section into a large vessel such that all refrigerant is present in the vapor phase. The amount of refrigerant mass is then calculated using a pressure-volume-temperature (p-v-T) relationship.

The QCVT is an indirect measurement technique and one of the oldest techniques for measuring the volumes the liquid and vapor phase occupy within a section. In 1931, Moore and Wilde [5] used the QCVT to measure the void fraction in a vertical gas lift. Lockhart and Martinelli [6], in 1949, relied on measurement data obtained using the QCVT to derive what is today known as the Lockhart-Martinelli parameter. In the 1960s, determining and predicting of steam void fraction in steady and transient conditions in steam generating power channels of nuclear reactors became increasingly important. The paper by Colombo et al. [7] is one of several papers which demonstrate that the QCVT can be used for heated two-phase flow and transient measurements.

Regarding refrigeration systems, Tanaka et al. [8] were the first in 1982 to use the QCVT on a residential 1-ton R-22 heat pump system to measure the transient refrigerant migration during start-up. Three magnetic valves were used to divide the system into three sections: the indoor heat exchanger, the outdoor heat exchanger and the compressor which included the accumulator. To measure the refrigeration masses inside each section, Tanaka et al. [8] describes the following secondary procedure. The refrigerant from each section is transferred into a cooled receiver due to the pressure difference between the evaporation and condensation points. The weight of the refrigerant in the cold cylinder is determined. The weight of the remaining

refrigerant gas in each section is added—knowing the volume of the section—by measuring the pressure and temperature and assuming the remaining refrigerant is at a superheated state. For the compressor section, the amount of refrigerant dissolved in the oil was added, too. Mulroy and Didion [9] used the QCVT and the same secondary procedure as Tanaka et al. [8] on a residential 3-ton R-22 heat pump system running in cooling mode. Mulroy and Didion [9] increased the number of valves—in their case pneumatically operated—to five which allowed them to measure the refrigerant mass in five sections—the outdoor heat exchanger, the liquid line, the indoor heat exchanger, the vapor line and the compressor including the accumulator. Hoehne and Hrnjak [10] applied the QCVT and RWT to measure the refrigerant charge distribution in a low charge (<150 g) hydrocarbon (propane) refrigeration system. They demonstrated that by cooling the receiver in liquid nitrogen less than 0.1 g of refrigerant is left in each section. Björk [4] presents a new secondary procedure to measure the refrigerant mass trapped in a section by using the QCVT. After the refrigerant is trapped in a section, it is expanded into a tank of known volume, and large enough to ensure a superheated state is reached. As thermodynamic equilibrium is reached, the temperature and pressure are measured. Using the p-v-T relationship, and the known volume of the tank and the section, it is possible to calculate the refrigerant mass. Björk [4] used a domestic refrigerator for his experiment in which the compressor was used to evacuate the expansion tank and therefore returned the refrigerant to the cooling system. Comparing his new secondary expansion technique to the liquid nitrogen technique, Björk [4] concludes the differences are small ranging from one percent for the evaporator to five percent for the filter drier.

The following authors applied the QCVT to measure the refrigerant mass contained in heat exchangers: Machado et al. [11], Margat [12], Zietlow and Pedersen [13], Marinhas et al. [14] and Traeger and Hrnjak [15]. They all used the RWT as the secondary procedure except for Marinhas et al. [14], who used a receiver attached to

the section. After closing the valves to trap the refrigerant mass in the section, the valve to the receiver—chilled in a cold bath at $-6°C$—is opened. After equilibrium is reached, the weight of the cylinder is measured and the refrigerant remaining in the section is calculated the same way as for the RWT. Then the receiver is heated and the refrigerant is transferred back into the section.

Contrary to the QCVT, the OLMT is a direct measurement technique. The basic idea is to put the section of interest on a scale to measure its weight while the refrigeration system is running. The OLMT allows a dynamic measurement of the refrigerant mass in a section without interrupting operation as it is the case for the QCVT. Miller [16] used the OLMT on a 3-ton, R-22 split-system air-to-air heat pump. The migration of refrigerant entering or leaving the outdoor unit was measured using a weight scale incorporating a counterbalance to act as a tare weight (weight of outdoor unit without a refrigerant charge). Flexible couplings between outdoor housing and the vapor and liquid line were used to eliminate vertical thrusts. Miller [16] reports an accuracy of 0.05 kg for the weighing system while the heat pump is operated and a 15 s response time for a 1.0 kg step change in weight.

Belth et al. [17] further developed the OLMT to be able to measure the change in mass of each component of a 3-ton split-system air-to-air heat pump. For the indoor and outdoor heat exchangers they used a double balance scale because—during start-up—liquid refrigerant moves inside the heat exchanger without leaving the coil and the center of mass of the heat exchanger changes location. The compressor was placed on a single balance beam using a brass proving ring force transducer. The accumulator was suspended from a steel proving ring. For both, the compressor and accumulator, Belth et al. [17] concluded it is necessary to install zig-zag copper tubing around those components to reduce the stiffness of the refrigerant tubing to below the stiffness of the force transducer. The zig-zag copper tubing, however, led to considerably more refrigerant mass in the system decreasing the dynamic response

time of the system.

Kuijpers and de Wit [18] used the OLMT to determine the mean void fraction of small evaporating and condensing heat exchangers. They determined the change in weight by measuring the displacement of the heat exchanger using springs fixed to a reference construction. Machado et al. [11] measured the refrigerant mass in an evaporator under transient conditions using the OLMT based on Miller [16] and Belth [19].

1.2 Experimental Results of Refrigerant Mass Distribution

Many indirect measurements of refrigerant migration have been done by measuring temperature, pressure and mass flow rates. These analyses give valuable insight into the dynamic performance of refrigeration systems, but cannot provide absolute numbers regarding the amount of refrigerant mass held up in components [2, 20, 21, 22]. Collins and Miller [23] concluded in 1996 “the distribution of charge in the system is a key parameter” and future work should be focused ”on obtaining accurate experimental descriptions of charge in the system in steady state and transient operation”. The following paragraphs give an overview of the available literature regarding direct measurements of refrigerant mass in components and systems.

Tanaka et al. [8] argue pressure and temperature measurements alone are not sufficient to evaluate the dynamic characteristics of a heat pump. The dynamic change of the refrigerant charge has to be considered. Therefore, Tanaka et al. [8] measured the refrigerant migration of a 1-ton R-22 heat pump in heating mode during start-up, stop-start and steady state operation in three sections (compressor including accumulator, condenser and evaporator). They found under steady-state operating conditions the outdoor heat exchanger holds 68.5 percent of the total refrigerant

charge in cooling mode operation and 35.7 percent in heating mode operation. They further observed the refrigerant mass in the outdoor heat exchanger—before start-up—exceeded half of the amount of the total refrigerant charge. During start-up the temperatures and pressures become stable after a stationary distribution of the refrigerant charge is achieved. Additional experiments showed the power drawn by the compressor is decreased during start-up if the refrigerant is kept in the condenser during the off-cycle time by closing the valve after the condenser.

Mulroy and Didion [9] measured the refrigerant migration of 3-ton R-22 heat pump system during start-up in cooling mode. They conclude turning off the indoor fan during off cycle operation has no significant influence on the off-cycle refrigerant migration. At the end of the off-cycle, 80 percent of the total charge was found in the low pressure components—evaporator, vapor line and accumulator/compressor. During steady-state operation 83 percent of the total charge was found in the condenser and liquid line. The experimental data of the refrigerant migration during start-up shows after 15 s of on-cycle time most of the refrigerant has left the evaporator, while at the same time the accumulator/compressor section contains a maximum amount of refrigerant (38 percent of the total charge). The amount of refrigerant in the accumulator/compressor section slowly decreases to its steady state value (5 percent of total charge). Mulroy and Didion [9] argue this a result of gradually release of liquid refrigerant held up in the accumulator into circulation and therefore "much of the cyclic loss can be attributed to the unit being in effect undercharged while the liquid refrigerant is stored in the accumulator".

Miller [16] measured the refrigerant migration of a 3-ton R-22 heat pump in heating mode during on-off periods of a cycle and at steady state operating conditions for two different ambient temperatures. By measuring the weight of the outdoor unit containing the compressor, condenser and accumulator, Miller [16] determined during steady state—operating at $-1°C$ outdoor temperature—the outdoor unit holds

53.7 percent of the total refrigerant charge. At 10°C outdoor temperature, the outdoor unit contains 34.2 percent of the total refrigerant charge. Miller [16] concludes a decrease in outdoor temperature causes an increase in the amount of refrigerant stored in the accumulator. From the on-off cycle experiments Miller [16] concludes the outdoor unit holds the majority (95 percent) of the refrigerant just before system start-up. The development of the charge distribution during start-up is similar to what Mulroy and Didion [9] reported, first a large amount of refrigerant is transferred from the low pressure components to the high pressure components in a short period of time—followed by a gradual migration of refrigerant mass over several minutes. Miller [16] speculates this gradual migration is caused by a gradual release of liquid refrigerant from the accumulator through the orifice at the bottom of the accumulator U-tube. Comparing the refrigerant migration during the on-period of the cycle for the two different outdoor temperatures shows the steady-state charge distribution is achieved in less time for the lower outdoor temperature. Miller [16] confirms the compressor power during start-up can be reduced by isolating the refrigerant in the condenser during off-cycle, as shown by Tanaka et al. [8].

Belth et al. [17] measured the refrigerant migration during start-up and shut-down of a 3-ton R-22 split-system air-to-air heat pump in cooling and heating mode. Their cooling mode results compare favorably with Mulroy and Didion [9]. Furthermore, they report three major conclusions. First, as the first to measure the refrigerant mass in the compressor, they show that there is "very little change" in the amount of refrigerant mass in the compressor. Second, confirming what Mulroy and Didion [9] and Miller [16] reported, at the beginning of start-up, a large quantity of refrigerant leaves the evaporator and enters the accumulator. Then, the refrigerant slowly leaves the accumulator over several minutes until a steady-state distribution is achieved. Third, during the compressor off period a large percentage of the refrigerant migrates to the evaporator. These three conclusions are valid for both, the heating mode and

cooling mode of the heat pump.

Hoehne and Hrnjak [10] present charge distribution data for an R290 (propane) refrigeration system under steady state conditions. The refrigerant charge was determined in the following six sections: compressor, condenser, high side receiver plus high pressure part of the internal heat exchanger, evaporator, low pressure part of the internal heat exchanger, and discharge line. The total system charge ranged from 110 g to 130 g. Although different ambient temperatures were investigated, the charge distribution remained constant because the cooling capacity was held between 1.1 kW and 1.3 kW. The results showed the majority of the refrigerant mass (80 percent) was found in the compressor, condenser and evaporator. Sheth and Newell [24] investigated a 1.5 kW R-22 window air conditioning unit at steady state conditions. They conclude for their particular system "the condenser and evaporator have the largest amount of oil and refrigerant out of all the components due to their size".

Björk and Palm [25] report experimental results of the charge migration in a steady cycling domestic refrigerator using R600a as the refrigerant, and having a rated cooling capacity of 108 W at AHSRAE conditions (54.4°C/−23.3°C). Their data shows the largest displacement of refrigerant charge during an on-off cycle occurs immediately after compressor start or stop. Similar to what the previously mentioned investigations of the R-22 heat pumps showed, the evaporator charge decreases sharply after a compressor start, reaches a distinct minimum after half a minute and then increases until it levels off after two minutes. The filter/dryer—positioned between the condenser and the capillary tube inlet—and the condenser show a "mirrored" behavior compared to the evaporator. The charge is first displaced into the condenser and then back to the evaporator. Björk and Palm [25] explain this behavior is a result of a high initial compressor mass flow rate and a low capillary tube mass flow rate. This displacement of charge towards the condenser leads to a relatively quick refilling of the evaporator as a result of a subcooled state at the capillary tube inlet.

Björk and Palm [25] point out that this confirms what Rubas and Bullard [2] already described based on their indirect analysis of refrigerant mass migration. In a separate paper Björk and Palm [26] present results from investigating the refrigerant charge distribution at steady state conditions with different thermal loads. The conclusion from this investigation showed the condenser refrigerant mass hold-up capacity and the compressor refrigerant vapor mass increase whereas the evaporator refrigerant mass hold-up capacity decreases upon increased thermal load. For the investigated range of thermal loads—74 W to 144 W—the evaporator showed the largest charge variation, decreasing by more than 30 percent from the lowest to the highest thermal load. Björk and Palm [26] also conclude that the accumulator acts as a charge buffer from which refrigerant mass is displaced to other parts of the system.

1.3 Lubricant Mass Migration

Compressors used in refrigeration systems require lubrication to reduce friction of their moving parts. The use of a lubricant is therefore essential in refrigeration systems to guarantee durability and reliability. Secondary benefits of the lubricant include serving as a sealing agent, reducing noise and/or serving as a heat transfer medium for cooling the compressor. Lubricants for refrigeration applications are divided into two categories—mineral oils and synthetic oils. Because lubricants for refrigeration applications are oil based the terms "lubricant" and "oil" are often used interchangeably. For automotive applications—using R134a as a refrigerant—synthetic lubricants based on polyalkylene glycol (PAG) are commonly used [27]. Although categorized as a partially miscible combination, R134a and PAGs oils are miscible over a wide range of temperatures and pressures [28].

Since the lubricant comes in direct contact with the refrigerant, it is unavoidable some lubricant leaves the compressor discharge. As a result, returning the lubricant

to the compressor must be insured during operation. Lubricant is, however, held up in components and tubes. Crompton et al. [29] showed that lubricant holdup is sensitive to quality, mass flux, tube type and lubricant concentration. The presence of lubricant induces changes in the flow configurations, increases pressure drops, and thermodynamic properties of the refrigerant—liquid-vapor equilibrium, enthalpy, viscosity, surface tension, etc. [1]. The influence of lubricants on system performance, however, is not well understood [27]. Experimental measurements of the distribution of lubricant in tubes and components under steady state operating conditions have been performed [30]; however, no experimental measurements have yet been published directly measuring the lubricant mass migration across the components of a clutch cycling orifice tube system during on/off cycling.

Chapter 2

Experimental Facility and System

This chapter describes the experimental facility and its instrumentation including an assessment of the measurement uncertainties. The experimental system and its configuration, including the determination of the system volume and relative heights of components are described as well. Additional pictures and component specifications can be found in Appendix A.

2.1 Laboratory and Instrumentation

The experimental facility used for all experiments presented in this study, consists of two environmental chambers shown in Figure 2.1. The chamber containing the condenser is referred to as the outdoor chamber, while the chamber containing the evaporator is referred to as indoor chamber. Controls and data acquisition are located in front of the outdoor chamber. The compressor stand is installed between the two chambers to minimize piping length. A schematic of the experimental facility, including the location of the components of the experimental system, is shown in Figure 2.2.

The outdoor and the indoor chambers are 4.7 m x 2.5 m x 2.3 m and 4.7 m x 2.2 m x 2.3 m, respectively. All refrigerant to air heat exchangers are installed in open-loop wind tunnels housed inside the chambers. The wind tunnels in the indoor and outdoor chambers are similar in design. The outdoor wind tunnel is build from 1.9 cm thick plywood, whereas the indoor wind tunnel for the evaporator is build

Figure 2.1: Experimental facility for R134a automotive A/C system

from 0.75 cm thick polycarbonate sheets. Radial blade blowers—controlled by variable frequency drives—are used to draw air through the wind tunnels. The condenser is installed at the entrance of the wind tunnel. The evaporator, however, remains installed inside the original heating ventilation air conditioning (HVAC) module, which is attached to the wind tunnel. Using the module's blower in combination with the radial blade blower creates a more realistic velocity and temperature profile at the evaporator. The flaps inside the HVAC module are set for fresh air intake without reheat—the heater core is bypassed. Air-side pressure drops across flow nozzles are measured with differential pressure transducers. Welded Type-T thermocouples measure the dry-bulb air temperature at the nozzle throats. The air flow rates are calculated using nozzle calibration curves and air properties. Thermocouple grids installed upstream and downstream of the heat exchangers measure the dry-bulb air temperatures. An external R404A chiller system—the evaporator being mounted on the outdoor chamber ceiling—compensates for the heat rejected by the condenser. Proportionalintegralderivative (PID) controllers adjust electric heaters—installed in both chambers—to heat the room to the specified test conditions. The heaters are mounted in separate forced-air heater ducts, eliminating the effects of heat conduction and thermal radiation into the test sections where temperature measurements

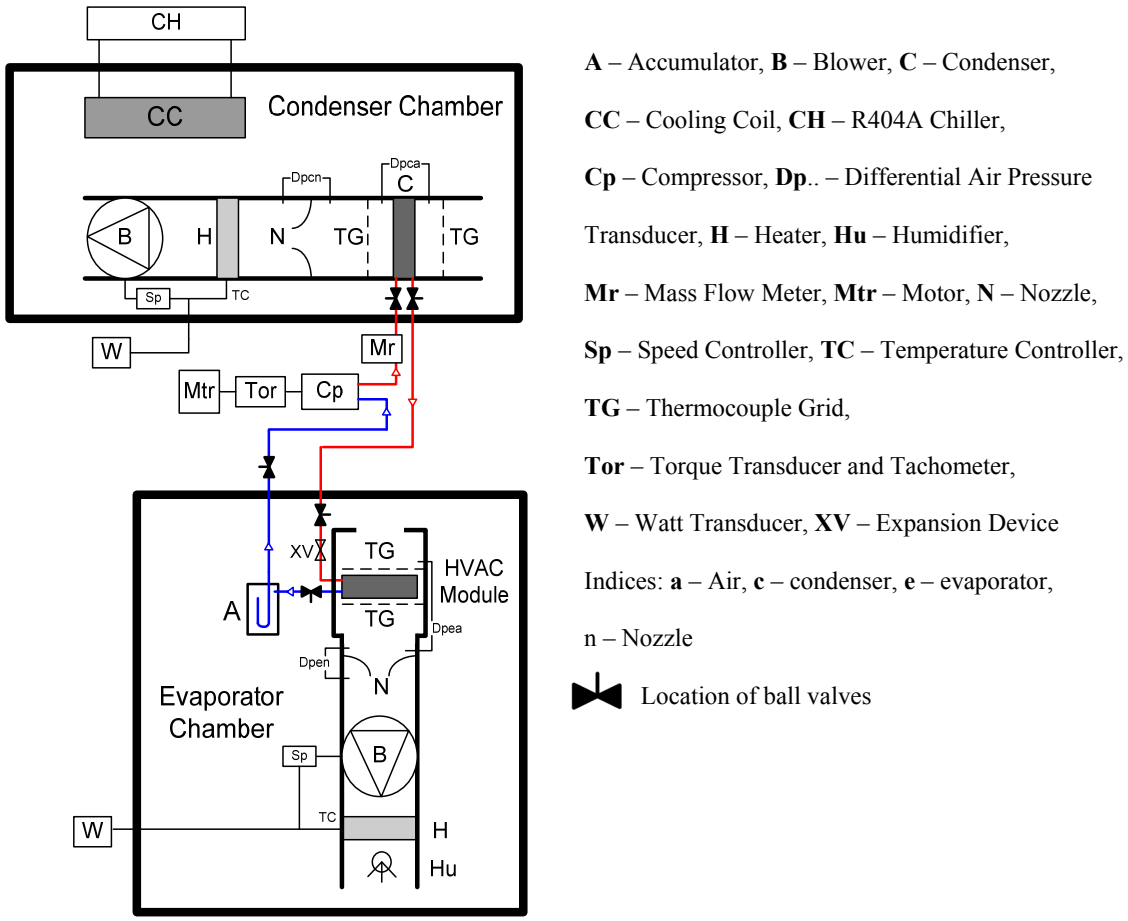

Figure 2.2: Schematic of experimental facility including breadboard system

are taken. Experiments requiring specified moisture content in the indoor chamber use a controlled steam injection. The steam is superheated using an additional heater before it is mixed into the air stream exiting the indoor heater duct. Chilled-mirror dew point sensors monitor the moisture content. The refrigerant side temperatures are measured by Type-T immersed thermocouples. Absolute pressure transducers measure the pressures within the system.

A Coriolis type mass flow meter measures the mass flow rate. The flow meter is installed between compressor and condenser. The device used reads mass flow rates accurately only for fluids in either liquid or gas phase. For steady state investigations of automotive refrigeration systems, the mass flow meter is usually installed between

the condenser and the expansion device—called the liquid tube—since the refrigerant is usually a saturated or subcooled liquid in this part of the system. In transient conditions the refrigerant is not always in the liquid phase in the liquid tube. During the off-cycle—when the compressor is turned off—the phase of the refrigerant changes from liquid to two phase to a gas phase. A reverse phase transition occurs during the start-up, which would leave a measurement gap for the mass flow rate during this phase transition. Therefore, the mass flow meter is located between the compressor and the condenser since the refrigerant is in the vapor phase almost always (for further details see Chapter 6.4.3).

The compressor power is determined using a torque transducer and tachometer. Both devices are installed between the compressor and the electrical motor, which drives the compressor. Therefore, the power calculated using measurements from both devices is the compressor shaft power. Two scales are used for the mass measurements. Depending on the amount of mass to be measured and the limit of each scale, the scale with the higher accuracy is always used.

Except for the mass measurements, all experimental data is recorded using a Hewlett-Packard 75000 data acquisition system consisting of a voltmeter module and three multiplexer cards, each having 16 channels. One multiplexer card has a thermistor on the board to provide direct temperature readings from the thermocouple signals. Agilent VEE data acquisition software displays data on screen and writes data to an Excel spreadsheet every four seconds. Faster sampling times of 1.5 seconds are achieved using the internal memory of the data acquisition system. The memory size and number of channels read limit this "fast sampling" to 10 minutes and an on screen observation is not possible. The data is read out of the memory after the 10 minutes and transferred into an Excel spreadsheet. All post-processing is done using the Engineering Equation Solver [31]. The following table 2.1 lists the measurement instruments and their specifications.

Table 2.1: Specifications of experimental instruments

Instrument	Range	Accuracy	Description or location
Type T welded thermocouple wire	-200°C to +200°C	greater of 0.5°C or 0.4% reading (above 0°C)	air temperatures
Type T immersed thermocouple	-200°C to +200°C	greater of 0.5°C or 0.4% reading (above 0°C)	refrigerant temperatures
Dew point sensor	-40°C to +60°C	±0.2°C	airflow upstream and downstream of evaporator
Differential pressure transducers	0 to 254 Pa	±0.25% full scale	pressure drop across heat exchangers
	0 to 762 Pa	±0.25% full scale	pressure drop across flow nozzles
Absolute pressure transducers	0 to 1379.0 kPa	±0.05% full scale	evaporator outlet
	0 to 1379.0 kPa	±0.05% full scale	accumulator outlet
	0 to 3447.4 kPa	±0.1% full scale	compressor inlet
	0 to 6894.8 kPa	±0.1% full scale	condensor in/outlet
Refrigerant mass flow meter	0 to 1.89 kg/s	±0.35% of Flow Rate	compressor outlet
Torquemeter	0 to 28.2 Nm	±0.15% full scale	compressor shaft
Tachometer	0 to 15,000 rpm	60 Voltage pulses/rev	compressor shaft
Scales	0 to 6100 g	±0.02 g	to measure mass of sampling cylinders and compressor
	0 to 12,000 g	±0.1 g	to measure mass of recovery cylinder
Hot wire anemometer	0.2 to 20.0 m/s	±1% full scale	air velocity

2.2 Measurement Uncertainty

The usefulness of reported measurement results depends on the uncertainty which accompanies them. Therefore, assessing the uncertainty of measurement results is essential in experimental research. A single standard on how to express the measurement uncertainty is not available. However, the National Institute of Standards and Technology (NIST) [32] and the American Society of Mechanical Engineers(ASME) [33] harmonized their guidelines with the International Organization for Standardization (ISO) Guide to Expression of Uncertainty in Measurement [34] to provide better comparisons of experimental results worldwide. Since differences still exist between these three guidelines, this section presents the approach used for expressing the measurement uncertainty in this document.

The uncertainty of a measurement consists of several components. The ISO guide [34] suggests identifying two components, random and systematic uncertainty, based on the method used to evaluate their numerical value. Based on NIST guidelines there is not always a simple correspondence between random and systematic uncertainty and therefore classification can be difficult. NIST [32] recommends avoiding the terms "random uncertainty" and "systematic uncertainty" altogether, and use the adjectives "random" and "systematic" in combination with the word "error". A systematic error β is the mean that would result from an infinite number of measurements of the same measurand (value of a physical quantity) carried out under repeatability conditions minus the value of the measurand. The random error ϵ is the result of a measurement minus the mean that would result from an infinite number of measurements of the same measurand carried out under repeatability conditions. The error of a measurement δ is then the sum of systematic and random error:

$$\delta = \beta + \epsilon \tag{2.1}$$

In general, the error of a measurement is unknown because the true value of the measurand is unknown. However, the uncertainty of the result of a measurement, y, can be evaluated. In most cases the measurement result y is calculated based on several directly measured variables or input quantities x_i. Therefore, y has a functional relation f with the N input quantities x_i.

$$y = f(x_1, x_2, \ldots, x_N) \tag{2.2}$$

Each input quantity contributes an uncertainty, $u(x_i)$, to the measurement result. The calculation of the propagation of the different uncertainties $u(x_i)$ results in the combined standard uncertainty, u_c. The combined standard uncertainty is calculated from a first-order Taylor series approximation of the function for y.

$$u_c = \sqrt{\sum_{i=1}^{N} \left(\frac{\partial y}{\partial x_i}\right)^2 u^2(x_i)} \tag{2.3}$$

Equation (2.3) is called the law of propagation of uncertainty or root sum of squares (RSS) method. Assuming a normal (Gaussian) distribution—an appropriate assumption in many practical measurement situations [32]—u_c defines a confidence interval.

$$y - u_c \leq Y \leq y + u_c \;\rightarrow\; Y = y \pm u_c \tag{2.4}$$

A normal distribution has a level of confidence of 68 percent, which means if the measurement is repeated 100 times 68 results would fall within the interval. An expanded uncertainty interval, U, is calculated as shown in Equation (2.5).

$$U = ku_c \text{ with k} = 2 \tag{2.5}$$

A coverage factor $k = 2$ results in a level of confidence of approximately 95 percent—out of 100 measurements 95 will be within the interval indicated by the value of U.

The uncertainty of a measurement result is expressed as shown in Equation (2.6).

$$y - U \leq Y \leq y + U \;\rightarrow\; Y = y \pm U \tag{2.6}$$

The expanded uncertainty interval is chosen over the combined standard uncertainty to represent the measurement uncertainty of the experimental results in this document unless otherwise stated.

2.3 Experimental System

The experimental refrigeration system chosen for this research is a 2007 production line R134a automotive A/C system. This system was chosen because, first, no experimental data regarding the refrigerant and oil migration within an automotive system has been published. Second, a setup using a fixed orifice tube and fixed displacement compressor eliminates control parameters, e.g., changes in expansion device opening, so the focus can be on the physical mechanisms. The system consists of a minichannel condenser, fixed orifice tube (FOT) expansion device, plate evaporator, suction side receiver—referred to as accumulator—and fixed displacement compressor. This section describes the experimental system, including the modifications from the original automotive system, the internal volumes of the sections, and the location of the components. The specifications of the individual components can be found in Appendix A.

2.3.1 Breadboard System

All of the original production line system components—compressor, condenser, expansion device, evaporator, accumulator—are used in the breadboard system. The original breadboard system was modified by replacing the original accumulator with

a transparent accumulator and surrounding transparent tubes. The configuration using the transparent accumulator results in minor differences regarding the tubing length, internal volume and horizontal position. The differences are denoted in Tables 2.2–2.4. To fit the original production line system into the experimental facility, and measure refrigerant-side properties—pressure, temperature, mass flow rate—several modifications were necessary. Additional tubing was used since the distances between components locations are dictated by the arrangement of the environmental chambers. Although the components are installed as physically close as possible to each other, the tubing length differs from the original system.

Table 2.2: Tube lengths comparison–original and breadboard system

Tube lengths in mm	Original	Breadboard
Compressor to Condenser	1036	3075
Condenser to Evaporator	1450	4920
Evaporator to Accumulator	0	660 (782)[1]
Accumulator to Compressor	699	1470 (1585)[1]

[1] for breadboard system with transparent accumulator section

As Table 2.2 shows, the breadboard system tubes are longer by a factor of three for the tubes connecting the compressor to the condenser and by a factor of 2.1 from accumulator to the compressor. The largest difference in tubing length between original and breadboard system—by a factor of 3.4—is the distance between the condenser and evaporator. In the original system, the accumulator is attached directly to the evaporator. This is changed in the breadboard system since pressure, temperature and charge ports are added. Figure 2.3 shows an overview schematic of the locations of all tubes, charge ports, temperature and pressure measurements, sight glass, refrigerant mass flow meter, and ball valves. The pressure taps, immersed thermocouples and charge ports are either separate tee assemblies or are a combined tee-cross assembly.

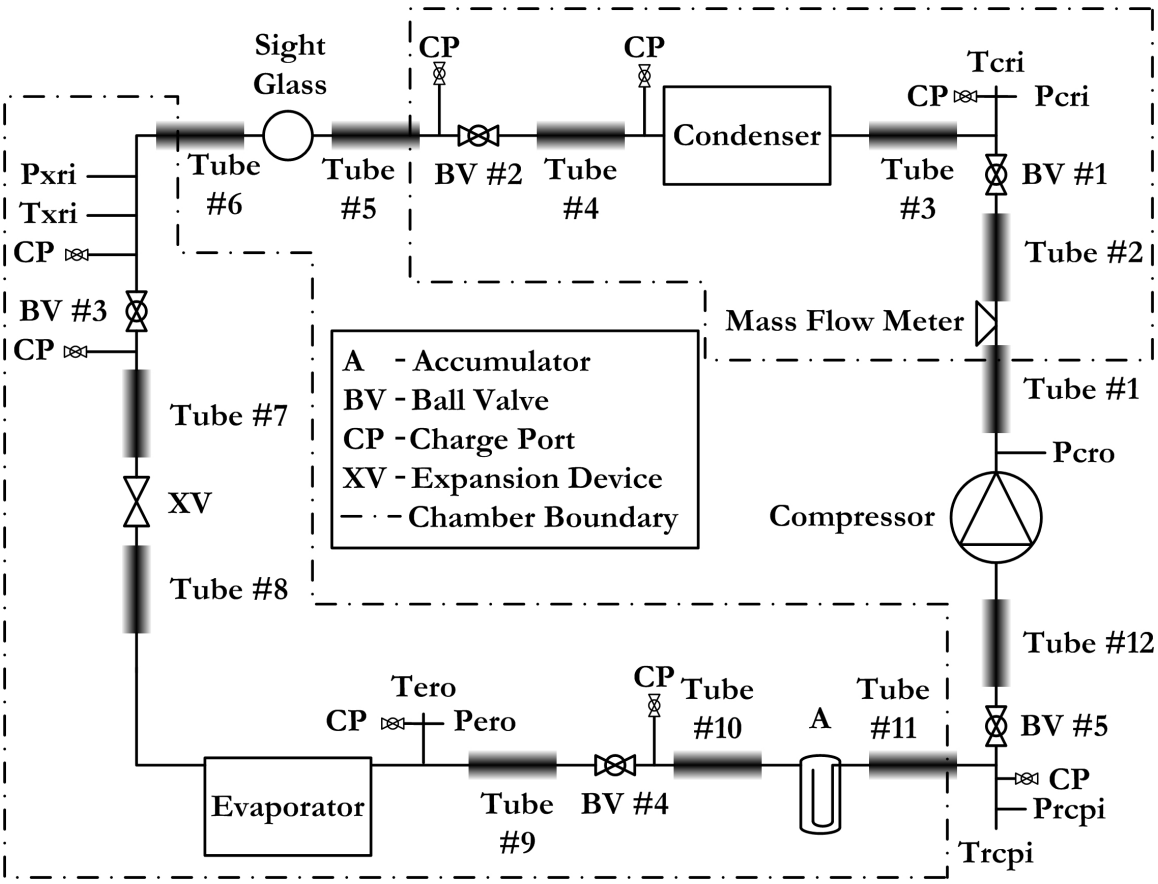

Figure 2.3: Schematic of breadboard system

Table 2.3 lists the lengths and diameters of all tubes, labeled according to Figure 2.3. The tubes used for the breadboard system are uninsulated copper tubes with a tolerance of ±0.0508 mm and ±0.076 mm for internal diameters of 10.21 mm and 15.75 mm, respectively. A tolerance regarding the internal diameter for the transparent tubes is not provided by the manufacturer. Since all tubes are measured as installed in the experimental facility, a tolerance of ±50 mm regarding the length of each tube is appropriate. For the breadboard system using the transparent accumulator tubes #10 and #11 are a combination of a copper tube and a transparent tube.

Table 2.3: Tube lengths and internal diameters–breadboard system

	Length (mm)	Internal Diameter (mm)
Tube #1	1735	10.21
Tube #2	450	10.21
Tube #3	890	10.21
Tube #4	250	10.21
Tube #5	2615	10.21
Tube #6	1675	10.21
Tube #7	130	10.21
Tube #8	250	10.21
Tube #9	500 (152)[1]	15.75
Tube #10	160 (430)[1]	15.75
Transparent part[1]	(200)[1]	13.36
Tube #11	720 (635)[1]	15.75
Transparent part[1]	(200)[1]	13.36
Tube #12	750	15.75

[1] for breadboard system with transparent accumulator section

2.3.2 Determination of System Volume

The internal volume of the system is important; it dictates how much refrigerant and lubricant mass can be stored in the system. Two approaches are taken to determine the volume. The first method calculates the volume based on geometrical information. For the second method, the system is filled with a known mass of gas. After the system reaches equilibrium, pressure and temperature readings are used to determine the gas density. By using the density of the gas, and the measured mass of gas filled into the system, the volume can be calculated.

Geometrical Method

The internal volumes of the system components—condenser, expansion device, evaporator and accumulator—are provided by the manufacturer. The internal volumes of the tubes are calculated based on the information given in Table 2.3. The uncertain-

ties regarding the internal diameters and lengths of the tubes are accounted for and the resulting uncertainty is shown for the summation of the volumes in Table 2.4, which presents an overview of the breadboard system internal volumes.

Table 2.4: Geometrical internal volumes of breadboard system

	Volume (cm^3)		Volume (cm^3)	
Tube #1	142			
Muffler	62			
Tube #2	37			
Valve	5			
Tube #3	73		Condenser Section	
Condenser	516		614	
Tube #4	20			
Valve	5			
Tube #5	214		Liquid Tube Section	
sight glass	12		369	
Tube #6	137			
Valve	5			
Tube #7	11		Evaporator Section	
Exp. Device	30		1045	(977)[1]
Tube #8	20			
Evaporator	881			
Tube #9	97	(30)[1]		
Valve	5			
Tube #10	31	(84)[1]	Accumulator Section	
Transparent part		(28)[1]	1508	(1503)[1]
Accumulator	1331	(1234)[1]		
Tube #11	140	(124)[1]		
Transparent part		(28)[1]		
Valve	5			
Tube # 12	146			
Sum	3927±50	(3854±50)[1]		

[1] for breadboard system with transparent accumulator section

The internal volume of the compressor is not known. The internal volumes of the pressure taps, immersed thermocouples, charge ports and tubing to the pressure transducers are excluded from the table. Although these volumes will hold refrigerant mass, the refrigerant is not actively flowing through them. The sum of these "inactive volumes" are estimated to be 100 cm^3 which is less than three percent of the "active volumes". The muffler—an original component—is part of tube #1 and its volume is listed as well as the volume of the sight glass. Since the measurements regarding the refrigerant and lubricant mass distributions are—as a result of the experimental methods used—by section, Table 2.4 also presents the section volumes. The replacement of the original accumulator with a transparent accumulator and additional transparent tubes results in a less than two percent—and therefore negligible—change of the volume.

Isothermal Gas Method

Since the compressor volume is unknown, the geometrical volume determination lacks this information. To determine the compressor section volume, and hence the total system volume of the breadboard system with the original accumulator, the isothermal gas method is used. Carbon dioxide—with a stated purity of 99.9 percent—is used as a gas. Before the carbon dioxide is filled into the system, the compressor is cleaned—using the procedure outlined in Chapter 4.3—to avoid diffusion of carbon dioxide into the lubricant. The system is evacuated, the carbon dioxide is filled in, and after a thermal equilibrium is reached, pressure and temperature measurements are taken. The density is calculated using EES [31] property data for carbon dioxide. The mass of carbon dioxide filled into the section is determined by weighing the charging cylinder. This procedure is repeated for each section and the results are presented in Table 2.5 which also includes the values of the section volumes based on the geometrical determination.

Table 2.5: Internal volumes of breadboard system–Isothermal gas method

Section	Pressure (kPa)	Temperature (°C)	Mass (g)	Calculated Volume (cm^3)	Geometrical Volume (cm^3)
Compressor	562.2	22.8	12.07	1160	1160[1]
Condenser	2063.0	23.0	30.22	688	614
Liquid tube	2474.0	24.0	21.76	388	369
Evaporator	1076.0	22.9	22.64	1072	1045
Accumulator	703.2	24.8	20.00	1506	1508
				4814±239	4695±224

[1] taken from the calculated volume since compressor geometrical volume is unknown

The internal volumes calculated using the isothermal gas method agree with the values from the geometrical volume determination. The sum of the internal volumes using the isothermal gas method include the "inactive volumes". Subtracting the "inactive volumes"—100 cm^3—from the sum of the volumes from the isothermal gas method gives an excellent agreement with the system value from the geometrical determination. It can be concluded that the breadboard system volume is 4705±164 cm^3 without the "inactive volumes". The original automotive system—using the volume for the compressor from the isothermal gas method and the manufacturer data—has an internal volume of 3880 cm^3. Therefore, the breadboard system volume is 21.3 percent (23.8 percent accounting for the "inactive volume") larger than the original automotive system

2.3.3 Relative Heights of System Components

The original components of the R134a automotive system are located at different heights in the vehicle. Figure 2.4 shows a to scale side view of the vehicle components. Gravity is acting in the negative Z direction. The compressor is located at the lowest location. This is usually the case for an automotive A/C system to allow lubricant

drained towards the compressor when the system is not operating or during an off-cycle. Using the compressor outlet as a reference height (Z=0), Table 2.6 lists the elevation differences of the components. These elevation differences were met within a tolerance of ±10 mm in the laboratory by adjusting the height of the compressor stand and the wind tunnel in the indoor chamber. The inlet of the transparent accumulator is at Z=403 mm and therefore 100 mm lower than the original location as a result of the installation of transparent tubes at the inlet and outlet.

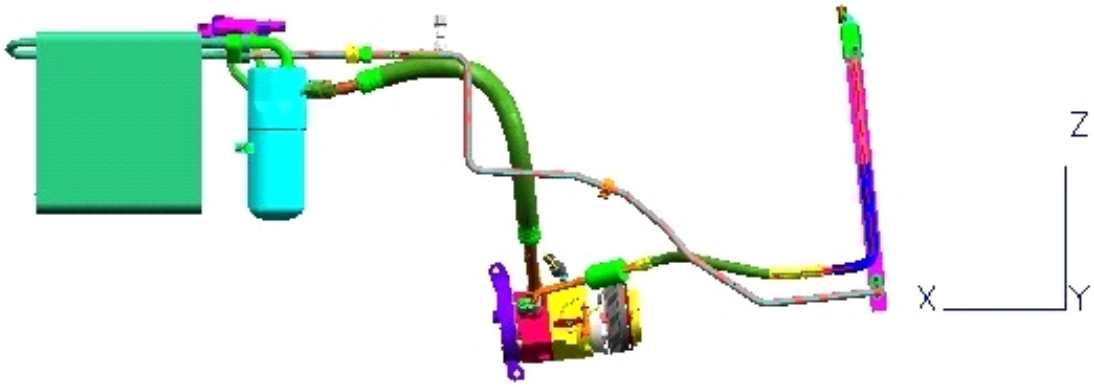

Figure 2.4: Side view of component locations in the vehicle

Table 2.6: Relative heights of components

Location	Relative height Z (mm)
Compressor outlet	0
Compressor inlet	20
Condenser inlet	385
Condenser outlet	28
Evaporator inlet	395
Evaporator outlet	413
Accumulator inlet	413
Transparent Accumulator inlet	403

Chapter 3

Experimental Method—Refrigerant Mass Distribution

To comply with the main research objective—measuring the refrigerant and lubricant migration over the major components of a refrigeration system—an experimental technique must include:

- Measurement of the refrigerant mass in each component at any given time
- Measurement of the lubricant mass in each component of the system at any given time

Two experimental techniques are found in the literature (see Section 1.1): The Quick-Closing Valve Technique (QCVT) and the On-Line Measurement Technique (OLMT). The main advantages of the QCVT are precise measurements—even at transient conditions [3, 4]. Another advantage is that only minimal physical changes to the system are necessary, e.g., installation of valves and ports to remove the refrigerant from the different sections. The major disadvantage of the QCVT is its time intensive procedure as a result of the intrusive nature of this technique. It requires stopping of the system, recharging the refrigerant, and reestablishing the operating conditions before another measurement can be done.

The advantage of using the OLMT is that the change in refrigerant mass can be measured continuously in each component of the system while the system is in operation. Using this direct measurement technique, many different transient scenarios can be measured in a relatively short amount of time. However, to implement the OLMT several expensive modifications to the original system are necessary as out-

lined by Belth et al. [17]. To account for movement of the refrigerant inside a heat exchanger a double balance beam must be used. The stiffness of the refrigerant lines and the air duct must be much less than the stiffness of the force transducers. Besides these physical changes to the system, careful calibration is needed to account for the lift force versus air velocity at the heat exchangers. Another disadvantage of the OLMT is that the refrigerant mass in the tubes cannot be measured. Furthermore, the water condensate formed on the evaporator during operation with dehumidification falsifies the measurement of the refrigerant mass. And, most significantly, since only the total mass contained within each component can be determined refrigerant and lubricant mass cannot be differentiated. Therefore, since the OLMT cannot meet the requirement of measuring the lubricant migration, the QCVT was chosen as the measurement technique.

As a secondary technique, the Remove and Weigh Technique (RWT) using liquid nitrogen to cool the receiver vessels was chosen because of the good accuracy reported by Hoehne and Hrnjak [10]. Björk [4] points out that his expansion technique may result in considerable errors if—for miscible refrigerant lubricant combinations—a large quantity of lubricant exists within the control volume because a considerable amount of refrigerant mass will still be dissolved in the lubricant. The technique Marinhas et al. [14] used only measures the refrigerant in the section, not the amount of lubricant. Both, Björk [4] and Marinhas et al. [14] techniques have the risk that if lubricant enters the receiver vessel it cannot be returned to the system, because for both methods the refrigerant is returned to the system in a vapor state, potentially leaving the lubricant behind.

3.1 Quick Closing Valve and Remove and Weigh Technique

The experimental system is divided into five sections by ball valves as shown in Figure 2.3. Ball valves are chosen because their high flow coefficient causes a minimal pressure drop. To estimate the pressure drop caused by a ball valve the following equations are used [35]:

$$K_v = \frac{\dot{Q}}{514}\sqrt{\frac{\rho \cdot T}{\Delta p \cdot p_{out}}} \tag{3.1}$$

$$K_v = \dot{Q}\sqrt{\frac{\rho}{1000 \cdot \Delta p}} \tag{3.2}$$

Equation (3.1) is used for gases and Equation (3.2) is used for liquids. The corresponding units for the quantities are given in Table 3.1. The calculated pressure drops Δp for a ball valve installed in the liquid tube and the suction tube of the experimental system at steady state operation condition are shown in Table 3.1. The calculated pressure drop is—as expected—lower for the liquid tube than for the suction tube. The suction tube is assumed to have the highest pressure drop but the calculated pressure drop of 1 kPa is negligible small and therefore the pressure drop caused by the ball valves can be neglected.

Table 3.1: Parameters and resulting Δp for equations (3.1) and (3.2)

	K_v	$\dot{Q}$	ρ	T	p_{out}	Δp
	m^3/h	m^3/h	kg/m^3	K	bar	bar
Suction Tube (3.1)	5.5	7.78	16.20	276.5	3.3	0.01
Liquid Tube (3.2)	5.5	0.113	1115	320.7	-	0.0005

The ball valves require a quarter turn to be fully closed. Since the ball valves

are manual operated, a strategy to close them simultaneously is necessary. Two ball valves are located in the indoor chamber, two are in the outdoor chamber and one ball valve is located between the chambers. Synchronization of closing is achieved by a light signal. To ensure that the compressor is not turned off before the ball valves are completely closed, a delay of one second is used.

For the remove and weigh technique, aluminum sampling cylinders are used. The cylinders have an internal volume of 700 cm^3 and have a 90 degree needle valve. Figure 3.1 shows a picture of the sampling cylinder and its placement in a styrofoam container when it is cooled with liquid nitrogen.

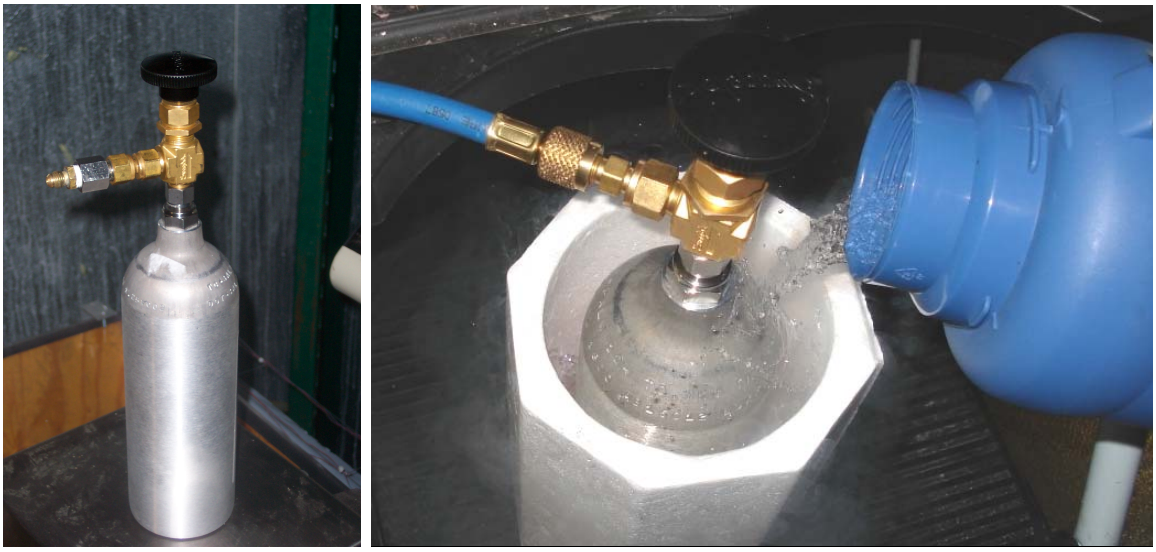

Figure 3.1: Sampling cylinder

3.2 Charging Procedure

Filling of an experimental system with refrigerant—referred to as charging—can be done manually or using charging equipment [27]. A manually charging procedure is used for all experiments conducted in this study. A cleaned recovery cylinder is filled with R134a from a commercially available R134a cylinder by placing the recovery cylinder in an ice bath. Checking the purity of the R134a after the distillation process

confirms a purity of at least 99.6 percent of R134a. The recovery cylinder mass is determined before and after the charging process and the difference is denoted as the filled-in-mass. The uncertainty of this value is obtained from the accuracy of the scale used. However, this uncertainty is misleading because the recovery cylinder has to be connected and disconnected from the system and R134a will be lost to the environment even if so called low-loss refrigerant hoses are used [36]. Experiments using low-loss refrigerant hoses showed that up to five grams of R134a can be lost during disconnecting if the hoses were filled with liquid phase R134a. To minimize the loss of R134a the following procedure is used. After the system is filled through the charge port located downstream of the evaporator, the valve between the system and the recovery cylinder is closed, leaving the hose connected. The experimental system is then turned on and operated to reach an evaporator exit pressure of 300 kPa. The valve between the system and the recovery cylinder is opened for five seconds to lower the pressure in the hose and to allow most of the liquid R134a to be transferred into the system. One concern with this approach is that lubricant from the system might enter the hose. However, examining the hose several times after a charging procedure showed that lubricant is not entering the hose.

3.3 Procedure for Extracting Refrigerant Mass

Simultaneously closing the ball valves traps the refrigerant mass and lubricant mass in each section. A step-by-step overview of the procedure to extract the refrigerant from each section is shown in Figure 3.2, including the time lengths of each step. At the start of the procedure, a cleaned and evacuated sampling cylinder is connected to a section. All sampling cylinders are connected using evacuated refrigerant hoses. The valve to the system is opened first followed by the needle valve of the sampling cylinder. The sampling cylinder is placed in a styrofoam container and chilled with

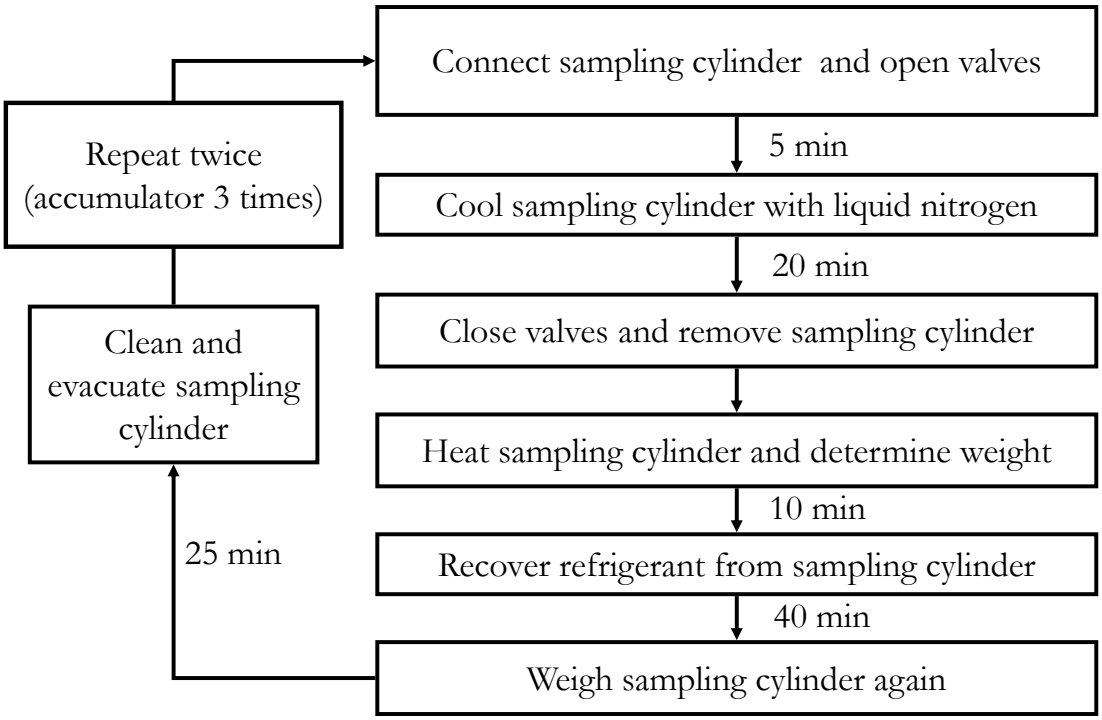

Figure 3.2: Procedure for extracting refrigerant mass

liquid nitrogen. Whenever liquid nitrogen is handled, safety goggles and protective gloves are used. Based on experience, it is sufficient to immerse the sampling cylinder about one quarter of its volume into the liquid nitrogen. After 20 minutes the valves are closed and the sampling cylinder is removed from the liquid nitrogen. To remove ice buildup on the sampling cylinder and to avoid further water condensation, the sampling cylinder is warmed to a temperature above the dew point in the room and dried. The weight of the cylinder is determined. Since lubricant can be carried with the refrigerant into the sampling cylinder, the refrigerant is recovered by the method described in Section 4.1. After the refrigerant is removed, the sampling cylinder is weighted again to determine the amount of lubricant removed from the system. The sampling cylinder is then cleaned with acetone and evacuated and its weight is checked against the tare weight to ensure proper cleaning. The whole procedure is repeated twice on each section, three times on the accumulator section

with the original accumulator. For the transparent accumulator section the amount of refrigerant in the section is determined during the 1st flush as described in Section 4.4.

The repetition of the procedure ensures a low pressure—less than 20 kPa—in each section. However, refrigerant remains dissolved in the lubricant and is released over time. A typical pressure increase curve is shown in Figure 3.3. The refrigerant

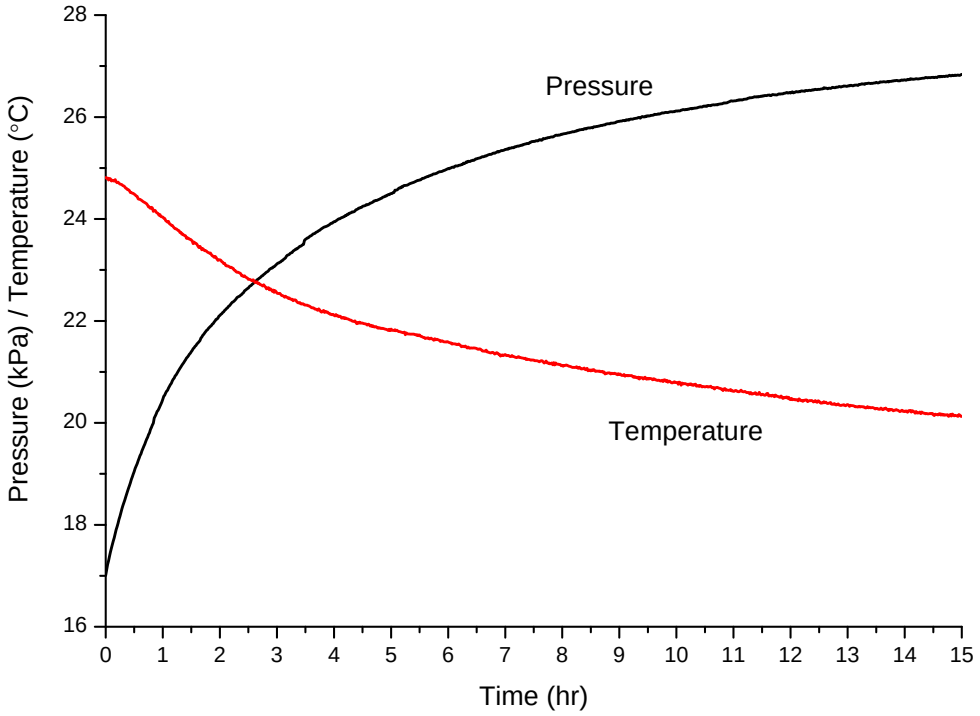

Figure 3.3: Temperature and pressure development after extracting refrigerant

released from the lubricant increases the pressure in the section until a pressure, temperature and concentration equilibrium is achieved. For the experimental system and its facility it takes 12 to 16 hours to reach near equilibrium. Therefore, after the refrigerant extracting procedure, the system is left at rest for at least 12 hours. The density of the refrigerant, ρ, based on the pressure P and temperature T in each section is then determined to calculate the mass of refrigerant, m, left in each section

by multiplying the section volume, V, by the density.

$$m = \rho(P, T) \cdot V \tag{3.3}$$

Table 3.2: Typical pressures, temperatures and resulting mass of refrigerant in sections 12 hours after extracting procedure

	Evaporator	Condenser	Liquid Tube	Compressor	Accumulator
Temp. (°C)	23.19	23.64	23.05	23.50	22.92
Pressure (kPa)	21.33	13.50	27.87	18.68	41.44
Mass (g)	0.95	0.39	0.45	0.90	2.62

Table 3.2 shows a typical pressure and temperature measurement 12 hours after the refrigerant was extracted. The mass of refrigerant is calculated using Equation (3.3). In this example, 5.31 g of refrigerant is left in the system and therefore is included in determining the amount of refrigerant mass in the system. Using Equation (3.3) the leftover refrigerant mass in each section was determined and added to the value from weighing the sampling cylinders.

3.4 Uncertainty and Repeatability

Besides the uncertainty as a result of the charging procedure, two more uncertainties arise. First, from the lubricant mass occupying part of the system volume and, second, the refrigerant mass dissolved in the lubricant after extraction. An estimation of the magnitude of two uncertainties can be determined. The amount of lubricant in the system is 230 g and having a density of 994 m^3/kg the volume the lubricant occupies is 231.4 cm^3. Assuming an equilibrium condition of 50 kPa at 20°C, 0.5 g of refrigerant could occupy the volume of the lubricant and therefore does not introduce a significant error.

The refrigerant dissolved in the lubricant—under the same conditions—can be estimated using the correlation from Seeton and Hrnjak [28] which predicts the concentration of R134a dissolved in PAG 46 lubricant at a given the equilibrium pressure and temperature. The correlation predicts—assuming an equilibrium condition of 50 kPa at 20°C—10 g of R134a would be dissolved in 230 g of lubricant.

As a result of the multitude of unknown sources of errors, a practical way to express the uncertainty regarding the total amount of R134a in the system is to compare the mass of R134a in the system from the charging procedure to the mass determined by using the Quick Closing Valve and Remove and Weigh techniques. Based on 30 experiments, the uncertainty between the filled-in R134a and extracted R134a is 4.2±4.0 g. A positive deviation is expected since refrigerant mass can only be lost and not gained during the extracting procedure.

The determination of R134a in each section has an additional uncertainty arising from how well the ball valves can be closed simultaneously. The ball valves used are hand operated by students. A light signal is used to signal the students to close the ball valves. Therefore, an uncertainty arises as a result of the reaction time of each individual. To estimate this unknown error, the system was run at steady state conditions—having a refrigerant mass flow rate of 35 g/s—when all the ball valves were closed simultaneously. This experiment was repeated three times, each time using different personnel to close the ball valves. The total system charge used was 1245 g. In Figure 3.4 the values above the bars are the standard deviations of the three measurements taken for each section. A conservative estimate—based on the three measurements—is that the refrigerant mass in each section can be determined with an accuracy of ±10 g. To check if this estimate is reasonable, the following calculation is performed.

The average reaction time of a university student exposed to light stimuli is 0.24 seconds [37]. According to the estimate of ±10 g and a refrigerant mass flow rate

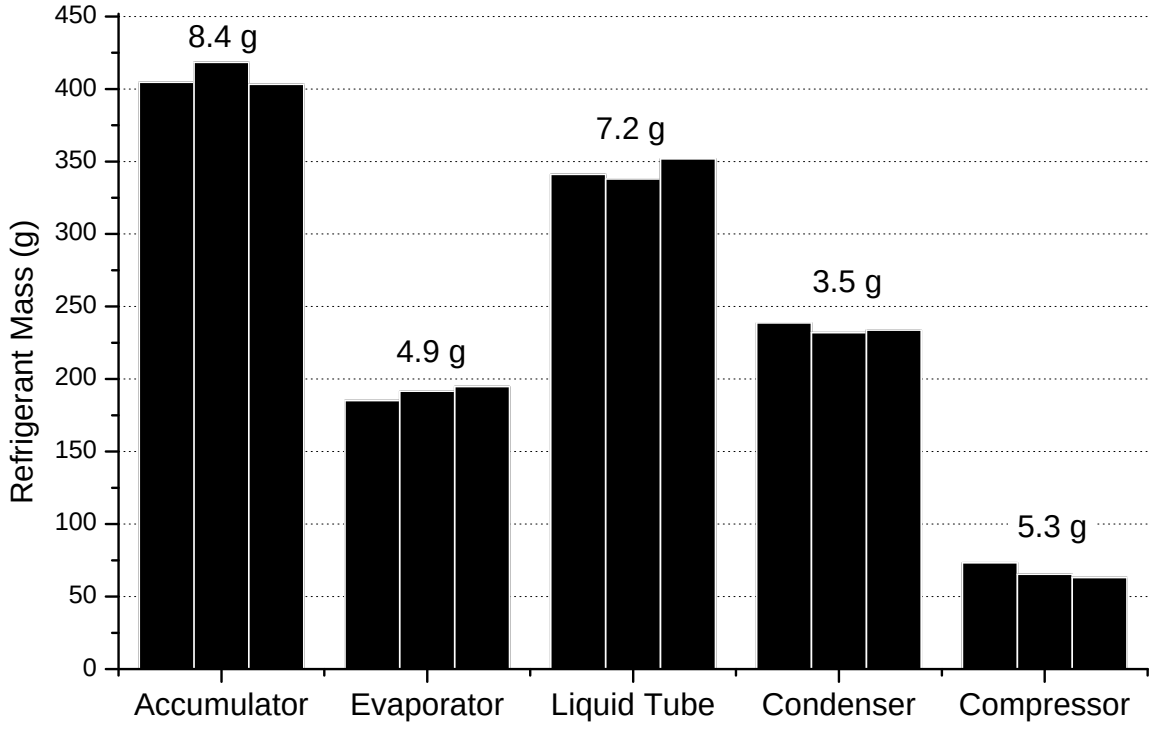

Figure 3.4: Repeatability and standard deviation of refrigerant mass measurements per section

of 35 g/s the maximum allowable difference in reaction time between students is 0.3 seconds. This means the students reacted with 0.24±0.15 s, which is reasonable and therefore confirms the estimate of ±10 g. Extrapolating this relationship allows the calculation of the expected uncertainty, U in grams, as function of refrigerant mass flow rate, $\dot{m}$ in grams per second, and the reaction time difference of 0.3 seconds, Δt:

$$U = \dot{m} \cdot \Delta t \tag{3.4}$$

Applying the Quick Closing Valve and the Remove and Weigh techniques to the breadboard system to determine the refrigerant mass distribution results in accurate measurements. The uncertainty of how much refrigerant mass is in a section is less than ±10 g—for a refrigerant mass flow rate of 35 g/s—and the uncertainty regarding how much total refrigerant mass is in the system is ±4.0 g. Applying these techniques,

however, is time consuming. For the investigated breadboard system with its five sections it takes ca. 40 hours to complete one set of data.

3.5 Generalization—Practical Guidelines

Based on the experience gained from applying the Quick Closing Valve and the Remove and Weigh techniques to an automotive air conditioning system, several guidelines can be deducted.

- Pressure rated aluminum sampling cylinder having a volume large enough to hold 75 percent of the total system refrigerant mass are recommended. Unless it is anticipated that more than 75 percent of refrigerant mass is present in a section—this sampling cylinder size to total system refrigerant mass ratio results in good tradeoff between the mass of the cylinder and the mass of refrigerant recovered. A larger—and therefore heavier sampling cylinder—might require the use of a larger, less accurate scale.

- A styrofoam container with a clearance of one centimeter around the sampling cylinder and the immersion of the cylinder one quarter of its length into liquid nitrogen is sufficient; a cover can be used to further reduces the heat loss.

- For miscible refrigerant and lubricant combinations more than one sampling procedure might be necessary for each section.

- After extracting the refrigerant, the section measured should be allowed to reach pressure and temperature equilibrium because refrigerant will be released from the lubricant. When an equilibrium is reached, the amount of refrigerant present in the section as vapor should be calculated and added to the value determined from weighing the sampling cylinder. Depending on the lubricant to refrigerant ratio, the volume occupied by the lubricant needs to be accounted for when

performing the calculation. The refrigerant left dissolved in the lubricant can be calculated using a vapor liquid equilibrium correlation—if available for the given refrigerant-lubricant combination.

- The sampling cylinder should always be checked for lubricant extracted from the system. This can be done as described in ANSI/ASHRAE Standard 41.4-1996 [38] or by the method described in Section 4.2. Lubricant extracted from the system should be replenished.

- Appropriate sized ball valves offer very low flow resistance and therefore are recommended.

- Manually operated ball valves introduce an error as a result of the reaction time of individuals. This uncertainty can be estimated using Equation (3.4) for any refrigerant. If automated ball valves are used, verification experiments should be performed. The closing speed of the ball valves should be as fast as possible to avoid a prolonged expansion effect in the valve which could influence the refrigerant and lubricant mass distribution.

- The charging procedure used should be described and a comparison between the refrigerant mass filled into the system and the refrigerant mass determined by extracting the refrigerant should be presented.

Chapter 4

Experimental Methods—Lubricant Mass Distribution

The technique used to recover the refrigerant from the sampling cylinders is described first since it is always the first step in the overall procedure to determine the lubricant content in a sampling cylinder. A technique to separate the refrigerant and the lubricant is described next. This technique—as well as the recovery technique—can be seen as an independent technique even if it is described here in the overall context of determining the lubricant mass distribution in the experimental system. Three different techniques—Remove and Weigh, Flushing, Mix and Sample—are necessary to determine the lubricant distribution within all the sections of the experimental system and are described in listed order in this chapter. All three techniques are intrusive—and therefore not on-line—but the advantage is the potential for a low degree of uncertainty.

4.1 Recovery Procedure

As described in Section 3.1 the refrigerant is removed from the system using sampling cylinders. Instead of using a commercial recovery device—used for servicing mobile air-conditioning systems [39]—to recover the R134a from the sampling cylinders, the following manual method is used.

A recovery cylinder is placed in an ice bath and the sampling cylinder—containing refrigerant and possibly lubricant—is connected to it. The connection includes a transparent tube connected directly at the sampling cylinder to monitor that only

vapor phase refrigerant leaves the sampling cylinder. A flow meter indicates the refrigerant vapor flow. The sampling cylinder is at room temperature when it is connected to the recovery cylinder. First the valve at the recovery cylinder is opened and then the needle valve of the sampling cylinder is carefully opened to avoid boiling inside the sampling cylinder. Boiling can lead to foaming of the refrigerant-lubricant mixture and lubricant potentially could leave the sampling cylinder. If the flow meter shows that the initial vapor flow has ceased, the sampling cylinder is placed in a bucket and warm water (ca. 40°C) is slowly added. Again, boiling of the refrigerant lubricant mixture is avoided. The sampling cylinder stays connected to the recovery cylinder for one hour, after which the sampling cylinder is disconnected and the separation technique—described in the next section—is applied.

4.2 Technique to Separate Refrigerant and Lubricant

The refrigerant lubricant combination used—R134a and a polyalkylene glycol oil with an ISO viscosity grade of 46 mm^2/s (PAG 46)—is a miscible combination over a wide range of pressure and temperatures [28]. Therefore, a technique is necessary to separate the refrigerant from the lubricant in order to determine the amount of lubricant in a sample. ANSI/ASHRAE Standard 41.4-1996 [38] describes a method aimed to measure the lubricant to refrigerant ratio at a location of a system during operation. The standard requires that after a sample is taken, the sampling cylinder is connected to a recovery system and evacuated to pressure of 2000 μmHg (0.27 kPa). Then the mass of the evacuated cylinder is determined to within ± 0.1 g. Comparing to the tare cylinder weight gives then the amount of lubricant—unless the value is smaller than 3 g which requires an additional procedure including the use of a solvent.

Following the standard an experiment was conducted. A sampling cylinder was

filled with 86.82±0.02 g PAG 46 lubricant and 20.81±0.02 g of R134a. The sampling cylinder was connected to a pressure calibrator and placed on a scale as shown in Figure 4.1. Following the recovery procedure, a vacuum pump was used as described

Figure 4.1: Sampling cylinder with pressure calibrator on scale

by the ANSI/ASHRAE Standard 41.4-1996 [38]. The vacuum pump was stopped when a pressure of 0.27 kPa was reached. The recovery procedure was repeated four times and the results are shown in Table 4.1.

As Table 4.1 shows, one evacuation is not sufficient to separate the refrigerant from the lubricant. It should be pointed out that the ANSI/ASHRAE Standard 41.4-1996 [38] is aimed to determine the concentration of small samples, e.g., for automotive systems the sample cylinder size should be 50 ml or smaller. The sampling cylinder

Table 4.1: Mass of R134a left in sampling cylinder after evacuation

Evacuation run	1	2	3	4
Mass of R134a left in sampling cylinder (g)	10.07±0.02	8.78±0.02	6.29±0.02	4.55±0.02

size used for the Flushing and the Mix and Sample techniques is 800 ml and due to the nature of these techniques the lubricant and refrigerant quantities can be of the order of 100 grams. Based on the results presented in Table 4.1 and knowing that the sampling cylinder size violates the ANSI/ASHRAE Standard 41.4-1996 [38] a new method has been developed.

To increase the separation of the refrigerant-lubricant mixture, the sampling cylinder is heated and stirred while being evacuated. The sampling cylinder—containing a magnetic stirrer added to the cleaned sampling cylinder before a sample is taken—was placed on a magnetic hot plate stirrer device. The procedure for the separation method is as follows. After the recovery procedure, the sampling cylinder is placed on a magnetic hot plate stirrer. The stirrer is set to 1100 revolutions per minute and the heating is set to keep the hot place surface temperature at 25°C. A vacuum pump is connected and the sampling cylinder is evacuated for 20 minutes. The hot plate surface temperature is increased to 90°C. The sampling cylinder is evacuated for 20 minutes. The sampling cylinder is removed and weighed.

4.2.1 Uncertainty of Technique to Separate Refrigerant and Lubricant

Several R134a and PAG 46 lubricant mass combinations listed in Table 4.2 were tested with the aforementioned procedure. For each combination, the R134a mass remaining in the sampling cylinder was less than 0.04 g. To determine if stirring actually has a significant influence on the release of refrigerant from the liquid refrigerant-lubricant

mixture, four experiments were conducted—except that the stirring was not used. The R134a and PAG 46 lubricant mass combinations for these experiments are listed in Table 4.2. The results are the same—less than 0.04 g of R134a remained after the separation procedure. Therefore, stirring does not have a significant influence on the separation procedure.

Table 4.2: Refrigerant lubricant combinations for verifying separation methods

Using a stirrer		No stirring	
PAG 46 lubricant (g)	R134a (g)	PAG 46 lubricant (g)	R134a (g)
49.62	436.02	49.58	299.44
49.65	550.94	49.67	119.91
147.70	185.96	49.70	117.76
147.70	556.72	157.85	466.25
147.70	545.23		
147.72	535.00		
157.87	164.48		

As a result of this finding the separation method was changed, and instead of a hot plate stirrer, a metal bucket filled with water was placed on top of a electric hot plate. The water was heated to 90°C and the sampling cylinder was placed into the water and connected to a vacuum pump. The sampling cylinder was evacuated three times for 20 minutes. After each evacuation run the sampling cylinder was placed on a scale to determine its weight and henceforth—knowing the tare weight—the amount of lubricant remaining in the sampling cylinder was determined. Comparing the weight of the sampling cylinder after the second and third evacuation was used as a check—the difference in weight was always less than the detection limit. The detection limit resulted from the measurement uncertainty of the scale used and the uncertainty associated with the determination of the tare weight of the sampling cylinder. In the presented case the detection limit was 0.02 g.

The method described above separates the refrigerant from the lubricant with less

than 0.04 g of refrigerant mass remaining in the lubricant in the sampling cylinder. It should be pointed out that this method does not require any solvent or heating the extracted lubricant above 90°C and therefore the lubricant can be reused. A practical advantage of using a bucket on top of an electric hot plate was that up to four sampling cylinders could be evacuated at the same time, the magnetic stirrer hot plate could only hold one sampling cylinder at a time.

4.3 Remove and Weigh Technique

The principle of the Remove and Weigh method is to physically remove a section from the system and compare the current weight to the tare weight. When this method is used to determine the lubricant mass in a section, three uncertainties arise. First, the uncertainty from determining the tare weight. Second, the uncertainty as a result of removing the refrigerant mass—especially if the refrigerant-lubricant mixture is miscible. Third, the uncertainty of determining the weight of a section containing the lubricant mass. The second uncertainty depends on the method of refrigerant extraction. The first and third uncertainties are related to the scale used. Besides the accuracy of the scale used, other uncertainties can arise from, for example, that a section cannot be easily placed on a scale—like a long tube—or the center of mass of the section is at an offset from its geometrical center.

The Remove and Weigh method—to determine the lubricant mass—was applied only to the compressor of the experimental system. The compressor was delivered containing lubricant but neither the amount of lubricant nor the tare weight of the compressor were known. To determine the tare weight of the compressor, the lubricant was first removed. Just removing the lubricant by draining, e.g., mounting the compressor upside down, was not sufficient to remove all the lubricant. However, the miscibility of the refrigerant-lubricant combination used—R134a and PAG

46—was exploited to remove the lubricant. The compressor was filled with liquid R134a to dissolve the lubricant. The liquid R134a and PAG 46 mixture was then recovered using a sampling cylinder chilled with liquid nitrogen. During this recovery procedure the compressor was mounted upside down to drain as much liquid refrigerant-lubricant mixture into the sampling cylinder. The amount of lubricant in the sampling cylinder was determined by the separation technique described in the previous section. This filling-recovering procedure was repeated ten times and Figure 4.2 shows the results. For filling-recovery run #5 the compressor was placed in an

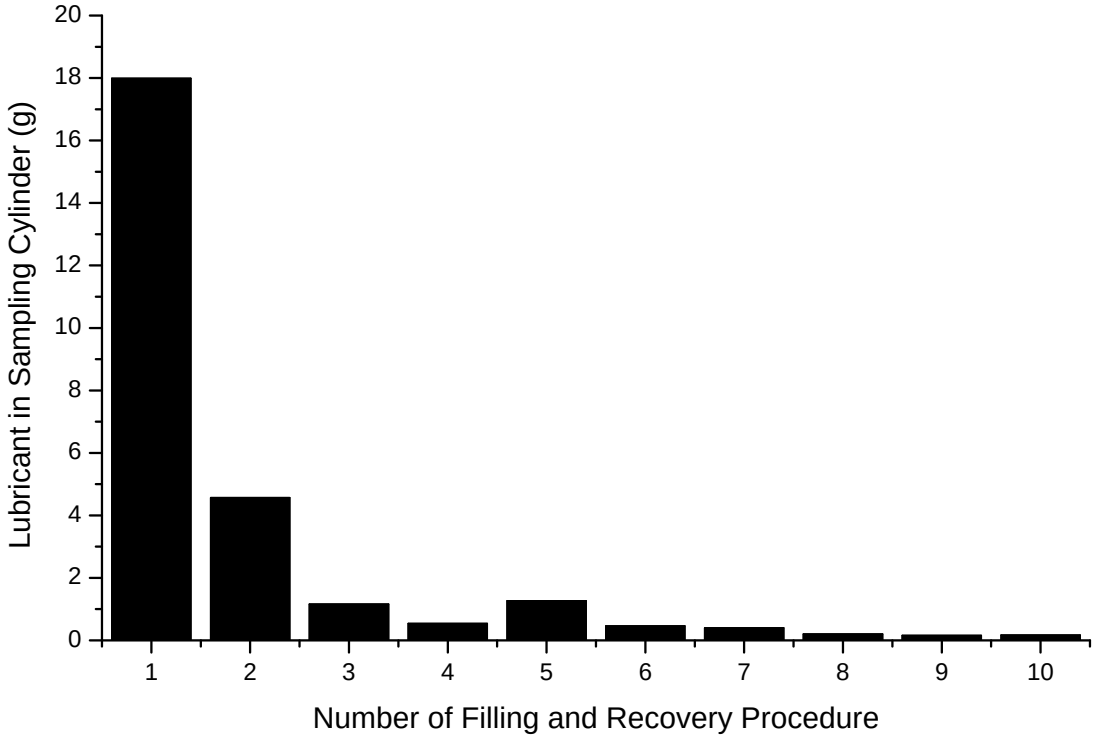

Figure 4.2: Determination of compressor tare weight

ice bath to increase the condensation of R134a, which explains the slight increase in recovered lubricant. Filling-recovery run #7 was changed such that the refrigerant had 60 hours to dissolve with the lubricant, but did not result in an increase in the recovered lubricant mass. After the #10 run only 0.16 g of lubricant was found in the sampling cylinder. Although this is slightly above the theoretical detectable limit

of 0.04 g, based on the decay of lubricant mass found during the previous runs it was estimated that ca. 1 g of lubricant mass remained in the compressor.

4.3.1 Uncertainty of Remove and Weigh Technique

To determine the uncertainty from removing the refrigerant mass from the compressor, the following procedure was used. The refrigerant was recovered from the compressor section using Quick Closing Valve and Remove and Weigh method twice. Then the compressor was connected to a vacuum pump and evacuated for 20 minutes. The weight of the compressor was determined and the compressor was evacuated again for 20 minutes. This procedure was repeated four times and the results are shown in Table 4.3.

Table 4.3: Verification of procedure to extract refrigerant from compressor

Time of vacuum (min)	20	20	20	20	20
Weight compressor (g)	5821.89	5821.45	5821.21	5821.22	5821.20
Difference weight (g)		0.44±0.04	0.24±0.04	-0.01±0.04	0.02±0.04

The weight of the compressor was determined by placing it on a scale and measuring its weight four times, each time rotating it by 90 degrees on the scale. The reported weight is the average of the four weights with an uncertainty of ±0.02 g which equals the detection limit. After the third evacuation—as shown in Table 4.3—the difference in weight was below the detection limit. A forth evacuation confirmed this result and therefore it was concluded that for the compressor used in this investigation an evacuation time of one hour was sufficient to remove the refrigerant.

The dominant uncertainty of the Remove and Weigh Technique to determine the lubricant mass in the compressor was the uncertainty of the tare weight. The uncertainty regarding the separation of refrigerant and lubricant was ±0.04 g and ±0.02 g regarding the measurement of the weight of the compressor. Therefore, if

the tare weight is known precisely the Remove and Weigh Technique has a very small uncertainty, which is primarily limited by the measurement uncertainty of the scale used.

4.4 Flushing Technique

The idea behind the Flushing Technique is to use a solvent—a chemical solvent or a refrigerant—and force it through a section. By capturing the solvent-lubricant mixture and separating it from the lubricant the amount of lubricant extracted can be determined. This method is used in industry to clean and/or retrofit systems [40, 41]. For mobile air conditioning systems SAE standard J2788 [39] establishes the specific minimum equipment performance requirements for recovery and recycling of R134a. A commercially available recycling device conforming to this standard is not only able to recovery R134a, but also to flush a section. The recycling device fills a section with R134a, circulates the R134a-lubricant mixture around, recovers the mixture, separates the lubricant, and purges it into a vessel.

To determine if the device can be used to measure the lubricant mass in a section, a test cylinder filled with 24.25 g of lubricant was connected to the device (Figure 4.3) and a flushing procedure was initiated.

After the first flushing procedure the test cylinder was removed and no lubricant ($<$0.04 g) was found. However, the lubricant separated out of the recycling device was less than the amount of oil in the test cylinder. This indicated that the recycling device retained some of the lubricant mass during the separation. Further tests revealed that the lubricant purged from the recycling device also contained lubricant from the recycling device itself—on average 1.6 g per purging. Both issues introduce an uncertainty in determining the amount of lubricant in a section. Several experiments were conducted on the evaporator and transparent accumulator section

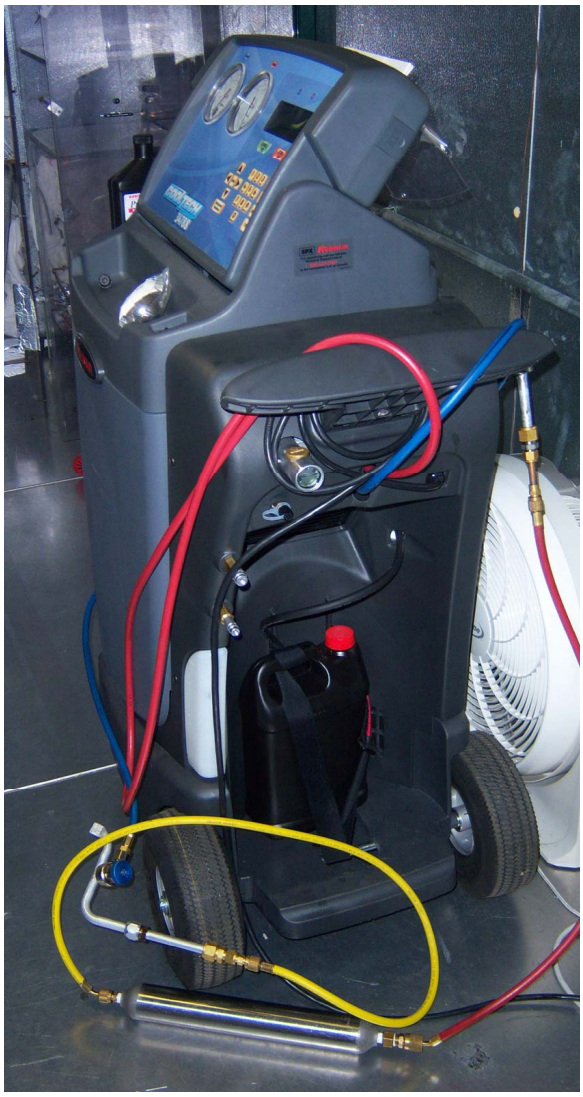

Figure 4.3: Recycling device connected to test cylinder

to determine this uncertainty. It was found that the uncertainty using the recycling device to measure the lubricant content is 30 g for more than 100 g of lubricant in a section and 10 g for less than 100 g of lubricant in a section after three flushing runs. In spite of this uncertainty, it was found that three flushing runs are sufficient to remove the lubricant mass from the accumulator section. The commercial recycling device is effective in removing lubricant mass from a section—which is its purpose—but has an uncertainty which is too high—for the purpose of this study—when used to determine the amount of lubricant in a section.

For the transparent accumulator section, a manual flushing method—using R134a as a flushing agent—was used to determine the amount of lubricant. The geometry of the automotive accumulator, however, makes the application of a flushing method challenging since the accumulator is designed to separate liquid and vapor effectively. In addition, the accumulator only allows refrigerant vapor and a small fraction of liquid refrigerant-lubricant mixture—entrained through a small hole at the bottom of the U-tube—to leave the accumulator. Therefore, during a flushing procedure, in which the accumulator is first completely filled with refrigerant, a significant amount of refrigerant can only be recovered by evaporation only. Figure 4.4 shows pictures of this process. In Figure 4.4c the evaporating refrigerant is visible. The evaporation and recovery of refrigerant leaves lubricant—dissolved in the liquid refrigerant-lubricant mixture—behind. Therefore, several flushing runs are necessary because only a fraction of the lubricant is removed with each flushing run.

(a) Before filling (b) Filling with pure R134a (c) Recover process

Figure 4.4: Photos of accumulator during flushing procedure before modification of accumulator

To avoid many flushing runs an outlet was installed at the bottom of the transparent accumulator. A sampling cylinder—chilled in liquid nitrogen—was connected and all liquid was drained into the sampling cylinder. The sampling cylinder stayed connected for 20 minutes. After the separation of refrigerant and lubricant, the refrigerant and lubricant masses were determined (this is referred to as the 1^{st} flush). However, some lubricant remained in the accumulator. Therefore, the accumulator was flushed through two times with liquid phase refrigerant, one time from the outlet side (2^{nd} flush) and one time from the inlet side (3^{rd} flush). The refrigerant-lubricant mixture is captured in a sampling cylinder—chilled in liquid nitrogen—connected to the outlet at the bottom of the accumulator. Figure 4.5 shows pictures of the accumulator after each flush.

(a) 1^{st} flush (b) 2^{nd} flush (c) 3^{rd} flush

Figure 4.5: Photos of accumulator after each flushing run

4.4.1 Uncertainty of Flushing Technique

Verification experiments were performed to determine the uncertainty associated with Flushing method applied to the transparent accumulator. Experiments were conducted with and without giving the refrigerant and lubricant time to diffuse. As Figure 4.6a shows, it was possible to create a visible layer indicating that lubricant and refrigerant are not completely mixed. To achieve a homogeneous refrigerant-lubricant mixture—as shown in Figure 4.6b—the refrigerant and lubricant were left in the accumulator for 15 hours. Overall, six experiments were conducted with a visi-

ble liquid layer present and four with a homogeneous mixture. For all experiments the accumulator was filled with 100 g of lubricant and 300 g of refrigerant before the first flushing procedure was initiated. Table 4.4 shows the results of these experiments.

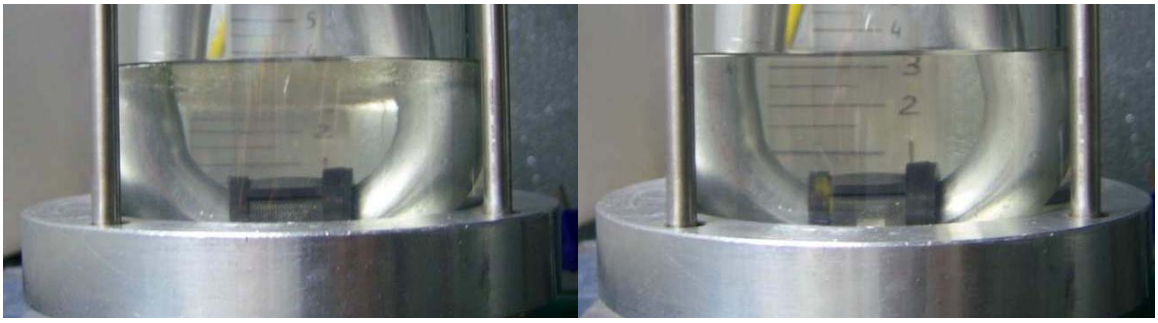

(a) Separated layer before flushing (b) Fully mixed before flushing

Figure 4.6: Photos of liquid refrigerant-lubricant mixture in accumulator before flushing

Table 4.4: Results of experiments to verify flushing method on accumulator

Flush	Separated layer Lubricant left (g)	Fully mixed Lubricant left (g)
1^{st}	6.18±2.37	5.42±2.15
2^{nd}	2.49±1.34	1.94±0.79
3^{rd}	1.97±1.16	1.43±0.61

As it can been seen, extracting the refrigerant-lubricant mixture through the bottom outlet of the accumulator (1^{st} flush), more than 5 g of lubricant remained in the accumulator and therefore justified the additional two flushes. More flushes most likely would remove even more lubricant from the section, but the tradeoff between better results and time commitment necessary dictated that three flushes are considered sufficient. Therefore, the accuracy of determining the amount of lubricant in the transparent accumulator section is 1.43±0.61 g for a homogeneous refrigerant-lubricant mixture or 1.97±1.16 g when a distinct layer was visible—indicating an

incomplete mixing of refrigerant and lubricant.

4.5 Mix and Sample Technique

Out of the previously described techniques the Remove and Weigh Technique would give the most accurate results if applied to the heat exchangers, assuming the tare weight is known. In practice, however, removing a heat exchanger is time consuming. For the experimental system used, the condenser is installed in a wind tunnel and the evaporator is installed inside the HVAC module. Removing these heat exchangers would take several hours, and after they have been reinstalled leak tests have to be performed. In addition, removing the liquid tube is not because it goes through to chamber walls, and therefore could only be removed in sections. Therefore, an in situ technique to determine the amount of lubricant inside a section was developed—called the Mix and Sample technique (MST).

The Mix and Sample Technique exploits the miscibility of a refrigerant and lubricant combination by filling a section with liquid refrigerant. After the refrigerant diffuses with the lubricant and forms a homogeneous mixture, a sample is taken and the concentration of lubricant in the mixture, ω_{sample}, is determined. By assuming the concentration of the sample is identical to the concentration in the section, $\omega_{section}$, the total amount of lubricant in the section, m_{lub}, can be calculated using Equation (4.1)—if the amount of refrigerant in the section, m_{ref}, is known.

$$\omega_{sample} = \omega_{section} = \frac{m_{lub}}{m_{lub} + m_{ref}} \rightarrow m_{lub} = \frac{m_{ref}\omega_{section}}{1 - \omega_{section}} \tag{4.1}$$

Since the calculation using Equation (4.1) is only correct if the sampled mixture is homogeneous, an experiment was conducted to estimate the time it takes for refrigerant and lubricant to diffuse. A sampling cylinder was filled with 50.0 g of PAG 46,

then R134a in a vapor phase was added. The sampling cylinder was placed on a scale and a pressure calibrator monitored the pressure and the temperature was measured by a thermocouple attached to the sampling cylinder outside wall. This experiment was repeated twice, once with the sampling cylinder in an up-right vertical orientation and a second time with the sampling cylinder in a horizontal orientation. The R134a was added quickly, so the amounts filled into the sampling cylinder were slightly different—24.5 g for the case of the vertical orientation and 26.0 g for the horizontal orientation. The surface area between the refrigerant and lubricant was greater for the horizontal orientation, so the refrigerant is expected to be absorbed quicker. For Fick's Law of diffusion—Equation (4.2)—the refrigerant mass flow rate, $\dot{m}$, is proportional to the surface area, A, times the diffusivity, D, and the concentration gradient.

$$\dot{m} = -A \cdot D \frac{\partial \rho}{\partial x} \tag{4.2}$$

The results from the experiment—shown in Figure 4.7—support the assertion that the refrigerant-lubricant mixture in the horizontal orientation reaches equilibrium quicker. However, the complete description of refrigerant absorption in lubricant oil is an issue that still remains open because of local density instability effects in the liquid phase [42].

The time to reach pressure equilibrium—as shown in Figure 4.7—was of the order of several hours. Therefore, to achieve a homogeneous mixture quicker, active mixing of the refrigerant and lubricant was necessary. A hermetic gear pump was used to circulate the liquid refrigerant and lubricant mixture after the refrigerant has been filled in. However, verification experiments on the condenser section showed that the uncertainty is ± 5 g even if the pump was running for two hours. A device was designed to improve this uncertainty while reducing the mixing time.

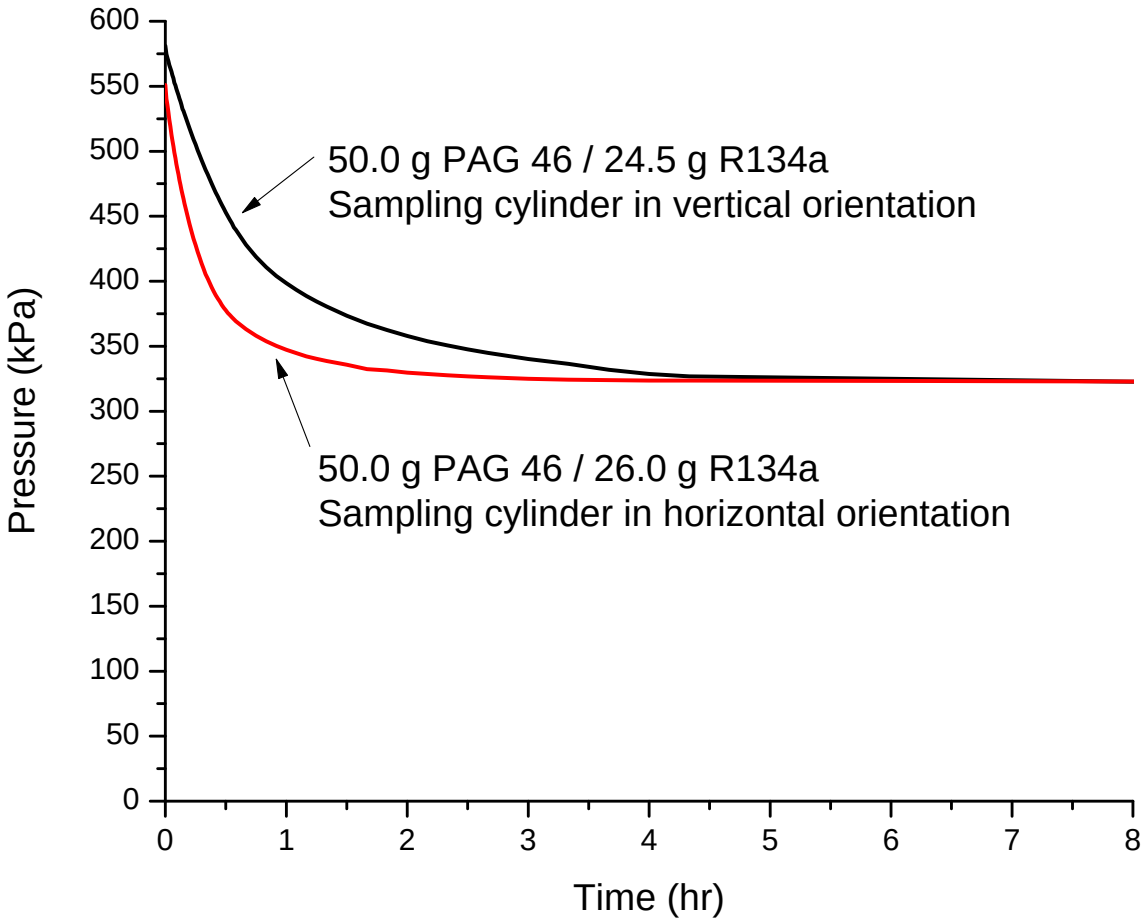

Figure 4.7: Time to reach pressure equilibrium for R134a and PAG 46 lubricant

4.5.1 Mix and Sample Device

The Mix and Sample Device (MSD)—developed for this study—has in addition to a gear pump—to circulate the liquid refrigerant and lubricant mixture—several features as shown in Figure 4.8. One feature is an added volume from a tank which provides space for the refrigerant and lubricant to be mixed. The tank doubles as a vapor separator. A transparent tube parallel to the tanks allows the liquid level within the tank to be monitored when a sample is taken. Another transparent tube is connected directly at the inlet to the sampling cylinder to monitor any flashing—separation of liquid and vapor—that may occur upstream of the sampling cylinder. The MSD and an attached section are filled through the charge port at the top of the device with

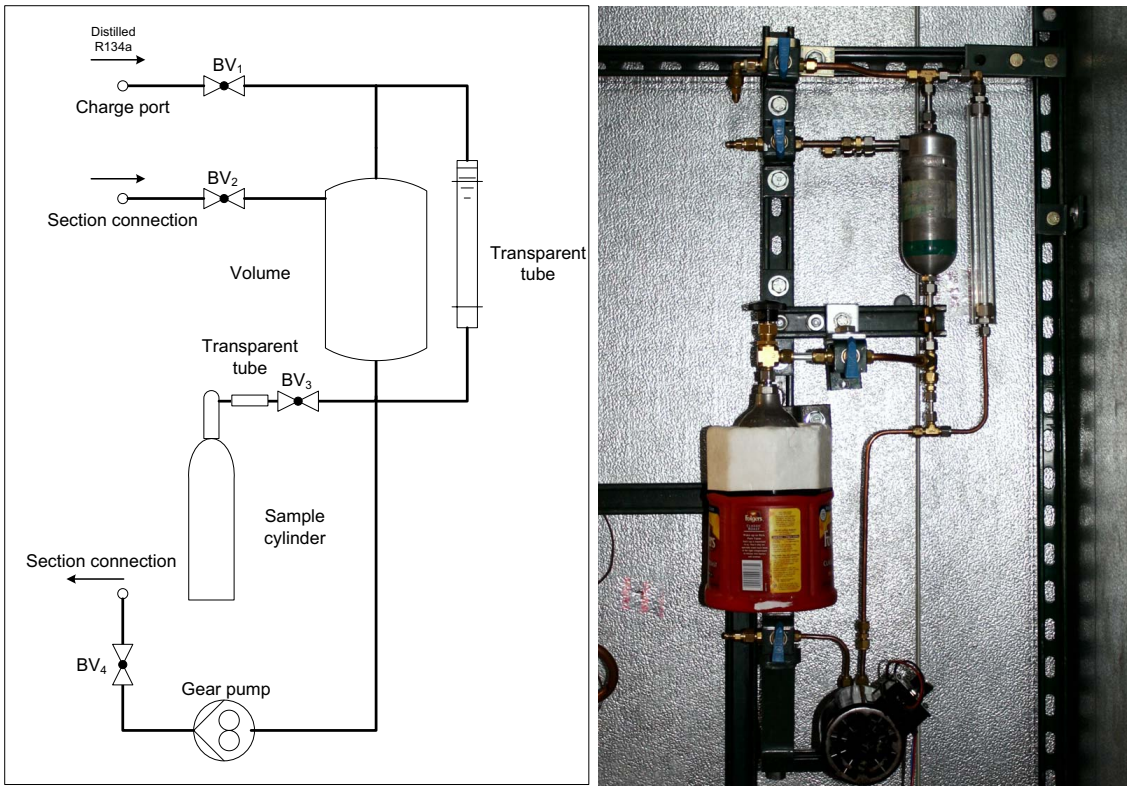

Figure 4.8: Schematic and picture of Mix and Sample Device

refrigerant. The MSD is mounted on a frame, making it portable and easy to install close to a section.

To clean the MSD the two ports—usually connected to a section—are short circuited using a copper tube. Acetone is then filled into the MSD through the charge port and the gear pump circulates the acetone for two minutes. Then the acetone is drained and the MSD is evacuated to remove leftover acetone. This procedure is repeated twice and measurements confirmed less than 0.04 g of lubricant remained in the MSD after the cleaning procedure.

The procedure to measure the amount of lubricant contained within a section started after the refrigerant is removed by the technique described in Section 3.3. The MSD was always mounted at a higher elevation compared to the section. After

the evacuated and cleaned MSD was connected to a section, liquid R134a having a purity of at least 99.6 percent was filled into the MSD from a recovery cylinder. The temperature of the recovery cylinder was maintained above room temperature and the filling was done slowly enough so the filled in R134a increased the temperature in a section. If the surface temperature in a section would be higher than the filled in R134a, evaporation of the liquid phase R134a would occur and pockets of vapor would form inside the section. An increase in temperature leads to a large change in pressure for saturated liquid R134a and therefore—as a safety precaution—the MSD and attached section was not completely filled with liquid R134a. The filling procedure was stopped when a small amount of vapor was still visible at the top of the transparent tube next to the tank. After the filling procedure the recovery tank is disconnected and its weight and henceforth the amount of R134a filled into the MSD and section was determined. The gear pump was turned on and left running for one hour. To take a sample, the sampling cylinder was cooled with liquid nitrogen and the valves are slowly opened in such a way that no flashing was visible in the transparent tube. Depending on the sample size, the sampling took several minutes. After the sampling was finished the sampling cylinder is removed. The amount of R134a and lubricant in the sample is determined using the technique described in Section 4.2.

The amount of lubricant in a section cannot be calculated using Equation (4.1) as a result of the design of the MSD and the procedure. Two corrections are necessary. First, when filling the cleaned MSD, the tube between ball valve #3 and the tee below the tank will be filled with liquid R134a. It is assumed that this volume, $Volume_{tube}$, stays filled with liquid phase R134a, $m_{R134a,tube}$—no measurable amount of lubricant will diffuse into this volume. Since this amount will be forced into the sampling cylinder, Equation (4.3) is used to calculate the mass of R134a in the tube using the

saturated liquid density as a function of temperature, $\rho_{R134a,sat,liq}$.

$$m_{R134a,tube} = \rho_{R134a,sat,liq} \cdot Volume_{tube} \tag{4.3}$$

Second, during the sampling procedure vapor will be generated within the MSD and attached section as a result of the sampling of liquid refrigerant-lubricant mixture. The release of R134a from the liquid phase into the vapor phase changes the concentration of the lubricant in the liquid refrigerant and lubricant mixture. Therefore, the lubricant concentration of the sampled liquid mixture changes over time as R134a vapor is released. To account for this change the final lubricant concentration of the sample, $\omega_{lub,s}$, is calculated as the average of the concentrations at the start of the sampling, $\omega_{lub,t0}$, and at the end of the sampling, $\omega_{lub,t1}$. Therefore, the change in lubricant concentration over time is assumed to be linear.

$$\omega_{lub,s} = \frac{\omega_{lub,t0} + \omega_{lub,t1}}{2} \tag{4.4}$$

The concentration of lubricant in the sample can also be expressed in terms of the mass of lubricant in the sample, $m_{lub,s}$, mass of R134a and lubricant in the sample, $m_{total,s}$, and the correction of R134a in the short tube, $m_{R134a,tube}$.

$$\omega_{lub,s} = \frac{m_{lub,s}}{m_{total,s} - m_{R134a,tube}} \tag{4.5}$$

The mass of R134a released from the liquid phase into the vapor phase during sampling, $m_{R134a,gas}$, is calculated by assuming the vapor phase R134a occupies the volume generated by the removed mass of R134a in the sample at the end of the sampling, $m_{R134a,s}$. Evaluating the specific densities for saturated vapor and liquid—based on the temperature during the sampling process—$v_{R134a,sat,gas}$ and $v_{R134a,sat,liq}$, the value

for $m_{R134a,gas}$ can be calculated using Equation (4.6).

$$m_{R134a,gas} \cdot v_{R134a,sat,gas} = m_{R134a,s} \cdot v_{R134a,sat,liq} \tag{4.6}$$

The equations for the lubricant concentrations at the beginning, $\omega_{lub,t0}$, and at the end, $\omega_{lub,t1}$, can then be expressed as follows.

$$\omega_{lub,t0} = \frac{m_{lub,section}}{m_{lub,section} + m_{R134a,in} - m_{R134a,tube}} \tag{4.7}$$

$$\omega_{lub,t1} = \frac{m_{lub,section} - m_{lub,s}}{m_{lub,section} + m_{R134a,in} - m_{R134a,tube} - m_{lub,s} - m_{R134a,s} - m_{R134a,gas}} \tag{4.8}$$

To calculate the amount of lubricant within the section of interest, $m_{lub,section}$, equations (4.3) through (4.8) are solved.

4.5.2 Uncertainty of Mix and Sample Technique

The Mix and Sample Device was short-circuited using a refrigerant hose to perform verification experiments and determine the measurement uncertainty of the device. Before each experiment the MSD and the refrigerant hose were cleaned. The refrigerant hose was filled with lubricant mass which was determined with an uncertainty of ±0.06 g. The MSD was run using the procedure described in the previous section, and the amount of lubricant mass was calculated using equations (4.3) through (4.8). The calculated amount of lubricant mass was compared to the amount of lubricant mass filled in. The difference between those values is the measurement uncertainty. Table 4.5 shows the results of the verification experiments. The column "Difference without corrections"—using only Equation (4.1)—shows a considerable error of more than half a gram. Accounting for the measurement uncertainties from using the scales and temperature measurements, the MSD can determine the amount of lubricant mass within ±0.1 g if equations (4.3) through (4.8) are used.

Table 4.5: Results of the verification experiments of the MSD

Amount of oil in MSD (g)	Prediction of oil based on MSD (g)	Difference (g)	Difference without corrections (g)
20.57 ± 0.06	20.51 ± 0.08	-0.06	0.58
19.58 ± 0.06	19.60 ± 0.08	0.02	0.63
20.70 ± 0.06	20.66 ± 0.08	-0.04	0.62

Although the MSD is produces a homogeneous mixture when short-circuited, the question remains if a homogeneous mixture is achieved when the MSD is applied to the condenser, liquid tube and evaporator sections. Therefore, verification experiments are performed. Each section was cleaned first, a known amount of lubricant was filled into the section, and the MSD was connected to the section. Tables 4.6 through 4.8 summarize the results of the verification experiments. A positive or negative difference between the measured and known value of lubricant mass indicates an inhomogeneous mixture. A consistently negative difference—as observed for the evaporator—indicates that the refrigerant did not mix with all the lubricant, e.g., one or several "dead spots" exist where lubricant remained unmixed. The average deviations are -0.42 g for the evaporator and -0.22 g for the condenser indicating an underestimation of the actual amount of lubricant in these sections. The liquid tube section average is 0.1 g indicating that for simple geometries the Mix and Sample method provides excellent results. As a result of the liquid tube verification experiments and verification experiments of the short-circuited MSD, the verification of the discharge tube was omitted since its length is in between the length of the short-circuited tubing used and the liquid tube length. Overall it can be concluded that the difference between known amount of lubricant and predicted amount using the MSD is less than 1 g for all sections.

Table 4.6: Results of the verification experiments of the MSD on the condenser section

Amount of oil in section (g)	Prediction of oil based on MSD (g)	Difference (g)	Difference (%)
18.92 ± 0.06	18.35 ± 0.08	-0.57	-3.01
22.60 ± 0.06	22.38 ± 0.08	-0.22	-0.97
22.44 ± 0.06	22.58 ± 0.08	0.14	0.62

Table 4.7: Results of the verification experiments of the MSD on the liquid tube section

Amount of oil in section (g)	Prediction of oil based on MSD (g)	Difference (g)	Difference (%)
36.18 ± 0.06	36.39 ± 0.08	0.21	0.58
29.19 ± 0.06	29.57 ± 0.08	0.38	1.30
21.58 ± 0.06	21.29 ± 0.08	-0.29	-1.34

4.5.3 Generalization—Practical Guidelines

The Mix and Sample Technique offers an in-situ measurement of the amount of lubricant mass contained within a heat exchanger or other part of a system. Using a Mix and Sample Device (MSD) gives researchers another tool to determine the lubricant distribution across a refrigeration system. An MSD—which can be built portable and compact—could also be used by service technician in the field, e.g., to determine if lubricant accumulates in one part of a system and potentially causes under lubrication of the compressor. Therefore, based on the experiences of applying the Mix and Sample Technique and designing a Mix and Sample Device, general advice and guidelines are presented.

To successful apply the Mix and Sample Technique it is important to have a

Table 4.8: Results of the verification experiments of the MSD on the evaporator section

Amount of oil in section (g)	Prediction of oil based on MSD (g)	Difference (g)	Difference (%)
42.97 ± 0.06	42.59 ± 0.08	-0.38	-0.88
38.68 ± 0.06	37.71 ± 0.08	-0.97	-2.51
35.98 ± 0.06	35.53 ± 0.08	-0.45	-1.25
22.80 ± 0.06	22.75 ± 0.08	-0.05	-0.22
20.39 ± 0.06	20.17 ± 0.08	-0.22	-1.08

lubricant-solvent combination which is miscible. Ideally, refrigerant can be used as the solvent if it is miscible with the lubricant—as is the case for the R134a and PAG 46 refrigerant-lubricant combination. The advantage is that no "foreign" fluid is introduced which could potentially harm the compressor, expansion devices or seals during the procedure or if not properly removed after the procedure. In addition, the uncertainty of determining the amount of lubricant mass in the sample will depend on the lubricant-solvent combination. The following list gives guidelines on how to design a Mix and Sample Device.

- A hermetic pump, e.g., magnetic driven gear pump, is recommended to avoid introducing another lubricant into the system. The flow rate of the pump should be chosen such that the complete mass inside the section and MSD is pumped around the system between 75 and 120 times per hour.

- An additional volume should be included in the design of the MSD, which can be achieved by using a cylindrical vessel similar to the one shown in Figure 4.8. A vessel having an internal volume of 25 percent to 50 percent of the section volume is recommended. A transparent tube installed parallel to the vessel to monitor the liquid level inside the vessel when a sample is taken is also

recommended. While the pump is running, the liquid level should be monitored to verify flow through the transparent tube.

- The pump should be run at least one hour before a sample is taken.
- The sampling cylinder connection should be physically below the vessel height but above the pump height. It is important to determine the volume between the sampling cylinder connection and the tube the liquid flows during sampling to account for the unmixed solvent in this volume using Equation (4.3).

The relationship between the mass extracted during sampling, lubricant mass in the section and the amount of solvent filled in is not trivial, and depends on the uncertainty of determining the amount of lubricant in the sample. For example, the lower the amount of lubricant mass in a section, the more mass has to be sampled to be able to determine the lubricant mass accurately. The method used to determine the amount of lubricant mass in a sample, e.g., based on ANSI/ASHRAE Standard 41.4-1996 [38] or as described in Section 4.2, dictates the minimum sampling size necessary to be within a prescribed uncertainty. For example, if the detection limit of determining the amount of lubricant mass in a sample is 0.25 g, any sample must contained more than 0.25 g of lubricant mass. The higher the amount of lubricant in the sample the lower the propagated uncertainty—0.25 g would result in an uncertainty of 100 percent and therefore more lubricant should be in the sample to decrease this uncertainty. The amount of lubricant in the section, the section volume and volume of the MSD determines the concentration of lubricant in the resulting homogeneous mixture and in turn how much mixture mass needs to be sampled. In helping to determine the sampling size Figure 4.9 can be used.

In Figure 4.9 the sampling size on the abscissa is expressed non dimensional—as the ratio of the sample mass divided by the total mass of lubricant and solvent in the section and MSD. For example, if 150 g are sampled and the total mass of solvent

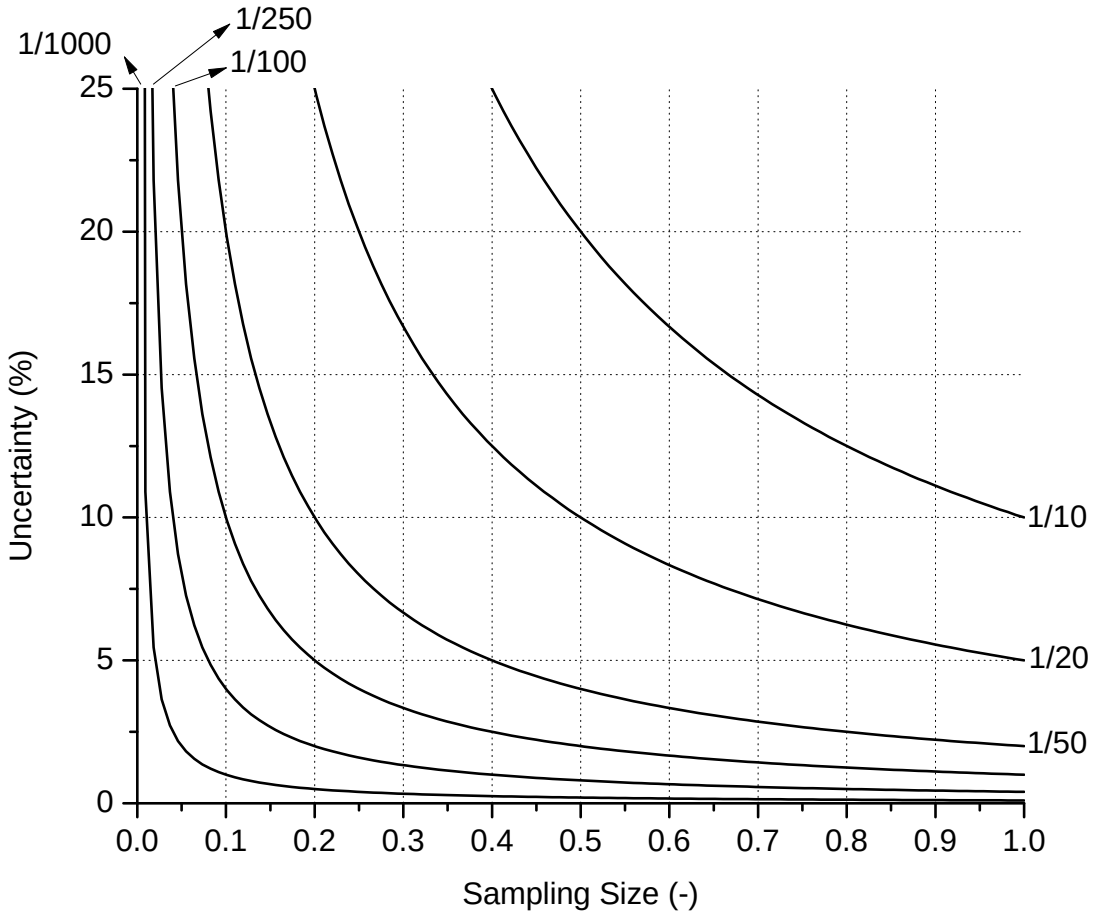

Figure 4.9: Graph to estimate sample size

and lubricant is 1500 g the sampling size is 0.1. The uncertainty plotted on the ordinate in Figure 4.9 is the uncertainty associated with determining the amount of lubricant within the sample in percent. The lines in Figure 4.9 represent the ratio of the detection limit of lubricant mass in a sample and the total mass of lubricant in the section. For example, if 25 g of lubricant are in a section, and the detection limit of the technique/equipment used to determine the lubricant mass in the sample is 0.25 g, the resulting ratio is 1/100. From Figure 4.9 it can be seen that to have an uncertainty of less than 10 percent—for a ratio of 1/100—the sample size has to be at least 0.1 times the amount of solvent filled into the system. To only use the amount of filled in solvent is sufficient in most cases, because—usually—the amount of lubricant in a sample is small compared to the amount of solvent. Also, in most

cases the amount of lubricant in a section is unknown but can possibly be estimated or guessed.

An important fact to keep in mind is that the larger the sample size the greater the potential for separation of solvent and lubricant during sampling and therefore the introduction of an additional uncertainty. Although equations (4.4) through (4.8) correct for this separation, depending on the geometry of the section and the solvent-lubricant combination used, the equations might not be applicable. As a general rule, the sampling size should be as small as possible while still providing the required/wished uncertainty.

4.6 Application of Techniques—Overall Measurement Uncertainty

As described in the previous sections, three different techniques are used to determine the lubricant mass distribution in the experimental system. All the techniques are applied after the QCVT is applied and the refrigerant has been removed from each section. The Remove and Weigh Technique is used for the compressor. However, since the lubricant mass only inside the compressor—without the surrounding tubing—is determined, the Flushing Technique is used for the discharge tube. The suction tube—also part of the compressor section, tube #12—is flushed at the same time as the accumulator section. The suction tube and accumulator section are flushed together for two reasons. First, for practicality—after the compressor is removed it is easy to connect the flushing cylinder to tube# 12—and second, tube #12 is angled downwards towards the compressor and therefore most of the lubricant is drained into the compressor. The Mix and Sample Technique using the Mix and Sample Device is applied to the condenser, liquid tube and evaporator section. The flushing technique is used on the accumulator section. Table 4.9 summarizes the techniques used on

each section with references to the sections describing each technique in detail.

Table 4.9: Overview of techniques used to determine lubricant distribution

Section	Technique (chapter)
Compressor	Remove and Weigh (4.3)
Discharge Tube	Mix and Sample (4.5)
Condenser	Mix and Sample (4.5)
Liquid tube	Mix and Sample (4.5)
Evaporator	Mix and Sample (4.5)
Accumulator	Flushing (4.4)

After the lubricant masses are determined the experimental system—except the compressor—is cleaned using a commercial recycling device (see Figure 4.3). Accounting for the lubricant mass already in the compressor, lubricant is filled into the accumulator to bring the total amount of lubricant to 230 g. Since the lubricant is filled in manually, the total amount of lubricant inside the system can vary. For all experiments conducted the total amount of lubricant ranges between 227.43 g and 231.11 g with an uncertainty of the filled in amount of lubricant of ± 0.06 g. Since the uncertainty of the filled in amount of lubricant mass is an order of magnitude lower than the Flushing and Mix and Sample techniques uncertainties, the filled in amount is taken as the "true value". Overall twenty experiments were conducted. For each experiment the actual mass of lubricant in the system was compared to the sum of masses of the lubricant determined by applying the three techniques. The results are presented in Figure 4.10.

Based on the verification experiments on each section, the combined expected deviation from the actual mass of lubricant in the system is -0.97 g which means on average the sum of the measured lubricant masses from all sections should be lower by one gram compared to the amount which was actually in the system. Figure 4.10 confirms this assumption showing that the average deviation between measured

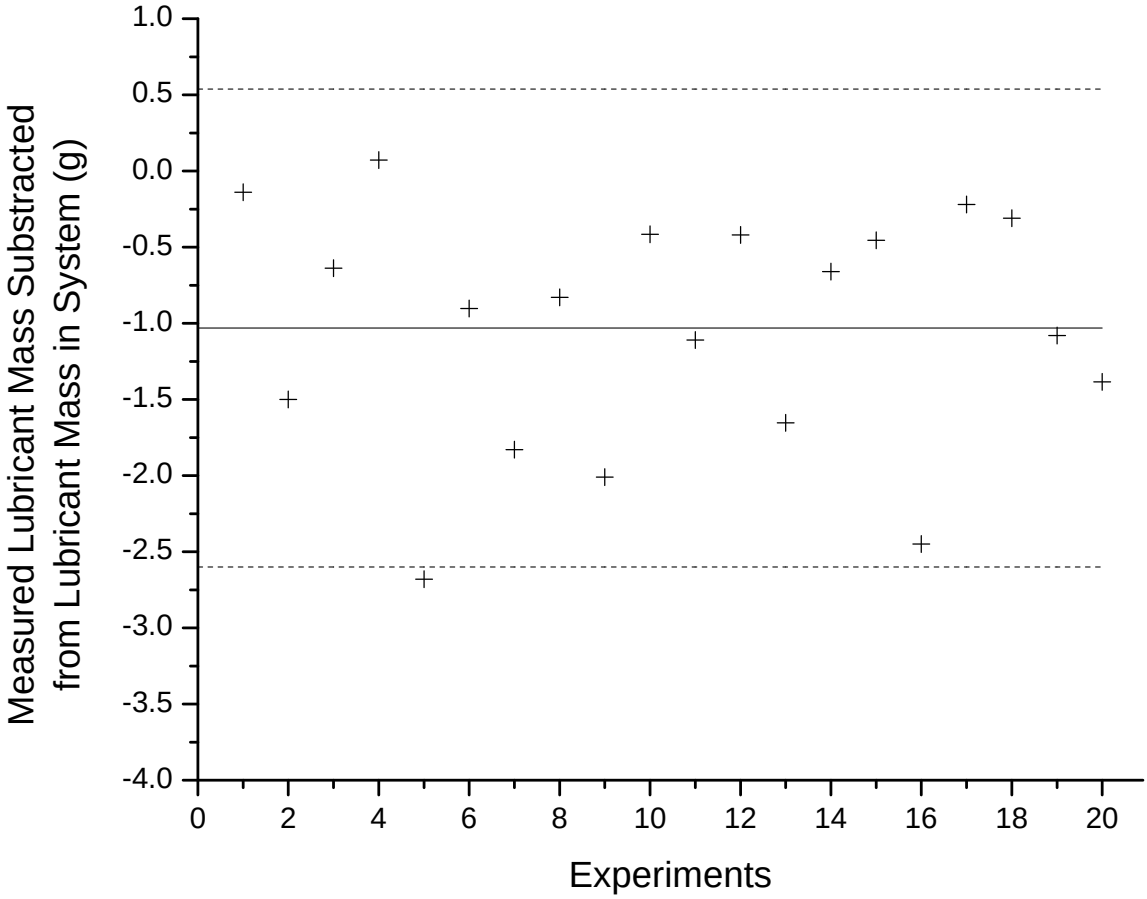

Figure 4.10: Comparison of measured and actual lubricant mass in the system

and filled in amount of lubricant is -1.03 g—denoted as the solid line. Overall, the measurement uncertainty of the total amount of lubricant within the system using the three measurement techniques can be expressed as -1.03 $\pm$1.57 g based on twenty experiments.

Chapter 5

Experimental Results

The first section of this chapter gives an overview of the experimental operating conditions at steady state and during a transient event. Cycling times vary for automotive air conditioning systems using clutch cycling to control the cooling capacity—from a couple of seconds to minutes—depending on the operating parameters and refrigerant charge [23]. The transient event investigated consists of an off-cycle period in which the compressor is turned off for three minutes, but the air flow rates and air inlet temperature conditions at the heat exchangers are maintained, followed by a start-up when the compressor is turned on again. The three minutes off-cycle period is atypical but it allows to investigate both types of mass migration—primary and secondary mass migration (see Section 6.1.1 on page 102). Using the Quick Closing Valve Technique requires that the breadboard system is recharged after each measurement, and an identical operating conditions has to be reached before another measurement can be taken. The precision of the experimental facility with respect to achieving identical steady state conditions and keeping the operating parameters steady during the transient event is presented.

The second section presents a comparison of the two breadboard system setups—using the original accumulator and the transparent accumulator. The objective is to determine if changing the accumulator and surrounding tubing affects the system performance and the refrigerant mass distribution. In addition, the desiccant package was removed from the transparent accumulator to visualize the flow inside the accumulator. The results show that using the transparent accumulator and removing the

desiccant package had no influence on the steady state performance and refrigerant mass distribution.

The third and fourth sections present the results of the refrigerant and lubricant migration experiments. Section 5.3 presents the refrigerant mass migration results including pressure, temperature, mass flow rate and compressor power measurements. Section 5.4 presents the results of the lubricant mass migration measurements. Since these results are unprecedented, they are shown without analysis to provide a condensed overview. Comprised analyses are given in Chapter 6.

5.1 Operating Conditions

Using the Quick Closing Valve and Remove and Weigh techniques to determine the refrigerant mass distribution results in very accurate measurements, but come with the disadvantage of being time intensive techniques (see Section 3.4). Therefore, the number of data points taken and operation conditions used had to be limited. Table 5.1 gives an overview of the steady state operating conditions used. All operation

Table 5.1: Operating conditions

	Compressor	Condenser		Evaporator		
	Speed	Temp.	Air flow	Temp.	Humidity	Air flow
	rpm	°C	m^3/h	°C	%	m^3/h
I45-dry	900	45	1650	45	-	490
I40-dry	900	40	1650	40	-	490
I35-wet	900	35	1650	35	40	490
I35-dry	900	35	1650	35	-	490
I25-dry	900	25	1650	25	-	340

conditions are idle conditions, meaning the compressor speed is at a minimum. Typically, automotive air conditioning systems are designed to provide a sufficient cooling capacity at the lowest allowed compressor speed since this is the most challenging

operation condition. For the purpose of this investigation the operating condition I35-dry is taken as a "design condition" and the amount of R134a necessary for the breadboard system to provide a sufficient cooling capacity was determined for this condition (see Section 6.2.1). Except for the I35-wet condition, the dew point is maintained below the evaporator refrigerant saturation temperature to avoid water condensation formation on the evaporator. The volumetric air flow rates are based on manufacturer specifications.

The measurement uncertainties—from an error propagation calculation—of the operating parameters are shown in Table 5.2. The uncertainty of the air inlet tem-

Table 5.2: Uncertainty of operating parameter measurements

Compressor	Condenser		Evaporator		
Speed	Temp.	Air flow	Temp.	Humidity	Air flow
rpm	°C	m^3/h	°C	%	m^3/h
±1	±0.3	±38.4	±0.5	±0.5	±3.4

peratures is a function of the number of thermocouple used—twelve for the condenser air inlet temperature and four for the evaporator air inlet temperature—and therefore have different uncertainties. Controlling the operating parameters introduces another limit to achieving the parameters exactly as shown in Table 5.1. For the facility used

Table 5.3: Acceptable range of steady state operating condition parameters

Compressor	Condenser		Evaporator		
Speed	Temp.	Air flow	Temp.	Humidity	Air flow
rpm	°C	m^3/h	°C	%	m^3/h
±3	±0.5	±50	±0.5	±1	±10

the acceptable range of steady state operating condition parameters are shown in Table 5.3. Steady state data was taken for 10 minutes. The averaged values during this

time period had to fall within the acceptable range of operating condition parameters before a measurement of refrigerant and/or lubricant mass distribution was initiated.

Another challenge is to keep the operating parameters constant during a transient event. As a result of the arrangement of the breadboard system using open loop wind tunnels inside two climate chambers, the air inlet temperatures are influenced when the compressor is stopped. The cause is the disruption of the steady state heat transfer balances—accomplished by removing or adding heat in the chambers with the chiller system and duct heaters—as a result of the decreasing heat transfer rates at the condenser and evaporator during the compressor stop period. Figure 5.1 shows the transient temperature profile for the condenser inlet temperature (T_{aci}) and evaporator air inlet temperature (T_{aei}) for the I35-dry and I35-wet conditions—the target temperature is 35°C. At time zero the compressor is switched off and is turned on at 180 seconds. For the dry condition experiments, no action was taken, that is, the PID-controller of the duct heaters kept the temperature as close as possible to the target temperature of 35°C. The evaporator air inlet temperature rose to 37°C and the condenser air inlet temperature fell to 33°C after 180 seconds and then slowly returned back to their target values. Therefore, the air inlet temperatures were within ±2°C of the target temperature during all dry condition transient experiments.

For the wet condition transient experiments, the temperature range was further reduced by applying a strategy—turning duct heaters and steam on and off during certain periods of the transient event as shown in Table 5.4. Since the condenser air inlet temperature drops during the off-cycle as a result of the decreased heat transfer from the condenser, a manually controlled duct heater is switched on to compensate. The opposite is done at the indoor chamber, the PID-controlled duct heater is switched off during the first half of the off-cycle and then is turned on again. At the same time a manually controlled duct heater is turned on for 170 seconds. The heat loss—which occurs when the indoor chamber door is opened shortly after

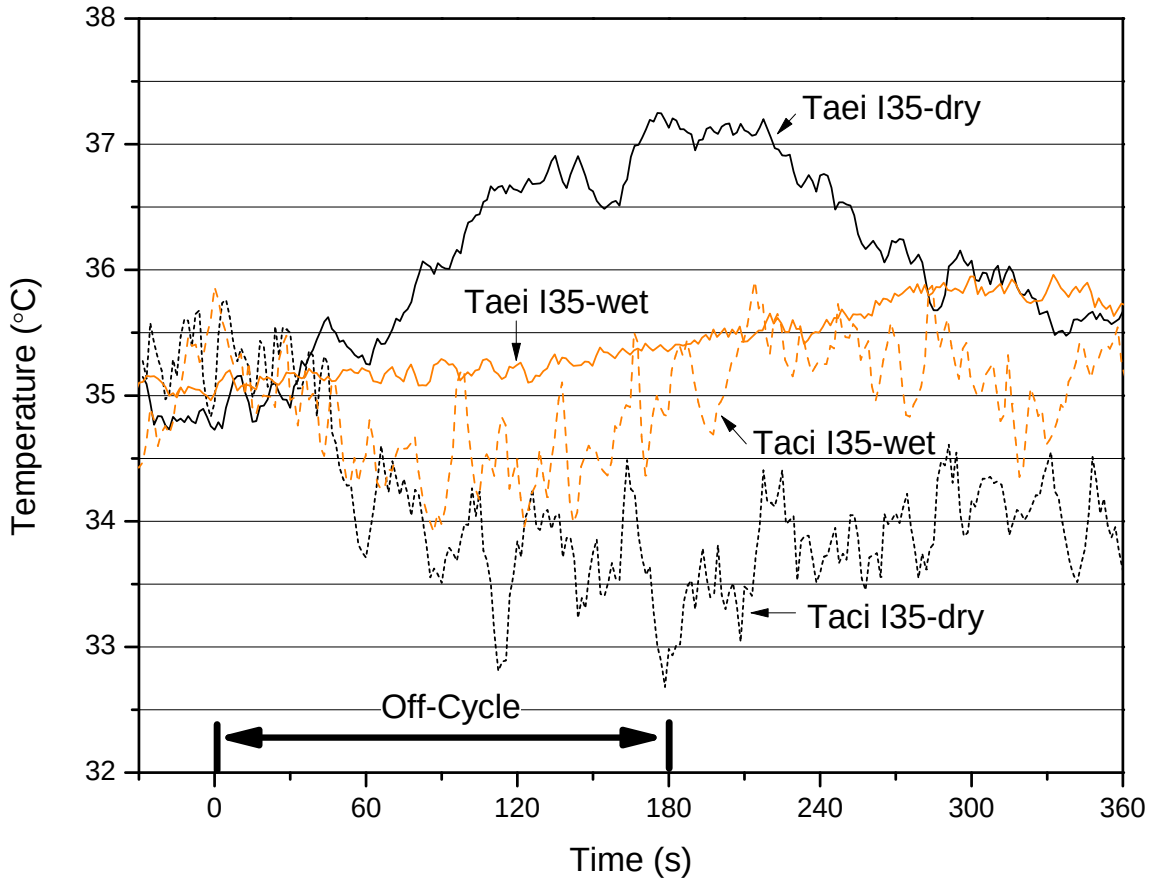

Figure 5.1: Air inlet temperatures during transient event

120 seconds—is thereby compensated. The door is opened to reduce the relative humidity in the chamber. How long the door is opened depends on the temperature and humidity in the room, but usually the door was open for 30 to 50 seconds. In combination with turning off the steam supply it was possibel to keep the dew point temperature within one degree of the target value of 19.4°C. Figure 5.2 shows that without a strategy the dew point temperature rose above 26°C.

The air inlet temperatures at the condenser and evaporator are held within ±2°C of the target temperature during all dry condition transient experiments. For the wet condition transient experiments, the temperatures—including the dew point temperature—are held within ±1°C. All data reported has the same preceding steady state condition within the ranges shown in Table 5.3.

Table 5.4: Schedule for strategy to keep operating parameters constant during the wet transient event

Time (s):	-30	-10	0	90	180	190	260
Indoor heater PID		OFF		ON			
Indoor heater manual				ON			OFF
Outdoor heater PID							
Outdoor heater manual	ON					OFF	
Steam	OFF					ON	
Compressor			OFF		ON		

5.2 Original Versus Transparent Accumulator Section

As described in Section 2.3 the breadboard system has two setups—using the original accumulator or the transparent accumulator. This sections details the work done to determine if changing the accumulator and surrounding tubing affects the system performance and mass distribution. Since the original and transparent accumulators have the same design and dimensions, no measurable difference was expected. However, for visualization purposes the desiccant package was removed from the transparent accumulator. The function of the desiccant package in a refrigeration system is to absorb water which might be present and thereby prevent corrosion of metal parts or freeze-up which could plug the expansion device. The desiccant package is usually placed where it is in contact with liquid phase refrigerant, either inside a high side receiver or accumulator. As Figure 5.3 shows, the desiccant package occupied part of the volume inside the accumulator, and is porous allowing liquid phase refrigerant to flow through it. To determine if the removal of the desiccant package influences the refrigerant mass distribution and the performance of the breadboard system, experiments were conducted under the I35-dry operating condition.

First, the original accumulator was used and the performance and refrigerant

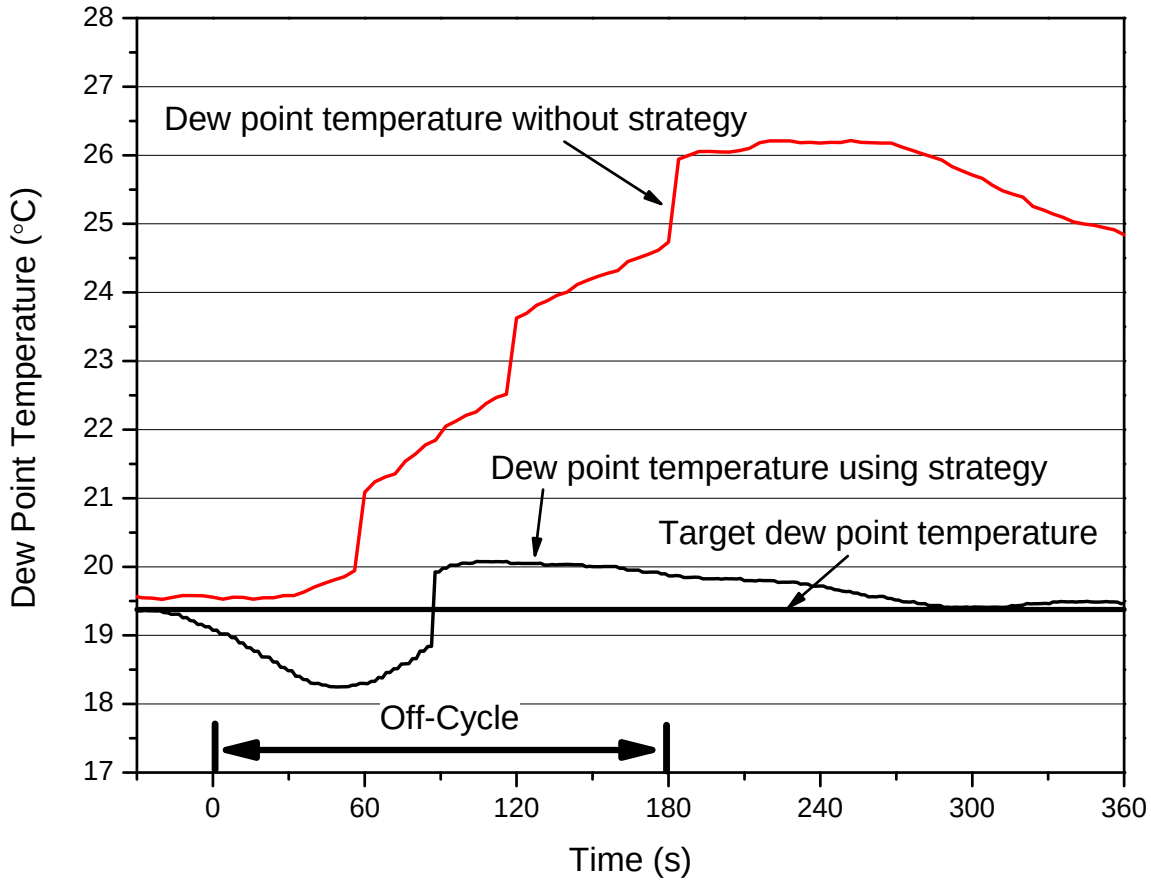

Figure 5.2: Comparison of dew point temperatures during transient event

mass distribution was determined under steady state operating conditions for three different total system refrigerant masses—1000 g, 1250 g and 1500 g. Second, the same experiments were repeated using the transparent accumulator without the desiccant package. Table 5.5 shows the cooling capacity and coefficient of performance (COP) results from the experiments. Based on these results, no measurable difference exists and therefore it can be concluded the desiccant package has no influence on the steady state performance of the breadboard system.

The comparison of the refrigerant mass distribution between the system using the original accumulator and transparent accumulator without desiccant package is shown in Figure 5.4. The difference in refrigerant mass distribution is within ±4% for all sections. In addition, no pattern is visible which could indicate a systematic

Figure 5.3: Original accumulator, transparent accumulator with and without desiccant package

difference. Overall, it can be concluded that the desiccant package does not influence the steady state refrigerant mass distribution.

In conclusion, the removal of the desiccant package for visualization purposes does not introduce a measurable deviation in performance or refrigerant mass distribution at steady state conditions.

5.3 Refrigerant Migration

The refrigerant mass migration was measured for a stop-start scenario using a stop period of three minutes during which only the compressor is turned off. The air flow rates and inlet temperature conditions at the heat exchangers were maintained within the ranges described in Section 5.1. Two refrigerant mass migration results are presented in this section. Table 5.6 explains the abbreviations used in Figures 5.6, 5.7, 5.9 and 5.10. The first result, Figure 5.5, is for an I35 dry operating condition and the breadboard system using the original accumulator. The second result, Figure 5.8, is for an I35 wet operating condition and the breadboard system using the transparent accumulator section without desiccant package. Both figures have two subfigures

Table 5.5: Comparison of performance of breadboard system with original and transparent accumulator without desiccant

Mass of R134a in system (g)	1000	1250	1500
	Cooling Capacity (kW)		
Original accumulator	4.15	4.16	4.02
Transparent, no desiccant	4.14	4.10	4.01
Difference	0.01	0.05	0.01
	COP (-)		
Original accumulator	2.47	2.43	2.34
Transparent, no desiccant	2.49	2.44	2.39
Difference	-0.02	-0.01	-0.05

focusing on the stop and start up periods. The main figure shows the amount of refrigerant mass in the system for each data point and the dotted line represents the target refrigerant mass of 1000 g. Breaks in the axes are used to focus on the parts of the results containing the dynamic changes. The time axis starts at zero seconds which corresponds to the time the compressor is turned off. The compressor is turned on again at 180 seconds, which initiates the start-up. Markers in Figures 5.5 and 5.8 denote data points. Lines are used between the data points to provide a better visual representation of the migration progression of refrigerant mass across the different sections. Since the measurement uncertainties associated with the refrigerant mass measurements are described in Section 3.4, error bars are omitted on the figures to maintain readability. The numerical values of the data points are given in Tables 5.7 and 5.8.

Additional figures present the air and refrigerant temperatures, refrigerant pressures, refrigerant mass flow rates and compressor power for the stop-start scenario for the I35 dry operating condition and the breadboard system using the original accumulator—Figures 5.6 and 5.7—and the I35 wet operating condition and the breadboard system using the transparent accumulator section without desiccant

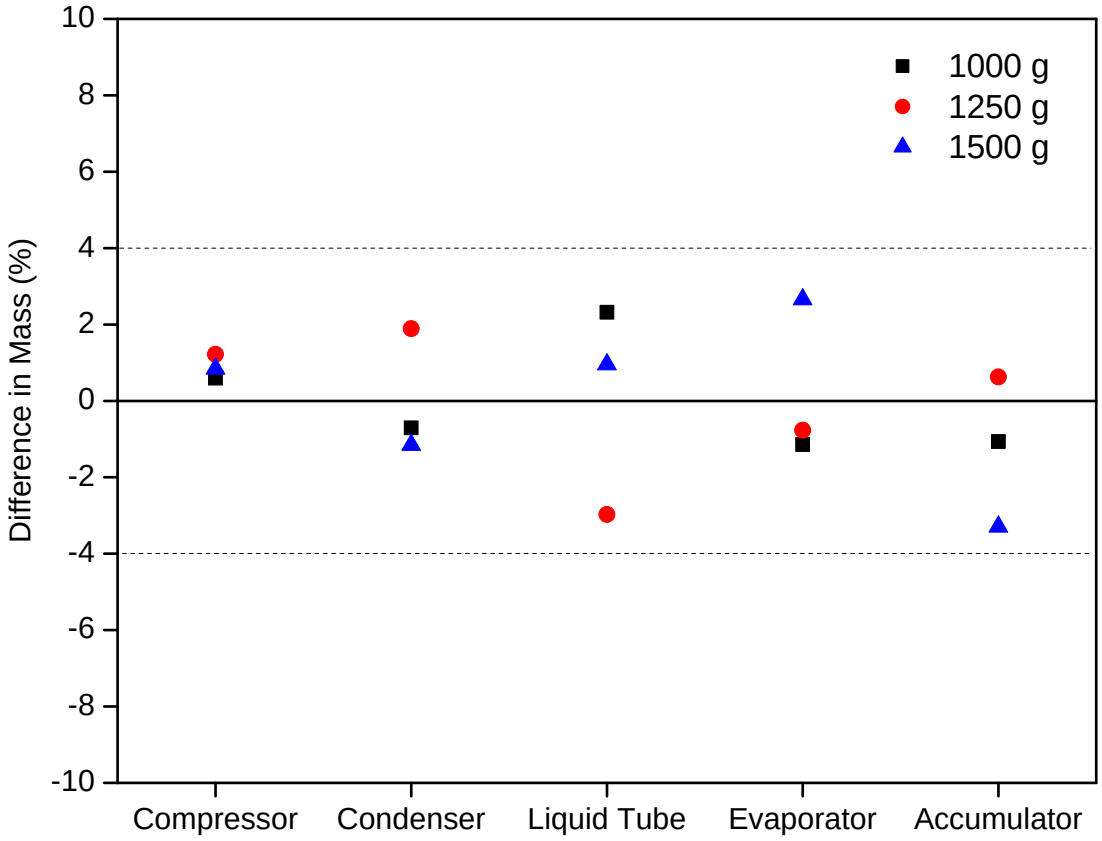

Figure 5.4: Difference in refrigerant mass distribution–original vs. transparent accumulator without desiccant

package—Figures 5.9 and 5.10. These data are taken every 1.5 seconds and are plotted as lines since symbols representing data points would overlap each other for the time scales used in the graphs—it is important to notice that symbols are only used to distinguish the different lines in these graphs. For Figures 5.7 and 5.10 a single symbol is used to mark the value of the refrigerant mass flow rate and compressor power at zero seconds. Error bars are again omitted on the figures to maintain readability. The corresponding measurement uncertainties can be obtained from Table 2.1.

Table 5.6: Explanation of abbreviations

Abbreviation	Explanation
T_{aei}	Air inlet temperature at evaporator
Taeo	Air exit temperature of evaporator
Taci	Air inlet temperature at condenser
Taco	Air exit temperature of condenser
Tdei	Air inlet dew point temperature at evaporator
Tdeo	Air exit dew point temperature of evaporator
Tral	Refrigerant temperature inside accumulator, measured at bottom and therefore represents the liquid phase refrigerant temperature
Trcpi	Refrigerant temperature at compressor inlet
Trcpi sat.	Refrigerant saturation temperature based on compressor inlet pressure
Trcpo	Refrigerant temperature at compressor outlet
Treo	Refrigerant exit temperature of evaporator
Treo sat.	Refrigerant saturation temperature based on evaporator exit pressure
Trxi	Refrigerant temperature before expansion device
Trxi sat.	Refrigerant saturation temperature based on pressure before expansion device
Prcpi	Refrigerant pressure at compressor inlet
Prcpo	Refrigerant pressure at compressor outlet
Preo	Refrigerant pressure at evaporator outlet
Prxi	Refrigerant pressure at expansion device inlet

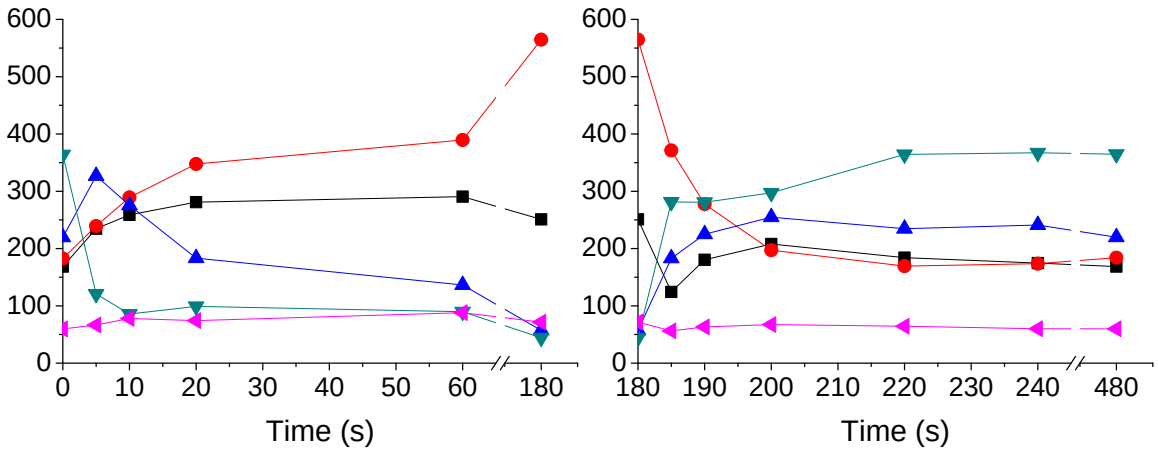

(a) Stop period

(b) Start up

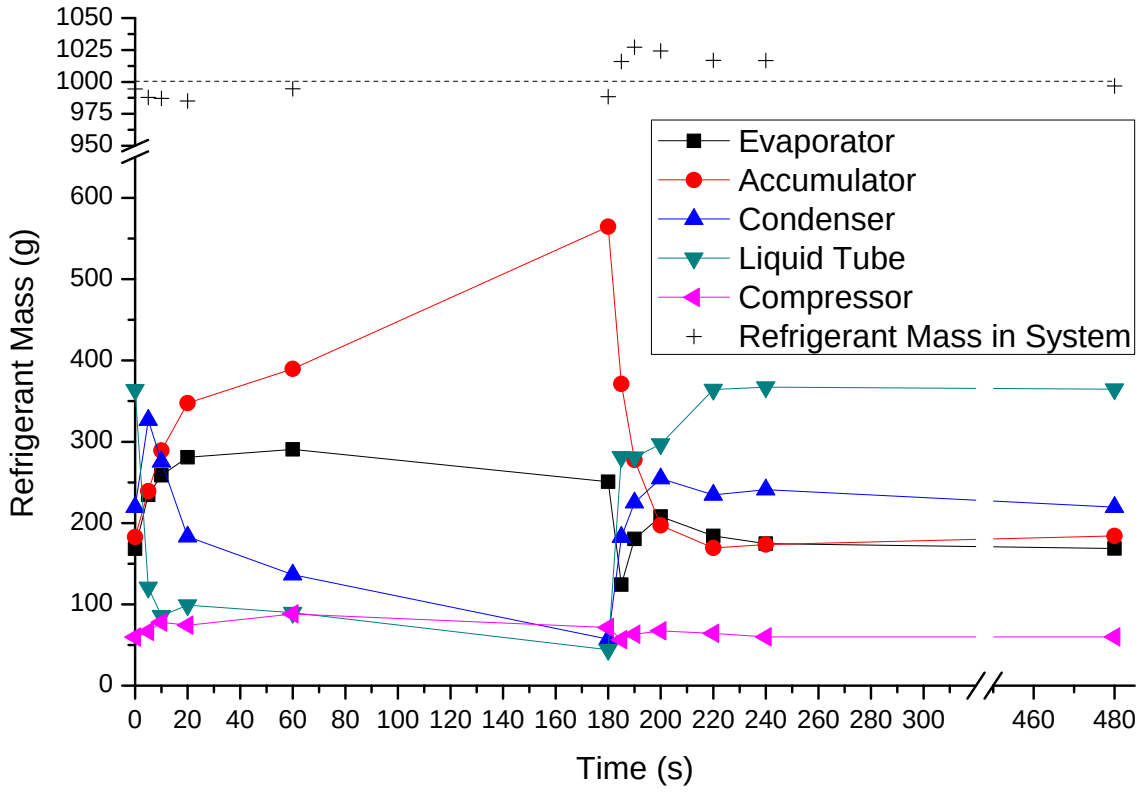

Figure 5.5: Refrigerant mass migration for I35-dry condition, original accumulator

Table 5.7: Refrigerant mass migration for I35-dry condition, original accumulator

Time	Evaporator	Accumulator	Condenser	Liquid Tube	Compressor	Sum
s	g	g	g	g	g	g
0	169	183	220	364	60	995
5	235	239	327	121	67	988
10	259	289	275	86	78	987
20	281	348	183	99	74	985
60	291	390	136	90	88	995
180	251	565	57	44	71	988
185	124	371	183	281	56	1016
190	180	278	225	281	63	1027
200	208	197	255	297	67	1024
220	184	169	235	364	64	1017
240	175	174	241	367	60	1017
480	169	184	220	365	60	997

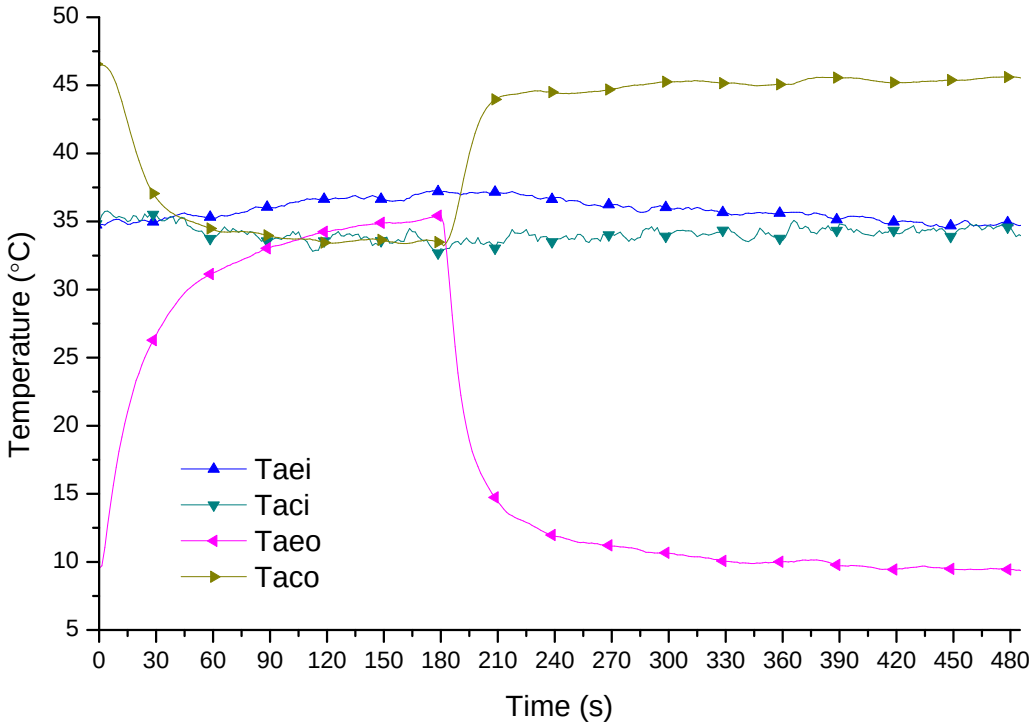

(a) Air temperatures

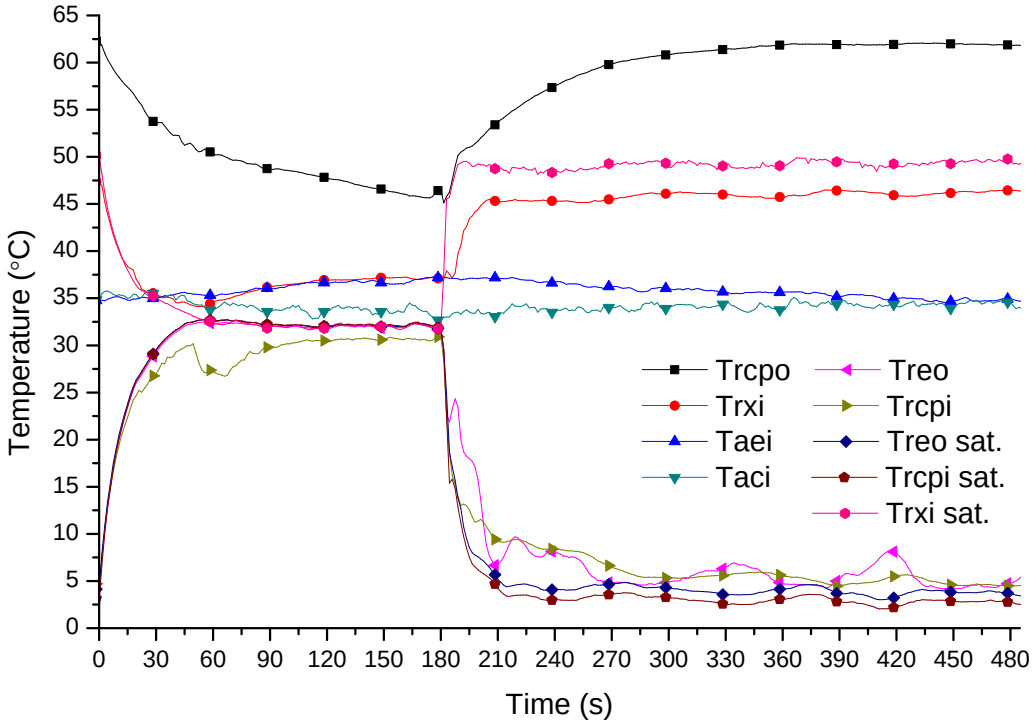

(b) Refrigerant and air inlet temperatures

Figure 5.6: Refrigerant and air temperatures for I35-dry condition, original accumulator

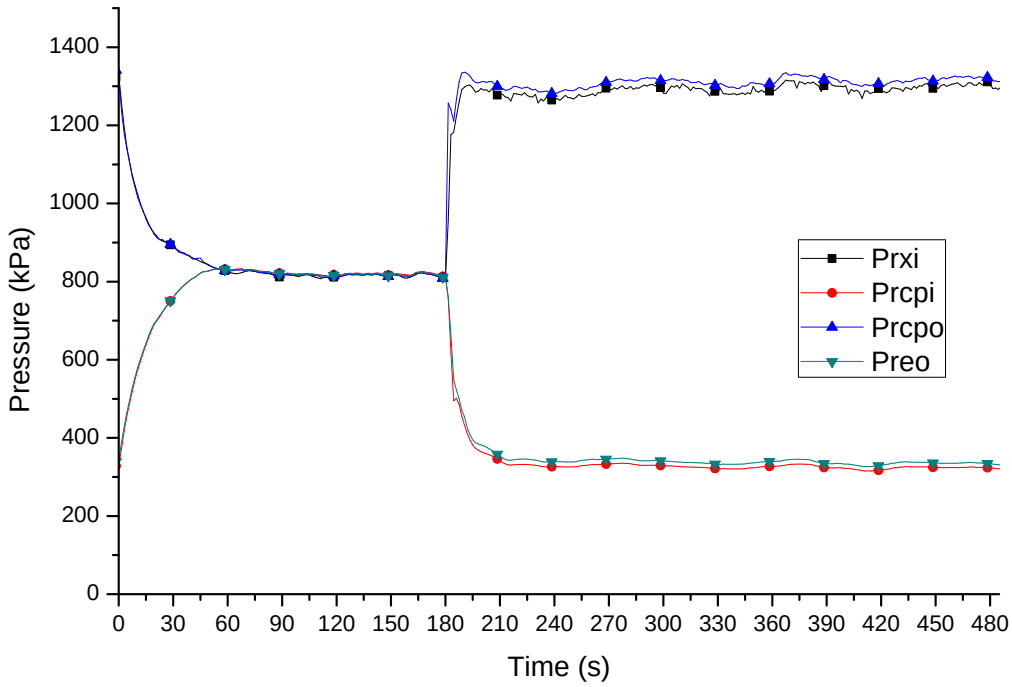

(a) Refrigerant pressures

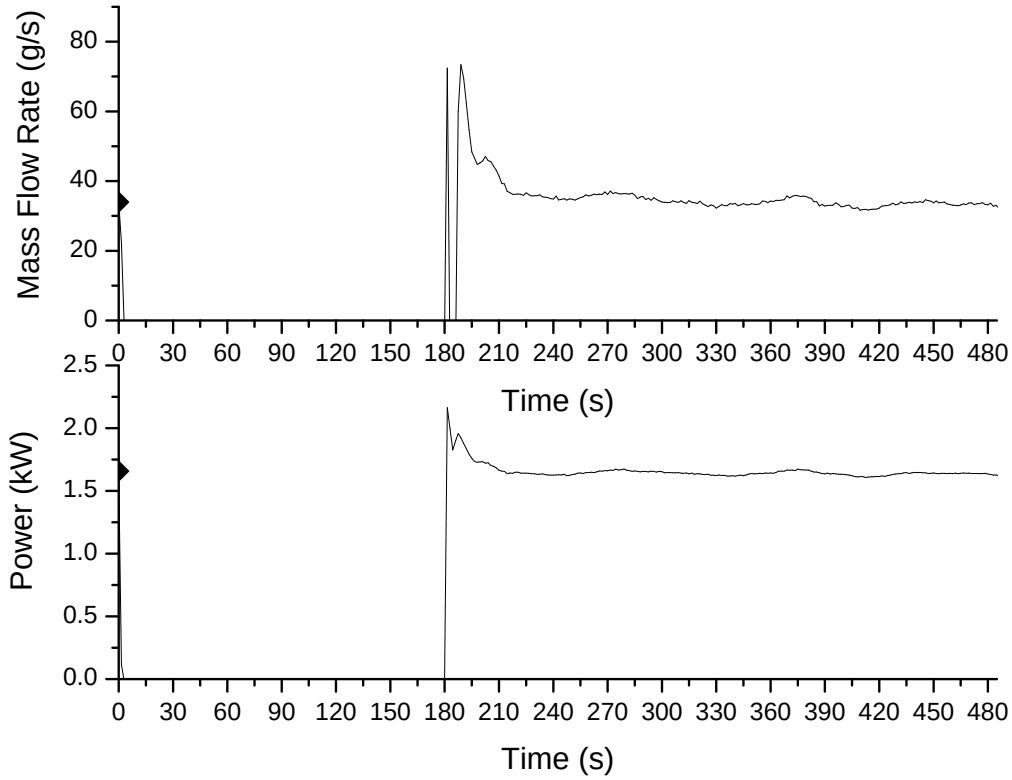

(b) Refrigerant mass flow rate and compressor power

Figure 5.7: Refrigerant pressures, mass flow rate and compressor power for I35-dry condition, original accumulator

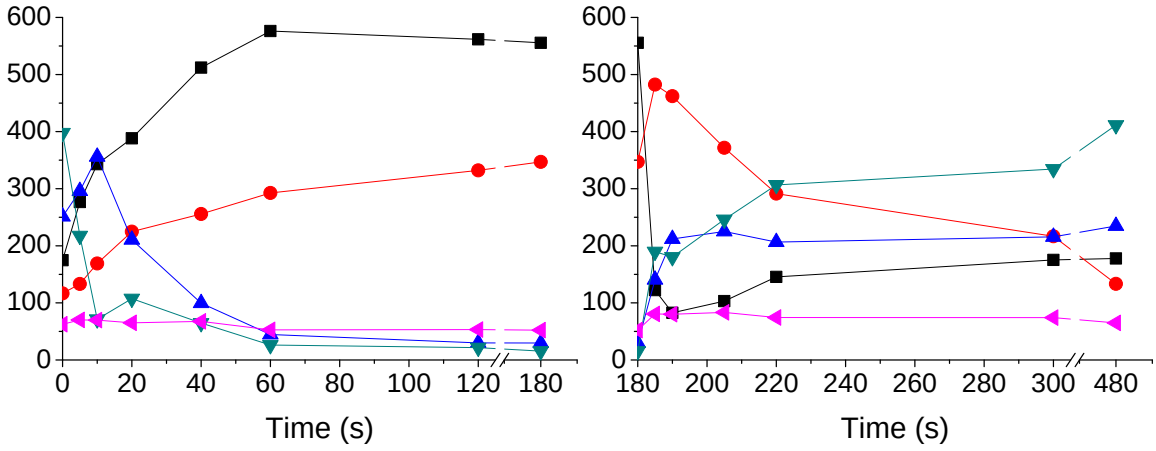

(a) Stop period

(b) Start up

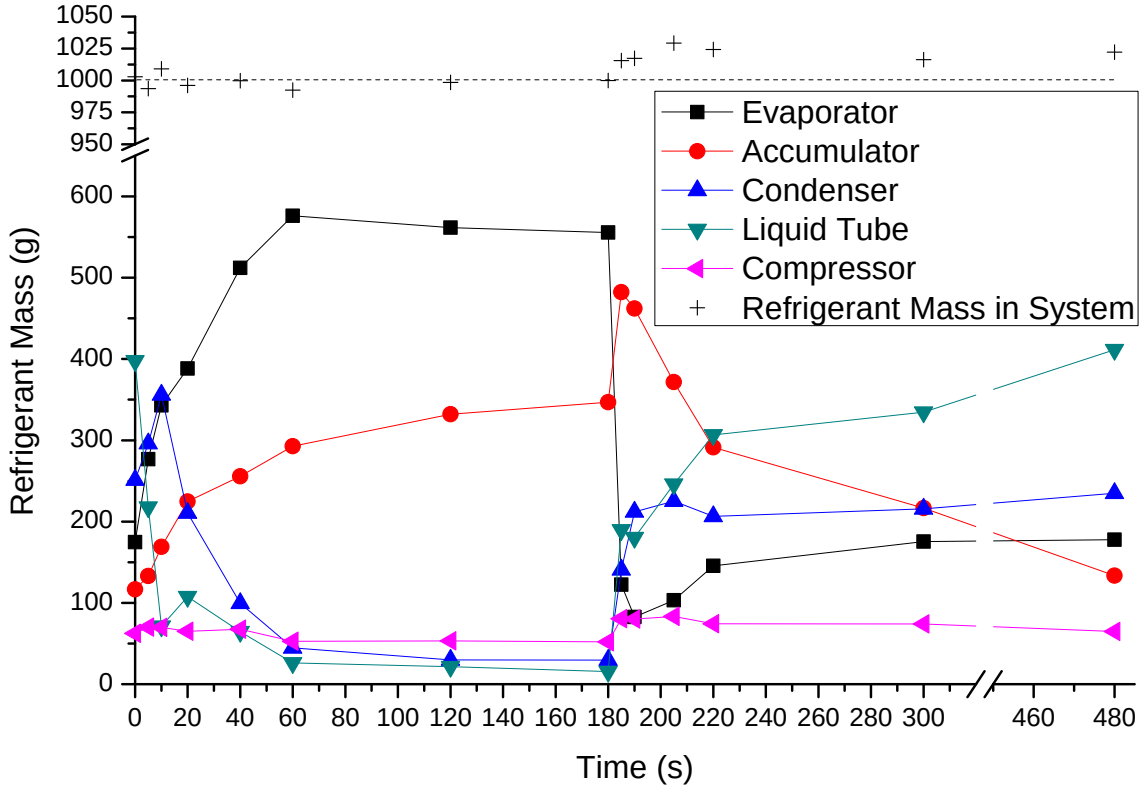

Figure 5.8: Refrigerant mass migration for I35-wet condition, transparent accumulator without desiccant package

Table 5.8: Refrigerant mass migration for I35-wet condition, transparent accumulator without desiccant package

Time	Evaporator	Accumulator	Condenser	Liquid Tube	Compressor	Sum
s	g	g	g	g	g	g
0	175	117	251	398	63	1003
5	277	133	296	218	70	994
10	343	169	356	71	70	1009
20	388	225	211	107	65	996
40	512	256	100	65	68	1000
60	576	293	45	26	53	992
120	562	332	30	22	53	998
180	556	347	30	16	52	1001
185	122	482	141	190	81	1016
190	83	462	212	180	80	1017
205	103	372	225	246	83	1029
220	145	291	207	307	74	1024
300	175	217	216	335	74	1016
480	178	133	235	411	65	1022

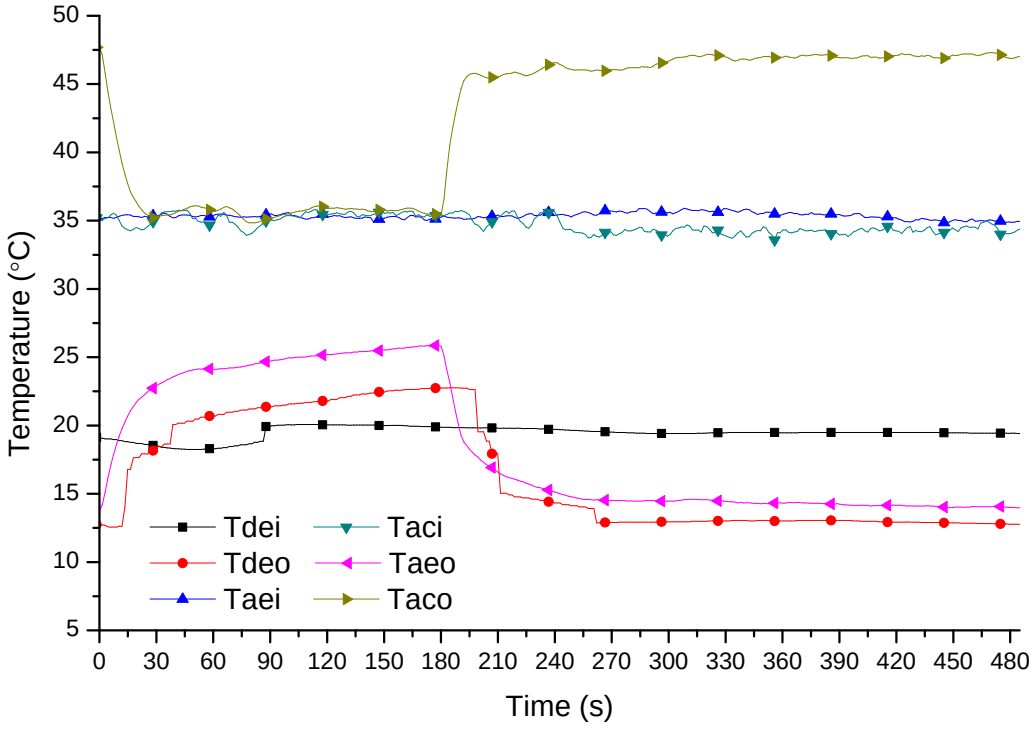

(a) Air temperatures

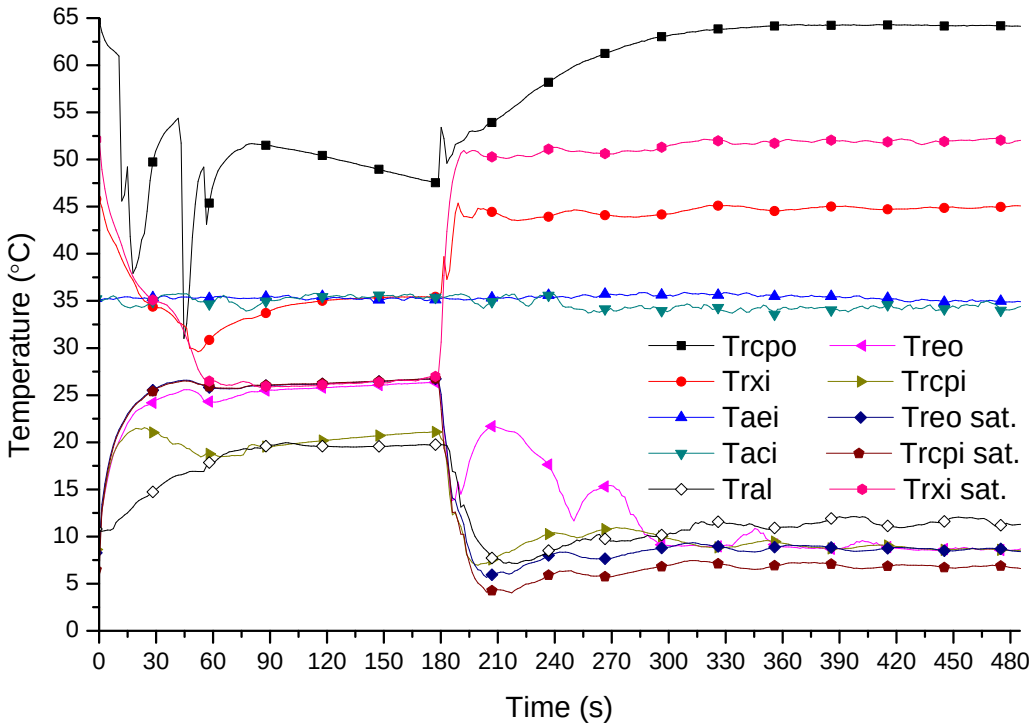

(b) Refrigerant and air inlet temperatures

Figure 5.9: Refrigerant and air temperatures for I35-wet condition, transparent accumulator without desiccant package

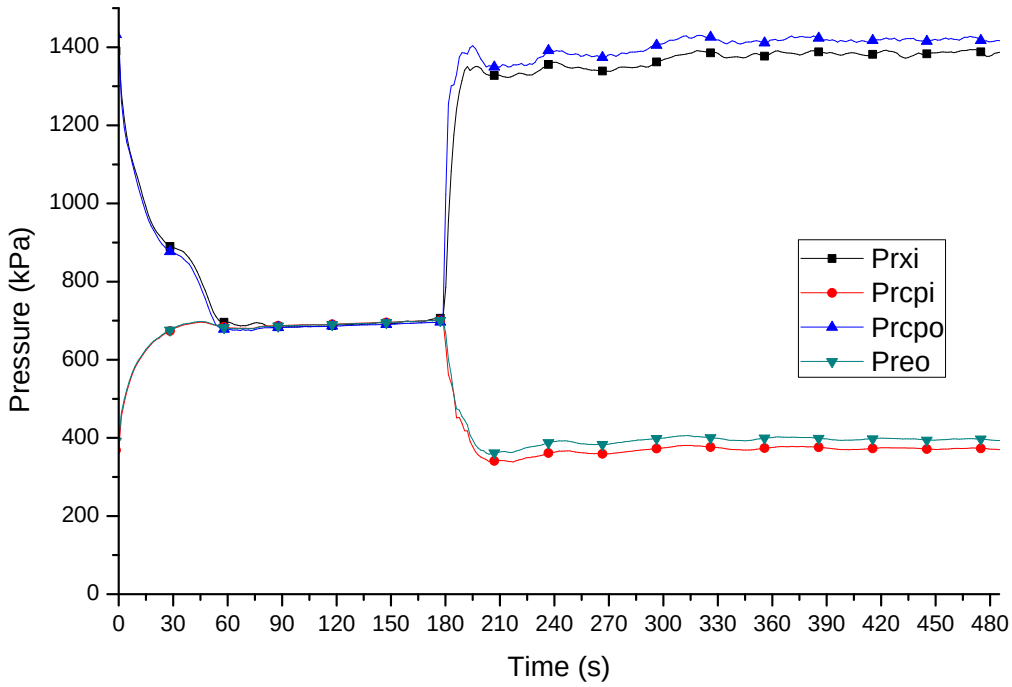

(a) Refrigerant pressures

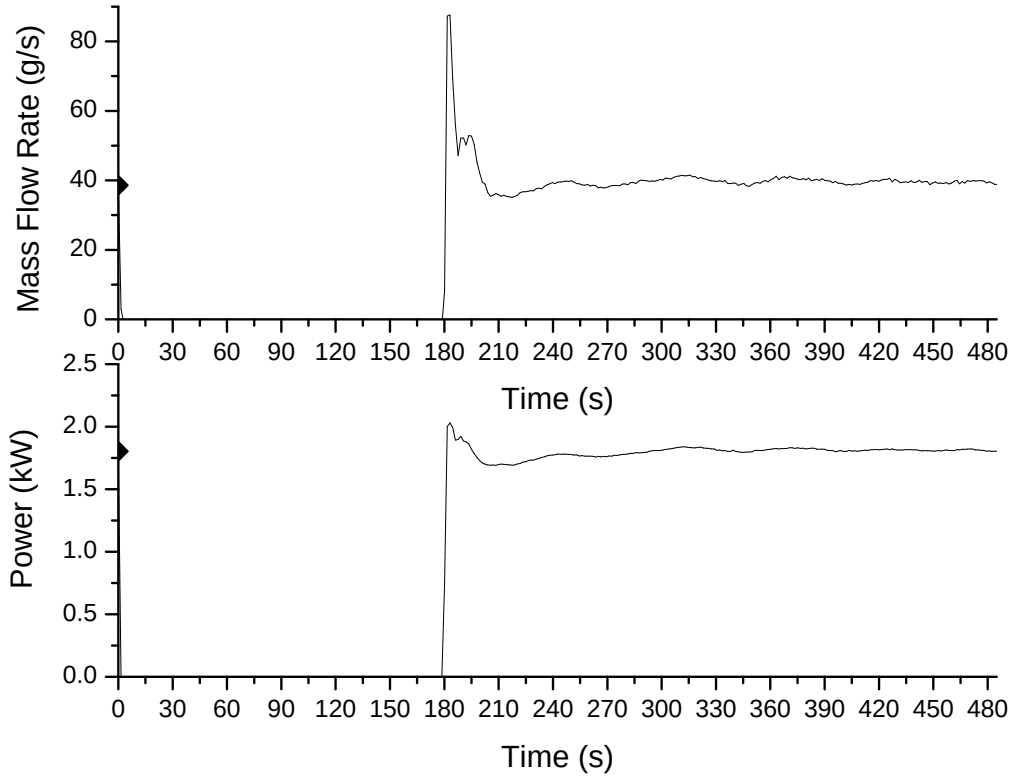

(b) Refrigerant mass flow rate and compressor power

Figure 5.10: Refrigerant pressures, mass flow rate and compressor power for I35-wet condition, transparent accumulator without desiccant package

5.4 Lubricant Migration

The lubricant mass migration was measured for the stop-start scenario used the I35 wet operating condition and the breadboard system using the transparent accumulator section without desiccant package. The results of the lubricant migration are shown in Figure 5.11. Since the accumulator contained over 100 g of lubricant, a second right-hand ordinate is used. This ordinate is also used to compare the total amount of lubricant mass in the system for each experiment compared to the target lubricant mass of 230 g—denoted by the dotted line. The two subfigures focus on the stop and start up periods with breaks in the axes to focus on the parts of the results containing the dynamic changes. The time axis starts at zero, corresponding to the time the compressor is turned off. The compressor is turned on again at 180 seconds, which initiates the start-up. Markers in Figure 5.11 denote data points. Lines are used between the data points to provide a better visual representation of the migration progression of lubricant mass across the different sections. Since the measurement uncertainties associated with the lubricant mass measurements are described in Chapter 4, error bars are omitted on the figures to maintain readability. The numerical values of the data points are given in Table 5.9. The second to last column shows the summation of the measured quantities of lubricant mass in each component. The last column shows the difference between the lubricant mass in the system based on the summation of the measured quantities of lubricant mass in each component and the amount of lubricant in the system. The lubricant measurements were taken right after the extraction of the refrigerant mass so Figure 5.8 shows the corresponding refrigerant mass migration. Figures 5.9 and 5.10 are the corresponding figures regarding the temperatures, pressures, refrigerant mass flow rate and compressor power.

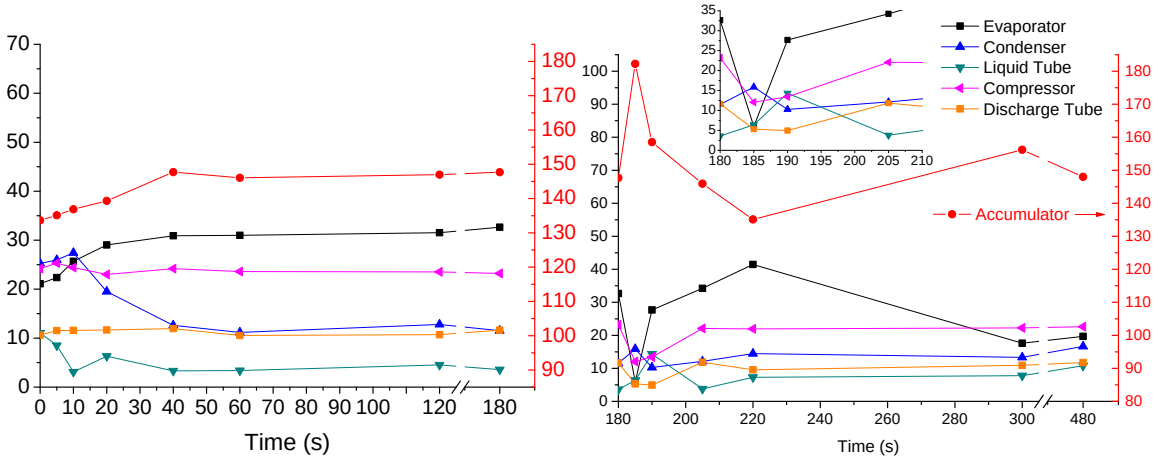

(a) Stop period

(b) Start up

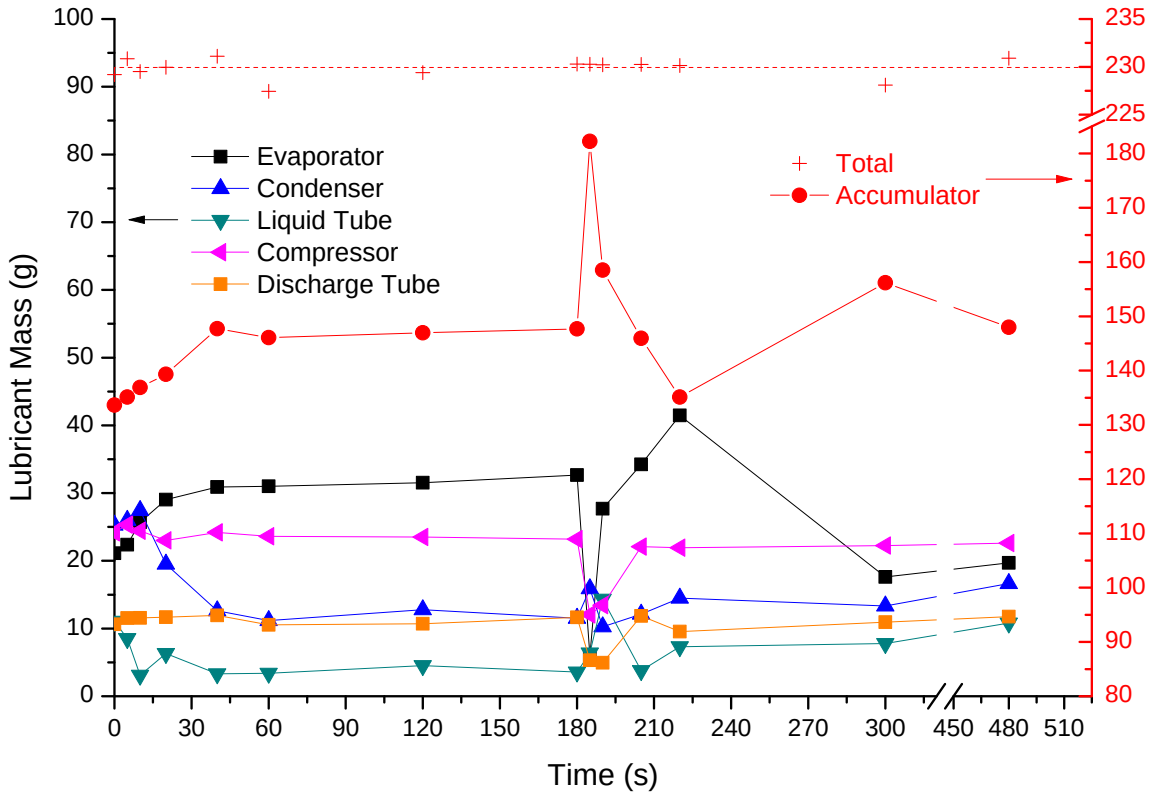

Figure 5.11: Lubricant mass migration for I35-wet condition, transparent accumulator without desiccant package

Table 5.9: Lubricant mass migration for I35-wet condition, transparent accumulator without desiccant package

Time	Evap.	Accu.	Cond.	Liquid Tube	Comp.	Dis. Tube	Sum	Diff.
s	g	g	g	g	g	g	g	g
0	21.1	133.6	25.3	11.1	24.2	10.6	225.9	-3.3
5	22.4	135.1	26.0	8.5	25.3	11.6	228.8	-2.0
10	25.7	136.9	27.4	3.1	24.4	11.6	229.1	-0.4
20	29.0	139.3	19.5	6.3	23.0	11.7	228.9	-1.1
40	30.9	147.7	12.6	3.3	24.2	12.0	230.7	-0.4
60	31.0	146.1	11.2	3.4	23.6	10.6	225.8	-1.7
120	31.5	147.0	12.8	4.5	23.5	10.7	230.1	-0.7
180	32.7	147.7	11.5	3.6	23.2	11.6	230.3	-0.5
185	6.0	182.2	15.9	6.4	12.1	5.3	227.8	-2.5
190	27.7	155.0	10.3	14.3	13.4	5.0	225.6	-1.0
205	34.2	145.9	12.1	3.8	22.1	11.8	230.0	-0.2
220	41.5	135.1	14.5	7.3	21.9	9.5	229.8	-0.3
300	17.6	156.2	13.3	7.8	22.2	10.9	228.1	-2.1
480	19.7	148.0	16.6	10.8	22.6	11.8	229.5	-1.4

Chapter 6

Analysis

The analysis chapter will first present a comparison between the experimental data and the data in the open literature. Next is a section analyzing the refrigerant distribution at steady state—including a detailed condenser model—and relationship between refrigerant and lubricant hold-up in the accumulator. The third section analyses the results of the cooling capacity during stop-start operation including a proposed curve fit. The fourth and fifth sections present the analysis of refrigerant and lubricant migration results. The last section presents how the knowledge gained from the previous sections can be used to improve the energy efficiency of refrigeration systems during cycling and start-up.

6.1 Comparison of Current Experimental Results to the Literature

Peuker and Hrnjak [43] were the first to report measurements of the refrigerant migration of an automotive refrigeration system. Experimental data of refrigerant migration is available for five other systems as reported by Tanaka et al. [8], Mulroy and Didion [9], Miller [16], Belth et al. [17] and Björk and Palm [25]. The literature review in Chapter 1 presents the authors own interpretation of their data. This chapter analyses the reported data and the data reported by Peuker and Hrnjak [43] to determine similarities and identify discrepancies.

Table 6.1: Overview of system parameters of literature reporting measured refrigerant mass migration

Author(s)	Type of system	Refrigerant	Mass (g)	Capacity (kW)
Tanaka [8]	Heat pump	R22	950	2.3
Mulroy [9]	Heat pump	R22	3920	10.6
Miller [16]	Heat pump	R22	5700	10.6
Belth [17]	Heat pump	R22	4570	4.0 [1]
Björk [25]	Household refrigerator	R600a	35.3	0.1
Peuker [43]	Automotive	R134a	1000	4.0 [1]

Author(s)	Cycle time	Ambient Temperature	Accu.	Expansion device
Tanaka [8]	10 min off; on	18°C	Yes	Capillary tube
Mulroy [9]	24 min off; 6 min on	27.8°C	Yes	Capillary tube
Miller [16]	30 min off; 8 min on	-1.1/10°C	Yes	Capillary tube
Belth [17]	24 min off; 6 min on	8.3/27.8°C	Yes	Capillary tube
Björk [25]	17 min off; 10 min on	25°C	Yes[2]	Capillary tube
Peuker [43]	3 min off; 5 min on	35°C	Yes	Short orifice tube

[1] Actual steady state capacity, all other are rated capacities
[2] Accumulator integrated in evaporator

Table 6.1 provides an overview of the six different systems and their parameters. The heat pump systems investigated by Tanaka et al. [8], Mulroy and Didion [9], Miller [16] and Belth et al. [17] all used R22 as a refrigerant and—except for the system investigated by Tanaka et al. [8]—are of the same size in terms of cooling capacity. Mulroy and Didion [9] and Belth et al. [17] used the same cycle time, ambient temperature and almost the same amount of refrigerant mass. It is expected that their results match closely and are therefore used as a starting point to compare to the other systems. Since no standard exist on how to present refrigerant mass migration data, either the original data is presented—modified to present it in the order of first off-cycle then on-cycle—or a new plot was generated based on the data reported in the corresponding literature.

Figure 6.1 shows the two plots presented by Belth et al. [17] for off- and on-cycle migration combined into one plot. It should be noted the actual off-cycle was 24 minutes, but Belth et al. [17] only presented data for the first 10 minutes. However, comparing the values after 10 minutes of off-cycle to the values at the beginning of the on-cycle shows no difference. It can be concluded that the refrigerant migration has ended after 10 minutes and therefore validates the decision to present the data in one plot.

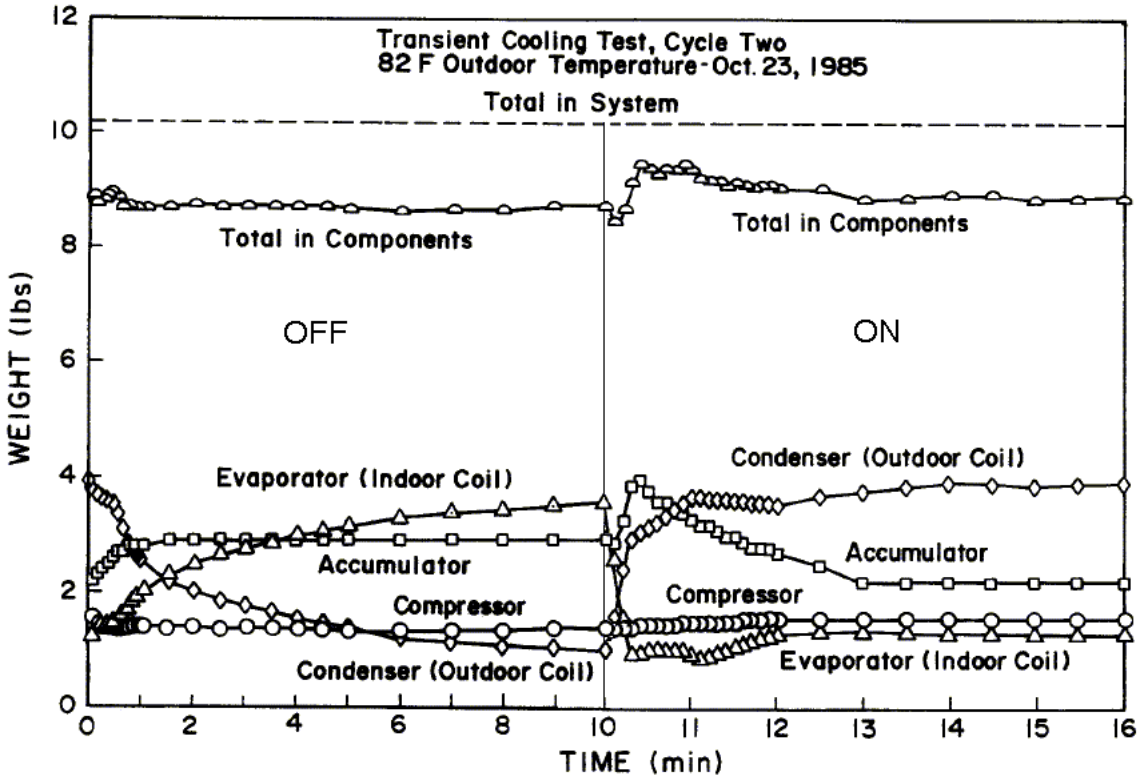

Figure 6.1: Refrigerant mass migration adapted from Belth et al. [17]; modified

Mulroy and Didion [9] did not present data for the off-cycle migration. Therefore, a plot based on their data is presented in Figure 6.2 which shows the refrigerant mass measured in each section during the on-cycle in percent of total mass of refrigerant in the system. The actual on-cycle was six minutes, but Mulroy and Didion [9]

presented a data point after 14 minutes when the system reached a steady state condition. Noting that in Figure 6.1 the total mass of refrigerant in the system is close to 10 lbs, the amounts reported in pounds for each section can be converted to percent of total mass of refrigerant in the system by multiplying each value by ten.

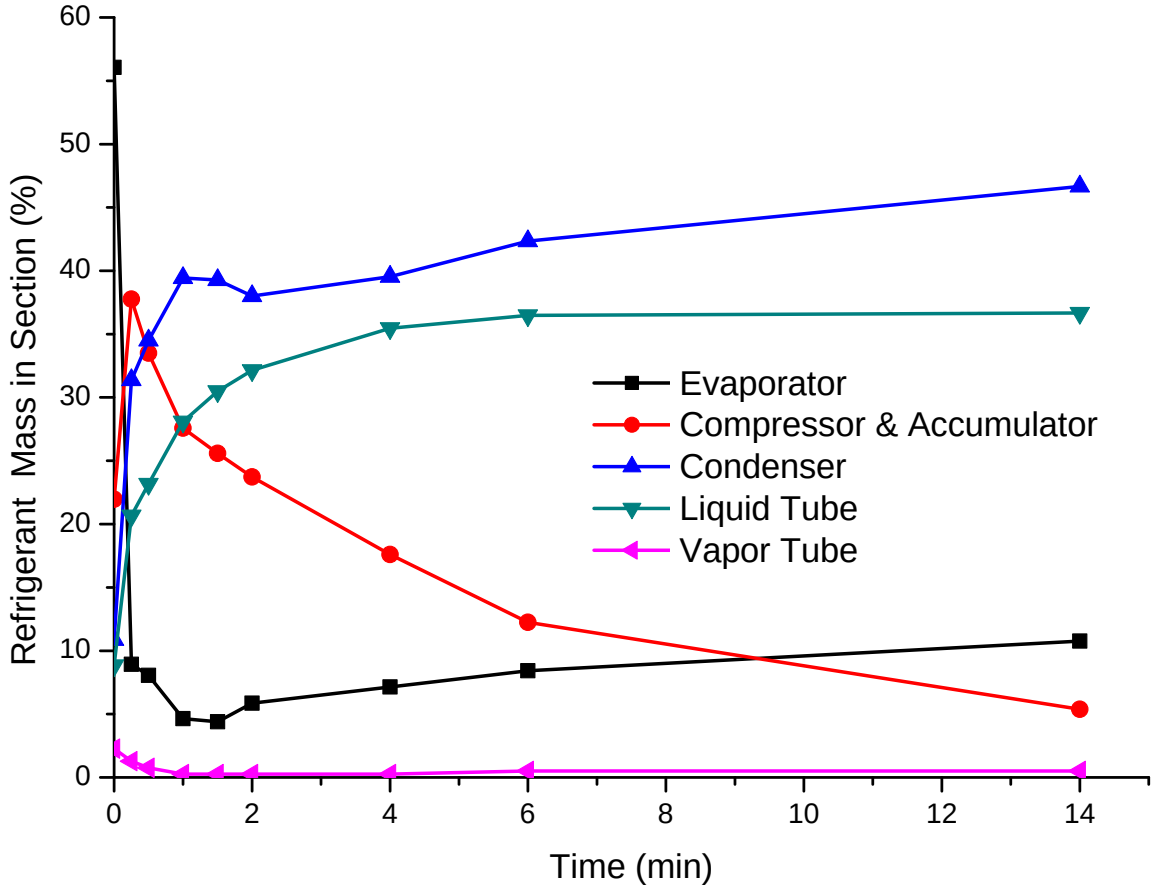

Figure 6.2: Refrigerant mass migration plotted based on reported data by Mulroy and Didion [9]

The on-cycle refrigerant mass migrations reported by Belth et al. [17] and Mulroy and Didion [9] in the condenser sections are almost identical, both in amplitude and time development. At the beginning of the on-cycle, both show the condenser section holds 10 percent of the total refrigerant mass in the system. The condenser refrigerant mass increases to a peak at 40 percent at one minute into the on-cycle, followed by a small decrease and a minimum at two minutes into the on-cycle. The evaporator

sections show the same dynamics, a rapid decrease within the first 20 seconds of the on-cycle, a minimum after one minute and a slow increase until a value of 10 percent is reached after six minutes. The only difference is the value at the beginning of the on-cycle, Mulroy and Didion [9] have 56 percent of the total refrigerant mass—and therefore 16 percent more mass—in the evaporator than Belth et al. [17]. One possible explanation for this discrepancy is that Belth et al. [17] did not measure the mass held up in the tubes since they used the OLMT and therefore only report the mass inside the components.

As it can be seen in Figure 6.1 the total mass in the components is ca. 1.5lbs less than the total mass of refrigerant in the system. If most of this mass migrates into the tubes surrounding the evaporator during off-cycle, the difference between the results from Belth et al. [17] and Mulroy and Didion [9] might be less. Another explanation is the fact that the OLMT employed by Belth et al. [17] includes the mass associated with the movement of lubricant. The lubricant movement could explain why the dynamics are almost identical for all sections, but the quantities are different.

Comparing the values of the accumulator and compressor sections from Belth et al. [17] to the reported values from Mulroy and Didion [9] show identical dynamics but different quantities. The latter measured the refrigerant mass in the accumulator and compressor as one component, and therefore report the combined value. At the beginning of the on-cycle Belth et al. [17] report 47 percent of the total refrigerant mass in the accumulator and compressor section, which does not match the 21 percent of total refrigerant mass reported by Mulroy and Didion [9]. The data by Belth et al. [17] give the insight that the compressor weight does not change and therefore the dynamic change occurs in the accumulator. The dynamics are the same for both, a sharp increase during the first 20 to 30 seconds followed by a decrease. After six minutes of on-cycle Belth et al. [17] reports 39 percent of the total mass—sum of the compressor and the accumulator masses—compared to 12 percent as reported by

Mulroy and Didion [9]. This offset between the two studies is present throughout the on-cycle. If the amount of lubricant is assumed to be the only cause for the difference—the mass reported by Belth et al. [17] includes the lubricant mass—the conclusion would be that most of the lubricant mass is located in the accumulator and compressor. This hypothesis is supported by Peuker and Hrnjak [43], who show that during steady state the compressor and accumulator combined contain 60 percent of the total lubricant mass.

Therefore, assuming the quantitative differences are a result of the experimental method used by Belth et al. [17]—the OLMT cannot distinguish between lubricant and refrigerant mass—the following conclusions can be made. The data regarding the on-cycle refrigerant mass migration presented by Belth et al. [17] and Mulroy and Didion [9] are identical and show that the majority of refrigerant migrates to the evaporator during the off-cycle. At the beginning of the on-cycle a significant amount of refrigerant mass—presumably in the liquid state—leaves the evaporator and consequently enters the accumulator. This refrigerant is then displaced from the accumulator to the condenser and liquid tube which—based on the data reported by Mulroy and Didion [9]—contain 83 percent of the total refrigerant mass after 14 minutes of on-cycle.

The refrigerant mass migration during on-cycle reported by Miller [16] is compared in Figure 6.3 to the data from Mulroy and Didion [9]. Since Miller [16] only measured the weight of the outdoor unit, the data from Mulroy and Didion [9] is modified for an easier comparison. In Figure 6.3b the reported values for the evaporator and compressor-accumulator sections are added together and labeled “Outdoor unit”. The sum of the refrigerant masses in the condenser, liquid and vapor tube sections is labeled “Indoor unit”. The qualitative transient development of refrigerant mass migration is similar between the two studies. This is expected since both systems are identical and the off-cycle time only differs by four minutes. However, the total mass

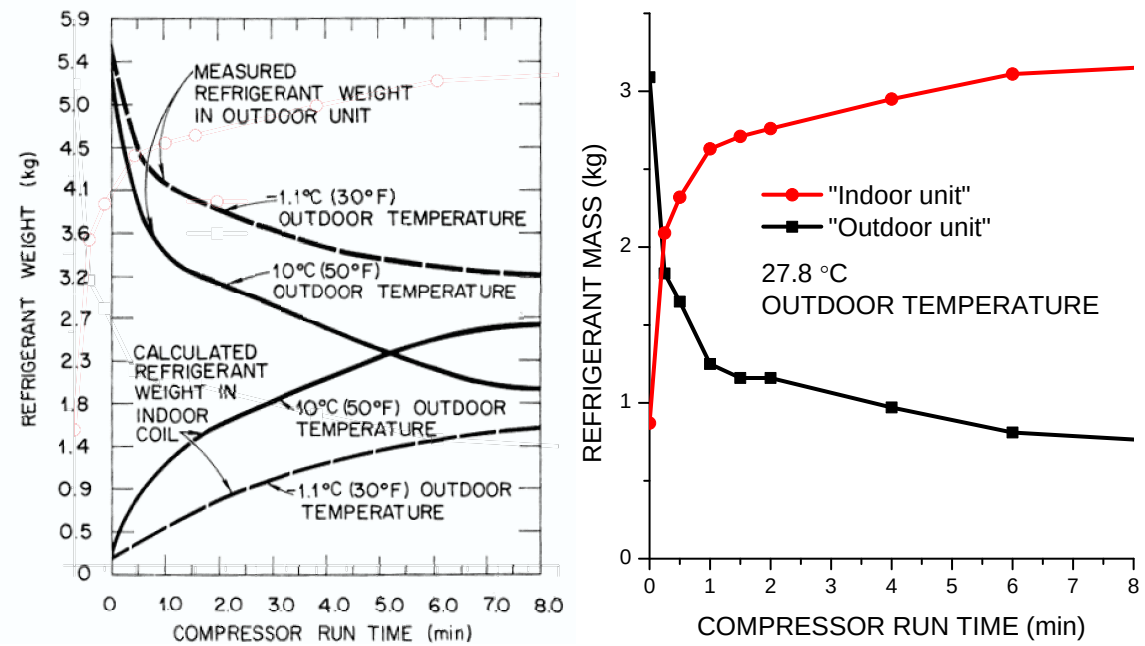

(a) Miller [16]

(b) Mulroy and Didion [9]; adapted

Figure 6.3: Comparison of on-cycle refrigerant mass migration between Miller [16] and Mulroy and Didion [9]

of refrigerant in the system and the ambient temperatures are different which leads to quantitative differences.

Despite these differences, the comparison gives insight on how the ambient temperature influences the refrigerant mass migration. For the lowest ambient temperature—$-1.1°C$—40 percent of the total refrigerant mass in the system migrates out of the outdoor unit during the first eight minutes of on-cycle. It should be noted the change in weight is assumed to only be the result of the refrigerant movement—the movement of lubricant mass is unknown. At an ambient temperature of 10°C, 57 percent of the total refrigerant mass in the system migrates out of the outdoor unit during the first eight minutes of on-cycle. For an ambient condition of 27.8°C—investigated by Mulroy and Didion [9]—63 percent of the total refrigerant mass in the system migrates out of the outdoor unit. Therefore, a higher ambient temperature leads to more refrigerant mass migrating and hence to higher energy losses during the on-cycle

since compressor energy is necessary to redistribute the refrigerant mass.

Tanaka et al. [8] used a different approach—the system was run at steady state conditions and then turned off for 16 hours (Case I) or 10 minutes (Case II) before it was started again. The data of the refrigerant mass migration is presented in the original paper as a ratio of the refrigerant mass at the steady state operating condition. For comparison, the data is modified and plotted as refrigerant mass in percent of total refrigerant mass in the system. Figure 6.4 shows the migration of refrigerant mass during the on-cycle for Case II.

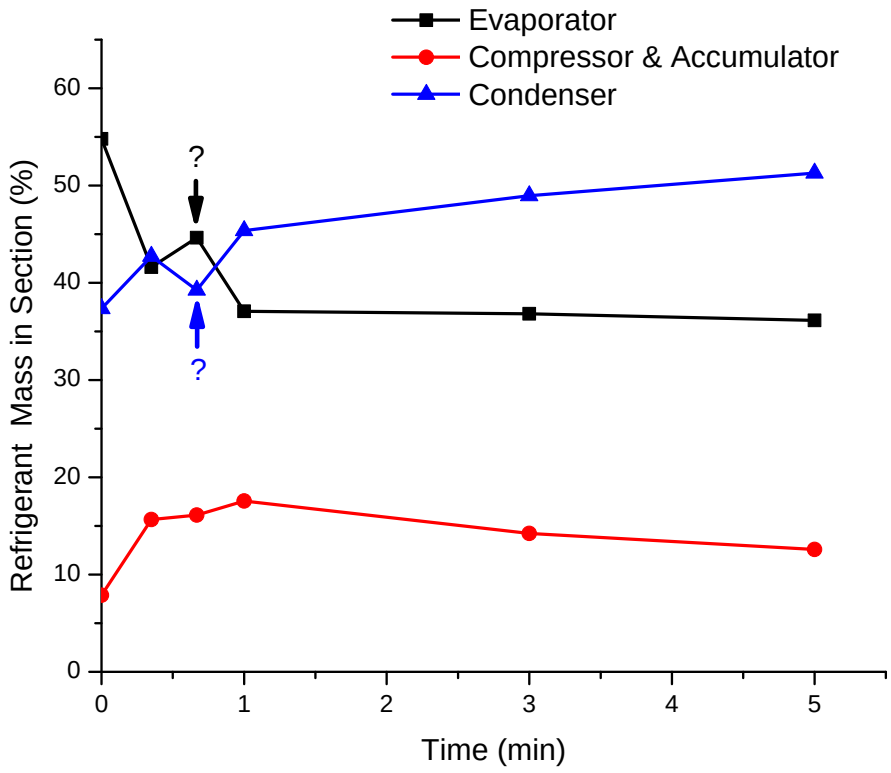

Figure 6.4: Refrigerant mass migration adapted from Tanaka et al. [8] Case II

Two issues make it difficult to compare the data presented by Tanaka et al. [8] to the data of Mulroy and Didion [9], Miller [16] and Belth et al. [17]. First, the system used by Tanaka et al. [8] is only separated into three sections and information about

the exact locations of the separation valves is not given. Therefore, it is unclear how much of the refrigerant mass reported in the evaporator section is actually in the liquid tube. Second, the changes in refrigerant mass in the condenser and evaporator sections show an odd behavior 40 seconds into the on-cycle. Both sections have an equal but opposite change in refrigerant mass. This phenomenon is not found in any of the other heat pump investigations, and raises the question if a mistake was made when creating the original plot. If the two values were swapped, the curves would be "smoother", and the development would be consistent with the data reported by the other three publications. Besides these difficulties, the general trend—refrigerant mass is transferred during the on-cycle from the evaporator to the condenser—is consistent with the other publications.

Björk and Palm [25] investigated a household refrigerator using isobutane (R600a) as a refrigerant. The total refrigerant mass used in their system is two orders of magnitude smaller compared to all the other systems. Furthermore, both of the heat exchangers are free convective type heat exchangers. The accumulator is integrated into the roll-bond (plate type) evaporator and is not a separate vessel and therefore is not comparable in design to the accumulators from all the other systems. The cycling time is 17 minutes off-cycle and 10 minutes on-cycle at an ambient temperature of 25°C at the condenser and an evaporator air inlet temperature of 5°C. Figure 6.5 shows the refrigerant mass migration as presented by Björk and Palm [25] rearranged as an off-on-cycle. The amount of refrigerant mass dissolved in the compressor oil is not directly measured, but determined by subtracting the amount of refrigerant masses in the other sections from the total mass of refrigerant in the system. In addition, the section labeled evaporator in Figure 6.5 shows the mass of refrigerant in the evaporator with integrated accumulator.

During the first three minutes of the off-cycle, 9.5 g of refrigerant mass migrates from the condenser to the evaporator, which then holds 62 percent of the total re-

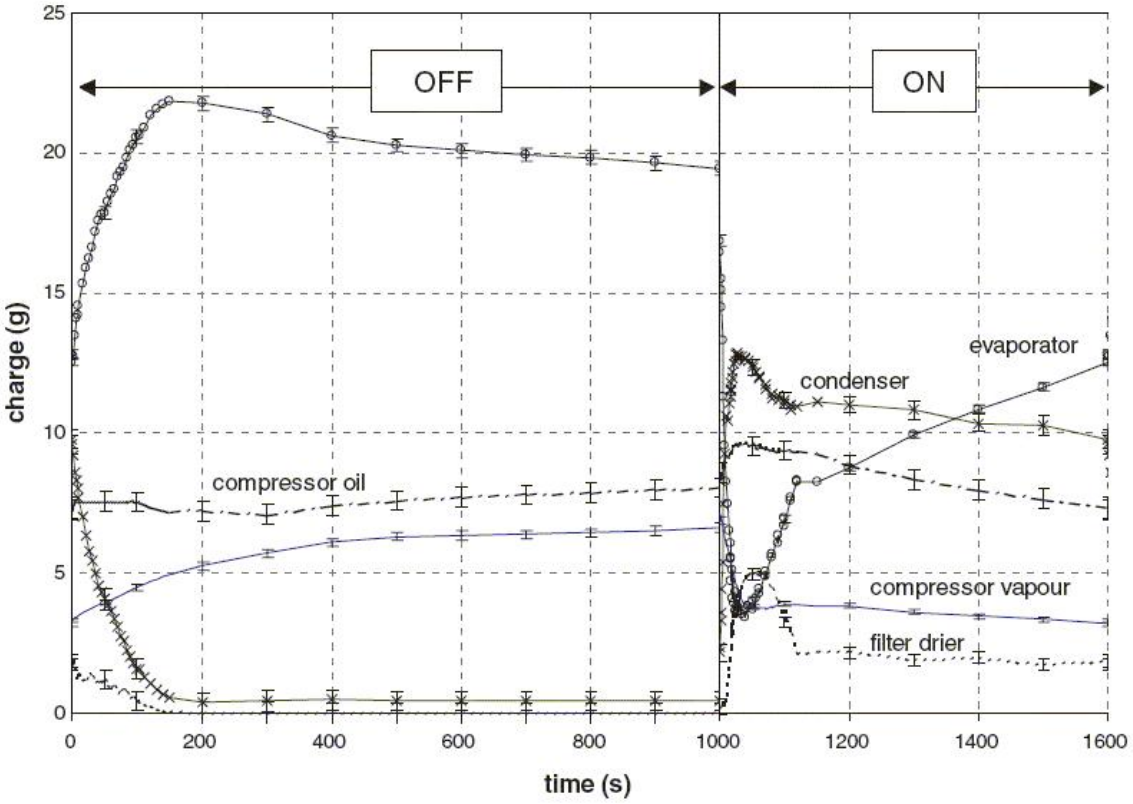

Figure 6.5: Refrigerant mass migration adapted from Björk and Palm [25]

frigerant mass. The remainder of the refrigerant mass—about 36 percent—is found in the compressor since the condenser and filter dryer contain only 0.5 g, which is less than two percent of the total system. This is a significant difference compared to the heat pump systems—they show less than 20 percent of the total refrigerant mass is in the compressor—but can be explained by the ratio of compressor volume to system volume. Mulroy and Didion [9] report a volume ratio of 44 percent for the compressor and accumulator, whereas the volume ratio is 87 percent for the compressor alone for the system investigated by Björk and Palm [25]. A larger compressor volume holds more refrigerant mass, but the refrigerant mass increase is less than in other components—if increased by the same volume—because the refrigerant inside the compressor is mostly in the vapor phase. The refrigerant mass—dissolved in the

lubricant and present in the vapor phase—within the compressor varies between 11 g and 14 g throughout the off-on cycle and therefore remains relatively constant.

During the on-cycle the refrigerant mass decreases sharply in the evaporator and reaches a minimum after 30 seconds. It then increases sharply again, but after two minutes there is a sudden leveling off observed before the refrigerant mass increases linearly. The condenser and filter/drier show the same but mirrored behavior. Although the peaks are more distinct, the behavior is similar to the on-cycle refrigerant mass migrations reported by Belth et al. [17] and Mulroy and Didion [9]. Overall the general behavior of the system investigated by Björk and Palm [25]—albeit different in magnitudes and timing—is similar to the heat pumps system investigated by Belth et al. [17] and Mulroy and Didion [9]. Björk and Palm [26] report in another investigation the refrigerant mass decreased in the evaporator if the thermal load was increased under steady state operating conditions. They did not report the off-cycle migration for those conditions, but it can be assumed—based on the conclusion made earlier from the comparison of the data provided by Miller [16] and Mulroy and Didion [9]—that an increase in thermal load increased the refrigerant mass migration during off-cycle.

Peuker and Hrnjak [43] investigated the refrigerant migration of an automotive refrigeration system during a stop-start event. They were the first to present refrigerant mass migration data measured in all sections of the system and distinguish between the refrigerant mass in accumulator and compressor. A detailed description of this system is presented in Section 2.3. The major differences compared to the other systems in Table 6.1 are the shorter cycling time, the higher ambient temperature and the expansion device. The results of the refrigerant mass migration are presented in Figure 6.6. The system is run at steady state condition and the compressor is stopped for three minutes and then started again. The values at 480 seconds are identical to the values at zero seconds. Therefore, the data in Figure 6.6 can be interpreted as

a repeatable off-on-cycle having a three minute off-cycle period and a five minute on-cycle period.

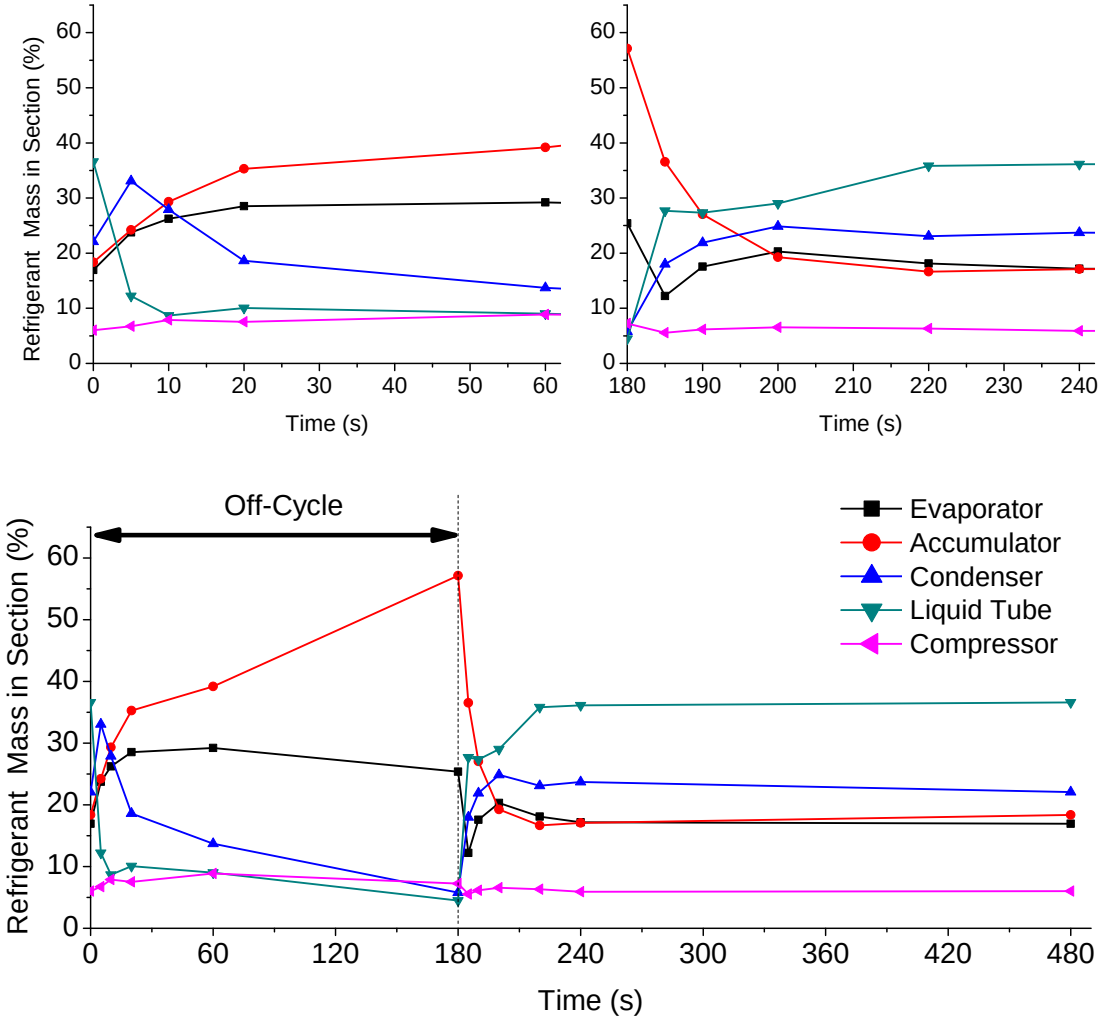

Figure 6.6: Refrigerant mass migration; Peuker and Hrnjak [43]

The upper right-hand plot in Figure 6.6 shows the first 60 seconds of the on-cycle. The steady state refrigerant distribution is reached after almost 60 seconds of on-cycle—the change in refrigerant mass in the condenser between time index 340 and 480 seconds is only two percent. The heat pump systems reached steady state refrigerant mass distribution between six minutes—Tanaka et al. [8]—and 14 minutes—Mulroy and Didion [9]. The household refrigerator investigated by Björk and Palm [25] did not reach steady state values after 10 minutes. The fast dynamics

of the automotive system are expected since automotive systems, in general, are designed to provide quick changes of cooling capacities based on human input or climate controllers to increase passenger comfort. In spite of the faster dynamics, the general trends are similar during the on-cycle—refrigerant mass is transferred from the accumulator and evaporator to the condenser and liquid tube. During the off-cycle, the reverse is observed, refrigerant mass migrates form the condenser and liquid tube to the evaporator and accumulator. Compared to Belth et al. [17] and Björk and Palm [25], the only qualitative difference—besides the faster dynamics—is the data by Peuker and Hrnjak [43] show a quick increase in refrigerant mass in the condenser section during the first five seconds before a constant decrease is observed. This unique phenomenon is further discussed in Section 6.4.1.

The dynamics of the refrigerant mass migration can be divided into two parts, a fast migration of the majority of refrigerant mass during the first 20 seconds, followed by a slower migration. This statement is true for both the off-cycle and on-cycle migration. In addition, this behavior—having different timing—is observed for the data presented by Belth et al. [17] and Björk and Palm [25]. The timing of the "fast migration" is approximately the same for the off-cycle and on-cycle migration and indicates that the compressor alone cannot be responsible for the time it takes to redistribute the refrigerant mass during the beginning of the on-cycle. The expansion device limits the refrigerant mass flow rate and therefore the time it takes for the "fast migration" to occur. Further explanation is provided in Section 6.4. The data by Peuker and Hrnjak [43] show a minimum in evaporator refrigerant mass five seconds into the on-cycle. The same is observed qualitatively by Mulroy and Didion [9], Belth et al. [17] and Björk and Palm [25] one minute into the on-cycle or 30 seconds into the on-cycle, respectively. The refrigerant mass increase in the condenser and liquid tube sections during on-cycle show strong similarities to the data provided by Mulroy and Didion [9], as well as the refrigerant mass decrease in the accumulator. The dynamics,

however, are roughly ten times faster for the system investigated by Peuker and Hrnjak [43] and the magnitudes of the refrigerant masses in the components are also different.

6.1.1 Generalization—Refrigerant Mass Migration

Comparing the experimental data of refrigerant migration presented by Tanaka et al. [8], Mulroy and Didion [9], Miller [16], Belth et al. [17], Björk and Palm [25] and Peuker and Hrnjak [43] gives the following general conclusions about the movement of refrigerant mass during cycling or stop-start operation.

- Refrigerant mass migrates from the high pressure components—condenser, liquid tube, high pressure receiver (filter/drier)—to the low pressure components during off-cycle or shut-down. The dynamic of this migration can be categorized into two parts. First a fast primary migration—20 seconds to three minutes depending on the system—of the majority of the refrigerant mass followed by a slow secondary migration over time. The secondary migration of the refrigerant mass differs by system, but the primary migration is qualitatively the same.

- During on-cycle refrigerant mass has to be transferred from the low pressure components—evaporator, accumulator—to the high pressure components. The initial mass distribution at the beginning of the on-cycle is identical to the mass distribution at the end of the off-cycle, if the cycling is steady. Therefore, the off-cycle migration has a direct influence on the on-cycle performance since compressor energy is necessary to redistribute the refrigerant mass.

- There is a relation between ambient temperature and the amount of refrigerant mass migration during off-cycle. Higher ambient temperatures lead to more refrigerant mass migration.

- The change in refrigerant mass in the compressor during both, the off and on-cycle, is the least of all components. It should be noted that this might be different for compressors with high pressure sumps.

- During the beginning of the on-cycle the evaporator shows a minimum below the amount of refrigerant mass found during steady state, indicating that more refrigerant mass is leaving the evaporator than is entering it from the expansion device.

6.2 Refrigerant and Lubricant Distribution at Steady State

6.2.1 System Charge and Refrigerant Distribution

The amount of refrigerant mass necessary for a particular system is determined by measuring the energy consumption of the compressor, and the cooling capacity provided by the evaporator for different refrigerant charges at a specified operation condition. Depending on the objective, the system is filled until a particular cooling capacity or coefficient of performance is achieved. Even simpler procedures, e.g., charging a system until the evaporator is flooded, are used in industry. This section discusses the refrigerant mass distribution for different system charges and how it affects the cooling capacity and coefficient of performance, and hence the choice of how much refrigerant mass should be used in a refrigeration system.

To determine the system charge for the breadboard system a charge determination test was necessary since the manufacturer's specification of 700 g of R134a is for a system having a volume 21 percent smaller than the breadboard system (see Section 2.3.2). Therefore, it was expected the breadboard system requires more R134a mass than the original system to provide an optimized performance at the design operating

condition I35dry (see Table 5.1). To determine the optimum mass of R134a, the breadboard system was run at steady state for five different system charges ranging from 580 g to 1500 g. The cooling capacity, $\dot{Q}_a$, of the evaporator is determined based on air side measurements—$\dot{m}_a$ is the dry air mass flow rate and h_{aei} and h_{aeo} are the enthalpies of the air entering and leaving the evaporator.

$$\dot{Q}_a = \dot{m}_a \cdot (h_{aei} - h_{aeo}) \tag{6.1}$$

The coefficient of performance is (COP) is solely based on the power of the compressor measured at the shaft, $\dot{W}_{comp}$, and does not account for the power necessary for the air blowers or any other power consumption of the system.

$$COP = \frac{\dot{Q}_a}{\dot{W}_{comp}} \tag{6.2}$$

Another measure used in charge determination tests is the degree of subcooled refrigerant liquid at the condenser exit and superheated refrigerant vapor at the evaporator exit. For an ideal vapor-compression cycle, the refrigerant exits the condenser as saturated liquid and enters the compressor as saturated vapor [44]. In an actual cycle, the superheat and subcooling is determined from on the temperature difference between measured refrigerant exit temperature, T_e, and pure refrigerant saturation temperature based on the measured exit pressure, $T_{sat}(P)$, as shown in Equation (6.3).

$$\Delta T = T_e - T_{sat}(P) \tag{6.3}$$

However, in an actual refrigeration system, the thermophysical properties of the refrigerant-lubricant mixture are different from the pure refrigerant properties. For example, the implied "superheated vapor" at the evaporator exit is actually the bubble point temperature minus the saturation temperature of the pure refrigerant [45].

Therefore, the degrees of superheat or subcooling should be regarded as apparent values.

Figure 6.7 presents the air side cooling capacity, the COP, the apparent degrees of subcooling at the condenser refrigerant exit, and the apparent degrees of superheat at the evaporator refrigerant exit. As the figure shows, the cooling capacity increases

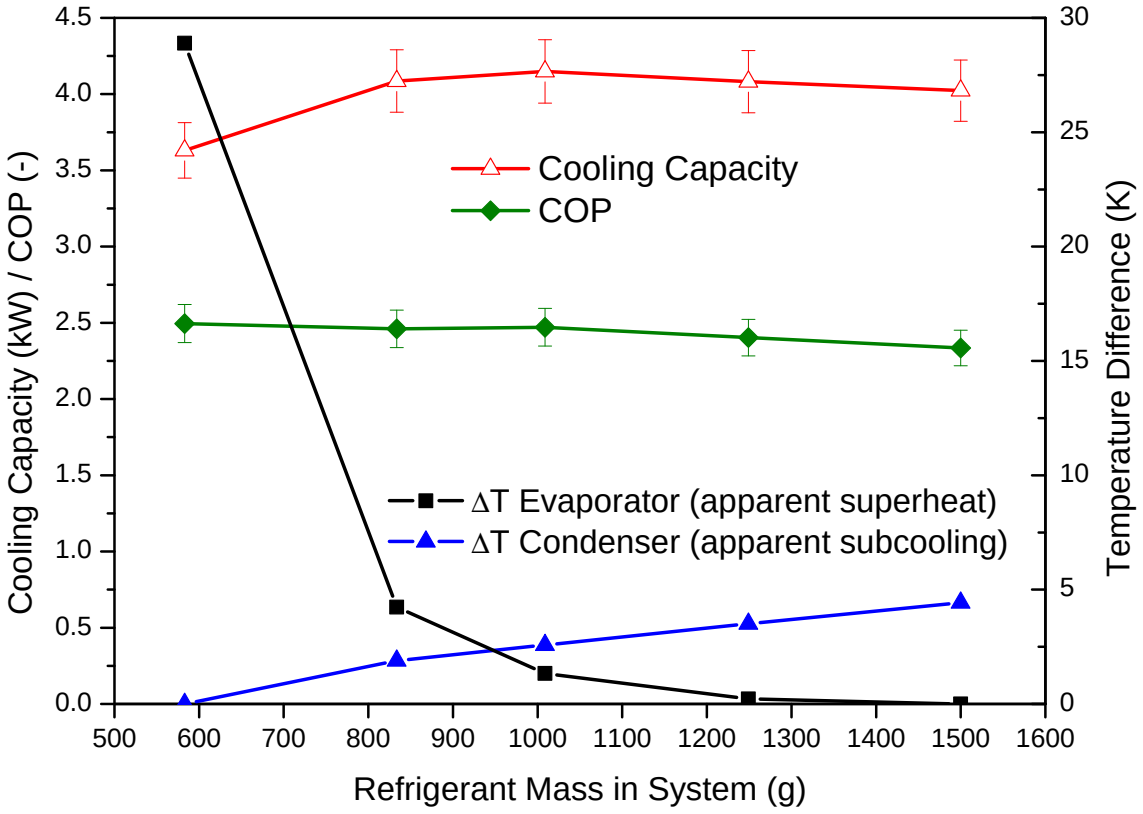

Figure 6.7: Cooling capacity, COP, apparent subcooling and superheat for different system charges

by 0.5 kW when the system refrigerant charge is increased from 580 g to 830 g. The highest value is reached for a system charge of 1000 g. For higher system charges the cooling capacity decreases slightly. The COP is constant at 2.5 and starts to decrease for system charges over 1000 g. Apparent subcooling is first observed for a system charge of 830 g and is linearly increasing for higher system charges. The apparent evaporator superheat is almost 30 K for a system charge of 580 g but decreases significantly to 4 K for a system charge of 830 g. For a system charge of

1000 g the apparent superheat is 1 K and essentially zero for higher system charges. Considering the optimum in cooling capacity and the fact that the COP is still 2.5 a system charge of 1000 g can be regarded as the optimum charge for the design condition. This coincides with the observation that both, the apparent subcooling and superheat, are present but below 3 K and therefore close to the ideal vapor-compression cycle values.

The manufacturer of the original system specifies a refrigerant charge of 700 g. However, the liquid tube for the breadboard system is 3.4 times longer than the liquid tube of the real vehicle system. This increases the volume of the breadboard system liquid tube section by 0.270 liter. Assuming the additional volume is filled with saturated liquid refrigerant, the additional refrigerant mass hold up can be calculated. The liquid saturation density at a pressure of 1300 kPa—the pressure measured for the breadboard system for a system charge of 1000 g—is 1105 kg/m^3. Multiplying the density by the additional volume results in a refrigerant mass of 300 g—the difference between the manufacturer specified charge and the optimum refrigerant mass for the breadboard system. An important conclusion from this observation is that the amount of refrigerant mass in the liquid tube section is directly proportional to the volume of this section—if the exiting refrigerant from the condenser is saturated or subcooled.

Because of the additional refrigerant mass the oil charge—220 g as specified by the manufacturer—of the breadboard system also needs to be corrected. The correction is done by multiplying the additional refrigerant mass by the lubricant in circulation ratio (LCR). For the breadboard system having a refrigerant charge of 1000 g, the LCR was measured to be 4.45 percent and therefore 10 g of lubricant were added to compensate for the additional volume of the liquid tube. The amount of lubricant used for the breadboard system was 230 g of Polyalkylene Glycol (PAG) having an ISO viscosity grade of 46 mm^2/s.

Based on the results presented in Chapter 5, the mass residence times in each section can be calculated by dividing the measured mass in a section by the measured mass flow rate. The mass flow rate of the lubricant is determined from the measured refrigerant mass flow rate times the LCR. Table 6.2 shows the result of the refrigerant mass residence times for the I35-dry and I35-wet operating condition and the lubricant mass residence times for the I35-wet operating condition. In the liquid tube section,

Table 6.2: Mass residence times at steady state condition

	Evap.	Accu.	Cond.	Liquid Tube	Comp.
	s	s	s	s	s
I35-dry R134a	4.8	5.2	6.3	10.4	1.7
I35-wet R134a	4.4	3.0	6.4	10.1	1.6
I35-wet PAG 46	19.1	121.2	23.0	10.1	31.6

the residence times of refrigerant and lubricant are identical since in this section no vapor is present as a result of the subcooled condition at the condenser exit. In all other sections, refrigerant vapor is present resulting in a differences in retention times between refrigerant and lubricant mass. Since the accumulator holds 133.6 g of the lubricant at steady state condition, the lubricant has the longest residence time in this section. The liquid tube section holds the most refrigerant mass at steady state condition and therefore has the longest residence time for the refrigerant. It should be noted that as a result of the longer liquid tube of the breadboard system the refrigerant mass residence time in the original vehicle system would be an estimated 3.0 s and therefore the condenser would have the longest refrigerant mass residence time.

To gain further insight about how the refrigerant mass is distributed within the system for different system charges, the refrigerant mass distribution was measured across the five sections for each of the five system charges. Figure 6.8 shows the results

of these experiments. The slope of the accumulator is constantly positive, meaning

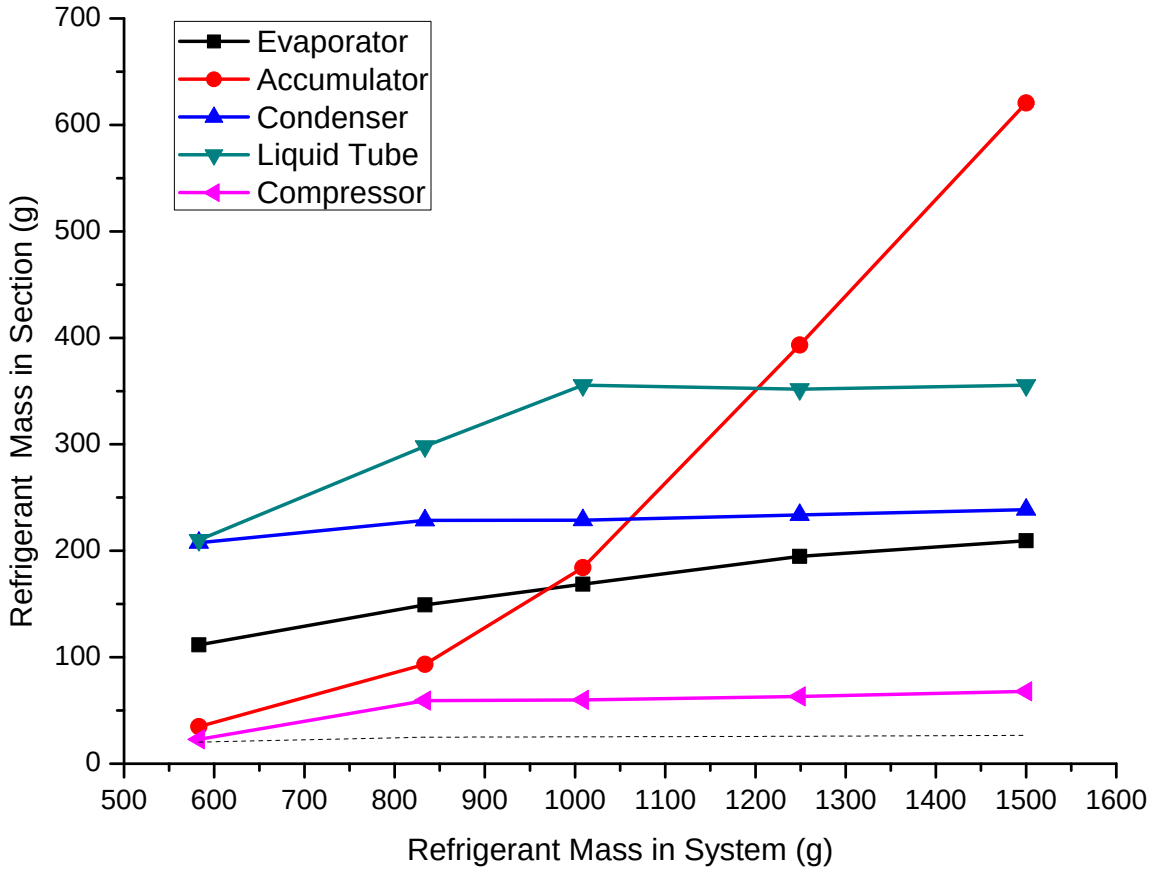

Figure 6.8: Refrigerant mass distribution across sections for different total refrigerant masses in the system

that by increasing the refrigerant charge in the system, more and more refrigerant mass will be held up in the accumulator. This behavior is desired since the role of an accumulator is to hold excess refrigerant mass when it is not needed for actual operation. The hold-up of refrigerant charge in the accumulator increases especially in the range from 1000 g to 1250 g. This observation can be explained by looking at the data of the liquid tube. Until a system charge of 1000 g, the refrigerant mass held up in the liquid tube increases at a constant rate. For system charges greater than 1000 g, the refrigerant mass in the liquid tube is constant, indicating that the liquid tube is almost completely filled with liquid phase refrigerant. Additional refrigerant mass cannot be stored there because the liquid refrigerant-lubricant mixture is nearly

incompressible.

The lubricant mass has a direct influence on the refrigerant mass distribution—especially in the accumulator. If the apparent superheat is taken as actual superheat, it is evident from Figure 6.7 that refrigerant should not be present in the liquid phase in the accumulator for system charges below 1250 g—the accumulator would be filled with only superheated refrigerant vapor. The dotted line in Figure 6.8 shows what the refrigerant mass in the accumulator section would be if only refrigerant in the vapor phase were present. For a system charge of 1000 g the difference—between the actual refrigerant mass and the refrigerant mass calculated using pure refrigerant properties—is 159 g. This difference demonstrates the potential underestimation of refrigerant mass when only pure refrigerant properties are considered. The next section looks further into the relationship between refrigerant and lubricant in the accumulator.

6.2.2 Relationship between Refrigerant and Lubricant Hold-Up in the Accumulator

The mechanism by which lubricant can return to the compressor from the accumulator is through entrainment of a small—one millimeter in diameter—hole at the bottom of the U-tube inside the accumulator. The amount of lubricant returned depends on how much liquid is entrained, as well as on the concentration ratio between refrigerant and lubricant inside the accumulator. A derivation of the relationship between refrigerant and lubricant hold-up in an accumulator for a fully miscible lubricant refrigerant combination is presented. This relationship—valid for any U-tube type accumulator since it is independent of geometrical parameters—links the lubricant in circulation ratio, the concentration of lubricant in the liquid mixture, and the entrainment ratio of liquid through the bleeding hole inside the accumulator.

The lubricant in circulation ratio can be defined as:

$$LCR = \frac{M_{lub}}{M_{lub} + M_{ref}} \tag{6.4}$$

where M_{lub} is the mass of the lubricant and M_{ref} is the mass of refrigerant in a given volume. The lubricant in circulation ratio at steady state operating conditions is assumed to be constant throughout the system. It is important to note that the LCR can only be determined for a volume in which there is no lubricant hold up. For the breadboard system, this is assumed to be the case for the liquid tube section if the liquid tube is filled with a liquid refrigerant and lubricant mixture. The concentration of the lubricant in the liquid mixture of lubricant and refrigerant in the accumulator, $C_{lub,accu}$, can be expressed as:

$$C_{lub,accu} = \frac{M_{lub}}{M_{lub} + M_{ref,liq}} \tag{6.5}$$

where $M_{ref,liq}$ is the mass of the refrigerant present in the liquid phase. For an accumulator having a U-tube and a small hole at the bottom of the U-tube, a certain amount of the liquid refrigerant and lubricant mixture is entrained into the refrigerant vapor flow. This entrainment ratio, E, can be expressed as:

$$E = \frac{M_{lub} + M_{ref,liq}}{M_{lub} + M_{ref,liq} + M_{ref,vap}} \tag{6.6}$$

where $M_{ref,vap}$ is the mass of the refrigerant that is present in the vapor phase. The relationship between equations (6.4), (6.5) and (6.6) can then be expressed as:

$$E = \frac{LCR}{C_{lub,accu}} \tag{6.7}$$

For the three system charges of 1000 g, 1250 g and 1500 g, the lubricant mass

measured in each section is presented in Figure 6.9. The amount of lubricant was held constant for these experiments—only the total refrigerant mass in the system is increased—to investigate the effect an increase in refrigerant mass has on the lubricant distribution. As Figure 6.9 shows, more than 50 percent of the total lubricant mass is

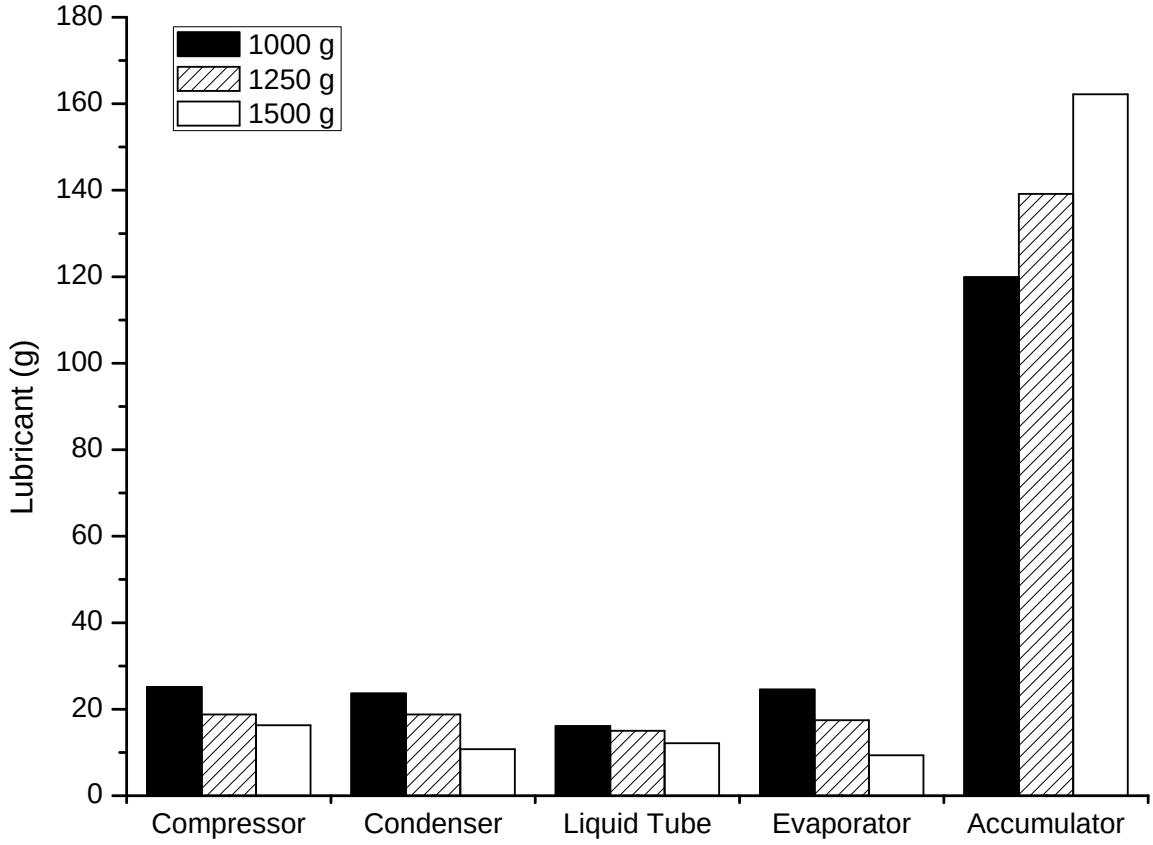

Figure 6.9: Lubricant mass distribution across sections for different total refrigerant masses in the system

found in the accumulator. As Figure 6.8 demonstrates, the amount of refrigerant hold up in the accumulator increases with increasing system charge. Figure 6.9 shows that the lubricant hold up also increases with increasing system charge. The consequence is a decreased amount of lubricant mass in all other sections—including the compressor. The lubricant mass in the compressor was reduced by 9 g when the system charge was increased from 1000 g to 1500 g. This decrease in lubricant mass in the compressor is an important observation since increasing the system charge without increasing

the amount of lubricant could lead to reduced lubrication of the compressor—and potentially to a failure of the compressor.

In order to further investigate the relationship of refrigerant and lubricant hold-up in the accumulator, the LCR was calculated for the three different system charges, 1000 g, 1250 g and 1500 g, based on the refrigerant and lubricant mass measured in the liquid tube section. To determine the concentration of the lubricant in the liquid mixture, $C_{lub,accu}$, it is necessary to determine the amount of liquid phase refrigerant in the accumulator. Carrying out a phase equilibrium calculation based on the measured pressure and temperature—the densities of the refrigerant-lubricant mixture were calculated from the correlation by Seeton and Hrnjak [28]—the amount of liquid phase refrigerant in the accumulator was determined. Table 6.3 shows the resulting ratios and corresponding propagated measurement uncertainties. The entrainment ratio, E, was calculated using Equation (6.6). Table 6.3 demonstrates that

Table 6.3: Refrigerant-lubricant concentration ratios for different system charges

System charge	LCR	$C_{lub,accu}$	E
g	%	%	%
1000	4.45±0.28	40.6±2.8	11.0±1.0
1250	3.75±0.22	26.4±1.1	14.2±1.0
1500	3.44±0.24	19.9±0.6	17.3±1.3

the entrainment of the liquid refrigerant-lubricant mixture through the hole in the U-tube of the accumulator increases with an increase in system charge. This increase is not unexpected since the liquid height above the hole increases, leading to a higher static pressure. The increase in refrigerant mass hold-up in the accumulator is greater than the increase in lubricant mass hold-up, reducing the concentration ratio of lubricant to liquid refrigerant in the accumulator. The increase in entrainment is not high enough to compensate for this decrease in lubricant concentration resulting in

a reduced lubricant in circulation ratio. Since the overall refrigerant mass flow rate changes by only 1.5 g/s from 1000 g to 1500 g of system charge it can be concluded that less lubricant is passed through the compressor—which could potentially lead to a failure of the compressor.

6.2.3 VLE-Correlations for R134a and PAG Oil

From the previous section, it is evident that the prediction of lubricant and refrigerant hold-up in the accumulator is important. Different refrigerant oil combinations can exhibit different behavior—vapor-liquid equilibrium (VLE), liquid-liquid equilibrium (LLE), vapor-liquid-liquid equilibrium (VLLE)—depending on the miscibility of the combination. The refrigerant-lubricant combination used in the experimental system was R134a and PAG 46—a miscible or soluble combination over a wide range of pressures and temperatures—and exhibits VLE behavior. Since a comprehensive physical model of refrigerant-lubricant mixtures has yet to be developed, empirical correlations have to be used to predict the vapor-liquid equilibrium. The following analysis addresses the question of if a VLE correlation can be used to predict the concentration of the liquid lubricant-refrigerant mixture inside the accumulator using temperature and pressure measurements during system operation.

Martz et al. [46] compared the local composition models based on Wilson [47], Tsuboka and Chao [48], Wang and Chao [49], Heil [50], Renon and Prausnitz [51] and the universal quasi-chemical theory [52] with respect to their applicability to predict VLE for seven refrigerant and lubricant mixtures. Their conclusion is that "the interaction parameters may not be optimal for predicting composition or temperature" and that "purely empirical models ... may be more attractive in some situations". Since the objective is to predict the composition of the liquid refrigerant-lubricant mixture, the following empirical models are considered: Grebner and Crawford [53], Thome [45] and Seeton and Hrnjak [28]. Raoult's law is applicable for an ideal liq-

uid mixture in equilibrium with an ideal gas. The assumption that the vapor phase behaves as an ideal gas makes Raoult's Law not suitable for high-pressure systems as it is the case here. For comparison reasons, however, Raoult's law is included in Figure 6.10, which shows a comparison of the predicted vapor pressure versus the concentration of R134a by mass evaluated at 20°C. The concentration of R134a by mass, w, in the liquid mixture of R134a and PAG 46 lubricant is defined as:

$$w = \frac{m_{R134a,liq}}{m_{R134a,liq} + m_{PAG46}} \rightarrow w = 1 - C_{lub,accu} \tag{6.8}$$

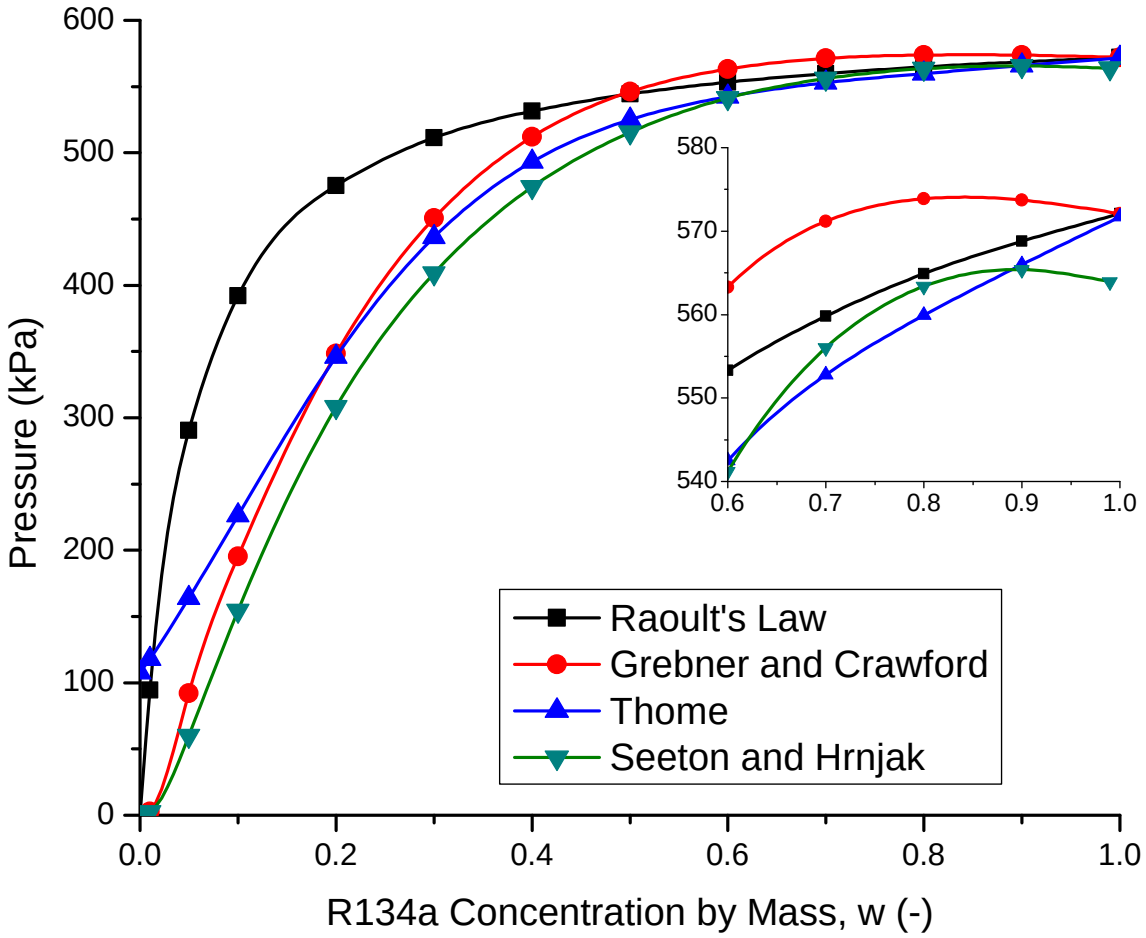

Figure 6.10: Vapor phase equilibrium pressure predictions for R134a-PAG 46 mixture at 20°C

As Figure 6.10 shows the three correlations are similar, but deviate at lower values

of w. Thome [45] uses a comprehensive thermodynamic approach, partly based on the empirical correlation from Takaishi and Oguchi [54]. Their correlation is valid for a concentration range of $0.3 < w < 1.0$, which explains why Thome's approach does not tend towards 0 pressure for $w < 0.2$ in Figure 6.10. Thome [45] argues that 90 percent or more of the evaporator will always have local concentrations of more than $w = 0.5$, and therefore recommends his approach to be used in research and industry. The correlations of Grebner and Crawford [53], and Seeton and Hrnjak [28] are both valid for almost the whole range of w, 0.01 to 1.0, and 0 to 0.99, respectively. Both correlations show a maximum in vapor pressure for large w values. If the mixture of R134a and PAG 46 is assumed to behave as a zeotropic mixture at 20°C, then this maximum is not physical. Because of the maximum, both correlations result in two values for w for the same vapor pressure, which needs to be recognized if these correlations were to be used in a calculation/simulation. In addition, the correlation by Seeton and Hrnjak [28] is the only one which does not converge to the physical boundary condition for $w = 1$—the saturation pressure of pure R134a.

To identify which correlation provides the best prediction for the given refrigerant-lubricant combination, pressure-temperature-concentration measurements were performed. The accumulator was filled with measured quantities of R134a and PAG 46 ranging from 100 g to 380 g, and 50 g to 150 g, respectively. The refrigerant and lubricant was left in the accumulator inside the climate chamber for a minimum of 24 hours—under a controlled temperature condition—to establish a vapor-liquid equilibrium. The temperature of the liquid refrigerant-lubricant mixture was measured by an immersed thermocouple, and the pressure of the refrigerant in the vapor phase was determined using a pressure transducer. The amount of vapor mass within the volume of the accumulator section was determined by using EES [31] property data to determine the R134a vapor density, and the equation provided by Seeton and Hrnjak [28] to determine the liquid refrigerant-lubricant mixture density. The con-

centration of R134a by mass in the liquid mixture, w, was determined using iteration, since the volume of the accumulator section, the masses of R134a and lubricant, and pressure and temperature are known. The concentration of R134a by mass in the liquid mixture, w, is defined by Equation (6.8) as the ratio of the R134a in the liquid mixture to the total mass of the liquid mixture. Table 6.4 compares the measurement results of temperature, pressure and concentration to the predictions based on the three different correlations.

Table 6.4: Comparison of concentration predictions

T (°C)	P (kPa)	w[1] (-)	Seeton and Hrnjak [28]	Thome [45]	Grebner and Crawford [53]
21.3	588.3	0.87	0.87	0.88	0.62
21.5	583.2	0.73	0.71	0.75	0.55
19.4	540.1	0.70	0.65	0.66	0.52
20.9	569.7	0.69	0.68	0.72	0.54
20.4	526.2	0.49	0.52	0.49	0.42
20.4	491.5	0.40	0.42	0.38	0.35
19.3	448.6	0.34	0.37	0.33	0.31

[1] Measurement uncertainty: w $< \pm 0.005$

The correlations by Seeton and Hrnjak [28] and Thome [45] provide excellent—within ±5 percent—predictions of the measured concentration w. An under prediction of the concentration is observed for the correlation based on Grebner and Crawford [53]. A possible explanation for this deviation could be the advancements in engineering more chemically stable, so called "end-capped", PAG lubricants compared to the PAG lubricant Grebner and Crawford investigated in 1992. Since the correlation by Seeton and Hrnjak [28] is applicable over almost the whole range of concentrations, and the correlation by Thome [45] is questionable for concentrations lower than 0.3, it is concluded that the correlation provided by Seeton and Hrnjak [28] is the best choice to predict the VLE concentrations of R134a and PAG 46 lubricant

under equilibrium conditions.

The question remains if the refrigerant-lubricant mixture inside the accumulator can be treated as a mixture in equilibrium at steady state operating conditions. If the answer were "Yes", VLE correlations can be incorporated into accumulator model calculations to account for the affect of lubricant on the refrigerant charge hold-up inside the accumulator. The refrigerant mass and lubricant mass inside the accumulator were measured at steady state operating conditions and different total refrigerant masses as shown in Table 6.5. The concentration of R134a by mass in the liquid mixture, w, was calculated using EES [31] property data to determine the R134a vapor density and the equation provided by Seeton and Hrnjak [28] to determine the liquid refrigerant-lubricant mixture density. For the studied breadboard system, the pressure at the inlet and exit of the accumulator were measured, but not inside the accumulator. The concentration of R134a by mass in the liquid mixture is different if the exit pressure and temperature—first listed values in Table 6.5—are used compared to the inlet pressure and temperature. However, the difference in w—calculated using either the inlet or exit pressures and temperatures—is an order of magnitude lower than the resulting measurement uncertainty and therefore only one value for w is listed in Table 6.5 for each condition.

The equilibrium temperatures at the inlet and exit of the accumulator were calculated using the VLE equation from Seeton and Hrnjak [28] and the values of w from Table 6.5, and inlet and exit pressures. In Figure 6.11 the solid lines are lines of constant w values. Since the w values are determined from measurements, the dotted lines correspond to the measurement uncertainty corresponding to the range shown in Table 6.5 in the last column. The inlet and exit pressure and temperature measurements are plotted with their respective measurement uncertainties. For the I35-wet experiment presented in Figure 6.11b, the temperature of the liquid refrigerant-lubricant mixture inside the accumulator was measured with an immersed

Table 6.5: Steady state measurements of refrigerant-lubricant concentration in accumulator

Condition	Lubricant	Refrigerant	Pressure	Temperature	w
	g	g	kPa	°C	-
Uncertainty	±0.61	±10	±3.45	±0.5	
I35-dry 1000g	119.9	197.1	329	5.0	0.60±0.028
			350	5.5	
I35-dry 1250g	139.2	405.4	337	4.3	0.74±0.010
			357	5.5	
I35-dry 1500g	162.2	669.4	341	4.4	0.80±0.006
			360	5.7	
I35-wet 1000g	133.6	116.7	370	10.8	0.41±0.054
			400	11.6	

thermocouple. This measurement was not available for the measurements shown in Figure 6.11a.

The exit temperatures—marked B in Figure 6.11—are consistently lower than the inlet temperatures as expected since there is a pressure drop across the accumulator which causes a decrease in saturation temperature. However, for the I35-wet condition, Figure 6.11b, the immersed thermocouple read a 2°C higher temperature for the liquid refrigerant-lubricant mixture compared to the inlet or exit temperatures—consistently observed for eight other measurements at the same operating conditions. The heat transfer from the environment to the accumulator explains the higher temperature. Water condensation was observed on the outside of the accumulator during the I35-wet steady state operating condition. The retention time of the refrigerant in the vapor phase inside the accumulator is one second—the retention time of the liquid phase refrigerant is 200 seconds. The longer retention time of the liquid phase refrigerant explain its higher temperature. The temperature intersects the line of the constant w value in Figure 6.11b in between the inlet and exit pressure and therefore

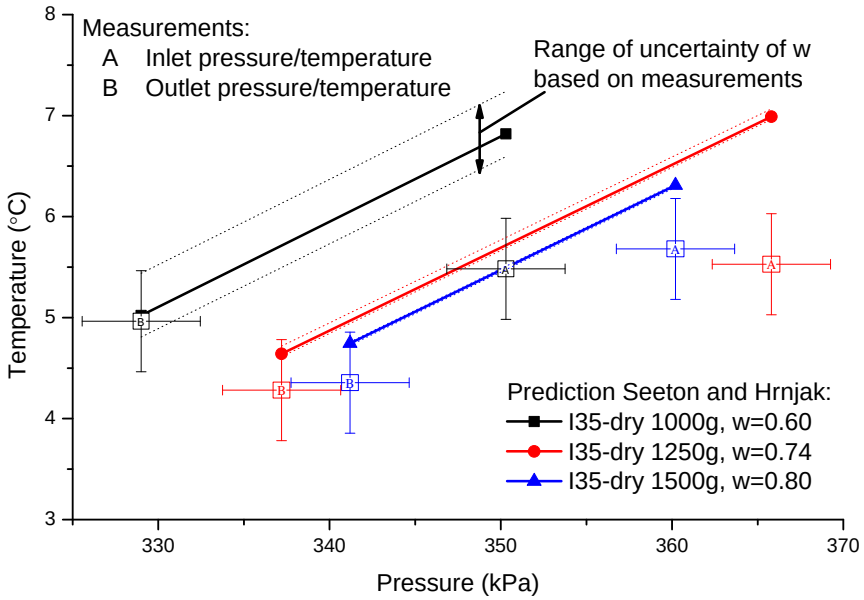

(a) Dry condition

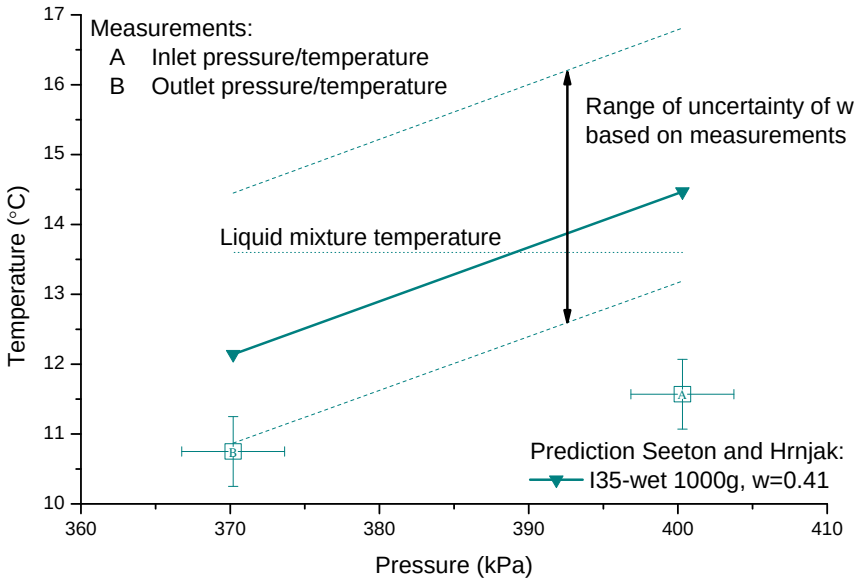

(b) Wet condition

Figure 6.11: Graphs to evaluate if inlet and exit conditions at accumulator can be used to predict concentration of liquid refrigerant-lubricant mixture

could indicate that the assumption of VLE inside the accumulator is valid.

Conclusive evidence if the refrigerant-lubricant mixture inside the accumulator can be treated as a mixture in equilibrium at steady state operating conditions cannot be derived from the presented data and further research is needed. The data shows

that the inlet and exit temperature and pressure measurements alone cannot be used in combination with a VLE equation to determine the concentration of R134a in the liquid refrigerant-lubricant mixture inside the accumulator under steady state operating conditions.

6.2.4 Condenser Model - Predicting Charge Inventory

Heat exchanger designers want to use models in order to accurately predict the performance of a certain design. Their objective is to achieve a given heat transfer rate while optimizing parameters such as pressure drop, heat exchanger size and weight. Two types of models are used—dynamic and steady state. Dynamic models are used to predict the dynamic response of a heat exchanger design at varying boundary conditions, e.g., changes in air and refrigerant mass flow rates. To achieve acceptable computation times and convergence, these models use more restrictive assumptions, e.g., constant two phase heat transfer coefficient or negligible void fraction. Steady state models are chosen to optimize the design of a heat exchanger because they allow more detailed assumptions.

This section investigates how accurately a steady state model of the condenser can predict the experimental data—including the refrigerant mass prediction. For this purpose a one dimensional finite element model of the experimental condenser was developed, and the complete EES-code can be found in Appendix B.2. The condenser model is divided into seven sections: inlet tube, inlet header, first pass, return header, second pass, outlet header, outlet tube. Table A.1 shows an overview of the internal volumes for each of the sections. The inlet and outlet tubes, as well as the headers, are modeled as single volumes and heat transfer and pressure drop were neglected. The first pass contains 31 channels and the second pass 17 channels. Each channel is 1.3 mm heigh and has 12 ports. Based on the given volumes, the resulting hydraulic diameter of one port is 0.9803 mm and therefore the channels can

be classified as minichannels [55]. The first and second pass are each divided into 135 one dimensional elements assuming an equal distribution of the refrigerant mass flow rate across the minichannels and a constant heat transfer coefficient within one element. The geometrical parameters for the multi-louvered fins are given in Table 6.6.

Table 6.6: Geometrical parameters for the multi-louvered fin of the condenser

Parameter	Unit	Value
Louver angle	Degree	28
Louver pitch	m	0.0014
Fin pitch	m	0.001429
Louver length	m	0.009651
Fin thickness	m	0.0001
Tube to tube distance	m	0.008835
Fin depth	m	0.018

To model the heat transfer between the air and the refrigerant the Effectiveness-Number of Transfer Units (ϵ-NTU) method as outlined by [56] was used. This method has been used frequently over the last three decades, e.g. [57, 58, 59, 60, 61]. For the presented case the smaller heat capacity rate, C_{min}—the product of the mass flow rate times the specific heat—is the air side when the refrigerant is present as a single phase fluid. When the refrigerant is present as a two phase fluid the ratio of the heat capacity rates, C_r, is defined as 0. The maximum possible heat transfer in one element is defined as

$$q = \epsilon C_{air} \left(T_{ref,in} - T_{air,in}\right) \tag{6.9}$$

The actual heat transfer rate in one element is given as

$$q = \epsilon C_{air} \left(T_{ref,in} - T_{air,in}\right) \tag{6.10}$$

and the effectiveness is defined as the ratio of the actual to the maximum possible heat transfer.

$$\epsilon = \frac{q}{q_{max}} \tag{6.11}$$

The effectiveness is a function of the NTU and heat capacity ratio. Since the condenser has a cross flow arrangement the effectiveness relation shown in Equation (6.12) is used when the refrigerant has a single phase, otherwise Equation (6.13) is used.

$$\epsilon = 1 - \exp\left[\left(\frac{1}{C_r}\right) \cdot NTU^{0.22} \cdot \left(\exp\left[-C_r \cdot NTU^{0.78}\right] - 1\right)\right] \tag{6.12}$$

$$\epsilon = 1 - \exp\left(-NTU\right) \tag{6.13}$$

The number of heat transfer units is a dimensionless parameter defined as:

$$NTU = \frac{UA}{C_{air}} \tag{6.14}$$

The overall heat transfer coefficient, UA, is defined in terms of the total thermal resistance to the heat transfer between the air and refrigerant.

$$\frac{1}{UA} = \frac{1}{\eta_0 h_{air} A_{air}} + \frac{L_w}{k_w A_{ref}} + \frac{1}{h_{ref} A_{ref}} \tag{6.15}$$

The conductivity of the wall, k_w, is calculated in the model at the average wall temperature. The heat transfer coefficients for the air and the refrigerant side, h_{air} and h_{ref} respectively, are assumed to be constant in an individual element. The air side heat transfer coefficient is calculated using the correlation given by Kim and Bullard [62] to determine the Colburn j-factor, a dimensionless heat transfer coefficient.

$$h_{air} = G \cdot c_p \cdot St \;\text{ where }\; St = j \cdot Pr^{-\frac{2}{3}} \;\text{ and }\; Pr = \frac{\mu c_p}{k} \tag{6.16}$$

In equation (6.16) G is the air mass flux, μ the viscosity of the air and k the thermal conductivity of the air.

To determine the refrigerant side heat transfer coefficient the model distinguishes between single phase and two phase refrigerant. Usually the refrigerant enters a condenser as superheated vapor, condenses, and leaves in a liquid phase. Therefore, a condenser typically has three zones—a desuperheating zone where the refrigerant is a vapor phase, a condensing zone or two phase zone, and a subcool zone where refrigerant is a liquid phase. The subcool zone may not always be present, e.g., if the overall heat transfer is not enough to condense all refrigerant vapor. To account for the different zones the condenser model has two different heat transfer coefficient correlations—one if the refrigerant is present as a single phase, vapor or liquid; and one if the refrigerant is present as two phases. In the single phase region, the heat transfer coefficient is calculated using the Nusselt number correlation of Gnielinski [63]. The friction factor is calculated using the correlation from Churchill [64]. The heat transfer coefficient in the two phase zone is calculated using the correlation presented by Cavallini et al. [65]. Although the correlation is valid for tubes with a diameter larger than 3 mm, Matkovic et al. [66] concluded that there is no significant discrepancy between the measured heat transfer in a minichannel having an internal diameter of 0.96 mm and the predicted heat transfer using models developed for condensation inside macroscale plain tubes.

To calculate the amount of refrigerant mass in a given volume containing both vapor and liquid, the void fraction must also be calculated. The void fraction gives information about the ratio between vapor and liquid phase refrigerant. This ratio can be expressed in different ways, e.g., as volume ratio (volumetric void fraction) or area ratio (cross sectional void fraction). If it is assumed that in a two phase flow the vapor and liquid phases have the same velocity, the void fraction, α, can be expressed

as a function of the quality, x, and vapor and liquid phase densities, ρ_v and ρ_l.

$$\alpha = \frac{1}{1 + \frac{1-x}{x}\frac{\rho_v}{\rho_l}} \tag{6.17}$$

The calculation of the void fraction using Equation (6.17) is referred to as the homogeneous void fraction model since it assumes a homogeneous mixture. However, if the two phases travel at different velocities, the resulting total mass inside a given volume will be different than if calculated based on the homogeneous assumption.

Since, as of today, no comprehensive physical model is available, an appropriate correlation must be chosen to calculate the void fraction. Rice [67] concluded that the choice of a two-phase void fraction model is of major significance in determining the total mass in a condenser. Numerous void fraction correlations are available, e.g., Woldesemayat and Ghajar [68] present 68 different void fraction correlations. As Jassim and Newell [69] point out no void fraction correlation accurately predicts the void fraction for all flow regimes. They make the same argument regarding the prediction of pressure drop. Jassim and Newell [69] present a two phase flow map based on flow regime time fractions which express the probability of encountering a certain flow regime for a given quality. Their approach has the advantage that void fraction and pressure drop correlations can be employed for each flow regime, and are "weighted" by the time fractions and thereby eliminating discontinuities which could arise when correlations are switched. Although the flow regime time fraction constants presented by Jassim and Newell [69] are for a 6-port minichannel and R134a at 10°C—and therefore do not exactly match the parameters and conditions encounter in the experimental condenser—their approach is used in the condenser model to predict the void fraction and pressure drop. The single phase refrigerant pressure drop is determined using the Darcy friction factor calculated for either laminar or turbulent flow conditions. For intermittent and annular two phase flow regime, the pressure

drop correlation from Niño et al. [70] is used. Similar to the heat transfer coefficients, the void fraction and pressure drop are taken as constant across an individual element. Table 6.7 gives an overview of the correlations used in the condenser model.

Table 6.7: Overview of correlations used in condenser model

	Heat Transfer		Pressure drop	Void fraction
Single phase	Gnielinski [63]		Re<2300 $f = \frac{64}{Re}$ Re>2300 $f = \frac{0.3164}{Re^{0.25}}$	
Two phase	Cavallini et al. [65]	Flow map	Jassim and Newell [69]	
		Intermittent flow	Niño et al. [70]	Armand [71]
		Annular flow	Niño et al. [70]	Niño [72]

Condenser Model Results

Experimental data regarding the condenser is available for five different operating conditions (see Table 5.1 on page 68) and from the charge determination tests. The following experimental parameters were used as input parameters for the condenser model—air inlet temperature, air mass flow rate, refrigerant inlet temperature, refrigerant inlet pressure, and refrigerant mass flow rate. Figure 6.12 presents comparisons between the experimental data and model prediction for the overall heat transfer, refrigerant outlet temperature, pressure drop, and mass inventory.

As Figure 6.12a shows, the condenser model predicts the overall heat transfer within ±10% and therefore has an excellent agreement with the experimental values. Figure 6.12b compares the predicted refrigerant outlet temperatures. Overall the model prediction is within ±5°C, tending to predict a higher outlet temperature. The prediction of the refrigerant outlet temperature can be significant regarding the prediction of the refrigerant inventory. If the predicted outlet temperature is too high such that the refrigerant is not subcooled at the condenser outlet, less refrigerant mass

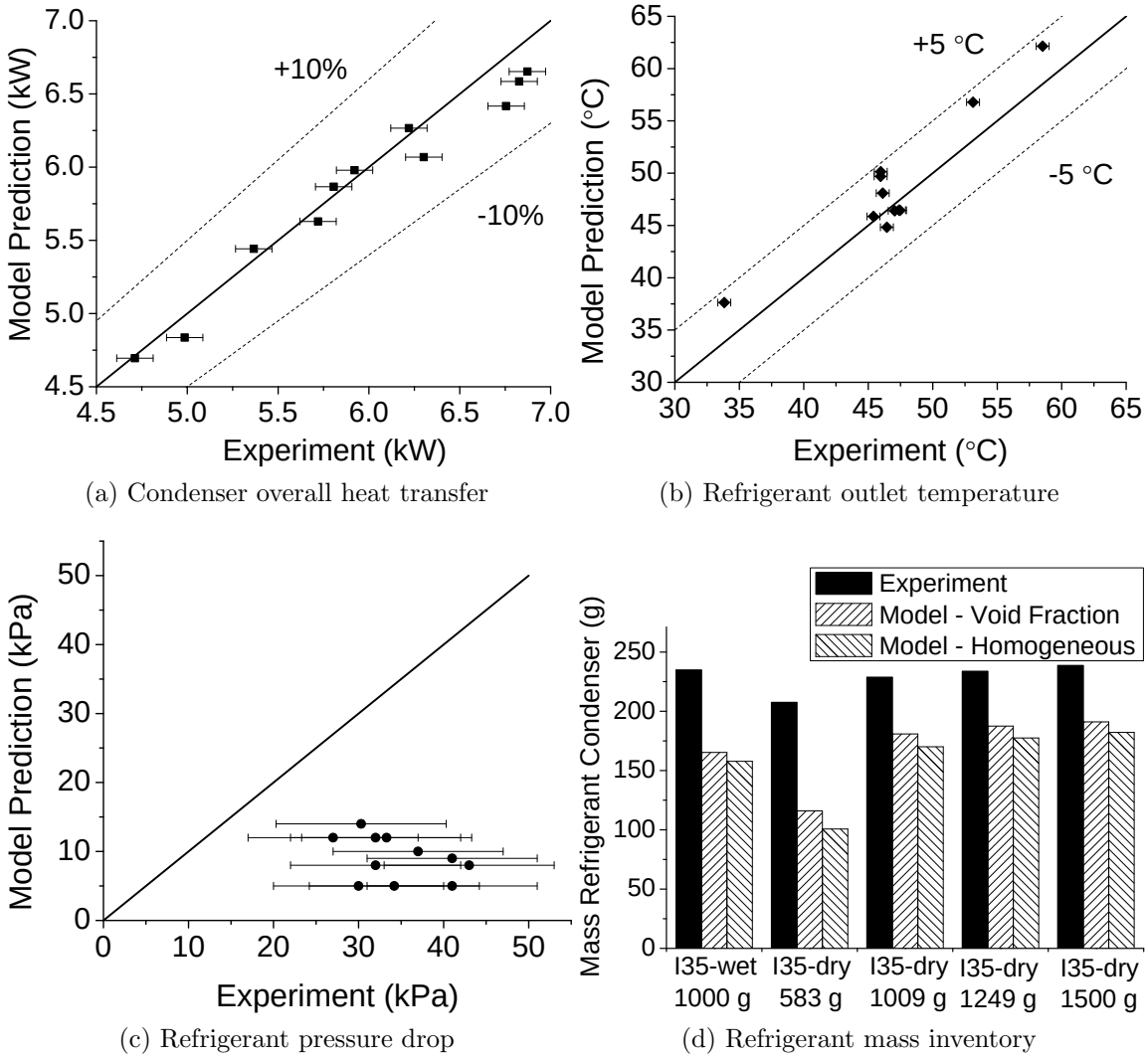

(a) Condenser overall heat transfer

(b) Refrigerant outlet temperature

(c) Refrigerant pressure drop

(d) Refrigerant mass inventory

Figure 6.12: Comparisons between condenser model predictions and experimental measurements

would be predicted. However, temperature alone is not sufficient to determine the state of the refrigerant at the outlet, pressure also needs to be considered. Figure 6.12c compares the predicted refrigerant pressure drop to the measured pressure drop. The predicted pressure drop is significantly lower than the measured pressure drop because the pressure drops in the inlet and exit tubes to the condenser and headers are not accounted for in the model. To determine the affect of neglecting the pressure drops in the inlet and exit tubes, and headers, the condenser model was run using

an imposed linear pressure drop to match the pressure drop of the experiment. The results show that, on average, the predicted overall heat transfer is decreased by 27 W and the refrigerant outlet temperature by 0.3°C for the imposed linear pressure drop. Therefore, the pressure drop prediction—even if more than 50 percent lower—does not significantly affect the prediction of the overall heat transfer.

The mass inventory prediction of the condenser model is compared in Figure 6.12d. Using the mentioned void fraction correlations in combination with the probabilistic flow map shows that 10 g more refrigerant mass is predicted compared to the homogeneous assumption. However, the differences between the experimental results and computational results are significant—the condenser model under predicts the refrigerant inventory by 46 g to 92 g. For the conditions shown in 6.12d, the experimental data had subcooled conditions at the condenser outlet for all cases except the I35-dry 583 g condition. The condenser model also shows subcooled conditions for all cases except for the I35-dry 583 g condition—ruling out that the underprediction of the mass inventory is a result of an inaccurate prediction of the condenser exit condition. This is a remarkable and important result demonstrating that if a model calculation predicts the overall heat transfer within ±10 percent, it does not necessarily predict the refrigerant mass inventory with the same accuracy. In the presented cases, the refrigerant mass inventory prediction is off by 20 to 40 percent. From where does this discrepancy between model prediction and experimental value arise? To answer this question, an additional measurement was necessary to investigate where the refrigerant mass is located inside the actual condenser.

6.2.5 Using Infrared Imaging as a Indirect Method to Determine Refrigerant Mass Distribution in the Condenser

The experimental techniques presented in Chapters 3 and 4 measure the refrigerant and lubricant mass in each section of the system to a high degree of accuracy. However, these techniques do not provide information about how the masses are distributed within a section. Optical methods are one possible approach to determine the refrigerant mass distribution, but are difficult to implement on heat exchangers as a result of their complex geometry and—in case of a condenser—the high temperature and pressure. Infrared imaging measures the surface temperature of an object, and this approach was explored to see if it can give further insight into the refrigerant mass distribution inside the condenser.

The condenser used in the experiments, its header arrangement, and the direction of the air and refrigerant flows is shown in Figure A.1. The infrared camera used for this investigation has a resolution of 240 x 320 pixels and an accuracy of ±2 K. The emissivity was set to 1.0 since the condenser is covered with black paint. The temperature reading of the camera and the temperature reading from several thermocouples where compared and the values were within the uncertainty range. The frontal area of the condenser is 44 x 72 cm. In one frontal picture of the condenser, one pixel represents an area of 1.8 x 2.25 mm. One minichannel, however, has a height of 1.3 mm, and therefore the resolution would not provide sufficient information regarding the frontal surface temperature of the minichannels. For this reason the condenser was divided into a 4 x 3 matrix resulting in 12 infrared pictures assembled into one picture. One pixel then represents an area of 0.6 x 0.6 mm, and at least two pixels—and hence temperature measurements—represent the minichannel frontal surface temperature in the horizontal direction. The infrared picture taken

at the I35-wet condition during steady state operating conditions is shown in Figure 6.13.

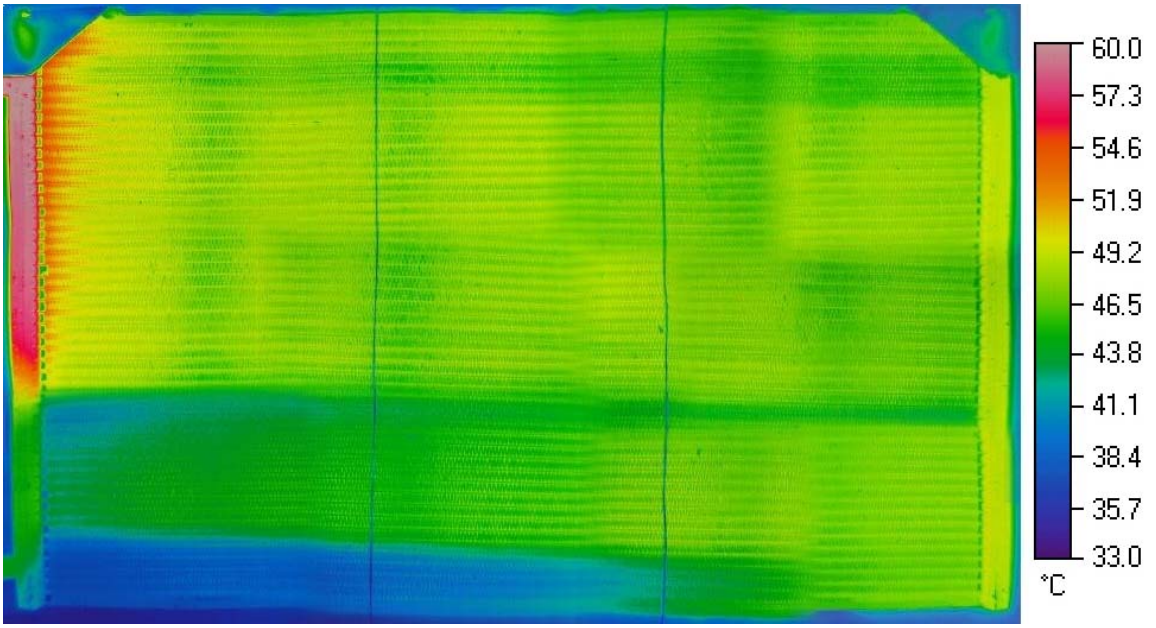

Figure 6.13: Infrared picture of condenser

The infrared camera measures the surface temperature, and therefore it is expected that—as a result of the thermal resistance of the tube material—the temperature reading of the camera is below the actual temperature of the refrigerant inside. Comparing the surface temperatures to the measured temperatures confirmed this expectation. The refrigerant enters the condenser as superheated vapor, at a temperature of 65°C based on an immersed thermocouple measurement. The infrared picture shows a surface temperature of 60°C at the surface of the inlet tube. Based on the pressure measurements the saturation temperature is 52°C. The infrared picture shows that the surface temperature of the return header is 49°C. The refrigerant outlet temperature of the condenser is 46°C measured using an immersed thermocouple. The surface temperature of the outlet tube is 43°C.

The infrared image can be used to identify the three different zones: the desuperheating zone, the two-phase zone and the subcooling zone. In Figure 6.13 a yellow-

ish color of a minichannel represents the presence of two-phase refrigerant. Figure 6.13 also shows subcooling does not start at the same horizontal location for each minichannel in the second pass.

To get a more quantitative result, temperature line profiles along the frontal surface area of three minichannels were determined from the infrared picture. The temperature line profiles start and end at the locations where the minichannels protrude from the headers. Counting the minichannels starting from the top of the condenser, Figure 6.14 shows the temperature profiles of minichannel #11 of the first pass, and minichannels #39 and #44 of the second pass. The profiles are plotted along the length of the minichannels, and the second pass continues at 0.718 m. The temperature of the refrigerant inside the minichannels based on the prediction of the condenser model is also shown in Figure 6.14. The desuperheating zone is relative short, ca. 0.1 m in length from the inlet header based on the temperature profile of minichannel #11. The condenser model prediction matches—showing a length of 0.101 m for the desuperheating zone length. The length of the subcooled zone predicted by the model—0.08 m—does not match with the temperature profiles of minichannel #39 and #44. Accounting for the temperature glide of 1°C as a result of the measured pressure drop, it can be interpreted that subcooling starts at 1.05 m for minichannel #39 resulting in a subcool zone length of 0.39 m. For minichannel #44, an immediate decrease in temperature starting at 0.718 m was observed, and therefore this minichannel might be already filled with liquid refrigerant. The decrease in temperature over the length is steeper compared to minichannel #39 and the lowest temperature is 36°C—close to the air temperature of 35°—indicating the refrigerant mass flow rates are not the same in minchannel #39 and #44. If the refrigerant mass flow rates would be equal in both minichannels, the temperature profiles should be identical. A measurement of the air velocity across the face area of the condenser showed an equal distribution (see Figure A.2 on page 233). Therefore, an uneven air

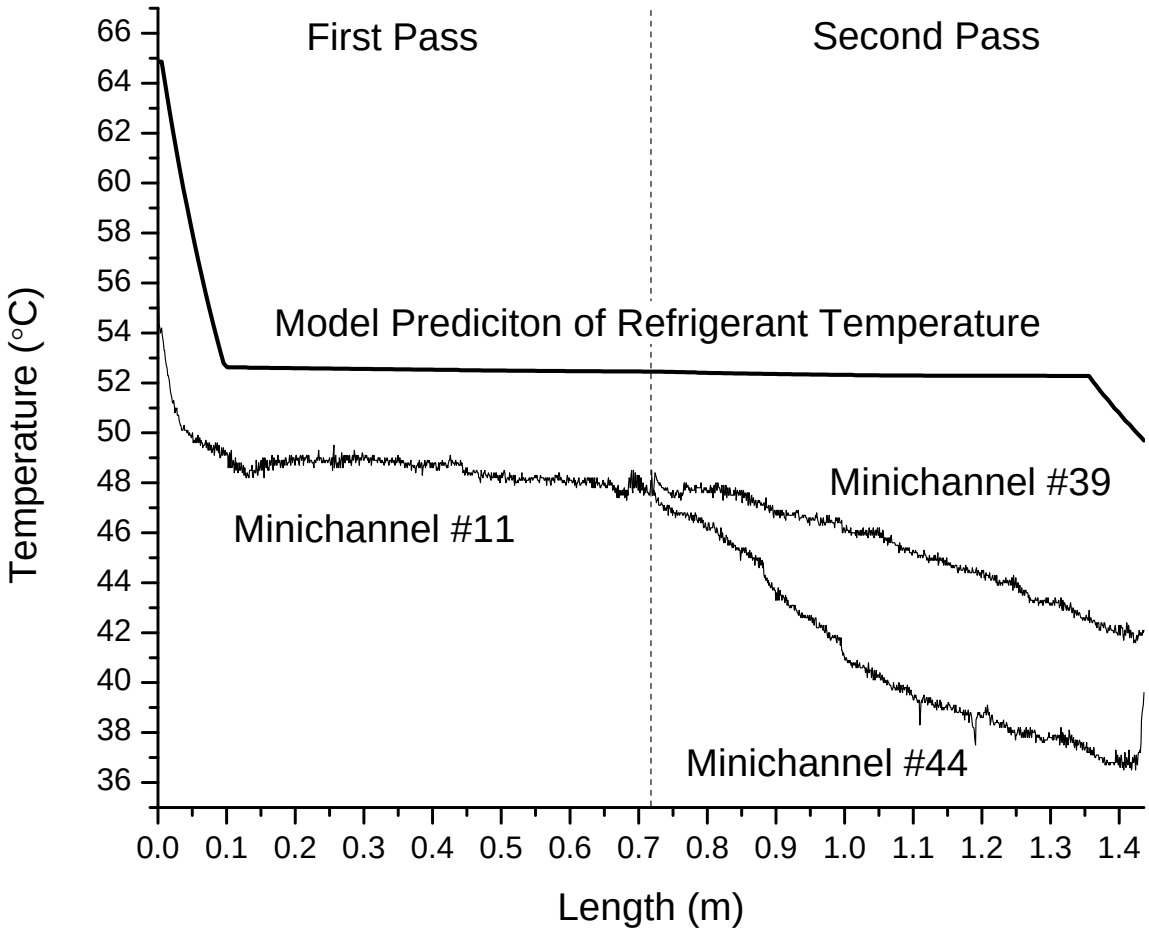

Figure 6.14: Measured surface temperature profiles and predicted refrigerant temperature inside minichannels versus length of condenser

flow rate distribution can be ruled out as a cause for the difference in the surface temperature profiles of minichannel #39 and #44.

To estimate the mass flow rates in the lower seven minichannels, #48 to #42, a control volume was drawn around the exit header as denoted by the dashed rectangle in Figure 6.15. The average inlet temperature for the control volume at location 1 is 45.3°C—determined from the average surface temperature using a line profile along the control volume border. The average surface temperature of the minichannels #48 to #42 is 36°C—which is used as the inlet temperature at location 2. The exit temperature at location 3 is 43.9°C—determined from the average surface temperature using a line profile along the control volume border. The combined mass flow rate of

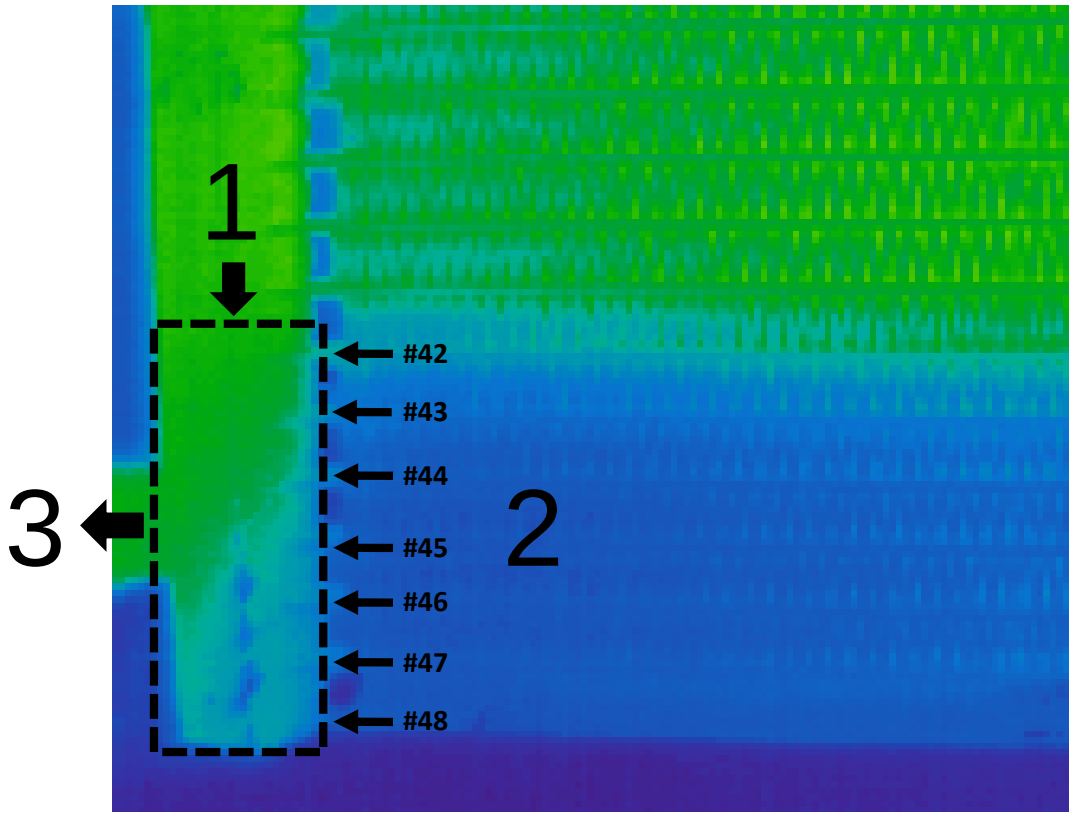

Figure 6.15: Infrared picture of exit header

the seven minichannels, $\dot{m}_2$, is calculated by applying the following mass and energy conservation equations.

$$\dot{m}_3 = \dot{m}_2 + \dot{m}_1 \tag{6.18}$$

$$\dot{m}_3 h_3 = \dot{m}_2 h_2 + \dot{m}_1 h_1 \tag{6.19}$$

The enthalpies, h, in Equation (6.19) were evaluated for R134a at the given surface temperature and measured exit pressure of 1390 kPa—all three locations show subcooled conditions—neglecting any pressure drop. The refrigerant mass flow rate—measured by the mass flow meter—at location 3, $\dot{m}_3$, was 39.5 g/s. Solving equations (6.18) and (6.19) using the given conditions results in a refrigerant mass flow rate of 0.6 g/s for $\dot{m}_2$. Although the calculation was done based on the surface temperatures—which are not identical to the actual refrigerant temperatures—it sup-

ports the assumption that the refrigerant mass flow rates in the lower seven minichannels are greatly reduced.

Combining all the evidence it can be concluded that the lower minichannels have significantly reduced refrigerant mass flow rates resulting in an increased subcooled zone. A longer subcooled zone leads to more refrigerant mass hold up in these channels. A possible explanation could be that in the return header liquid phase refrigerant is separated and—as a result of gravity—liquid accumulates in the bottom part of the return header filling the lower minichannels with liquid refrigerant.

Applying the findings from the infrared picture analysis to the condenser model, the following assumptions were made. First, the lower seven minichannels are filled with liquid phase refrigerant. Second, the lower part of the return header—where the lower seven minichannel connect—is filled with saturated liquid. The results of the prediction of the refrigerant mass inventory in the condenser are shown in Figure 6.16.

The model predictions of the refrigerant mass inventory in the condenser using the homogeneous model to calculate void fraction were 24 to 51 percent below the experimental measurements. By including the void fraction models by Armand [71] and Niño [72] using the probabilistic flow map by Jassim and Newell [69] the refrigerant mass inventory predictions increased between 3 and 7 percent compared to using the homogeneous model. However, the predictions of the refrigerant mass inventory were still below the experimental measurements by 20 to 44 percent. Applying the assumption of liquid filled minichannels in the lower part of the condenser, improved the refrigerant mass inventory prediction significantly. The model predictions were within 10 percent compared to the experimental results—except for the I35-dry 583 g condition for which the difference was 20 percent. It should be pointed out that lubricant is not accounted for in the model. Future research should be directed to investigate the effect of lubricant—for miscible refrigerant-lubricant combination—on the refrigerant

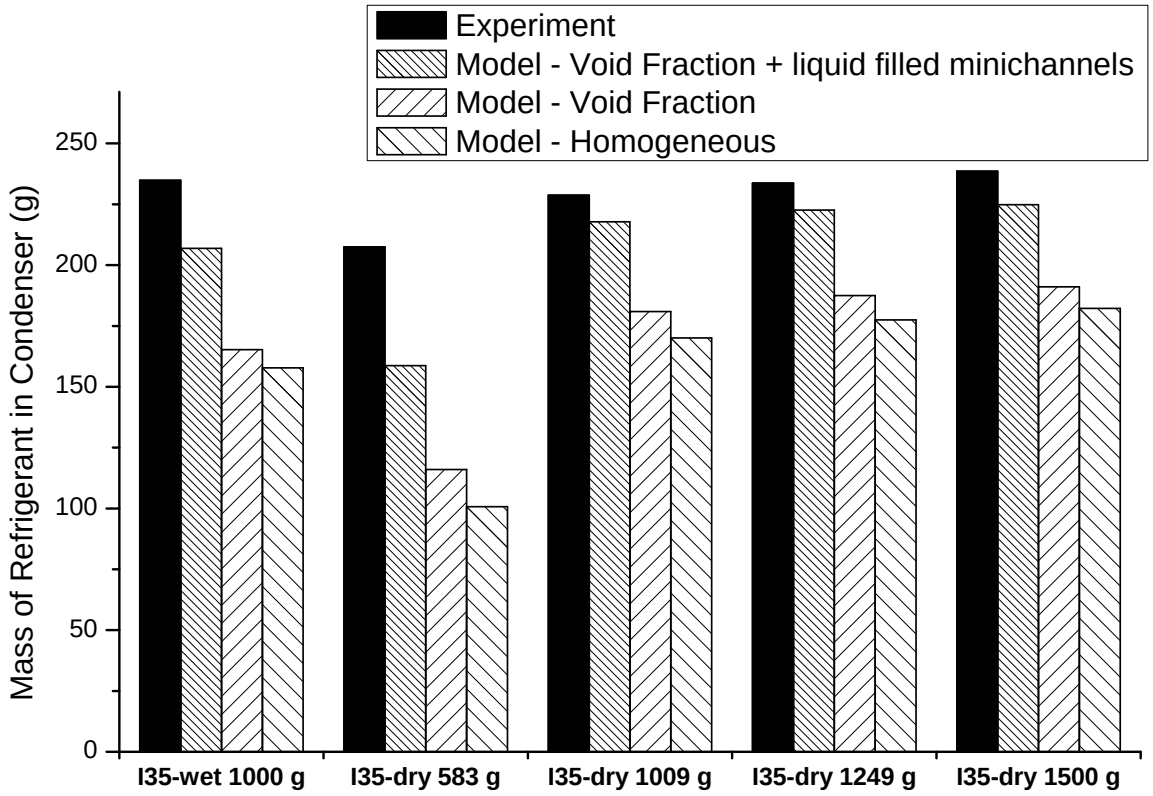

Figure 6.16: Condenser model refrigerant mass inventory prediction

mass hold up during condensation, and the physical mechanisms within the headers, e.g., regarding the separation of liquid and vapor phase refrigerant.

6.3 Transient Cooling Capacity

This section consists of four parts. The first part discusses how transient cooling capacities can objectively be compared between different systems. The second part presents a literature review of curve fits developed for representing the transient cooling capacity. The third part discusses the experimental results of the transient cooling capacities during an on-off cycle under dry operating conditions. A comprehensive curve fit to represent the transient cooling capacity for an off-on cycle is presented. The last section discusses the influence of latent heat transfer—dehumidification at the evaporator—on the transient cooling capacity.

6.3.1 Comparing Transient Cooling Capacities

Comparing the cooling capacities during start-up between refrigeration systems can be difficult as a result of the difference in steady state cooling capacities, e. g., comparing a household refrigerator ($\approx$ 100 W) to an automotive air conditioning system ($\approx$ 5000 W). Even for the same system the steady state cooling capacity can vary depending on the ambient condition making it difficult to analyze the time dependent development. To better compare the dynamic development of the cooling capacity a nondimensional approach is proposed, which scales the transient cooling capacity using the steady state cooling capacity. To illustrate this approach, Figure 6.17 shows a comparison of the start-up development of the cooling capacity for four different systems. The system investigated by Murphy and Goldschmidt [73] is a 10.5 kW residential air conditioner using R22 as a refrigerant. The system of Kim and Bullard [21] is a split air-conditioning system using R410A as refrigerant and has a nominal cooling capacity of 4.13 kW. Peuker and Hrnjak [74] present the start-up cooling capacity for a prototype automotive system using R744 as a refrigerant and for the automotive R134a system described in Chapter 2.3.

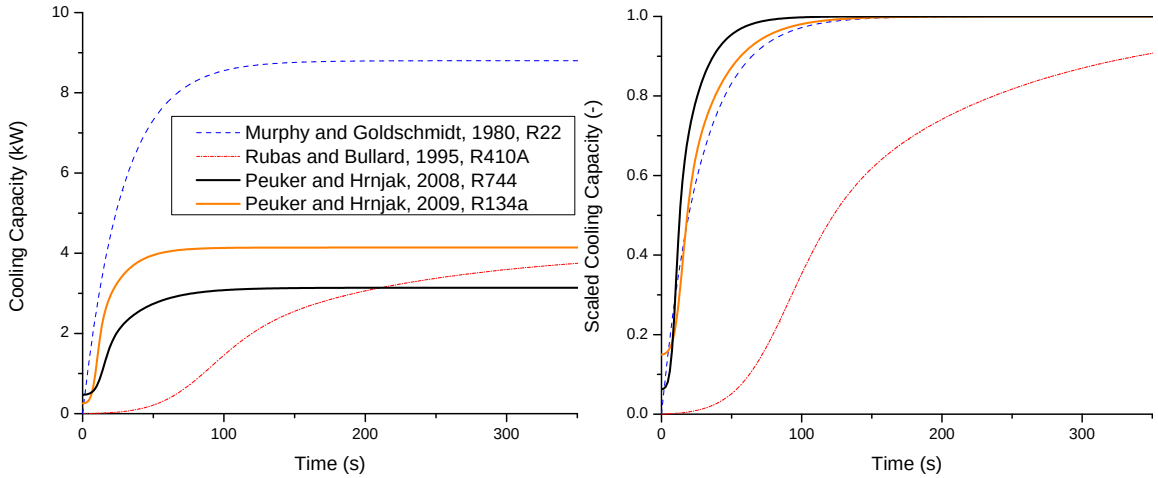

(a) Cooling Capacity (b) Scaled Cooling Capacity

Figure 6.17: Using scaled transient cooling capacity for better comparison of cooling capacity dynamics

From Figure 6.17a it is not readily seen when a system reaches, e.g., 80 percent of its steady state cooling capacity. A nondimensional transient cooling capacity, $\dot{Q}^*(t)$, resulting from dividing the transient cooling capacity, $\dot{Q}(t)$, by the steady state cooling capacity, $\dot{Q}_{ss}$,

$$\dot{Q}^*(t) = \frac{\dot{Q}(t)}{\dot{Q}_{ss}} \tag{6.20}$$

provides a straightforward comparison of the development of the transient cooling capacities. From Figure 6.17b it can readily be determined when a system reaches 80 percent of its steady state cooling capacity—the R744 system reaches 80 percent first.

6.3.2 Literature Review of Curve Fitting Transient Cooling Capacity

The developments of the cooling capacities in Figure 6.17 indicate that the developments are qualitatively similar. Researchers have developed curve fits for the cooling capacity development during start-up condition over the last 30 years and Table 6.8 shows a summary of the historical development. Murphy and Goldschmidt [73] pro-

Table 6.8: History of curve fitting start-up cooling capacity

Publication	Year	Equation
Murphy & Goldschmidt [73]	1980	$\dot{Q}^*(t) = 1 - \exp\left(\frac{-t}{S}\right)$
Mulroy and Didion [9]	1985	$\dot{Q}^*(t) = \left(1 - \exp\left(\frac{-t}{S_1}\right)\right)\left(1 + A\exp\left(\frac{-t}{S_2}\right)\right)$
Kim and Bullard [21]	1995	$\dot{Q}^*(t) = \frac{1-\exp\left(\frac{-t}{S_1}\right)}{1+A\exp\left(\frac{-t}{S_2}\right)}$
Peuker and Hrnjak [74]	2008	$\dot{Q}^*(t) = \left(1 - \dot{Q}^*\vert_{t=0}\right)\left(\frac{1-\exp\left(\frac{-t}{S_1}\right)}{1+A\exp\left(\frac{-t}{S_2}\right)}\right) + \dot{Q}^*\vert_{t=0}$

posed an exponential curve fit for the transient start-up cooling capacity using a single time constant. Mulroy and Didion [9] tried to link the single time constant

to the physical quantities of the evaporator—namely the evaporator coil mass, the UA value determined from the steady state cooling capacity, and the temperature difference between the air and refrigerant saturation temperatures. Their conclusion, however, was that a single time constant curve fit is not sufficient, and therefore proposed a new curve fit based on a product of two exponential functions having two time constants and one additional constant. All constants, however, are purely curve fitting constants and are not tight to any physical quantity. Kim and Bullard [21] improved the curve fitting equation further by using a division of two exponential functions. The equation provided an excellent fit (root mean square value of 0.998) to their transient start-up cooling capacity. Peuker and Hrnjak [74] modified the equation by Kim and Bullard [21] to account for a possible residual cooling capacity at start-up. They showed that the equation provides an excellent fit for the start-up cooling capacity of an R744 and R134a automotive system (root mean square value of 0.998 and 0.997, respectively).

The conclusion from these investigations is that the qualitative development of the cooling capacity at start-up is not a function of the refrigerant. Comparing the systems for which the curve fit based on Kim and Bullard [21] provides excellent fits, the following similarities are found, providing some conditions which should be met to apply the equation to other systems:

- The system has a fixed expansion valve setting or capillary tube.
- When the compressor is turned on it reaches its target speed linearly.
- The air flow rates are fixed during start-up.
- The ambient condition does not change during start-up.

6.3.3 Transient Cooling Capacity Without Latent Heat Transfer

A comparison of the start-up cooling capacities for the operating conditions at I25-dry, I35-dry and I45-dry (see Table 5.1) is shown in Figure 6.18. The cooling capacities were calculated using the air side measurements. Again, the usefulness of plotting

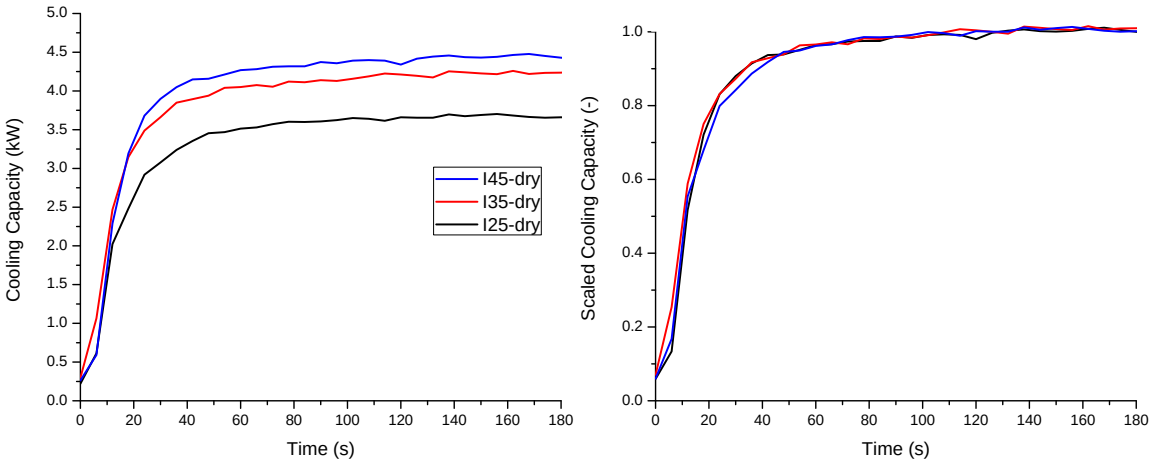

(a) Cooling Capacity (b) Scaled Cooling Capacity

Figure 6.18: Comparing dynamic development of start-up cooling capacity for three different air temperatures

the scaled cooling capacities is apparent. As Figure 6.18b shows, the dynamic development of the cooling capacities are identical although the ambient temperatures differ by 20°C. The ambient temperature, therefore, has little influence on the dynamic development of the cooling capacity. Furthermore, applying the equation from Peuker and Hrnjak [74], it is possible to have one curve fit—valid for air temperatures between 25°C and 45°C—using the curve fitting coefficients shown in Table 6.9. The curve fit provides an excellent fit, it is not plotted in Figure 6.18b since the curve would be on top and therefore indistinguishable from the other curves.

The development of the cooling capacity during the off-cycle period of 180 seconds for the operating conditions at I25-dry, I35-dry and I45-dry is shown in Figure 6.19. The dynamic development of the start-up cooling capacities during the off-cycle time

Table 6.9: Coefficients and goodness of fit for start-up cooling capacity

	$\dot{Q}^*\|_{t=0}$	A	S_1	S_2
	-	-	s	s
Coefficients	0.06773	77.06	15.57	1.534
	I25-dry	I35-dry	I45-dry	
RMS	0.995	0.989	0.994	

are identical as Figure 6.19b demonstrates, and the cooling capacity decays during the off-cycle. Mulroy and Didion [9] use an exponential decay curve fit based on

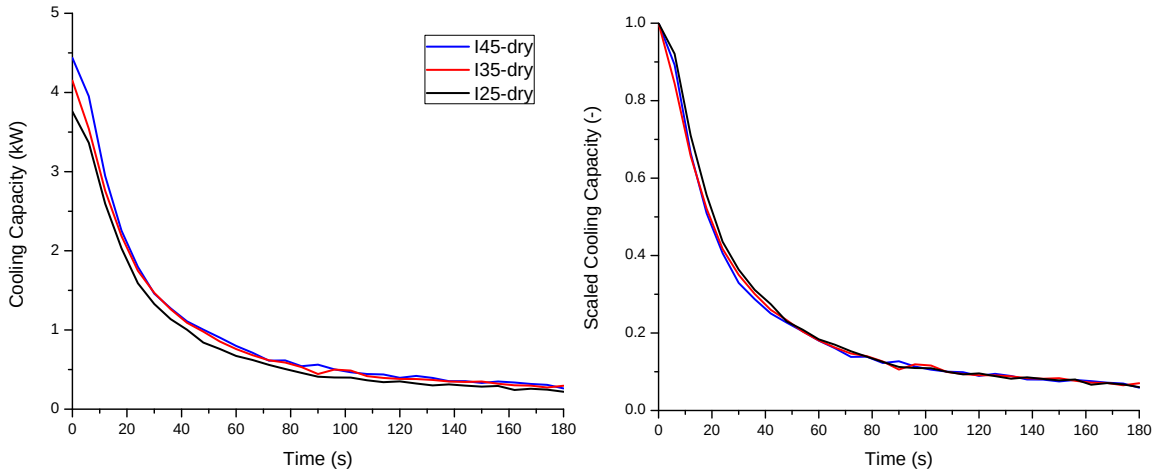

(a) Cooling Capacity (b) Scaled Cooling Capacity

Figure 6.19: Comparing development of off-cycle cooling capacity for three different air temperatures

Equation (6.21) to represent the decaying cooling capacity during the off-cycle.

$$\dot{Q}^*(t) = B \exp\left(\frac{-t}{O_1}\right) \tag{6.21}$$

Fitting Equation (6.21) to the data shown in Figure 6.19b gives B=0.9510 and O_1=36.61 s and a root mean squared value of 0.953. An improved fit for the data

presented in Figure 6.19 can be achieved by using Equation (6.22).

$$\dot{Q}^*(t) = B \exp\left(\frac{-t}{O_1}\right) + (1-B)\exp\left(\frac{-t}{O_2}\right) \tag{6.22}$$

The curve fit coefficients for Equation (6.22) to represent the decaying cooling capacity and the goodness of fit are listed in Table 6.10. Both curve fits can be combined

Table 6.10: Coefficients and goodness of fit for off-cycle cooling capacity

	B	O_1	O_2
	-	s	s
Coefficients	0.8739	24.46	301.1
	I25-dry	I35-dry	I45-dry
RMS	0.994	0.998	0.995

as shown in Equation (6.23) to represent one off-on cycle shown in Figure 6.20. Equation (6.23) is written so that $t = 0$ is the start of the off-cycle and t' is the time when the off-cycle ends. The dotted lines correspond to off-on cycles for which t' is 60, 120, 240 and 300 s.

$$\dot{Q}^*(t) = \begin{cases} B \exp\left(\frac{-t}{O_1}\right) + (1-B)\exp\left(\frac{-t}{O_2}\right) & \text{for off-cycle} \\ \left(1 - \dot{Q}^*|_{t=t'}\right)\left(\frac{1-\exp\left(\frac{t'-t}{S_1}\right)}{1+A\exp\left(\frac{t'-t}{S_2}\right)}\right) + \dot{Q}^*|_{t=t'} & \text{for start-up} \end{cases} \tag{6.23}$$

The practical importance of Equation (6.23) is demonstrated in Figure 6.20. If the steady state capacity is known—by either experiment or steady state simulation—then only one experiment is necessary to determine the curve fit constants. The absolute cooling capacity values are obtained by multiplying the scaled cooling capacity values by the steady state capacity for a given ambient temperature. Engineers can evaluate the transient cooling capacity at different ambient temperatures to find, e. g., the optimum cycle period, without a sophisticated transient simulation model

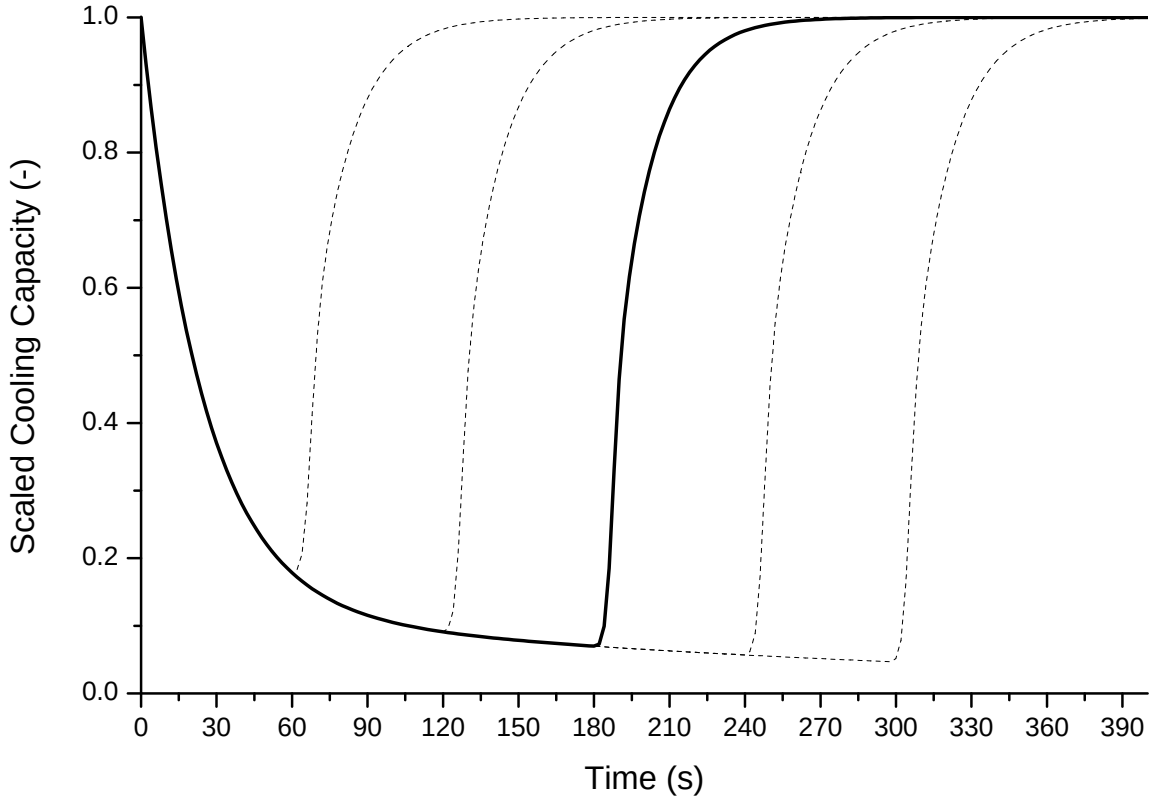

Figure 6.20: Scaled cooling capacity for different off-cycle times based on Equation (6.23)

or an extensive experimental test matrix. For example, Figure 6.20 shows the scaled cooling capacity for five different cycle periods. To experimentally evaluate the transient cooling capacity for these five different cycle periods at three different ambient temperatures would result in 15 experiments. It should be noted, however, that this is only possible for refrigeration systems which met the criteria listed previously on page 137.

6.3.4 Transient Cooling Capacity with Latent Heat Transfer

For the I35-wet operating condition dehumidification occurs and therefore the latent heat transfer at the evaporator needs to be accounted. A steady state energy rate balance, neglecting potential and kinetic energies, can be written for the air flowing across the evaporator coil, as shown in Equation (6.24), to calculate the rate of heat

transfer, $\dot{Q}$, expressed as positive if heat is transferred from the air to the refrigerant.

$$\dot{Q} = (\dot{m}_a h_{a1} + \dot{m}_{v1} h_{v1}) - \dot{m}_{w2} h_{w2} - (\dot{m}_a h_{a2} + \dot{m}_{v2} h_{v2}) \tag{6.24}$$

In Equation (6.24), subscript 1 denotes that properties are evaluated at the inlet air conditions and 2 at the air conditions after the air passed through the evaporator coil. Subscript a denotes dry air properties, v water vapor properties and w condensate properties. The enthalpies, h, are evaluated at the respective inlet and exit air temperatures. The air dew point temperatures at the inlet and exit of the evaporator were measured and therefore the corresponding humidity ratios, ω_1 and ω_2, are calculated as a function of dry bulb temperature, pressure and dew point temperature. The air flow rate is determined using flow nozzles after the evaporator coil and therefore is the sum of the dry air flow rate and water vapor flow rate, $\dot{m}_a + \dot{m}_{v2}$. All other flow rates are determined as shown in Equation (6.25).

$$\dot{m}_a = \frac{(\dot{m}_a + \dot{m}_{v2})}{1 + \omega_2} \quad \dot{m}_{v1} = \omega_1 \dot{m}_a \quad \dot{m}_{w2} = \dot{m}_a (\omega_1 - \omega_2) \quad \dot{m}_{v2} = \omega_2 \dot{m}_a \tag{6.25}$$

The latent and sensible heat transfer rates can be calculated using Equations (6.26) and (6.27), the sum of both are equal to the overall heat transfer rate, $\dot{Q}$.

$$\dot{Q}_{sensible} = \dot{m}_a (h_{a1} - h_{a2}) + \dot{m}_{v2} (h_{v1} - h_{v2}) \tag{6.26}$$

$$\dot{Q}_{latent} = (\dot{m}_{v1} - \dot{m}_{v2}) (h_{v1} - h_w) \tag{6.27}$$

Experimental data was taken every 1.5 seconds and an EES code (see Appendix B.1) was used to calculate the heat transfer rates at each time step using Equations (6.24), (6.26) and (6.27) during an off-on-cycle having a three minute off-cycle period. Figure 6.21a presents the heat transfer rates and Figure 6.21b the dew point

temperatures. The dew point temperatures jump as a result of the dew point sensors

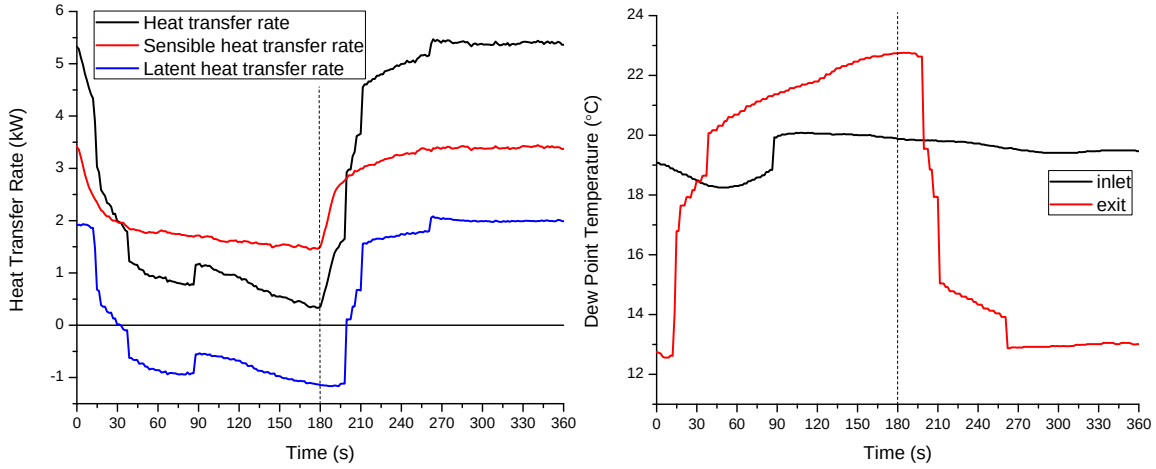

(a) Heat transfer rates (b) Dew point temperatures

Figure 6.21: Dynamic heat transfer rates and dew point temperatures

being used. The chilled mirror dew point sensors have a dew point cooling rate of 1.5°C per second and an update time of one second. In addition, since the sensors are not placed inside the air flow stream, a time delay of one second results as the air passes through the tubing to the sensors. Figure 6.21a shows a delayed reaction of the latent heat transfer rate of 10 seconds at the beginning of the off-cycle—at 0 seconds—and at the beginning of the on cycle—at 180 seconds. Correcting for this delay and applying Equation (6.23) results in Figure 6.22. The solid lines of the sensible and total heat transfer rates are curve fits using Equation (6.23) with the coefficients shown in Table 6.11. The solid line of the latent heat transfer rate is the

Table 6.11: Coefficients used to generate sensible and overall heat transfer rates for Figure 6.22

	B	O_1	O_2	$\dot{Q}^*\|_{t=0}$	A	S_1	S_2
	-	s	s	-	-	s	s
Sensible	0.4382	12.80	671.9	0.4398	15.12	18.6	0.3285
Overall	0.4726	5.024	89.72	0.06605	23.33	13.78	0.4248

difference between total and sensible heat transfer rates. The dashed lines in Figure

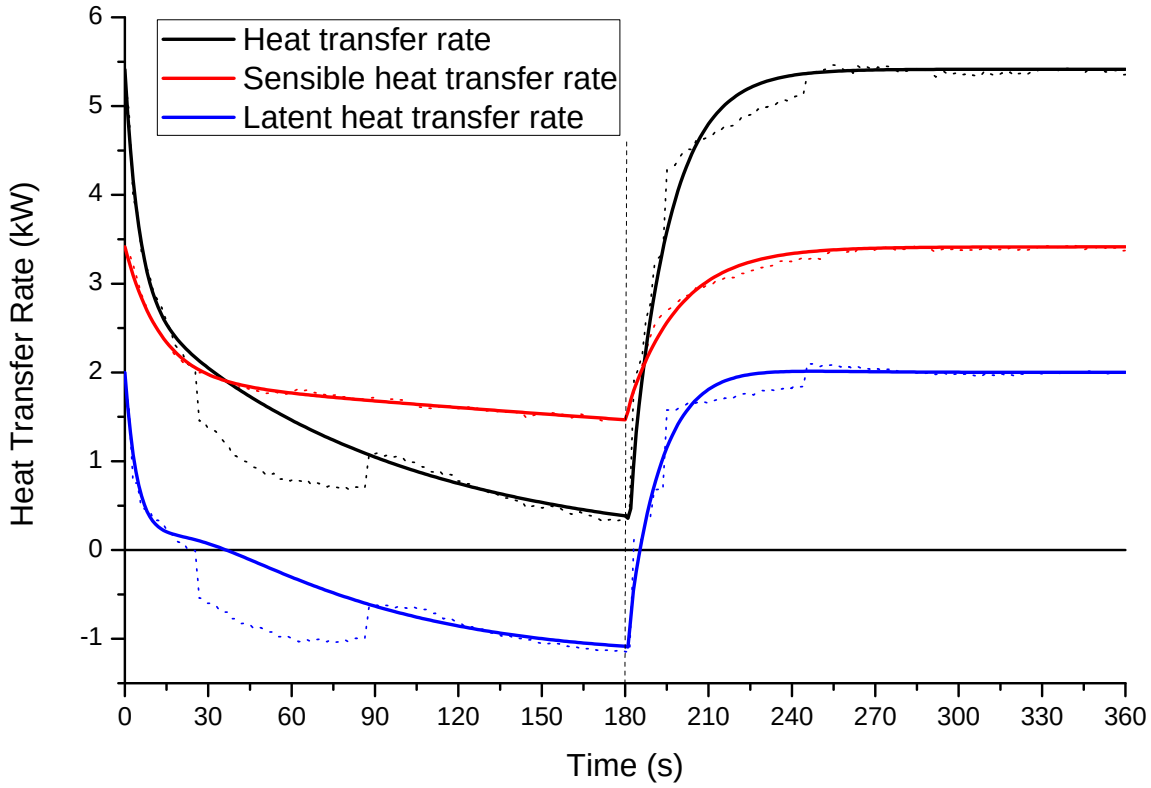

Figure 6.22: Heat transfer rates for off-on cycle for I35-wet condition

6.22 are based on the original measurements without any corrections. As Figure 6.22 demonstrates, the curve fit using Equation (6.23) provides a better representation of the heat transfer rates by smoothing the jumps caused by the dew point sensors and correcting for the tubing time delay.

The development of the latent heat transfer rate shows a reversion in the direction of the heat transfer rate during the off-cycle period. For the first 37 seconds of the off-cycle, the latent heat transfer is positive, and therefore water vapor is still condensing as the air passes through the evaporator coil. After 37 seconds, the latent heat transfer rate is negative and water is evaporating from the surface of the evaporator coil. It should be pointed out that the heat transfer rates in Figure 6.22 are based on the air inlet and outlet conditions. It is possible—and probably most likely—the transition from condensing water vapor to evaporating water on the evaporator coil surface does not happen uniformly in time across the evaporator coil. Some areas might still

condense water vapor, while other areas already evaporate water. These competing effects could explain the shallow gradient of the latent heat transfer rate between 15 and 30 seconds.

The evaporation of the water is dominant after 37 seconds and leads to an evaporative cooling effect. Consequently the air outlet temperature is still 10°C lower than the air inlet temperature 180 seconds into the off-cycle as shown in Figure 6.23. The dry bulb evaporator air exit temperature crosses the evaporator air inlet wet

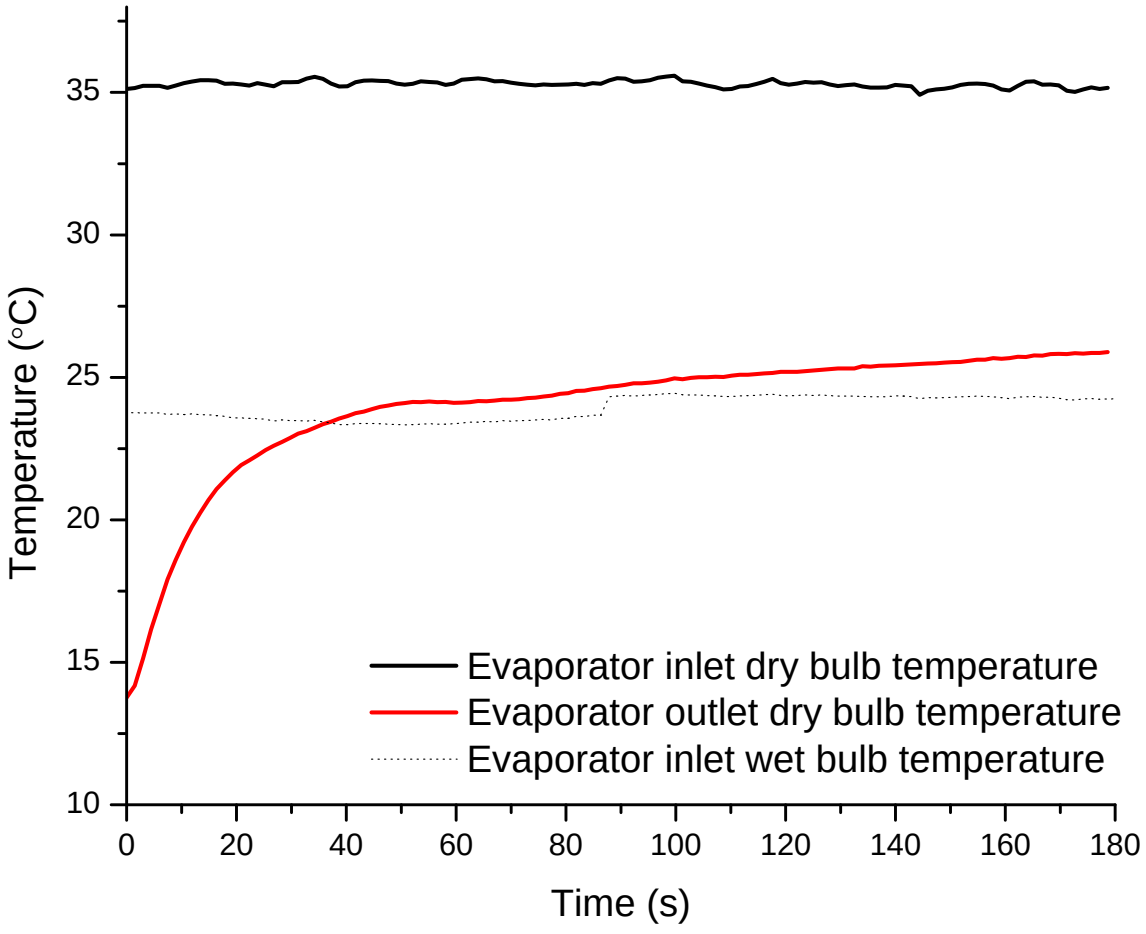

Figure 6.23: Wet bulb and dry bulb air temperatures during off-cycle for I35-wet condition

bulb temperature at 37 seconds and then stays within a couple of degrees of the wet bulb temperature. Since the wet bulb temperature is the lowest temperature that can be reached by the evaporation of water only, the evaporator dry bulb air exit

temperature after time index 37 seconds is another indication of evaporative cooling occurring. Evaporative cooling significantly affects the refrigerant charge migration, and is further investigated in Section 6.4.2.

A question remaining is whether the latent heat transfer and condensed water on the evaporator, have an influence on the transient cooling capacity. To answer this question Figure 6.24 compares the transient cooling capacities (heat transfer rates) for the I35-dry and I35-wet conditions during the off-on-cycle. For the comparison

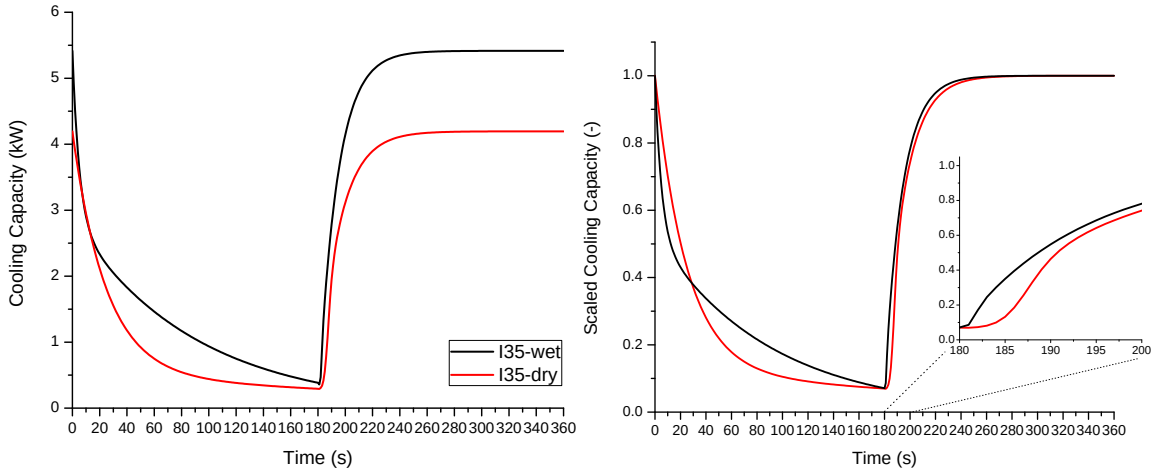

(a) Cooling Capacity (b) Scaled Cooling Capacity

Figure 6.24: Comparing development of cooling capacities for I35-wet and I35-dry operating condition during stop-start event

in Figure 6.24b, curve fits using Equation (6.23) were used. The on-cycle cooling capacity for the I35 wet condition is 5.4 kW and for the I35 dry condition it is 4.2 kW. The difference in cooling capacities makes it difficult to see the difference in the dynamics between the two cases during the on-cycle. Using the scaled cooling capacity approach, as shown in Figure 6.24b, reveals that the start-up development is faster for the I35 wet case during the first ten seconds. After 190 s the difference between the development of the cooling capacities is less than 5 percent and identical after 270 s. The difference of the development of the cooling capacities between the two cases during the off-cycle, however, is larger. The scaled cooling capacity

decreases rapidly for the I35 wet case for the first seconds, but a change in gradient can be observed around 20 seconds. At 30 seconds the scaled cooling capacity for the I35 wet case crosses the I35 dry case, coinciding with the onset of the reversion in latent heat transfer. As a result of the evaporative cooling effect, the overall cooling capacity, Figure 6.24a, is higher throughout the off-cycle for the I35 wet case, but approximates the I35 dry cooling capacity at 180 seconds.

The following conclusions can be drawn. First, the presence of water condensate on the evaporator coil has a strong influence on the cooling capacity during the off-cycle. As a result of the evaporative cooling effect, the cooling capacity decreases less rapidly than without the presence of water condensate on the evaporator. Second, the presence of water condensate on the evaporator coil has a minor effect on the start-up development of the cooling capacity.

6.3.5 Conclusions - Transient Cooling Capacity Investigation

A nondimensional approach was presented which scales the transient cooling capacity using the steady state cooling capacity. This approach allows for a better comparison of the dynamic development of the cooling capacity for different systems. A literature review of equations used to curve fit transient cooling capacity was presented. A comprehensive curve fit, Equation (6.23), was presented which represents the transient cooling capacity during on-off cycling. This curve fit was validated for R410A, R134a and R744 at operating conditions with and without dehumidification. The practical importance of this curve is that it allows engineers to evaluate the transient cooling capacity at different ambient temperatures to find, e. g., the optimum cycle period, without a sophisticated transient simulation model or an extensive experimental test matrix.

Different ambient temperatures do not influence the dynamics of the cooling capacity during on-off cycling. The presence of water condensate on the evaporator coil, however, does change the dynamics of the cooling capacity during the off-cycle. An evaporative cooling effect was observed slowing down the decrease in cooling capacity during the off-cycle. For practical applications it should be kept in mind that the evaporative cooling effect will increase the relative humidity of the air exiting the evaporator which could be perceived as uncomfortable by humans or even be a safety hazard in case of fogging on a vehicle's windshield.

6.4 Refrigerant Migration

The main objective of this dissertation is to provide the scientific community with experimental data regarding the refrigerant and lubricant migration. These experimental data are presented in Chapter 5. The following sections discuss and analyze the experimental results to provide a better understanding of the physics of refrigerant and lubricant migration. As it will be evident, the migration of refrigerant and lubricant during the investigated stop-start scenario is complex and requires measurement techniques in addition to the refrigerant mass measurements. Therefore, besides the refrigerant mass measurements and the basic measurements—temperatures, pressures and mass flow rates—infrared photography, high speed and real time videography are used. As mentioned in Chapter 2.3, the breadboard system has a sight glass installed in the liquid tube and the original accumulator was replaced by a transparent accumulator, and—upstream and downstream of the accumulator—transparent tubes were installed. Figure 6.25 shows a picture of the transparent accumulator section—inlet tube, accumulator, outlet tube—where the rectangles mark the video capturing areas.

For high speed visualization a Vision Research Phantom V4.2 high speed camera

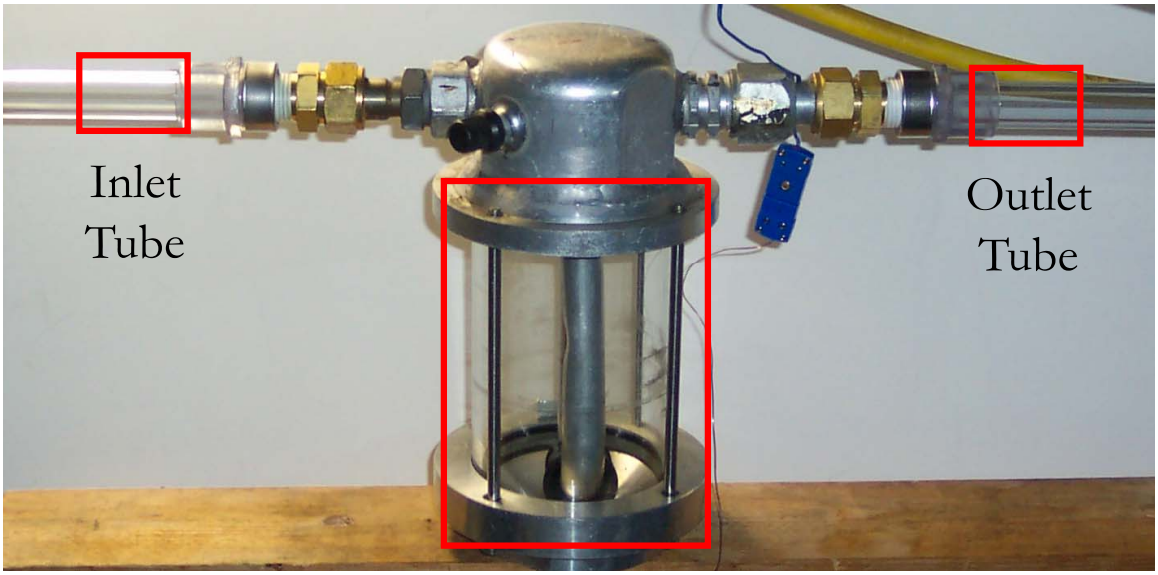

Figure 6.25: Transparent accumulator section with video capturing areas

was used. For real time visualization two Digital Video Camera Recorders—Sony DCR-TRV19 and DCR-TRV130—and a Logitech Quickcam Messenger webcam were used.

This section is divided into four sections—two discuss the refrigerant mass migration during the compressor stop period, and two discuss the refrigerant mass migration during the start-up. For each case—the compressor stop period, and the start-up period—one section discusses the effect the presence of water condensate on the evaporator has on the refrigerant mass migration. It should be noted that the experiments were conducted as one stop-start event and therefore the term "stop period" will be used instead of "off-cycle". The refrigerant and lubricant distribution at the end of the stop period is the initial condition for the start-up. Because of this relation, the reader should read and consider both parts and not treat them as individual unrelated subsections.

6.4.1 Refrigerant Migration During Stop-Period

Two refrigerant mass migration experiments were conducted for a transient event in which only the compressor was stopped for three minutes and then started again. The first experiment was for the I35-dry operating condition and the breadboard system using the original accumulator, and the second experiment was for the I35-wet operating condition and the breadboard system using the transparent accumulator section without desiccant package. A single logical order on how to present a discussion regarding the refrigerant migration results does not exist. The approach taken is to first look at the combined refrigerant masses in the high pressure sections—condenser and liquid tube—and low pressure sections—evaporator and accumulator—and then analyze each section individually. The refrigerant migration results for the I35-dry operating condition are discussed in this Section. Section 6.4.2 compares the results for the I35-dry operating condition to the I35-wet results to determine how the presence of condensate on the evaporator affects the migration of refrigerant mass during the stop period.

As concluded in Section 6.1, the movement of refrigerant mass from the high pressure components to the low pressure components during an off-cycle or compressor stop period happens in two parts—a primary fast migration of the majority of refrigerant mass followed by a secondary slow migration. However, the question of what causes these two different types of refrigerant mass migration has not been answered yet.

The refrigerant mass migration plotted as the sum of the masses in the condenser and liquid tube, and evaporator and accumulator sections is shown in Figure 6.26. In addition, the pressures in the high and low pressure sections are shown. As Figure 6.26 shows the pressure difference across the expansion device is 980 kPa when the compressor is stopped. This pressure gradient induces a mass flow rate of 34 g/s

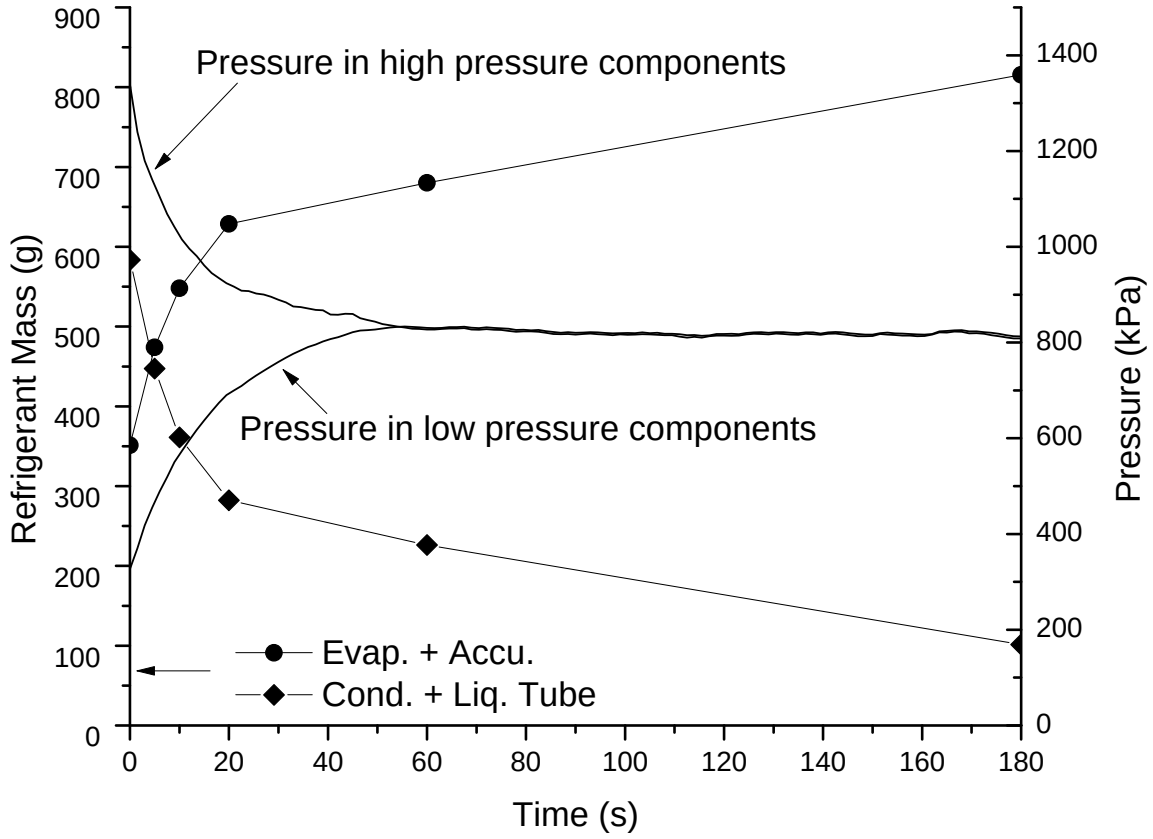

Figure 6.26: Stop period refrigerant mass migration in high and low pressure sections and pressure development

at steady state operation. When the compressor is stopped the pressures begin to equilibrate. However, the pressure gradient does not disappear instantaneously. As Figure 6.26 shows, it takes 54 seconds until the pressure gradient across the expansion valve is below 10 kPa, and both pressures reach an equilibration pressure of 820 kPa. A pressure difference between the high and low pressure components of less than 10 kPa is within the measurement uncertainty of the pressure transducers used, and cannot be detected. Therefore, the term "equilibration pressure" denotes to the pressure when both—the high and low side—pressures have a difference of less than 10 kPa, and should be understood as an apparent pressure equilibration. Figure 6.26 also shows that in the first 20 seconds, 280 g of refrigerant migrates from the condenser and liquid tube sections to the evaporator and accumulator section followed

by another 55 g in the next 40 seconds. Therefore, the primary refrigerant migration is caused by and follows the diminishing pressure difference across the expansion device.

Based on the observation that both pressures reach a value of 820 kPa after 54 seconds, it is expected that the refrigerant mass migration ends at this time. However, the migration of refrigerant mass does not ceases after 54 seconds as Figure 6.26 shows.

To analyze the secondary refrigerant mass migration a look at the data for each individual section is necessary. Figure 6.27 shows the refrigerant mass migration for

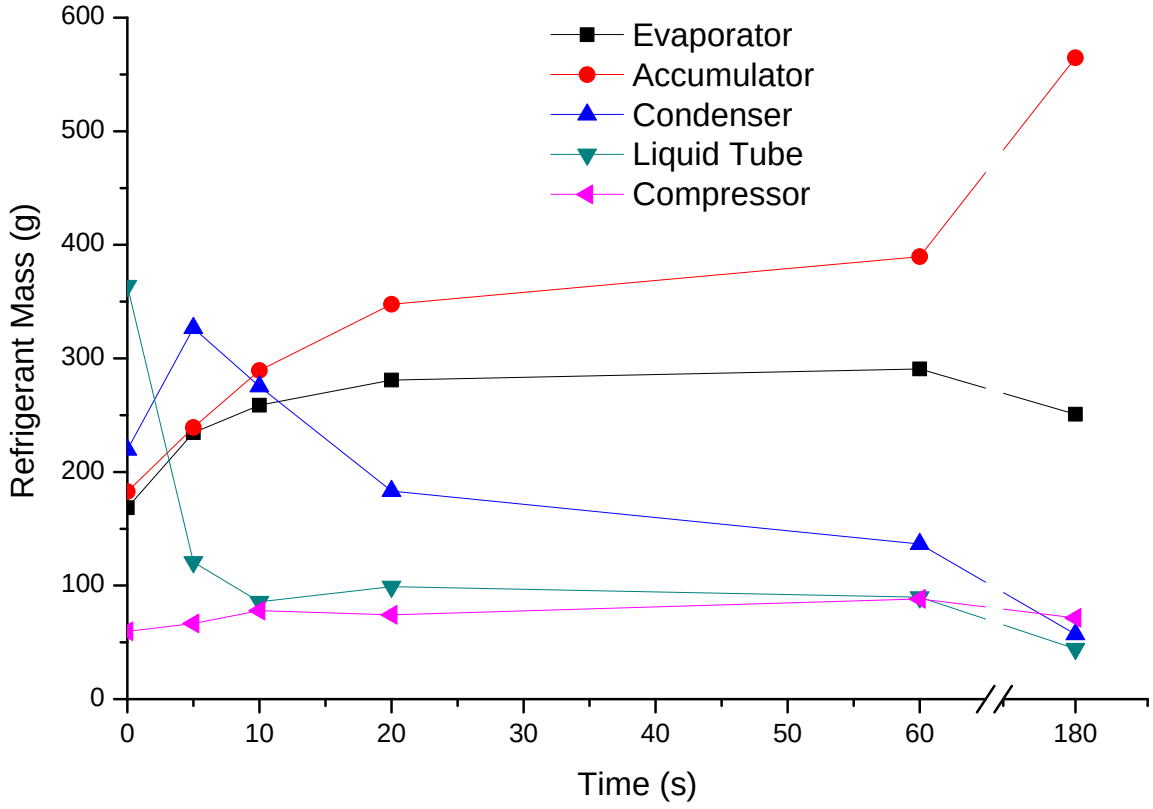

Figure 6.27: Stop period refrigerant mass migration for I35-dry condition

all five sections during the compressor stop period. From 60 to 180 seconds, 175 g of refrigerant migrates from all sections to the accumulator section. The hypothesis to explain this mass migration is that the metal mass and the liquid refrigerant mass inside the accumulator have a lower temperature than the saturation temperature.

Since the air flow rates were maintained at the heat exchangers, their metal mass will reach the ambient temperature quicker than the accumulator. Therefore, while refrigerant evaporates in the heat exchangers, it condenses inside the accumulator at the metal surfaces and at the surface of the liquid refrigerant-lubricant mixture. The condensation of vapor induces a pressure gradient large enough to drive the measured mass migration. The transparent accumulator used for the I35-wet experiment had a thermocouple placed inside the accumulator 1 cm from the bottom. As Figure 5.9b shows, the temperature of the liquid refrigerant inside the accumulator is 17°C below the saturation temperature at 60 seconds and therefore the liquid refrigerant is subcooled. The metal surface temperature of the accumulator was not measured, but the visualization videos do not show evidence of pool boiling inside the accumulator, which would occur if the metal surface temperature were higher than the liquid refrigerant temperature. Therefore, the metal surface inside the accumulator has the same or a colder temperature than the liquid refrigerant. Since the accumulator was exposed to the ambient environment of the indoor climate chamber, there was a free convective heat transfer from the 35°C warm air to the outside metal surface area of the accumulator. This outside convective heat transfer, however, is significantly smaller than the heat transfer inside as a result of vapor condensation inside the accumulator—the convective condensation heat transfer coefficient inside is three to four orders of magnitude larger than the free convective heat transfer coefficient at the outside of the accumulator [56]. All this evidence supports the hypothesis that the secondary refrigerant migration is caused by a pressure gradient as a result of thermal nonequilibrium within the system, and that only vapor phase refrigerant migration occurs.

The previous paragraph showed how the accumulator plays an important role for the secondary refrigerant mass migration. As mentioned earlier, the original accumulator was used for the refrigerant mass migration measurements for the I35-dry

operating condition, but a transparent accumulator section was used for visualization. The stop-start experiment was repeated twice, first using the transparent accumulator including the desiccant package and second after the desiccant package was removed. Real time videos were taken for both cases and snapshots of these videos are presented in Figures 6.28 and 6.29. The images are presented at the same time intervals as the refrigerant mass distribution measurements in Figure 6.27.

(a) 0 s (b) 5 s (c) 10 s

(d) 20 s (e) 60 s (f) 180 s

Figure 6.28: Snapshots of accumulator with desiccant package during stop period for I35-dry condition (arrow indicates liquid level)

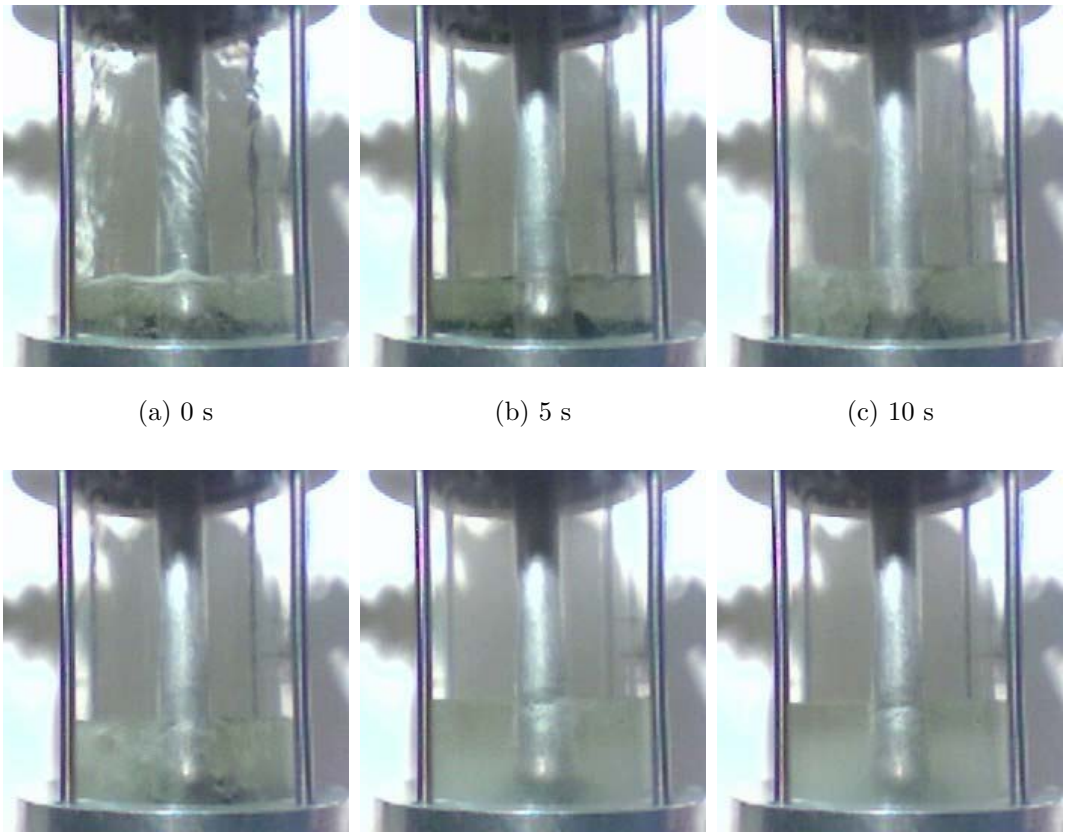

(a) 0 s (b) 5 s (c) 10 s

(d) 20 s (e) 60 s (f) 180 s

Figure 6.29: Snapshots of accumulator without desiccant package during stop period for I35-dry condition

As shown in Chapter 5, the removal of the desiccant package does not introduce a measurable deviation of the refrigerant mass in the accumulator at a steady state operation. Comparing Figures 6.28 and 6.29 shows, however, that the desiccant package increases the height of the liquid column inside the accumulator. The images of the accumulator without the desiccant package show that the liquid column does not seem to change between 60 seconds and 180 seconds. The measurement results show a refrigerant mass increase of 135 g during this time which seems to contradict the visual observation. To explain this contradiction Figures 6.30 and 6.31 show the images of the inlet and outlet tube, respectively.

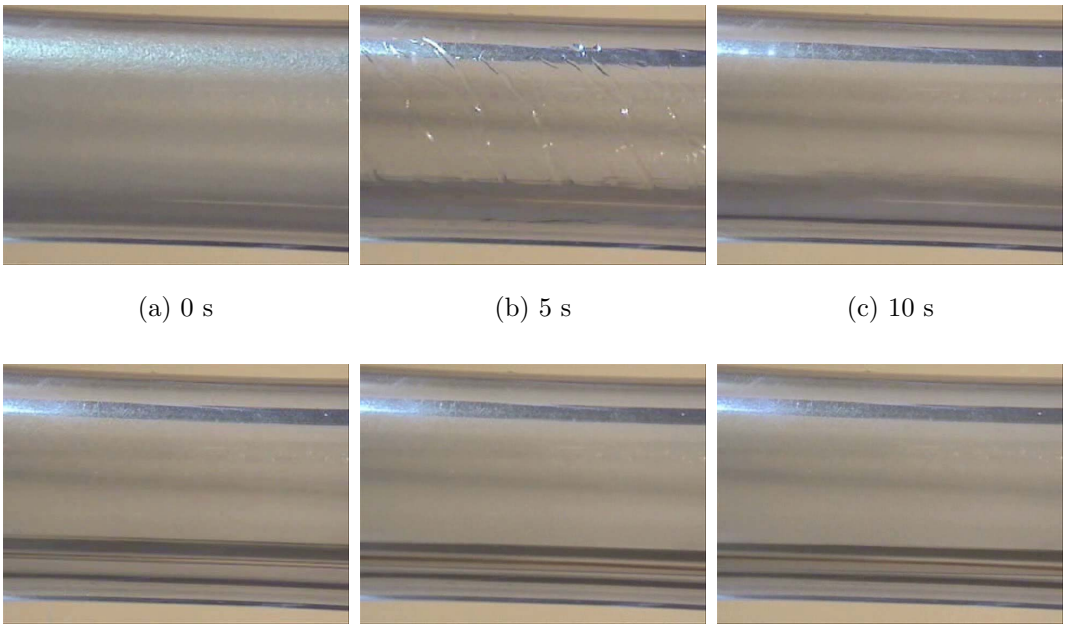

(a) 0 s (b) 5 s (c) 10 s

(d) 20 s (e) 60 s (f) 180 s

Figure 6.30: Snapshots of inlet tube to accumulator during stop period for I35-dry condition

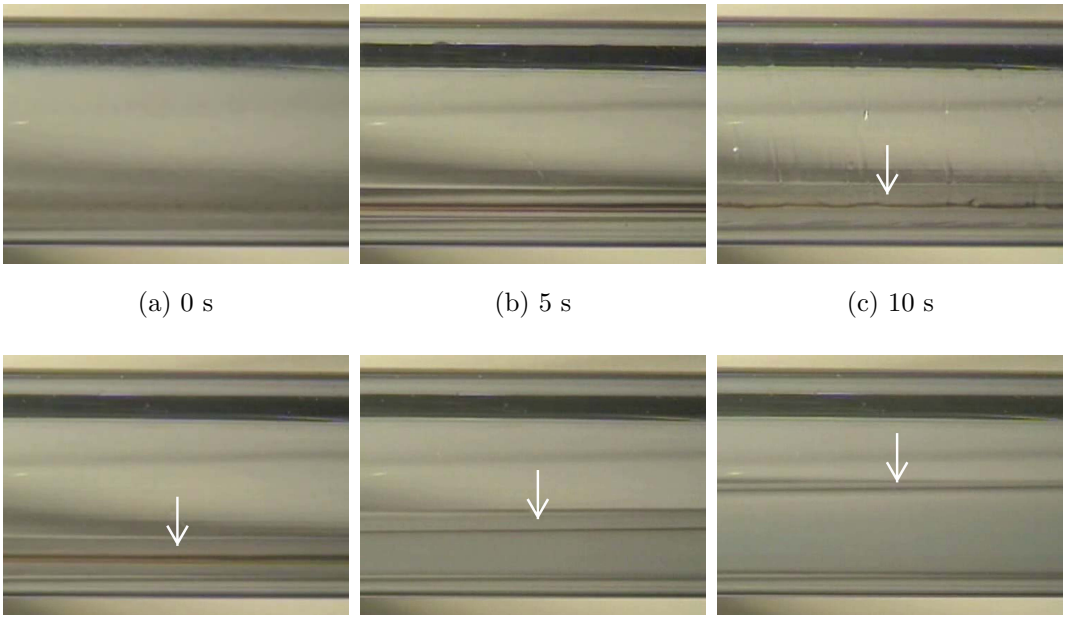

(a) 0 s (b) 5 s (c) 10 s

(d) 20 s (e) 60 s (f) 180 s

Figure 6.31: Snapshots of outlet tube of accumulator during stop period for I35-dry condition (arrow indicates liquid-vapor interface)

The images of the inlet tube show that after the compressor is stopped, the liquid film at the inner surface of the tube breaks down—as shown in Figure 6.30b. The liquid streaks are at an angle indicating flow from left to right, from the evaporator to the accumulator. Although the images do not represent it, the video shows that the amount of liquid at the bottom of the inlet tube decreases until 60 seconds, after which the tube appears to hold no visible liquid anymore. The disappearance of the liquid coincides with the observed pressure equilibration shown in Figure 6.26. This indicates that the 40 g of refrigerant mass leaving the evaporator and entering the accumulator during 60 seconds and 180 seconds had to be in the vapor phase.

The images of the outlet tube show that the liquid film at the inner surface of the tube breaks down—similar to what is observed for the inlet tube—but with a time delay of 5 seconds. The liquid streaks visible in Figure 6.31c are vertical indicating no flow. The video reveals that there is a tendency of some streaks to move to the right indicating minor flow out of the accumulator which ceases visibly after 15 seconds. After 20 seconds, however, liquid flows into the outlet tube from left to right. As Figures 6.31d to 6.31f show the liquid level rises inside the liquid tube. This evidence now explains the contradiction between the accumulator images of Figure 6.29—which indicate no change in liquid level during 60 seconds and 180 seconds—and the measured increase in refrigerant mass by 135 g during this time. Since the outlet tube is part of the accumulator section, the refrigerant mass measurement includes the refrigerant mass inside the outlet tube.

The refrigerant mass inside the compressor section does not increase between 60 seconds and 180 seconds—as shown in Figure 6.27—although liquid was observed in the outlet tube of the accumulator. As shown in Figure 2.4 the original system has an upward bend in the tubing connecting the accumulator and compressor. This upward bend is kept for the breadboard system and prevented that the liquid—visible in the outlet tube—was not drained by gravity into the compressor section during

the compressor stop period.

To understand the physical mechanism by which liquid refrigerant can enter the outlet tube of the accumulator during the compressor stop period, a closer look at the design of the accumulator is necessary. The accumulator used is a U-tube type accumulator. The inlet of the accumulator opens into a vessel at the top to allow a separation of liquid and vapor phase refrigerant. The vapor phase refrigerant exits the accumulator via a tube opening near the top of the accumulator. This tube forms a U-shape at the bottom of the accumulator and exits through the top—shown in the first schematic of Figure 6.32. Any mass leaving the accumulator passes through the U-tube. To avoid separating the lubricant inside the accumulator, the U-tube has a small opening—approximately 1 mm in diameter—at the bottom of the U-bend. This small opening allows the entrainment of the liquid refrigerant-lubricant mixtures and guarantees the return of lubricant to the compressor. Figure 6.32 shows four schematics of the accumulator and U-tube during the stop period. As soon as

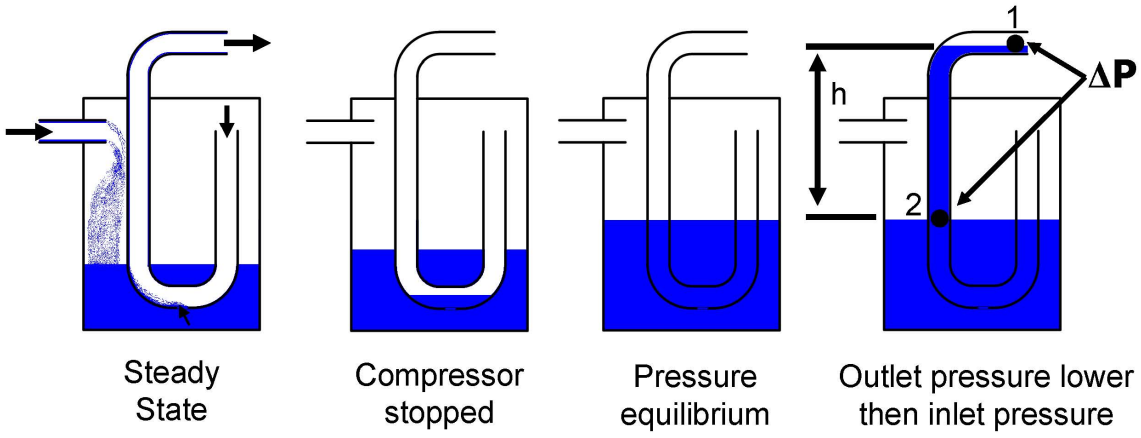

Figure 6.32: Schematic of accumulator during stop period

the compressor is stopped, a liquid refrigerant lubricant mixture starts to fill the U-tube through the small opening at the bottom of the U-tube. A liquid plug can form as soon as the lower U-tube bend is filled. If the inlet pressure and outlet pressure are in equilibrium, both legs of the U-tube will be filled to the same height with

liquid. Assuming the pressure at the outlet of the accumulator is lower than the pressure inside the accumulator, the liquid column in the leg of the U-tube closer to the exit will rise while additional liquid is entering the U-tube through the small hole at the bottom. The liquid column in the U-tube leg with the opening inside the accumulator will remain at the same height as the liquid level inside the vessel, assuming the flow rate through the small hole at the bottom can keep up with the rising liquid column. In order to raise the liquid level to point 1—as shown in the far most right schematic of Figure 6.32—a pressure difference between points 1 and 2 is necessary. An estimation of this pressure difference can be made by assuming a liquid density of $\rho = 1250$ kg/m^3, a height difference of h = 0.12 m and applying Bernoulli's equation between points 1 and 2 using a local acceleration of gravity of g = 9.8 m/s^2:

$$P_2 - P_1 = \rho g h = 1.5\ kPa \tag{6.28}$$

As this estimation shows, only a small pressure difference of 1.5 kPa is necessary to raise the liquid up the U-tube where it then can flow into the horizontal outlet tube. A smaller pressure difference is sufficient if a desiccant package is present since the liquid level inside the accumulator is higher as shown in the snapshot of Figure 6.28f. The accumulator outlet tube filling has a negative effect on the start-up performance, and is discussed in detail in Section 6.6. It is important to note that without visualization of the accumulator section, the described phenomenon would have not been observed.

The refrigerant and air inlet temperatures during the stop period are shown in Figure 6.33, where markers are used to distinguish between the different temperatures. The actual data points were taken every 1.5 seconds and are not shown to maintain readability of the figure. Before taking and analyzing the videos of the transparent accumulator section it was unclear why the thermocouple located between accumulator and compressor—T_{rcpi}—starts to show a lower temperature than

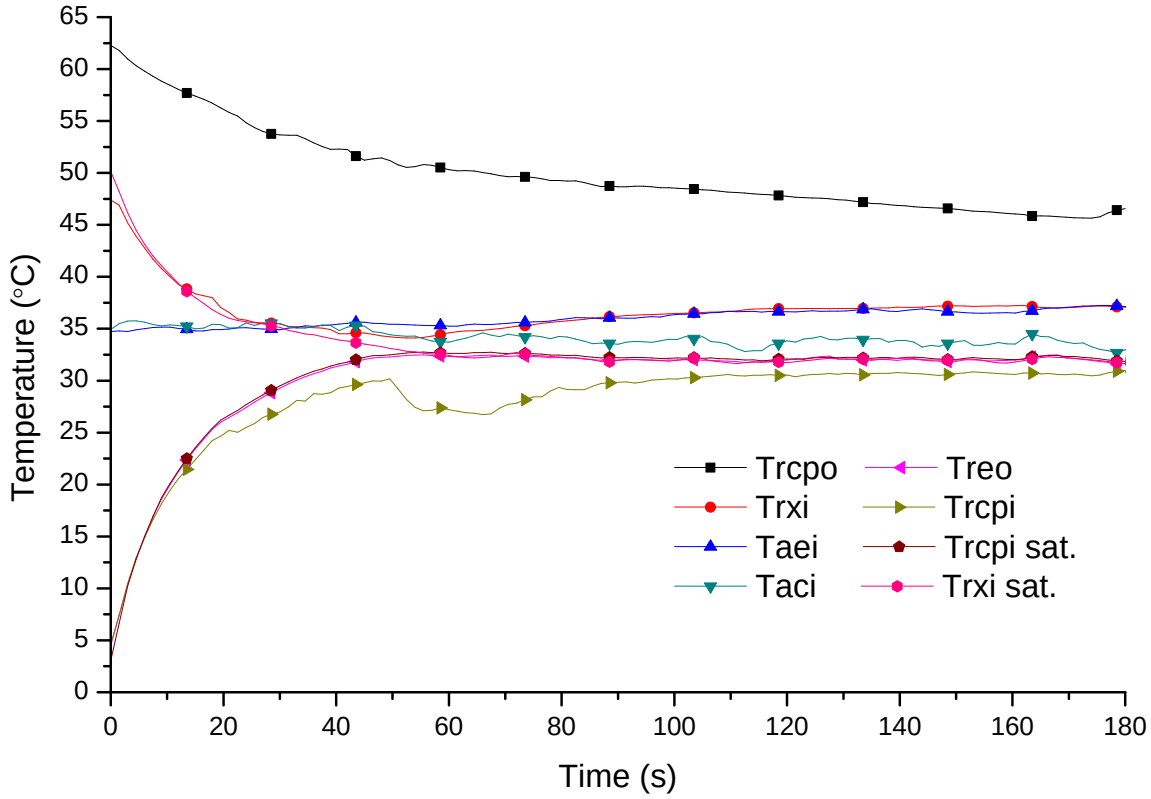

Figure 6.33: Stop period refrigerant temperatures and air inlet temperatures for I35-dry condition

its saturation temperature—$T_{rcpi\ sat.}$—after 20 seconds. The deviation coincides with the observation of liquid draining into the outlet tube of the accumulator. A seal is formed between the liquid plug in the accumulator U-tube and the compressor, and therefore no refrigerant flows across the thermocouple. It is assumed that the liquid draining into the outlet tube is subcooled liquid to explain the below saturation temperature reading.

The hypothesis for the secondary refrigerant mass migration is based on the condensation of vapor inside the accumulator. This requires a flow into the accumulator and—as a result of the liquid plug in the U-tube—this flow can only enter the accumulator from the evaporator side. Furthermore, the hypothesis postulates that only refrigerant in the vapor phase migrates after 60 seconds. The temperature based on the thermocouple located between the evaporator and accumulator—T_{reo}—shows

the same temperature as its saturation temperature—$T_{reo\ sat.}$—during the entire stop period. The temperature measurement alone is not sufficient proof for the presence of only saturated vapor since there could be also saturated liquid present. The visualization of the inlet tube, however, shows that after 60 seconds no liquid is visible inside the tube.

The temperatures upstream—T_{rcpo}—and downstream of the condenser—T_{rxi}—both start to decrease after the compressor is stopped. The temperature upstream of the condenser stays above the saturation temperature—$T_{rxi\ sat.}$—throughout the stop period. The temperature downstream of the condenser is three degrees below the saturation temperature when the compressor is stopped but quickly approaches the saturation temperature within 10 seconds. It follows the saturation temperature, but deviates after 60 seconds and follows the evaporator air inlet temperature. The immersed thermocouple measuring the temperature downstream of the condenser is located inside the evaporator chamber. Since the flow rate after 60 seconds is 1 g/s and the copper liquid tube length inside the evaporator chamber is 1 m, temperature reading follows the evaporator chamber temperature and not the condenser chamber temperature. Figure 6.34 shows snapshots of the video taken of the sight glass located between the condenser and expansion device.

(a) 0 s (b) 5 s (c) 10 s

(d) 20 s (e) 60 s (f) 180 s

Figure 6.34: Snapshots of sight glass between condenser and expansion device during stop period for I35-dry condition

Before the compressor is stopped the sight glass is filled with liquid, except for a small vapor pocket at the top of the sight glass above the tubing entrance/exit. After 10 seconds, only the liquid at the bottom of the sight glass—below the piping entrance/exit—remains as shown in Figure 6.34c. This remaining liquid is the result of liquid pooling below the tube entrance/exit and is an important observation since it demonstrates that liquid can accumulate in convexities during the stop period. During the secondary mass migration—starting after 60 seconds—the liquid in the sight glass gradually evaporates, and after 180 seconds almost no liquid is visible. The bubbles seen in the snapshots indicate the presence of lubricant, since a bubble consisting of a pure liquid is not stable and a dissolved surfactant is needed to stabilize the bubble.

Referring back to Figure 6.27, 279 g of refrigerant leaves the liquid tube during the first 10 seconds. However, Figure 6.26 shows that during the same time only 197 g pass through the expansion device. The difference of 82 g can be explained by focusing on the refrigerant mass in the condenser. Figure 6.27 shows an increase in refrigerant mass in the condenser by 107 g during the first five seconds. Since the compressor mass increases by 7 g, the only possible explanation is that refrigerant mass flows from the liquid tube back to the condenser during the first five seconds. As a result, the liquid tube is "drained" from two sides during this time which explains how 243 g of refrigerant mass left the liquid tube within five seconds.

Since this back flow to the condenser is unprecedented, the following hypothesis was formulated to explain the reversion in the flow direction. As soon as the compressor is turned off, the mass flow rate to the condenser is suddenly stopped. At steady state operating conditions 34 g/s of refrigerant vapor condenses inside the condenser. The condensation, however, does not stop immediately. Without a supply of refrigerant vapor from the compressor, the condensation of the refrigerant vapor inside the condenser leads to a reduction in pressure inside the condenser. This reduction in pressure is assumed to be faster during the first five seconds than the reduction in pressure caused by the expansion device. The resulting pressure gradient is towards the condenser, and because the exit of the condenser is filled with liquid refrigerant, 107 g of refrigerant mass flows back into the condenser. To confirm this hypothesis precise pressure measurements would have to be taken at several locations within the condenser and the liquid tube. Between 10 and 20 seconds the refrigerant mass flow rate leaving the condenser is higher than the mass flow rate leaving the liquid tube through the expansion valve which explains the increase of 13 g after 20 seconds in the liquid tube. The video of the sight glass shows that liquid flows through the sight glass until one minute into the stop period.

The compressor section shows the least change in refrigerant mass of all sections

during the stop period. During the first ten seconds the refrigerant mass increases by 18 g and at 60 seconds the compressor reaches its highest value of 88 g. During the secondary refrigerant mass migration refrigerant evaporates from the liquid refrigerant-lubricant mixture inside the compressor and after 180 s the measured refrigerant mass is 71 g.

6.4.2 Refrigerant Migration During Stop-Period - Effect of Water Condensate on Evaporator

The second refrigerant migration results are for an I35-wet operating condition and the breadboard system using the transparent accumulator section without desiccant package. The same stop-start scenario as for the I35-dry operating condition was used. Therefore, the only difference is the dew point temperature—set to 19.4°C—which corresponds to 40 percent relative humidity at 35°C dry bulb temperature. Running the breadboard system at the steady state I35-wet operating condition resulted in an evaporation saturation temperature of 9°C, and as a result water vapor condensed on the evaporator surface. This section discusses how the presence of water condensate on the evaporator surface influences the refrigerant migration during the compressor stop time.

The refrigerant mass migration plotted as the sum of the masses in the condenser and liquid tube, and evaporator and accumulator sections for both, the I35-dry and I35-wet cases, is shown in Figure 6.35. In addition, the pressures upstream and downstream of the expansion device are shown. The pressure difference across the expansion device is 20 kPa higher for the I35-wet condition when the compressor is stopped at 0 seconds. This is a result of an increase in the absolute pressures of 60 kPa and 80 kPa upstream and downstream of the expansion device, respectively. The measured mass flow rate at steady state operation was 39 g/s for the I35-dry

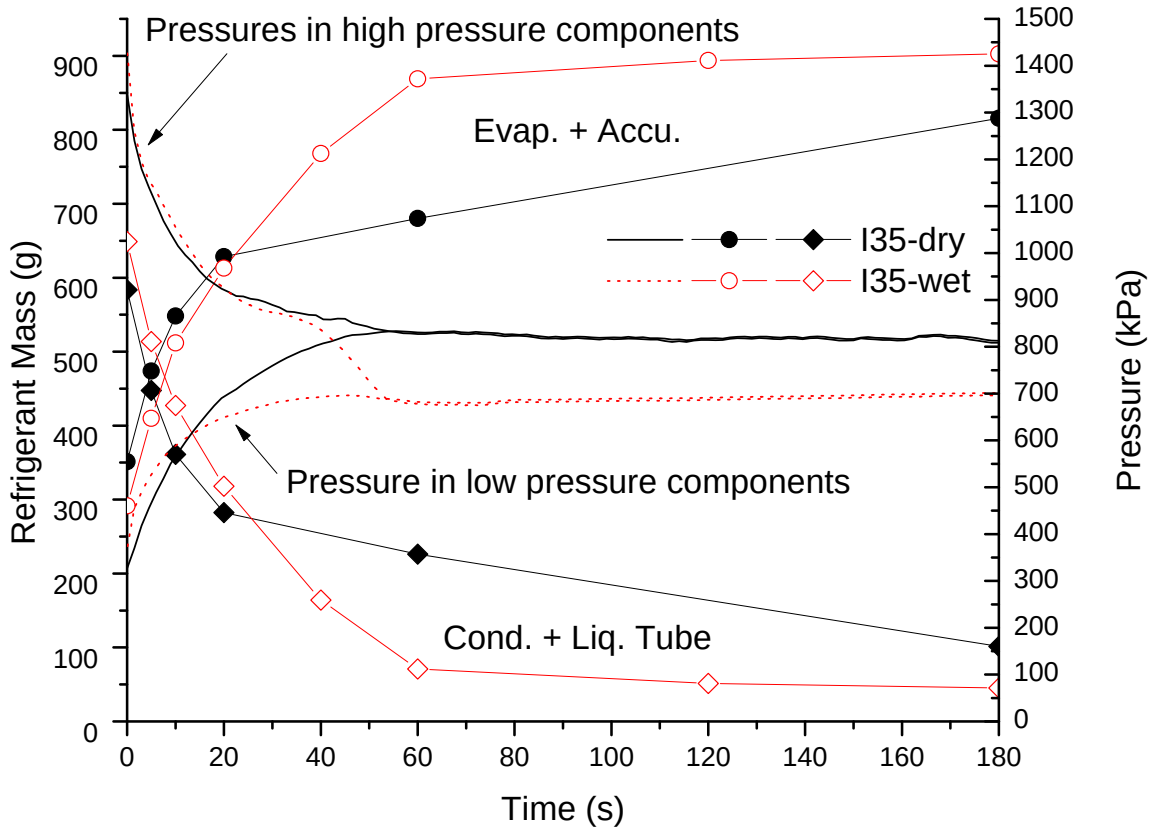

Figure 6.35: Stop period refrigerant mass migration in high and low pressure sections and pressure development for I35-dry and I35-wet conditions

condition—5 g/s higher than for the I35-dry condition. At steady state operation 50 g more of refrigerant is in the high pressure components and 50 g less in the low pressure components for the I35-wet condition compared to the I35-wet condition. During the first 20 seconds after the compressor is stopped the dynamic developments—besides the mentioned offsets—of the pressures and refrigerant masses are the same. After 20 seconds, however, the pressure in the low pressure components for the I35-wet condition deviates from the I35-dry condition and starts to level out. The pressure in the high pressure components follows the pressure of the I35-dry condition until 40 seconds and then starts to drop. The pressure difference is below 10 kPa across the expansion valve after the same time—54 seconds—for both conditions. However, the apparent equilibration pressure is 700 kPa—100 kPa lower than for the I35-dry condi-

tion. The reason for the lower apparent equilibration pressure is the reversion of the latent heat transfer which occurs at 37 seconds and the ensuing evaporative cooling effect as described in Section 6.3.4. For R134a, a pressure of 700 kPa corresponds to a saturation temperature of 26.7°C, which is within 2°C of the wet bulb temperature of the evaporator air inlet temperature after 37 seconds. Hence the evaporator saturation pressure from 37 seconds to 180 seconds is influenced by the water condensate temperature on the surface of the evaporator. For the I35-wet condition 200 g more of refrigerant migrates to the evaporator and accumulator between 20 seconds and 60 seconds. This increased refrigerant mass migration coincides with a higher pressure difference across the expansion valve for the I35-wet condition during this time. This confirms the conclusion drawn from the I35-dry condition results—the primary refrigerant migration is caused by and follows the diminishing pressure difference across the expansion device.

The distribution of the refrigerant mass after 60 seconds—when the primary refrigerant mass migration has ceased—is significantly different for the I35-wet condition, shown in Figure 6.36, compared to the I35-dry condition, shown in Figure 6.27 on page 152. At 60 seconds the evaporator holds 576 g of refrigerant for the I35-wet condition—281 g more of refrigerant than for the I35-dry condition. The amount of refrigerant mass in the accumulator at 60 seconds is 293 g for the I35-wet condition—97 g less than for the I35-dry condition. The refrigerant mass migrating to the accumulator during the first 60 seconds differs by 31 g, 176 g for the I35-wet compared to 207 g for the I35-dry condition. The differences in refrigerant mass migration are notably higher in other sections—279 g more for the evaporator section, 122 g more for the condenser section and 98 g more for the liquid tube section for the I35-wet condition. Overall, it can be concluded that the primary refrigerant mass migration is higher for the I35-wet condition compared to the I35-dry condition as a result of the presence of water condensate on the evaporator

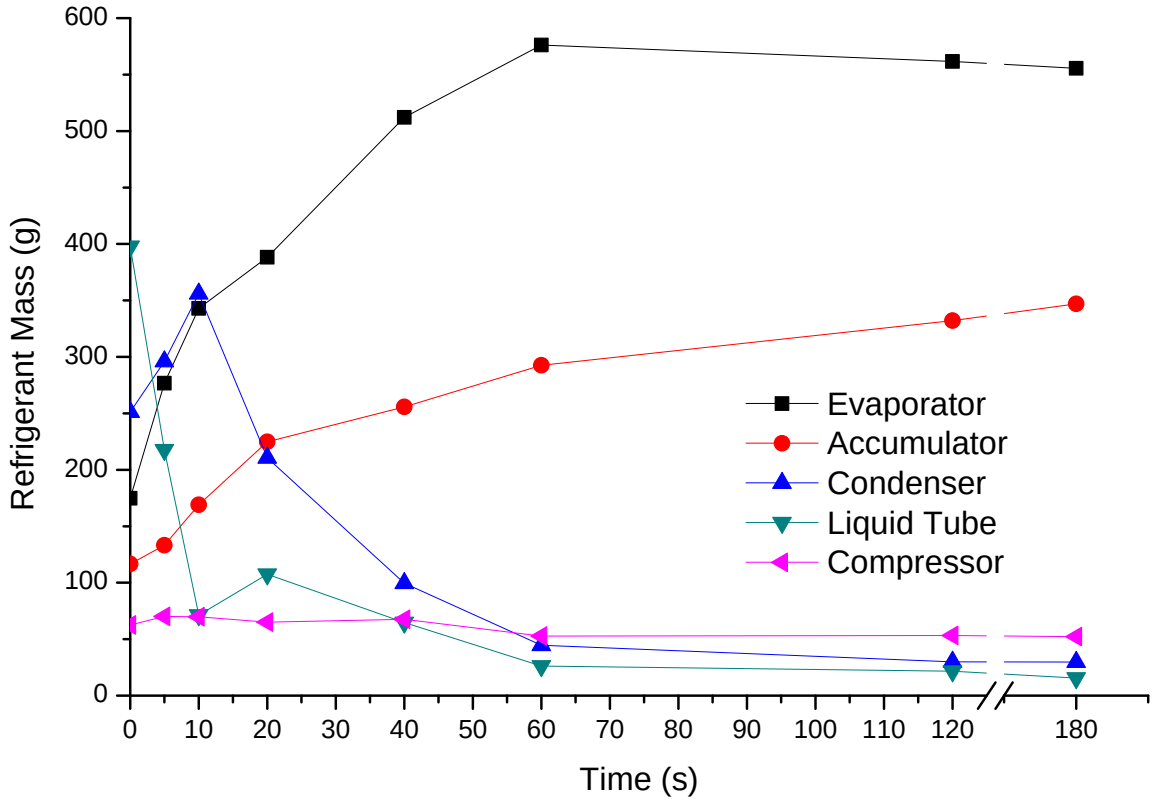

Figure 6.36: Stop period refrigerant mass migration for I35-wet condition

The dynamics of the refrigerant mass migration are similar between the I35-dry and I35-wet condition during the first 20 seconds. The refrigerant mass in the condenser increases by 105 g during the first 10 seconds and then starts to decrease. The decrease leads to an increase in refrigerant mass in the liquid tube between 10 seconds and 20 seconds. The refrigerant mass increases in the accumulator and evaporator during the first 20 seconds for both cases, but a major difference occurs after 20 seconds. Both, the liquid tube and the condenser sections show a faster decrease in refrigerant mass for the I35-wet case between 20 seconds and 60 seconds. After 60 seconds, the refrigerant mass in both sections decreases by less than 15 g. Therefore, most of the liquid refrigerant is drained out of these sections after 60 seconds. The video snapshots shown in Figure 6.37 of the sight glass support the conclusion of similar dynamics during the first 20 seconds. The images from the first 20 seconds do not

show a significant difference compared to the snapshots in Figure 6.34 on page 162. At 60 s, Figure 6.37f, bubbles are visible indicating evaporation of refrigerant, but a liquid level is not visible as observed for the I35-dry condition—Figure 6.34e. From 120 s to 180 s, Figures 6.37g and 6.37h, no liquid is visible in the sight glass for the I35-wet condition. The visual qualitative observations of the sight glass agree with

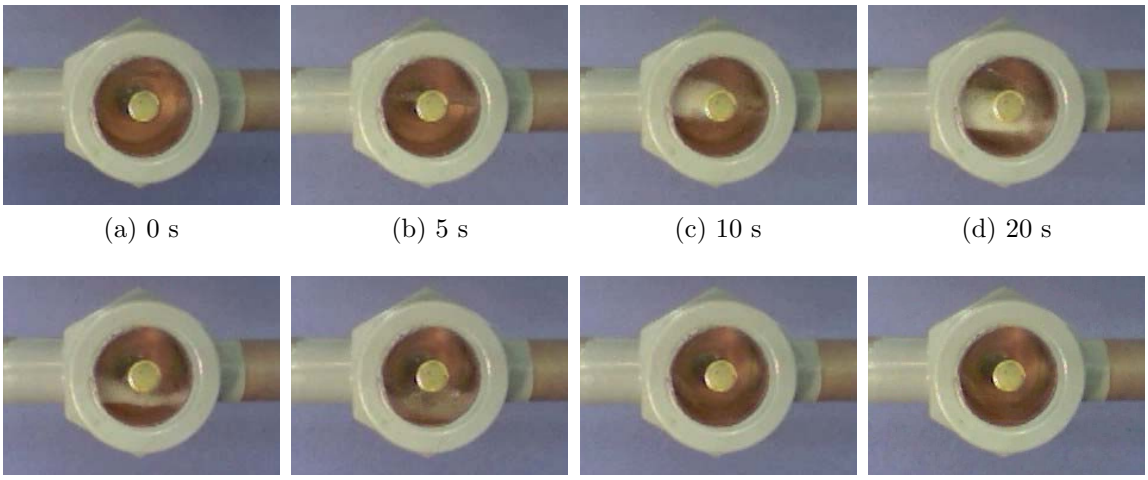

(a) 0 s (b) 5 s (c) 10 s (d) 20 s

(e) 40 s (f) 60 s (g) 120 s (h) 180 s

Figure 6.37: Snapshots of sight glass during stop period for I35-wet condition

the quantitative refrigerant mass measurements in the liquid tube. At 60 seconds 26 g of refrigerant was measured in the liquid tube, 64 g less than for the I35-dry condition. Similarly, the condenser section held 45 g of refrigerant at 60 seconds, 91 g less than for the I35-dry condition.

Since the primary refrigerant mass migration is higher for the I35-wet condition—221 g more refrigerant mass passes through the expansion device—the secondary refrigerant mass migration is consequently smaller. Between 60 seconds and 180 seconds the refrigerant mass in the accumulator increased by 54 g for the I35-wet condition—175 g was the increase for the I35-dry condition.

As outlined for the I35-dry condition results, the hypothesis for the secondary refrigerant mass migration relies on the assumption that the accumulator inside walls and the liquid refrigerant lubricant mixture have temperatures below the saturation

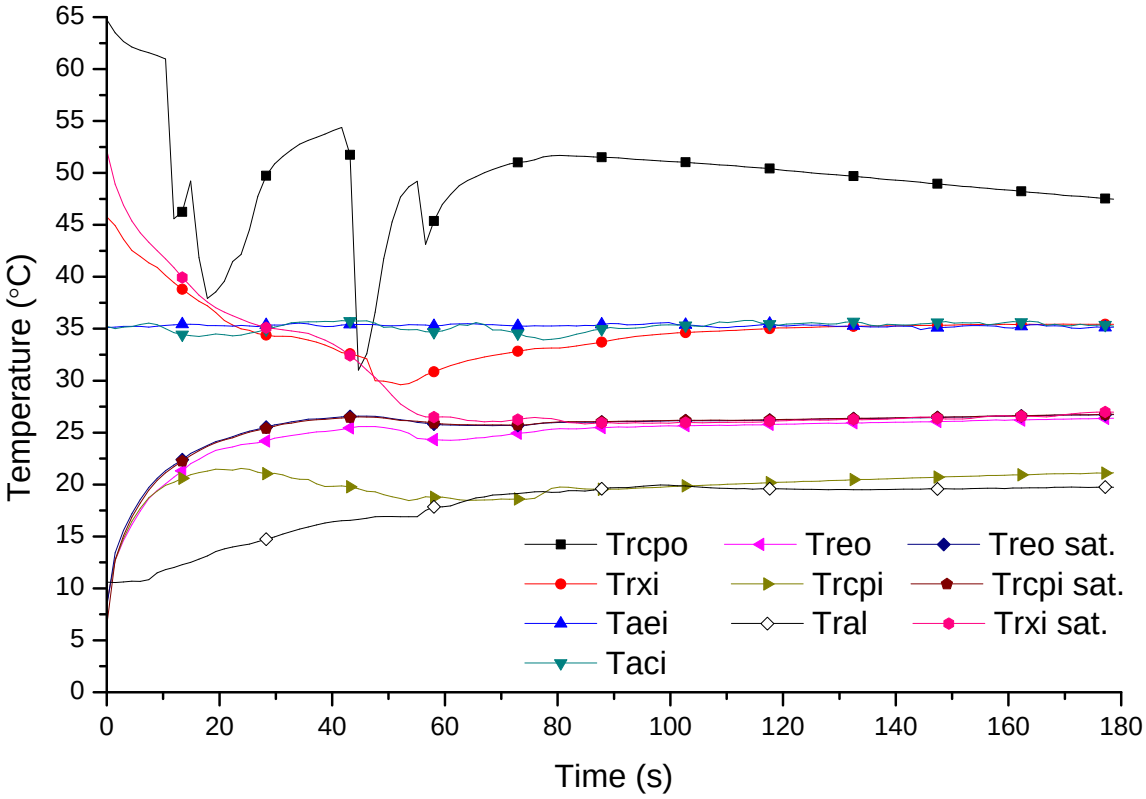

Figure 6.38: Stop period refrigerant temperatures and air inlet temperatures for I35-wet condition

temperature and henceforth refrigerant vapor can condense inside the accumulator. The refrigerant temperatures during the stop period for the I35-wet condition are shown in Figure 6.38. For the I35-wet condition the temperature of the liquid inside the accumulator was measured by an immersed thermocouple located at the bottom and labeled as T_{ral} in Figure 6.38. During the first 7 seconds the temperature stays constant, and then it starts to increase. The video of the accumulator indicates that the incoming liquid flow reaches the bottom of the accumulator after six seconds which corresponds closely to the measured change in temperature. It is therefore assumed that the increase in the liquid temperature is a result of the incoming warmer liquid flow from the evaporator being mixed with the liquid inside the accumulator. The temperature of the incoming flow, T_{reo}, is at an increasingly warmer temperature as measured by the thermocouple located between evaporator and accumulator.

The temperature of the liquid inside the accumulator remains below the saturation temperature—a constant difference of 7°C is measured after 70 seconds—throughout the stop period. The saturation temperatures are 8°C below the ambient temperature as a result of the water condensate temperature on the surface of the evaporator.

Similar to the I35-dry condition, the temperature at the expansion device inlet—T_{rxi}—follows the saturation temperature—$T_{rxi\ sat.}$—but deviates after the primary refrigerant migration ceases and approaches the evaporator chamber temperature—T_{aei}. The temperature downstream of the compressor—T_{rcpo}—shows several jumps during the first 60 seconds. The temperature decreases sharply down to the saturation temperature, but not below indicating refrigerant is evaporating in the vicinity of the thermocouple. These temperature jumps did not occur every time a stop-start experiment was preformed, indicating that the decrease is most likely caused by evaporating droplets on the thermocouple, and not by a flow across the thermocouple. The temperature between accumulator and compressor—T_{rcpi}—increases during the first 20 seconds, but then decreases, and after 60 seconds it reaches the temperature of the liquid inside the accumulator.

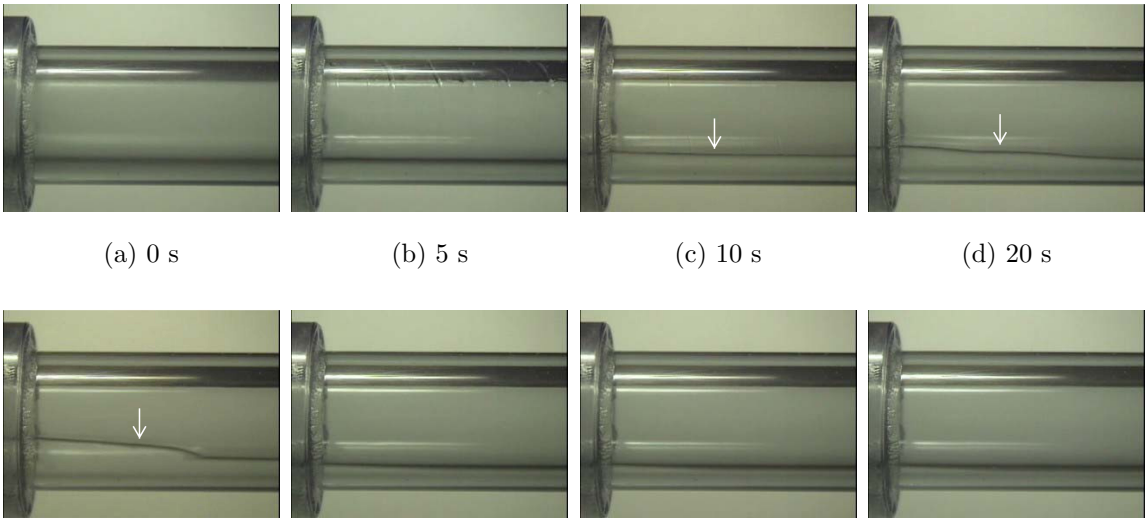

(a) 0 s (b) 5 s (c) 10 s (d) 20 s

(e) 40 s (f) 60 s (g) 120 s (h) 180 s

Figure 6.39: Snapshots of outlet tube of accumulator during stop period for I35-wet condition (arrow indicates liquid-vapor interface)

Snapshots of the video taken of the accumulator outlet tube are shown in Figure 6.39. After five seconds, the liquid film on the inside of the tube breaks down and liquid is visible at the bottom at the tube. Figure 6.39d shows that liquid is flowing into the outlet tube from the accumulator after 20 seconds—at the same time as observed for the I35-dry condition. The flow into the outlet continues—clearly visible at 40 seconds in Figure 6.39e—but stops after 45 seconds. It is observed from the video that the liquid flow is reversed and the liquid is drawn back into the accumulator, and from 60 seconds to 180 seconds no visible liquid is observed as shown in Figures 6.39f to 6.39h. This is a notable deviation from what is observed for the I35-dry condition—the liquid level increases in the outlet tube between 60 seconds and 180 seconds. Therefore, the presence of water condensate on the evaporator influences the migration of refrigerant mass out off the accumulator. As shown for the I35-dry condition, the pressure difference between the accumulator inside and outlet tube must be 1.5 kPa or higher to allow liquid to enter the outlet tube. One possible explanation for why the pressure difference is lower than 1.5 kPa after 45 seconds for

the I35-wet condition is the onset of the evaporative cooling effect after 37 seconds. If more liquid refrigerant evaporates than can be condensed in the accumulator, the pressure inside the accumulator is higher than in the outlet tube as a result of the liquid plug in the U-tube of the accumulator. Liquid is then pushed into the outlet tube as observed for the I35-dry condition. The evaporative cooling effect possibly causes less evaporation of liquid refrigerant, and therefore the pressure difference is less than 1.5 kPa after 45 seconds. The back-flow of liquid into the accumulator leads to a visible increase in the liquid level in the accumulator.

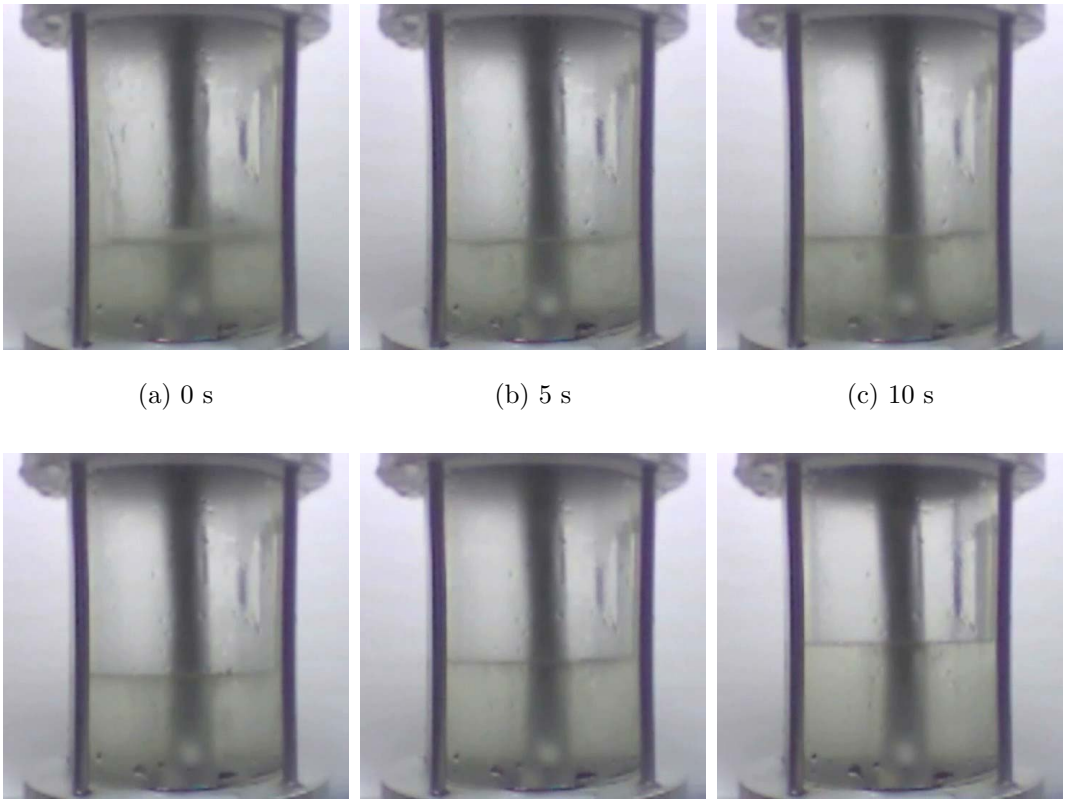

(a) 0 s (b) 5 s (c) 10 s

(d) 40 s (e) 60 s (f) 180 s

Figure 6.40: Snapshots of accumulator during stop period for I35-wet condition

The liquid level in the accumulator also increases between 60 seconds and 180 seconds—as shown in Figure 6.40 when comparing Figure 6.40e to 6.40f. For the I35-dry condition an increase in the liquid level is not observed—see Figure 6.29e and 6.29f

on page 155—because liquid is draining into the outlet tube. The conclusion is the liquid level inside the accumulator cannot be used as a measurement for refrigerant mass migration—no change in the liquid level would lead to the interpretation that no refrigerant mass migrates whereas in fact refrigerant mass is migrating through the accumulator.

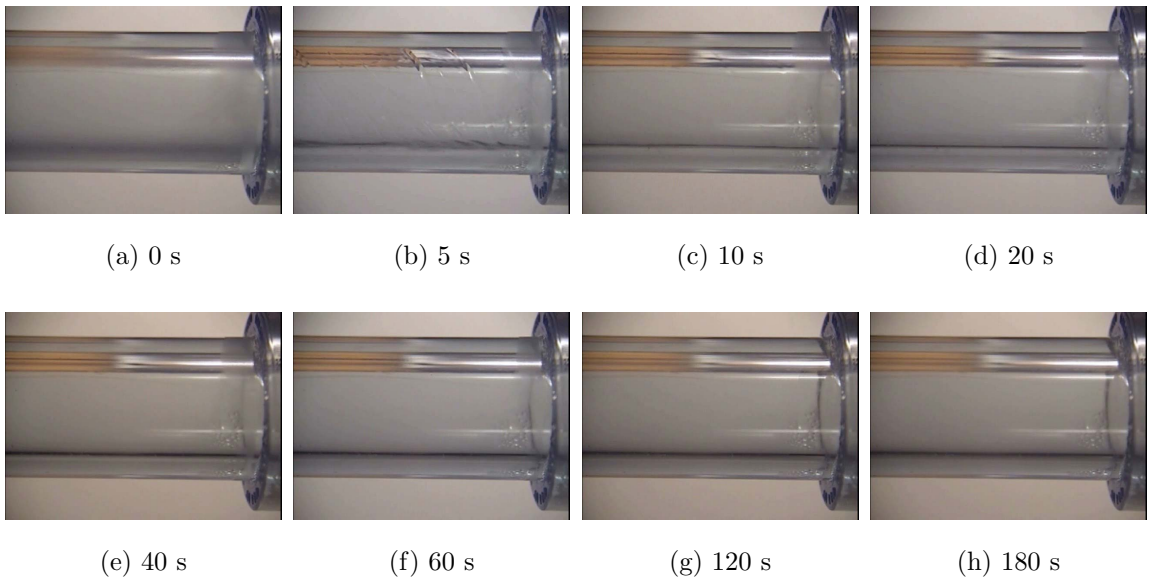

(a) 0 s (b) 5 s (c) 10 s (d) 20 s

(e) 40 s (f) 60 s (g) 120 s (h) 180 s

Figure 6.41: Snapshots of inlet tube of accumulator during stop period for I35-wet condition

The snapshots of the accumulator inlet tube during the stop period of the compressor for the I35-wet condition are shown in Figure 6.41. The images of the inlet tube show that after the compressor is stopped, the liquid film at the inner surface of the tube breaks down as shown in Figure 6.41b. The visible liquid streaks are at an angle indicating flow from left to right—from the evaporator to the accumulator. Although the individual images do not represent it, the video shows the liquid at the bottom of the inlet tube is reduced until 60 seconds, after which the tube appears to hold liquid anymore. It should be noted that the disappearance of the liquid coincides with the observed pressure equilibration shown in Figure 6.35. Therefore, any refrigerant mass leaving the evaporator and entering the accumulator between

60 seconds and 180 seconds must be in the vapor phase. Overall, the images of the inlet tube for the I35-wet and I35-dry conditions show no apparent differences.

For the I35-wet condition stop-start experiment, pictures of the condenser were taken with a Mikron Midas infrared camera having a resolution of 240 x 320 pixels. As a result of the positioning and space inside the climate chamber, the upper left corner of the condenser was not captured. Figure A.1 in the appendix shows a picture of the condenser used in the experiments, its header arrangement and the direction of the air and refrigerant flows. The images in Figure 6.42 show the front of the condenser and Figure 6.42h the temperature scale for all images.

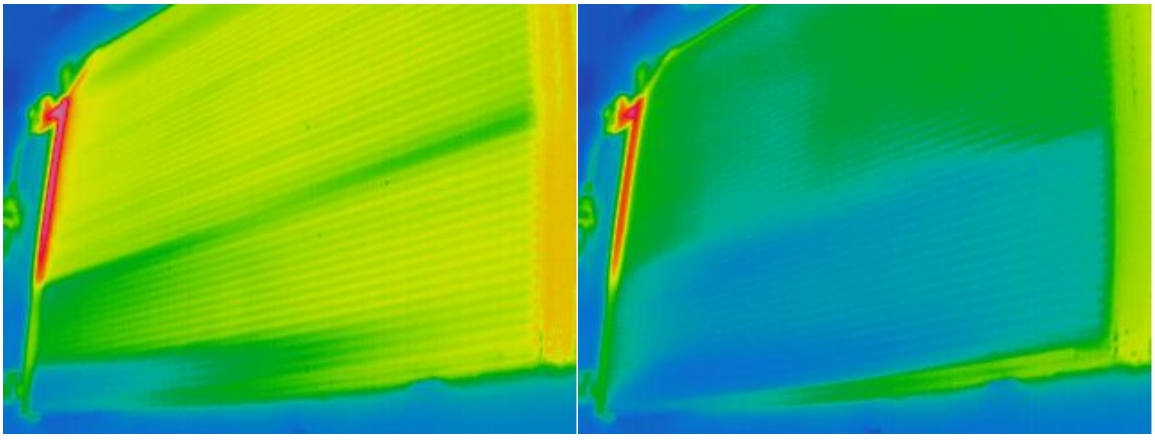

(a) 0 s (b) 5 s

Figure 6.42: Sequence of condenser infrared images during stop period for I35-wet condition

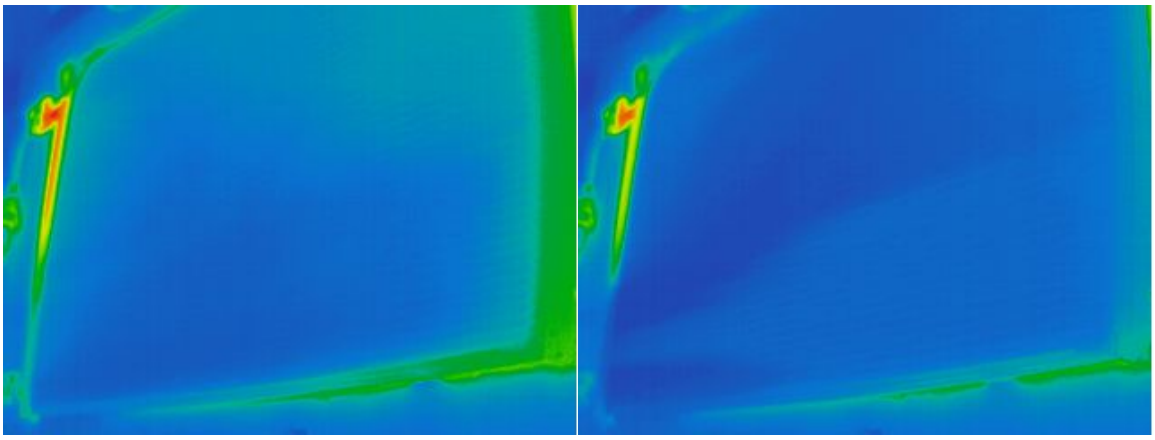

(c) 10 s (d) 20 s

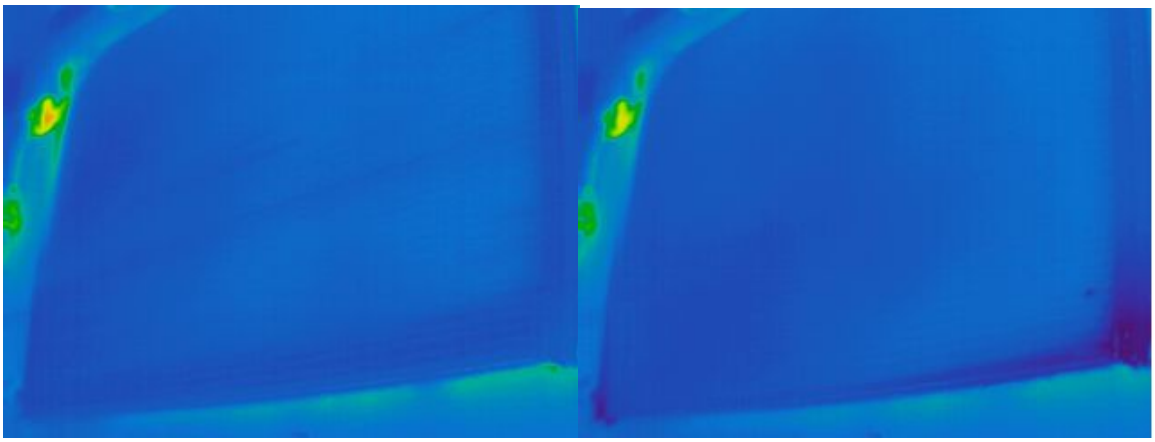

(e) 40 s (f) 60 s

(g) 180 s

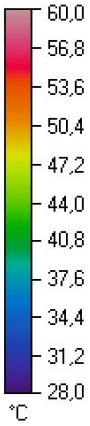

(h) Temperature scale

Figure 6.42: Sequence of condenser infrared images during stop period for I35-wet condition (cont.)

As soon as the compressor is turned off, the surface temperature of the finned part of the condenser decreases. As Figure 6.42b shows, the second pass is close to the ambient temperature of 35°C within 5 seconds after the compressor is stopped, whereas the first pass still has a higher temperature. After 10 seconds, the surface temperature in the first pass is the same as in the second pass. However, the return header surface temperature, as well as the inlet header surface temperature, are still at higher temperatures. After 20 seconds, the return header surface temperature reaches 35°C, indicating the refrigerant flows through the return header and hence cools the metal mass of the return header. Another indication that refrigerant flows through the return header is the shape of the temperature profile in the second pass, which looks similar to the steady state profile seen in Figure 6.42a. The return header surface temperature reaching 35°C after 20 seconds coincides with the refrigerant mass measurement which indicates that the refrigerant mass is leaving the condenser at its highest rate between 20 and 40 seconds after the compressor is stopped. Focusing on the lowest minichannels and the return header at time index 40 s, Figure 6.42e, shows that the surface temperature is 28°C, and therefore below the ambient temperature. A surface temperature lower than the ambient temperature indicates the presence of evaporating liquid refrigerant inside the lower parts of the condenser—the refrigerant saturation temperature as a result of the pressure is 27°C. This is another indication—in addition to the observation of the sight glass—that liquid can accumulate in convexities during the stop period. At 120 seconds, the infrared picture is identical to the one shown in Figure 6.42g indicating that most of the liquid refrigerant has evaporated—confirmed by the refrigerant mass measurements which show no change in refrigerant mass in the condenser between 120 seconds and 180 seconds.

The compressor section shows only a minor change in refrigerant mass during the stop period. After five seconds, the refrigerant mass increases by 7 g to 70 g and then

reduces to 52 g at the end of the stop period. From both, I35-dry condition and the I35-wet condition results, it can be concluded that the compressor section has the least charge migration by an order of magnitude compared to the other sections—tenths of grams instead of hundredths of grams in the other sections.

6.4.3 Refrigerant Migration During Start-Up

The refrigerant mass distribution in the components before a start-up is the result of the refrigerant mass migration during the off-cycle or—as it is the case here—the compressor stop period. Two identical stop-start scenarios were investigated—the difference being the operating condition—I35-dry and I35-wet—and the use of a transparent accumulator section for the I35-wet condition. As described in the previous section the presence of water condensate on the evaporator influences the refrigerant migration during the stop period. Because of the difference in refrigerant mass distribution, the I35-dry start-up results are discussed first, followed by the I35-wet start-up results (Section 6.4.4, page 185).

The refrigerant mass migration during the start-up for the I35-dry condition is shown in Figure 6.43. The time index is continued from the stop period and the compressor is turned on at 180 s. The data points are denoted by markers, the lines connect the data points to visualize the trends of refrigerant migration across the sections. One minute after the compressor is started—time index 240 s in Figure 6.43—98 percent of the steady state refrigerant redistribution is reached. The first five seconds show that 363 g of refrigerant mass is migrating to the liquid tube and condenser. Since this refrigerant has to pass through the compressor, the resulting average refrigerant flow rate over the first five minutes is 73 g/s—39 g/s higher than the steady state refrigerant mass flow rate. The question is—how does the compressor provide such an increased refrigerant flow rate during the first five seconds? To answer this question a combined analysis of measurement data—temperature, pressure, mass

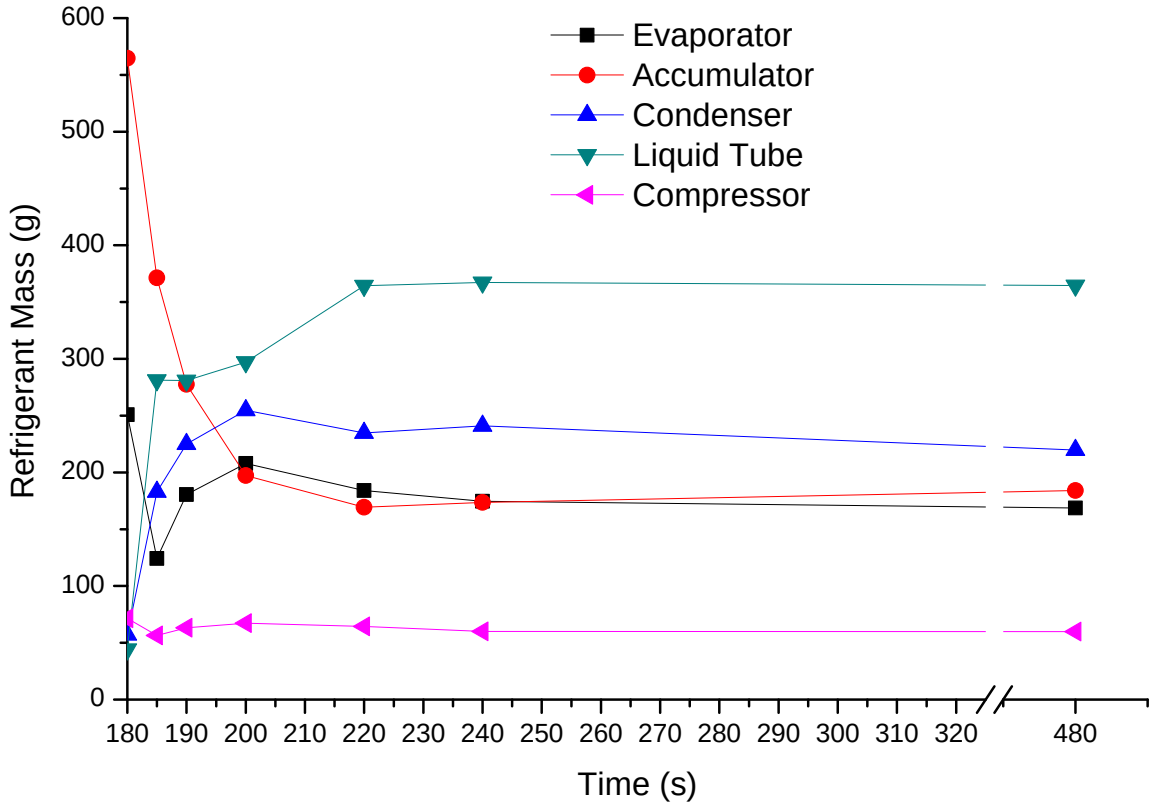

Figure 6.43: Start-up refrigerant mass migration for I35-dry condition

flow rate, compressor power—high speed and real time video images are necessary.

Images from high speed videos taken at the accumulator inlet tube and outlet tube are presented in Figure 6.44 and Figure 6.45, respectively. The exposure time for each image was 0.004 ms. The time index is in accordance with Figure 6.43 starting at 180 s. In Figure 6.44 the accumulator entrance is at the right side of each image and for Figure 6.45 the accumulator outlet is at the left side—the normal direction of refrigerant flow is from left to right in both figures. Figure 6.45a shows liquid at the bottom of the outlet tube at 180 s—the result of the stop period migration. The first sign of flow movement in form of ripples is observed—Figure 6.45b—followed by a front of visibly dense foam entering from the left—Figure 6.45c. This foam sweeps all the liquid at the bottom out of the tube towards he compressor. There is a short gap of 36 ms before another front of visibly dense foam enters

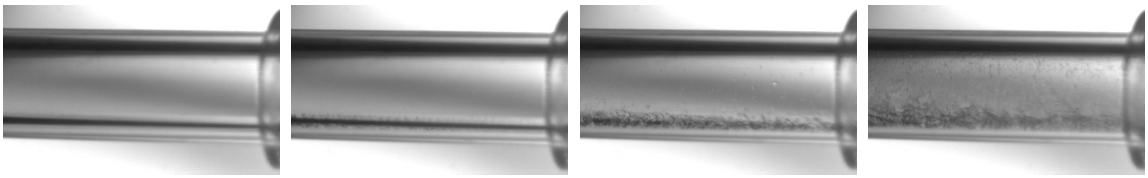

(a) 180.000 s (b) 180.024 s (c) 180.075 s (d) 180.224 s

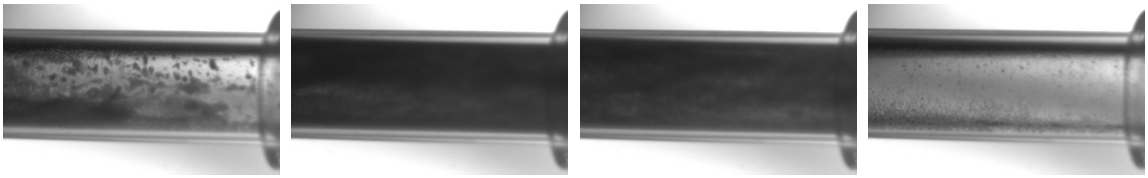

(e) 180.571 s (f) 181.000 s (g) 181.500 s (h) 183.000 s

Figure 6.44: Snapshots from high speed video of inlet tube of accumulator during start-up for I35-dry condition

the outlet tube—Figure 6.45e. The darker the foam, the higher is the amount of liquid phase refrigerant in the foam. The foam density of the second front visibly decreases gradually as shown in Figures 6.45f to 6.45h. The observation of the inlet tube—Figure 6.44—shows that until 180.571 s no significant amount of refrigerant mass enters the accumulator. Therefore, the refrigerant mass leaving the outlet tube during the first half second is the refrigerant mass originating from the U-tube in the accumulator. From observing the outlet tube high speed video it can be concluded that the liquid refrigerant inside the U-tube leaves and sweeps the liquid present in the outlet tube towards the compressor. Consequently liquid phase refrigerant enters the compressor leading to a spike in compressor power and refrigerant mass flow rate as shown in Figure 6.46.

Mass flow measurements were taken every 1.5 seconds and the refrigerant mass flow meter recorded a value of 70 g/s 1.5 s after the compressor start, but then does not show a value until 7.5 s. The mass flow meter—installed downstream of the compressor—is a Coriolis type and does not provide a value if the fluid is present in two phases. The absence of a reading indicates the presence of two phase refrigerant after the refrigerant passed through the compressor. The temperature measurements

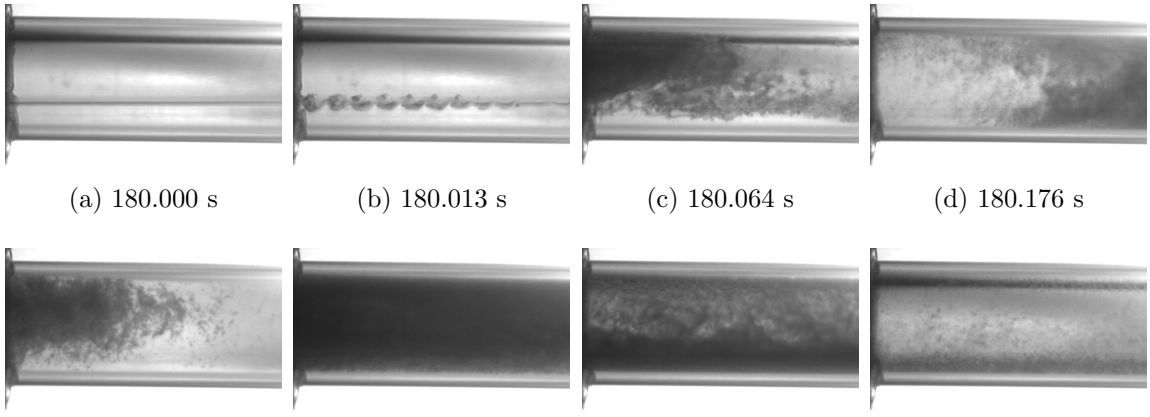

(a) 180.000 s (b) 180.013 s (c) 180.064 s (d) 180.176 s

(e) 180.212 s (f) 180.267 s (g) 180.400 s (h) 180.800 s

Figure 6.45: Snapshots from high speed video of outlet tube of accumulator during start-up for I35-dry condition

during the start-up—Figure 6.47—also indicate the presence of two phase refrigerant. The inset shows the compressor exit temperature—T_{rcpo}—and the saturation temperature—$T_{rcpo\ sat.}$—during the first ten seconds, and the markers denote the actual measurements. At 181.5 s the compressor exit temperature is 3°C below the saturation temperature but approaches the saturation temperature within three seconds. From 184.5 s to 190 s the two temperatures are equal—within measurement uncertainty. After 190 s the compressor temperature exceeds the saturation temperature.

The combined analysis of the high speed images and measurement data explains how the compressor can provide an increased refrigerant mass flow rate during start-up. The refrigerant entering the compressor contains liquid phase refrigerant causing an increase in the density of the refrigerant. The higher density of the refrigerant—compared to steady state operation—results in a refrigerant mass flow rate exceeding 70 g/s.

The increased density of the refrigerant also causes the compressor power to increase. At 181.5 s the compressor power is 0.5 kW higher than the steady state compressor power. Since data was taken every 1.5 s the actual peak may be higher.

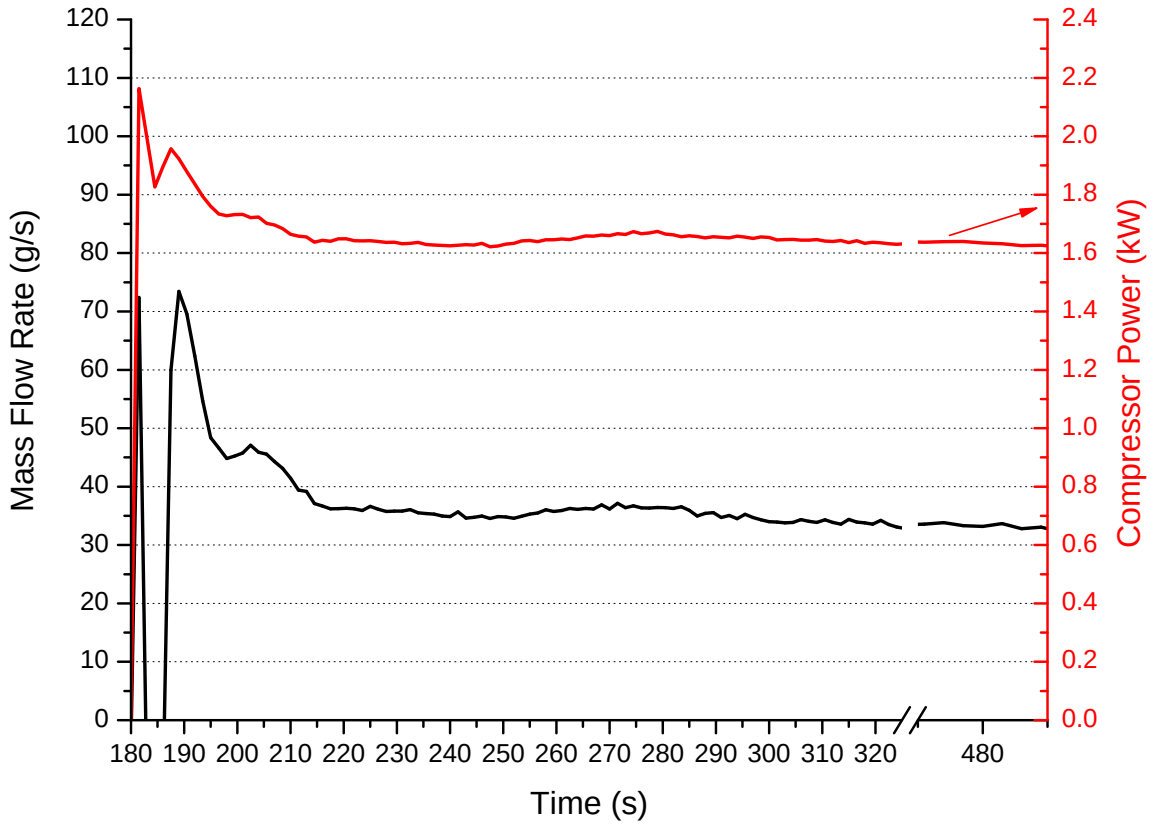

Figure 6.46: Refrigerant mass flow rate and compressor power during start-up for I35-dry condition

The high speed video snapshots revealed the cause for the first peak, but do not explain the refrigerant migration after the first five seconds. Images taken from the real time video of the accumulator explain the secondary refrigerant migration after five seconds. The visible dense foam entering the accumulator—as observed from the high speed video snapshot of the inlet tube half a second after the compressor start—reaches the liquid layer inside the accumulator after one second, shown in Figure 6.48b. Between 181 s and 200 s the accumulator is visibly filled with foam. Since the foam reaches to the top of the accumulator, foam can enter the U-tube resulting in the entrainment of additional liquid refrigerant compared to the steady state condition. The foam gradually disappears until 220 s. The occurrence of foam inside the accumulator, the refrigerant mass flow rate, and compressor power are related.

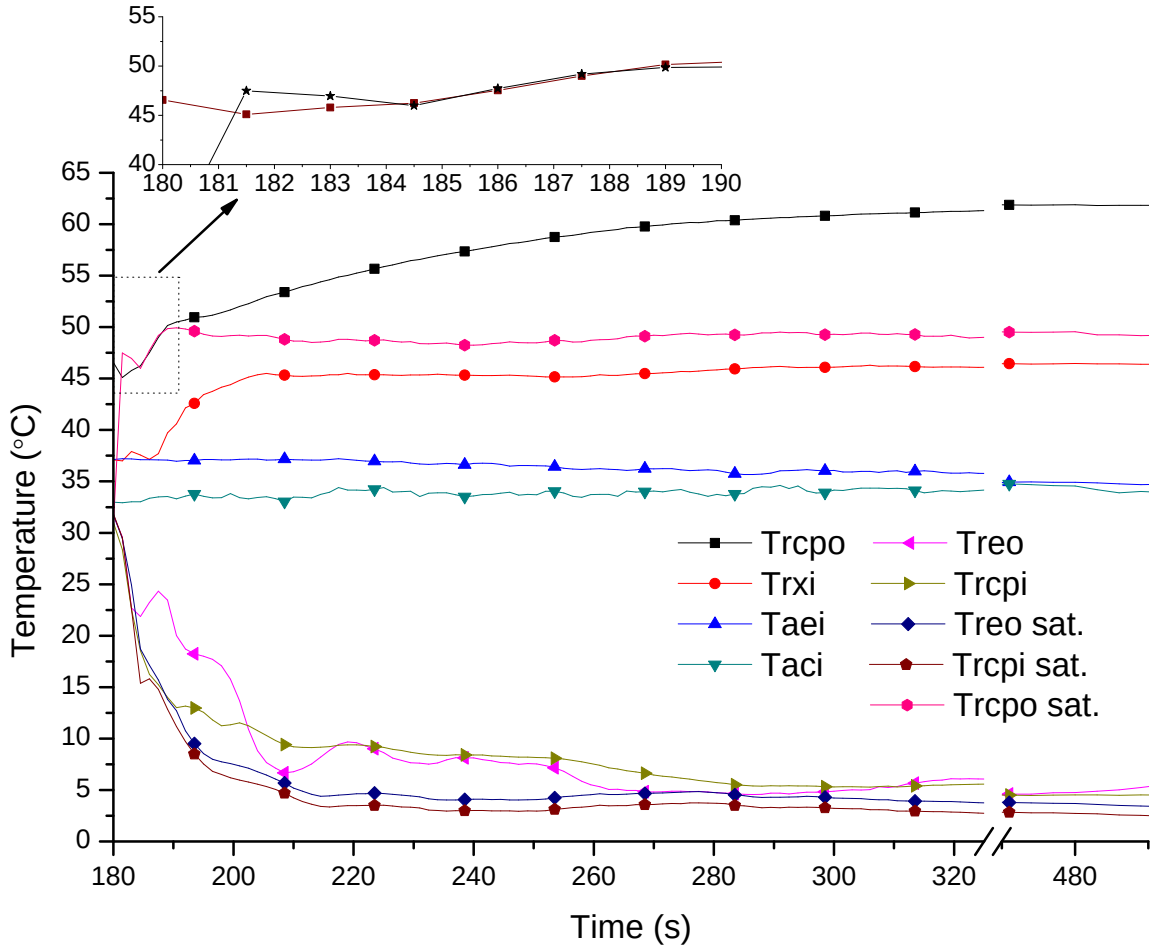

Figure 6.47: Start-up refrigerant and air inlet temperatures for I35-dry condition

As Figure 6.46 shows, the mass flow rate reaches its steady state value after 220 s—as does the compressor power—which coincides with the disappearance of foam in the accumulator. In addition, after 220 s the refrigerant mass migration out off the accumulator stops.

The refrigerant mass in the liquid tube and condenser increases by 363 g during the first five seconds—237 g of this increase is found in the liquid tube and 126 g in the condenser. The high refrigerant mass flow rate above 70 g/s during the first five seconds in combination with the condensation of refrigerant vapor inside the condenser is responsible for this quick increase in refrigerant mass. Snapshots of the sight glass—

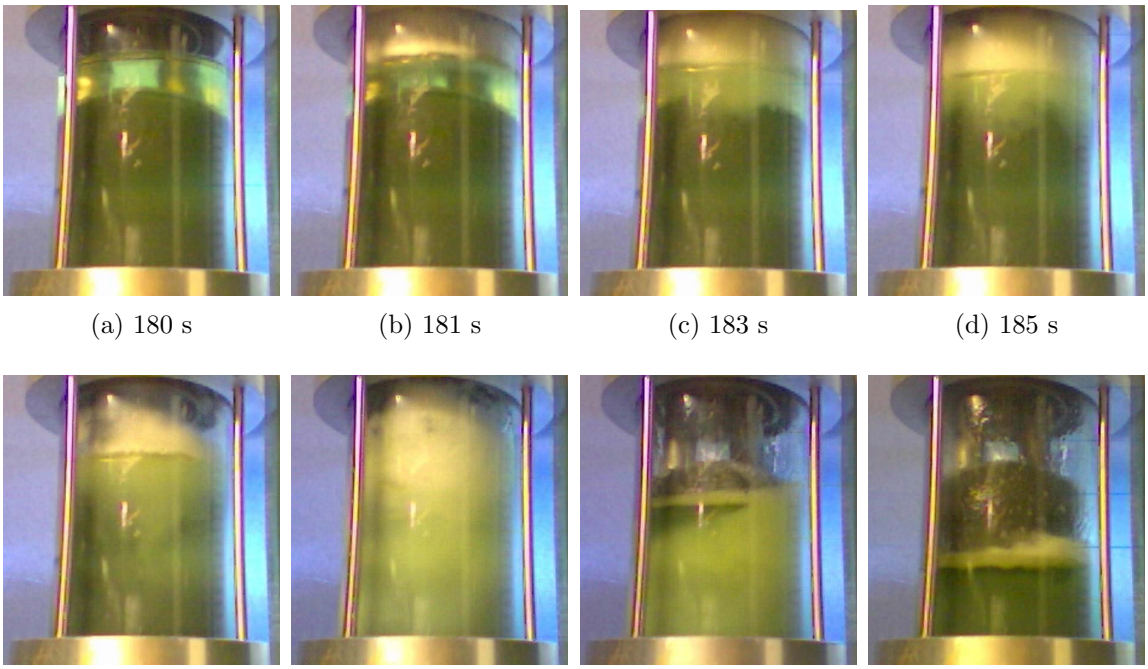

(a) 180 s (b) 181 s (c) 183 s (d) 185 s

(e) 190 s (f) 200 s (g) 220 s (h) 480 s

Figure 6.48: Snapshots of accumulator with desiccant package during start-up for I35-dry condition

located in the liquid tube section—during the start-up are shown in Figure 6.49. At 180 s the sight glass contains vapor phase refrigerant, except for a small amount of lubricant rich liquid at the bottom forming bubbles as shown in Figure 6.49a. After three seconds, the sight glass suddenly shows a flow, which could be described as fast moving foam as shown in Figure 6.49b. The foam disappears within one second and a distinct liquid layer is visible—Figure 6.49c. Figures 6.49c, 6.49d and 6.49e show a gradually increase of the liquid layer indicating an increase in refrigerant mass in the liquid tube from 186 s to 220 s. The refrigerant mass measurements—Figure 6.43—confirm this observation, showing an increase of refrigerant mass from 281 g to 364 g from 190 s to 220 s. The condenser does not show an increase in refrigerant mass after 200 s. The consequence is that after the condenser reaches its refrigerant mass storing capacity any refrigerant migrating from the accumulator and evaporator is being stored in the liquid tube.

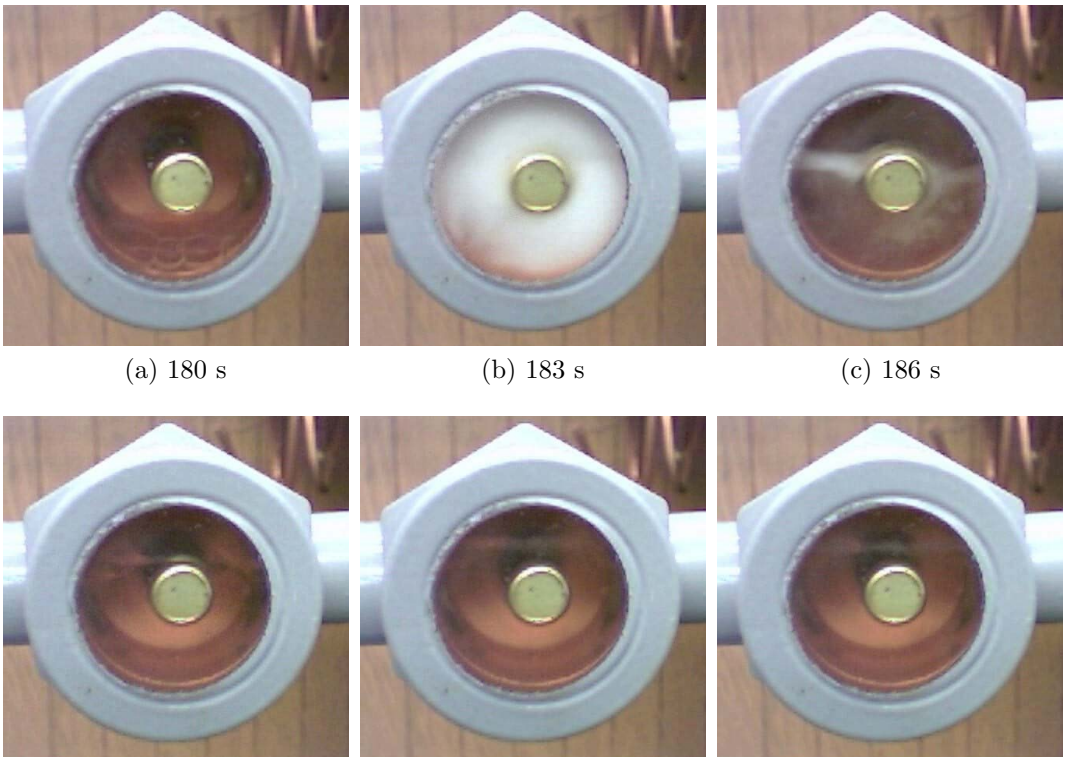

(a) 180 s (b) 183 s (c) 186 s

(d) 200 s (e) 220 s (f) 480 s

Figure 6.49: Snapshots of sight glass between condenser and expansion device during start-up for I35-dry condition

The refrigerant mass in the evaporator, as shown in Figure 6.43, decreases by 127 g during the first 5 s. The high speed videos of the accumulator inlet tube—Figure 6.44—show that liquid phase refrigerant is leaving the evaporator during the first 3 s. Based on the sight glass snapshots, during the first three seconds the expansion device has vapor phase refrigerant at its inlet, and therefore the flow through the expansion device is not high enough to compensate the refrigerant mass leaving the evaporator. After five seconds, the refrigerant mass in the evaporator starts to increase, indicating that the mass flow rate into the evaporator is higher than the mass flow rate out of the evaporator—coinciding with the observation of the sight glass showing the presence of liquid and vapor in the liquid tube. The evaporator refrigerant exit temperature is 5°C higher than the saturation temperature between 190 s and 200 s—indicating that the evaporator contains superheated refrigerant vapor, and, as a result of its low

density, less refrigerant mass can be stored.

From all sections, the compressor shows the least change of refrigerant mass during the start-up. It holds 71 g at 180 s—11 g more than at steady state operation. After 185 s the refrigerant mass is slightly higher—between 3 g and 7 g—than the steady state value which is reached after 240 s. The higher refrigerant mass in the compressor between 185 s and 220 s coincides with the obeserved entrainment of foam into the U-tube of the accumulator.

6.4.4 Refrigerant Migration During Start-Up - Effect of Water Condensate on Evaporator

Water condensate on the evaporator influences the refrigerant mass distribution during the compressor stop period. Table 6.12 shows a comparison of the refrigerant mass distribution at the end of the three minute stop period for both conditions.

Table 6.12: Refrigerant mass distribution before compressor start

	Evaporator	Accumulator	Condenser	Liquid Tube	Compressor	Sum
	g	g	g	g	g	g
I35-dry	251	565	57	44	71	988
I35-wet	556	347	30	16	52	1001
Diff.	+305	-218	-27	-28	-19	+13

The refrigerant mass distribution for the I35-wet condition is significantly different from the I35-dry distribution—the evaporator refrigerant mass is higher by 305 g and the accumulator refrigerant mass is lower by 218 g. Figure 6.50 shows the refrigerant mass migration plotted as the sum of the masses in the condenser and liquid tube; and the evaporator and the accumulator sections for both—the I35-dry and I35-wet conditions. The markers denote actual measurements and lines connecting the

markers show the trends. The pressures upstream and downstream of the compressor are shown as lines—data was taken every 1.5 seconds but markers are omitted. For

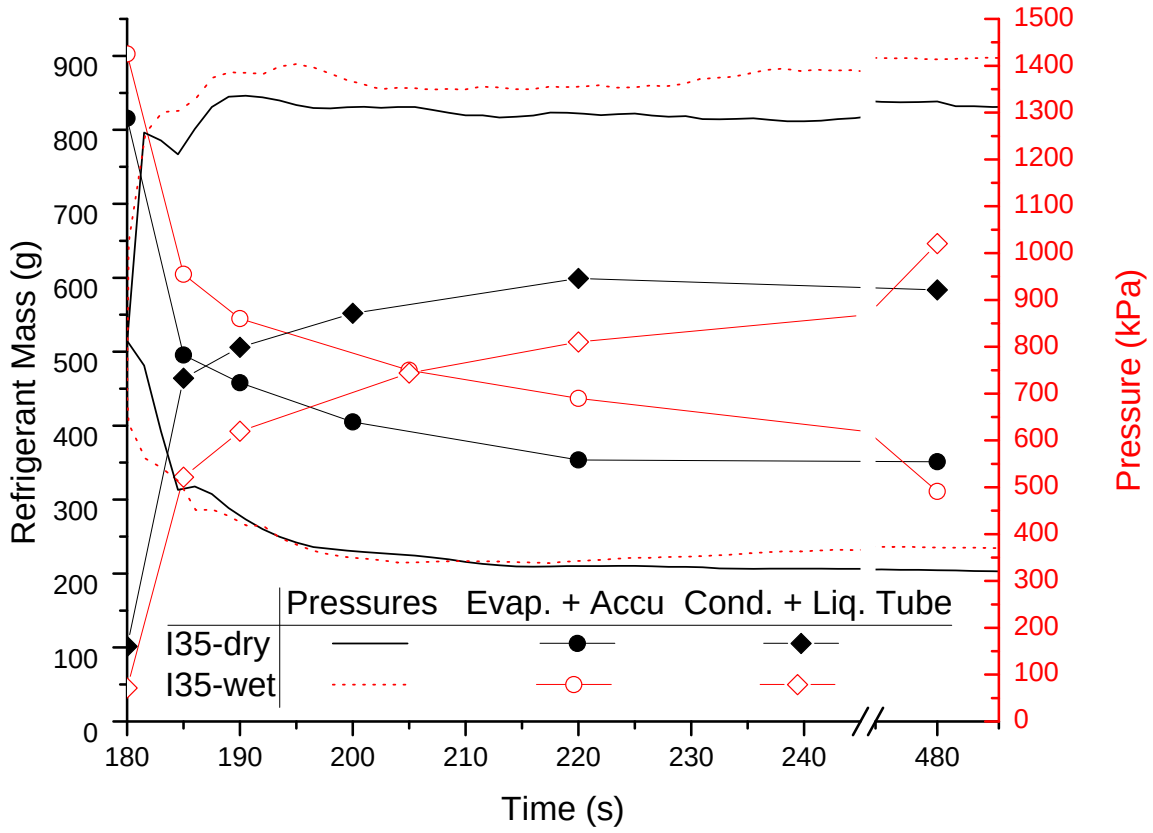

Figure 6.50: Start-up refrigerant mass migration in high and low pressure sections and pressure development for I35-dry and I35-wet conditions

both conditions, the pressure difference across the expansion valve is within 100 kPa of its steady state value 15 s after the compressor is turned on. However, the point in time when the refrigerant mass becomes equally distributed across the low and high pressure sections is significantly different—7 s for the I35-dry condition but 25 s for the I35-wet condition. The steady state refrigerant mass distribution is reached after one minute for the I35-dry condition but not for the I35-wet condition. As shown in Section 6.3.4, the developments of the cooling capacities during the compressor stop period are different for the I35-dry and I35-wet conditions, as a result of water condensate on the evaporator. The result is the difference in refrigerant mass

distribution as shown in Table 6.12 at the end of the stop period. The developments of the cooling capacities are the same, however, for both conditions during the start-up. The main objective of this section is to explain why the refrigerant mass migration during start-up for the I35-wet condition is different from the I35-dry condition.

The refrigerant mass migration during the start-up for the I35-wet condition is shown in Figure 6.51. The markers denote individual measurements, and the lines connecting the markers show the trends. The first major difference—compared to the

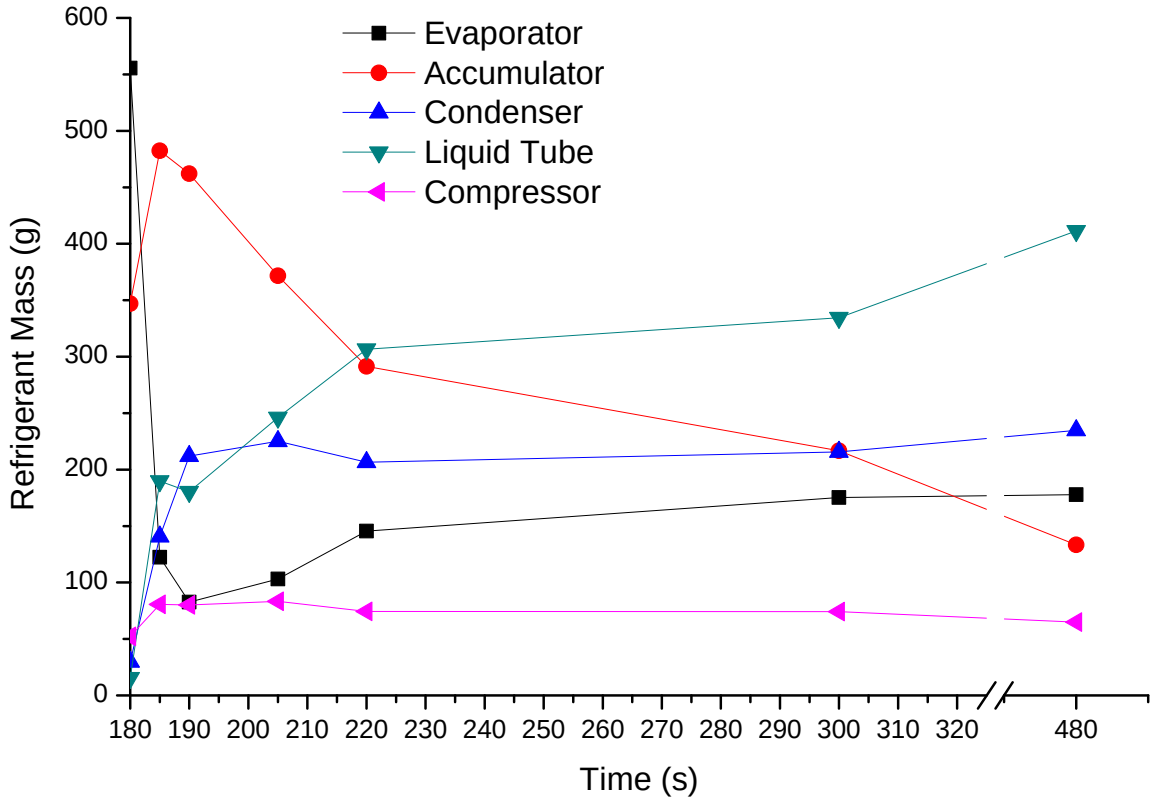

Figure 6.51: Start-up refrigerant mass migration for I35-wet condition

I35-dry condition—is the migration of refrigerant mass out of the evaporator during the first 5 s after compressor start—434 g compared to 127 g for the I35-dry condition.

To explain how 434 g of refrigerant can leave the evaporator in five seconds, an analogy to what was observed in the accumulator is made. During the compressor stop period, liquid refrigerant pools at the bottom of the accumulator as a result of

gravity. The same is assumed in the evaporator, the bottom headers—headers #2 and #4 in Figure A.3—fill with liquid refrigerant. Considering the refrigerant pressure, temperature and mass—and neglecting the presence of lubricant—the liquid in the evaporator at 180 s occupies 448 cm^3. The sum of the volumes of both bottom headers is 218 cm^3. Therefore—although the distribution of the liquid within the evaporator was not measured—it is evident that, at least in one header, the liquid level has to be above where the header and channels are connecting. The liquid provides a liquid plug—analogous to the U-tube in the accumulator—and the liquid is drawn out by the decreasing pressure at start-up. The video snapshots of the inlet tube to the accumulator, Figure 6.52, show that after 0.5 s fast moving foam appears. The foam gradually reduces until 185 s—434 g of refrigerant have left the evaporator.

Since 434 g of refrigerant leaves the evaporator in five seconds, the accumulator shows a significant increase in the liquid level at 5 s as shown in Figure 6.53b. A

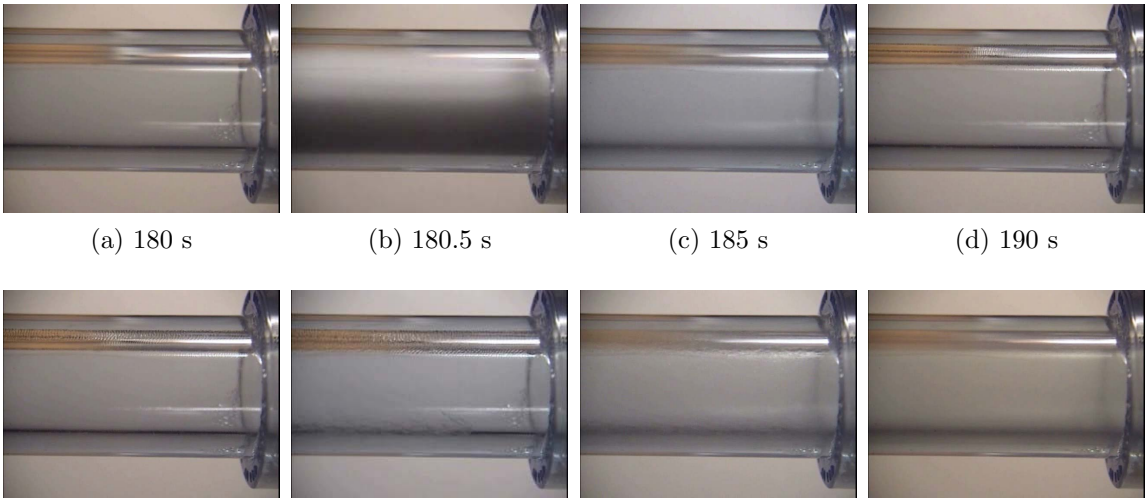

(a) 180 s (b) 180.5 s (c) 185 s (d) 190 s

(e) 205 s (f) 218 s (g) 300 s (h) 480 s

Figure 6.52: Snapshots of inlet tube of accumulator during start-up for I35-wet condition

refrigerant mass balance on the accumulator section shows that 299 g of refrigerant mass migrates out of the accumulator during the first five seconds after the compressor start. For the I35-dry condition, 321 g of refrigerant leaves the accumulator during

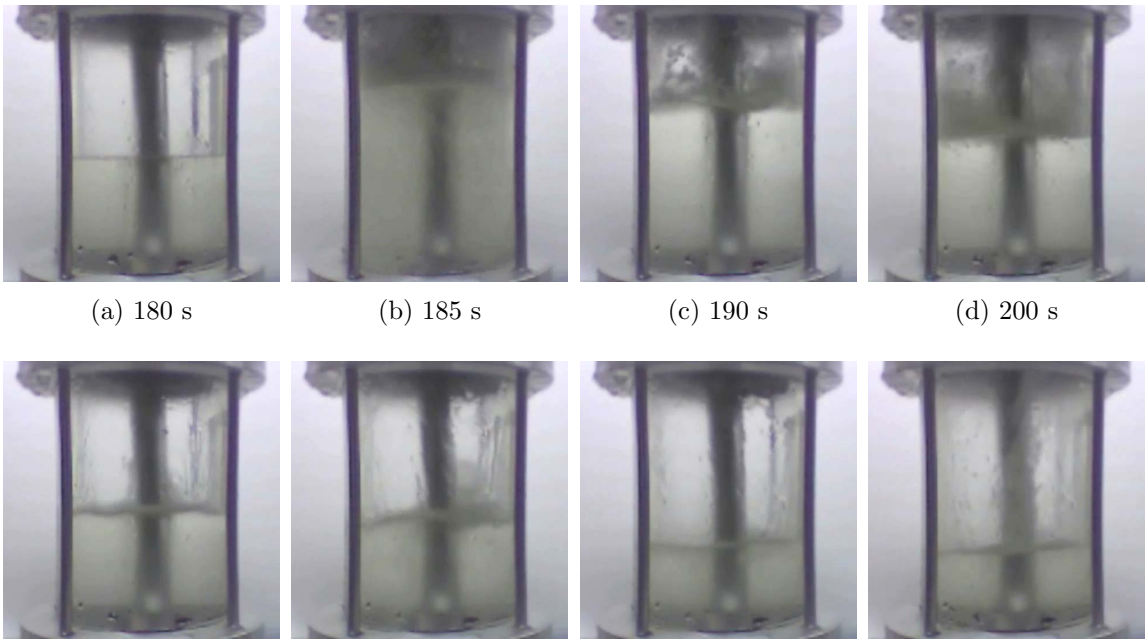

(a) 180 s (b) 185 s (c) 190 s (d) 200 s

(e) 220 s (f) 240 s (g) 300 s (h) 480 s

Figure 6.53: Snapshots of accumulator during start-up for I35-wet condition

the same time frame. The images of the accumulator outlet tube show a fast moving foam leaves the accumulator after 300 ms, Figure 6.54b; an identical observation as for the I35-dry condition. At 181 s—one second after the compressor is started—foam enters the accumulator and fills the accumulator leading to entrainment of foam into the U-tube; an identical observation as for the I35-dry condition. Therefore, the dynamics of refrigerant mass migration out of the accumulator are identical for both the I35-dry and I35-wet conditions during the first five seconds.

The accumulator holds—as a result of the refrigerant mass migration from the evaporator—329 g more refrigerant mass 10 s after compressor start than it holds under steady state conditions. For the I35-dry condition the same difference is only 94 g. Figure 6.51 shows that the rate, at which refrigerant mass decreases in the accumulator section, changes after time index 220 s. The reason for this change in the rate can be found from observing the videos of the accumulator and its outlet tube. Between 190 s and 220 s, foam repeatedly reaches the top of the accumulator.

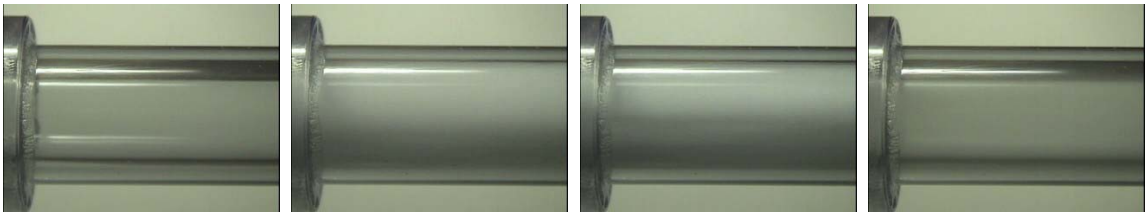

(a) 180 s (b) 180.3 s (c) 182 s (d) 185 s

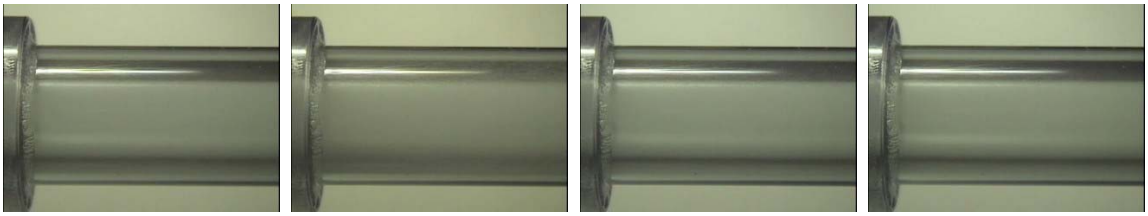

(e) 190 s (f) 200 s (g) 300 s (h) 480 s

Figure 6.54: Snapshots of outlet tube of accumulator during start-up for I35-wet condition

The observation of the video shows a periodic change in transparency of the outlet tube, corresponding to when foam visibly reaches the top of the accumulator. After 220 s, foam is not visibly reaching the top of the accumulator, corresponding to the change of rate at which refrigerant mass migrates out of the accumulator. The exact time when the system reaches its steady state refrigerant mass distribution cannot be concluded from the presented data. However, the measurement of the refrigerant mass distribution at 480 s is identical—within the measurement uncertainty—to the steady state refrigerant distribution.

The refrigerant and air inlet temperatures for the I35-wet condition during start-up are shown in Figure 6.55. The developments of the refrigerant temperatures are the same compared to the I35-dry condition, except for the temperature downstream of the evaporator—T_{reo}. The evaporator refrigerant exit temperature exceeds the saturation temperature by more than 5°C for 85 seconds—from 195 s to 280 s—compared to 10 seconds for the I35-dry condition—from 190 s to 200 s. The maximum difference is 16°C observed at 205 s for the I35-wet condition. The temperature difference starts to drop notably after 218 s. The video snapshots of the accumulator

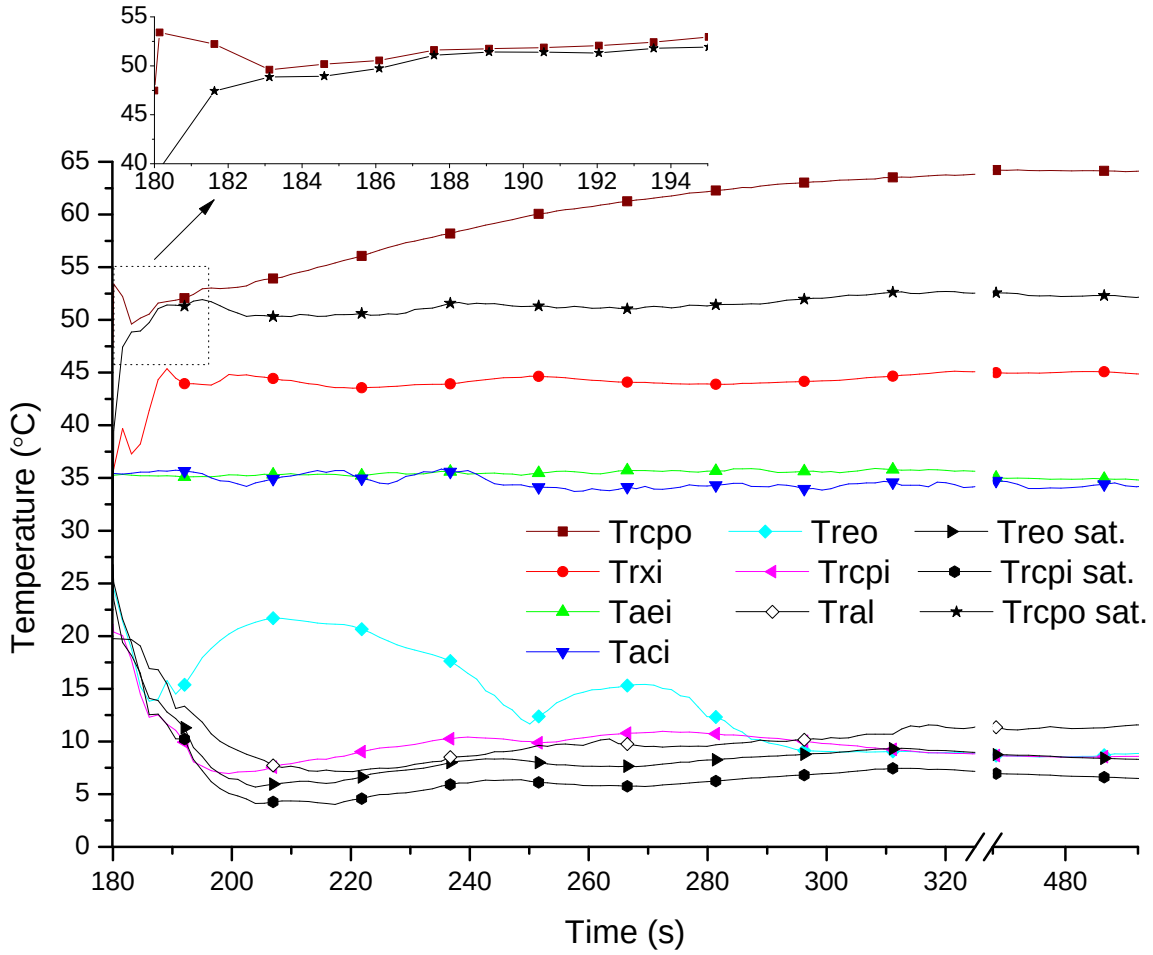

Figure 6.55: Start-up refrigerant and air inlet temperatures for I35-wet condition

inlet tube show between 185 s—Figure 6.52c—and 218 s—Figure 6.52f—a thin liquid film. The film is visible as a result of small slow moving ripples—the estimated speed of the ripples from the video is less then 5 mm/s. Assuming the thin film contains a negligible amount of refrigerant (and lubricant), only superheated refrigerant vapor is leaving the evaporator during this time frame. At 218 s a visibly thicker liquid films enters the inlet tube—Figure 6.52f shows the moment when the film has entered half way from the right side of the image. Figure 6.51 shows that between 190 s and 220 s the refrigerant mass in the evaporator increases at a faster rate than after 220 s. The evaporator holds 95 g less refrigerant mass at 190 s than at steady state. As a

result of the starved evaporator, the overall heat transfer coefficient of the evaporator drops, resulting in a lower evaporation pressure [75]. The evaporation pressure is at a minimum of 360 kPa at 200 s, before increasing to its steady state value of 400 kPa at 300 s. The saturation temperatures development in Figure 6.55—$T_{reo\ sat.}$ and $T_{rcpi\ sat.}$—follow accordingly. The measurement data and the video snapshots together indicate that the increase in refrigerant mass in the evaporator after 190 s is related to the decreasing superheated vapor in the evaporator. The higher degree of apparent superheated vapor and the longer occurrence—compared to the I35-dry condition—is a result of water condensate on the evaporator causing a latent heat transfer. Although there is the longer lasting and higher degree of superheat for the I35-wet condition, the cooling capacity development is not delayed compared to the I35-dry condition. Therefore, the observance of apparent superheat conditions at the evaporator exit does not correlate to the development of the cooling capacity for the two investigated cases.

The refrigerant mass flow rate and compressor power measurements—taken every 1.5 s—during start-up for both conditions are compared in Figure 6.56. As already mentioned, the dynamics regarding the refrigerant mass leaving the accumulator are identical during the first five seconds of start-up. The refrigerant mass flow rate peaks out at 90 g/s during the first 5 seconds for the I35-wet condition. The mass flow meter has a reading during the first five seconds—compared to the I35-dry condition—as a result of two effects. First, no liquid is observed at start-up in the outlet tube of the accumulator. Second, the temperature at the compressor outlet—T_{rcpo}—does not drop below its saturation temperature as it does for the I35-dry condition. The first reason explains why the peak in compressor power is only 0.2 kW above the steady state value compared to 0.5 kW for the I35-dry condition. For the I35-wet condition the refrigerant mass flow rate follows the compressor power as observed for the I35-dry condition. The decrease below the steady state mass flow rate between 200 s and

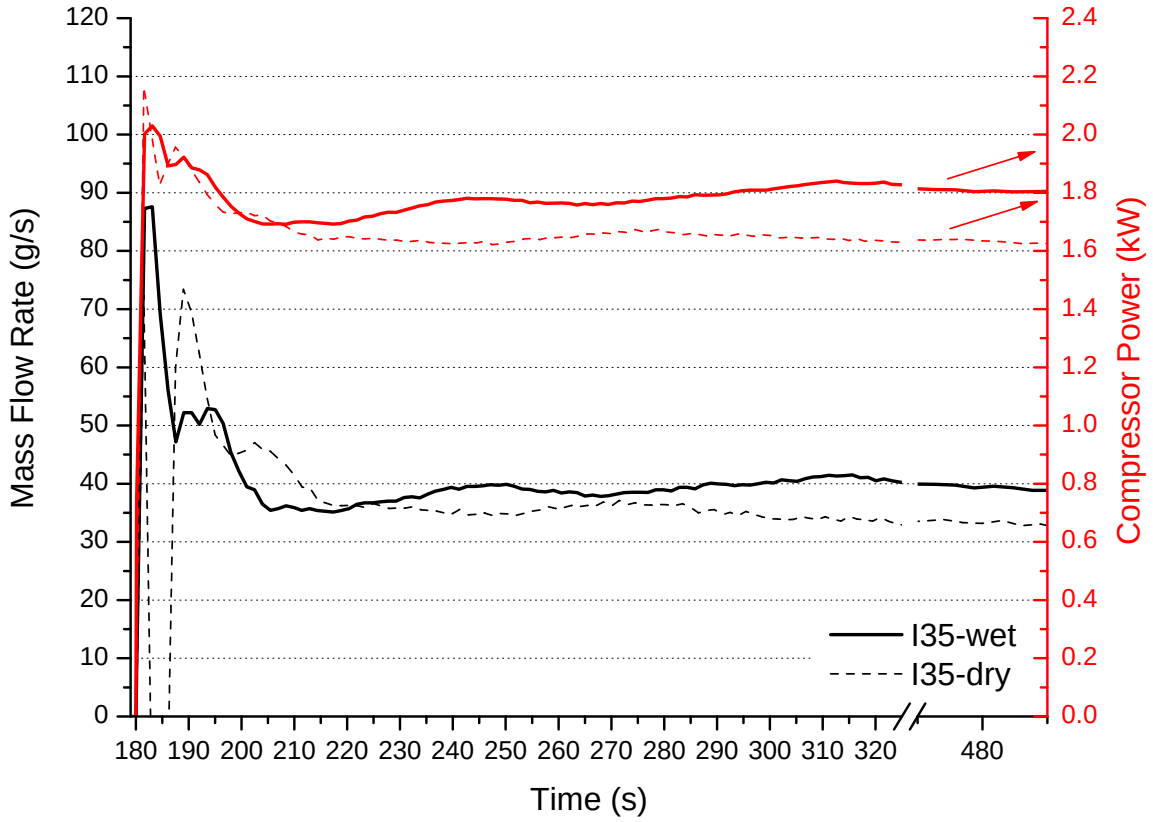

Figure 6.56: Start-up refrigerant mass flow rate and compressor power for I35-dry and I35-wet conditions

240 s coincides with the observed decrease in evaporation pressure as a result of the starved evaporator. The lower pressure and the lower refrigerant temperature at the compressor inlet—T_{rcpi} in Figure 6.55—result in a lower refrigerant density at the compressor inlet reducing the refrigerant mass flow rate.

The condenser section shows an increase of 182 g of refrigerant mass during the first 10 seconds to a value of 212 g—while 225 g is observed for the I35-dry condition. After 10 seconds, the refrigerant mass remains within 35 g of the steady state refrigerant mass storage capacity; identical to the I35-dry condition. The snapshots from the sight glass video show that it takes 5 seconds before two phase flow is visible—Figure 6.57b. The infrared pictures of the condenser—Figure 6.58—show an increase in the surface temperature from 35°C to 47°C during the first five seconds.

The temperature increase proceeds in the direction of the refrigerant flow. After 10 seconds—Figure 6.58g—the temperature distribution is almost identical to the steady state temperature distribution. The only significant change occurs at the inlet header. Its surface temperature slowly increases, corresponding to the measured compressor outlet temperature—T_{rcpo}—as shown in Figure 6.55, and reaches its steady state value at 300 s. Figure 6.58g shows that after 190 s, the lower minichannels are already being filled with liquid based on the conclusion drawn from the condenser model investigation—Section 6.2.4. The conclusion from all these observations is that the condenser refrigerant mass migration dynamics during start-up are not affected by water condensate on the evaporator—they are identical for both conditions.

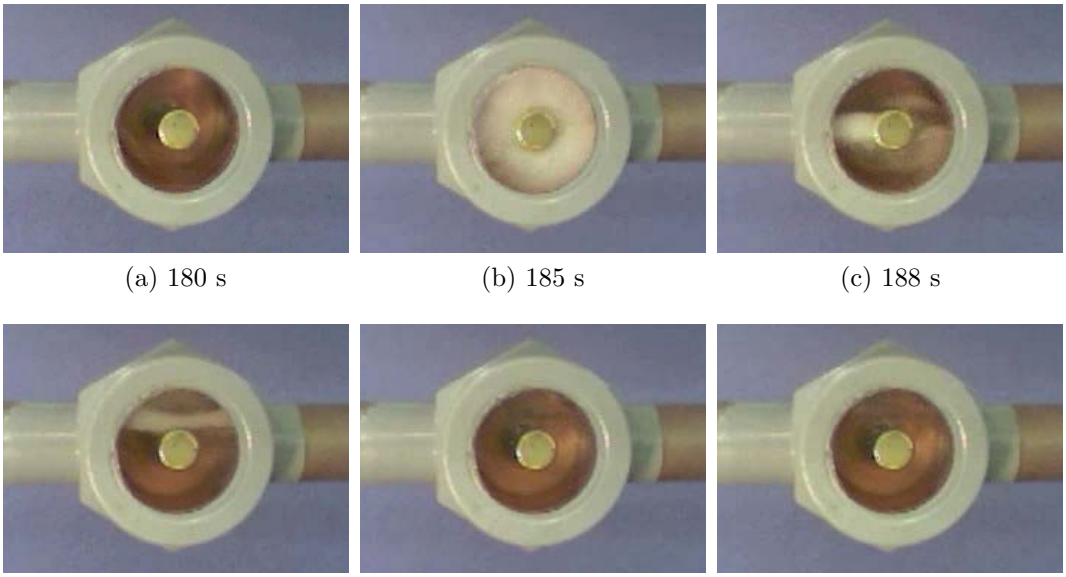

(a) 180 s (b) 185 s (c) 188 s

(d) 205 s (e) 220 s (f) 480 s

Figure 6.57: Snapshots of sight glass between condenser and expansion device during start-up for I35-wet condition

The liquid tube section shows a similar trend during start-up as observed for the I35-dry condition—first a sharp increase in refrigerant mass followed by a slower increase. The snapshots of the sight glass—shown in Figure 6.57—indicate that until 5 seconds after start-up no liquid refrigerant is present. Figure 6.57b shows the sight

glass is suddenly filled with fast moving foam at 185 s which gradually dissipates until a distinct liquid layer is visible at 188 s. The liquid layer height increases between 188 s and 480 s, corresponding to the measured increase in refrigerant mass shown in Figure 6.51. The delay until foam is visible in the sight glass indicates that the condenser is filled with refrigerant mass first before the liquid tube. Another conclusion is that only refrigerant vapor passes through the expansion device during the first 5 seconds. The result is a tremendous imbalance between the refrigerant mass flow rate provided by the compressor—in excess of 50 g/s—and the refrigerant mass flow rate through the expansion device—less than 10 g/s based on the data by Singh et al. [76]. After 10 seconds, the condenser sections reaches its steady state refrigerant mass storage capacity and all additional refrigerant mass is stored in the liquid tube after this time. At 220 s the evaporator refrigerant mass is close to its steady state refrigerant mass storage capacity. The result is that refrigerant mass leaving the accumulator after 220 s migrates to the liquid tube section.

The compressor section shows the least change in refrigerant mass during the start-up. For the I35-wet condition, the compressor section holds 19 g less refrigerant mass at start-up compared to the I35-dry condition. The refrigerant mass increases by 29 g to 81 g during the first 5 s of start-up and then decreases to the steady state value of 65 g as measured at 480 s.

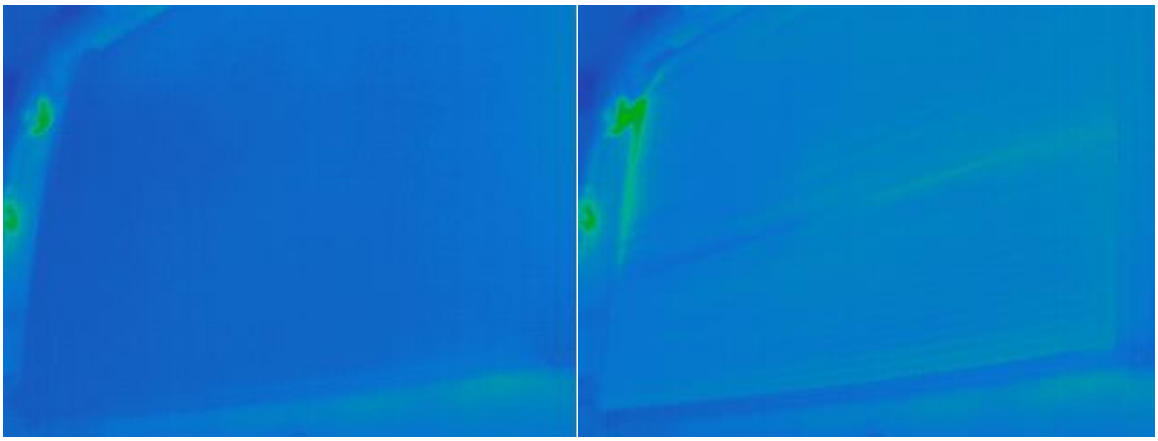

(a) 180 s (b) 181 s

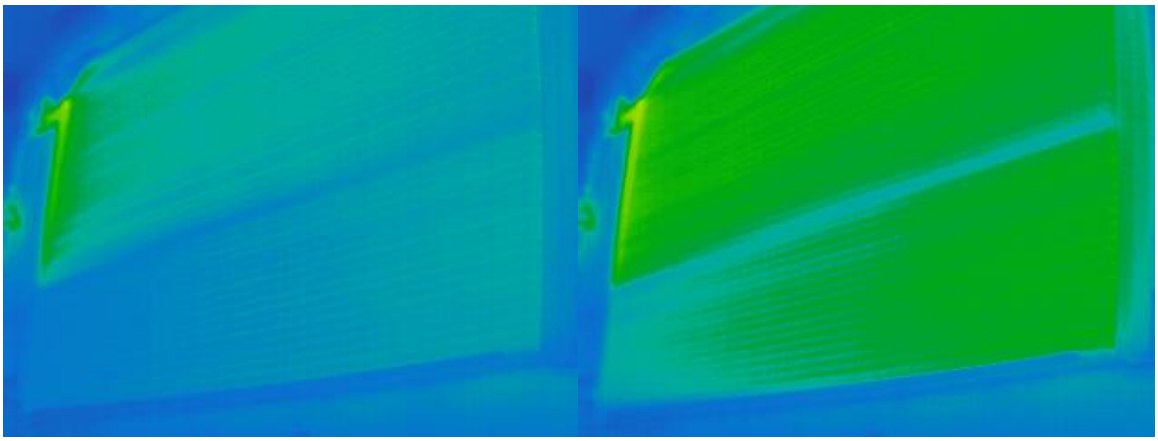

(c) 182 s (d) 183 s

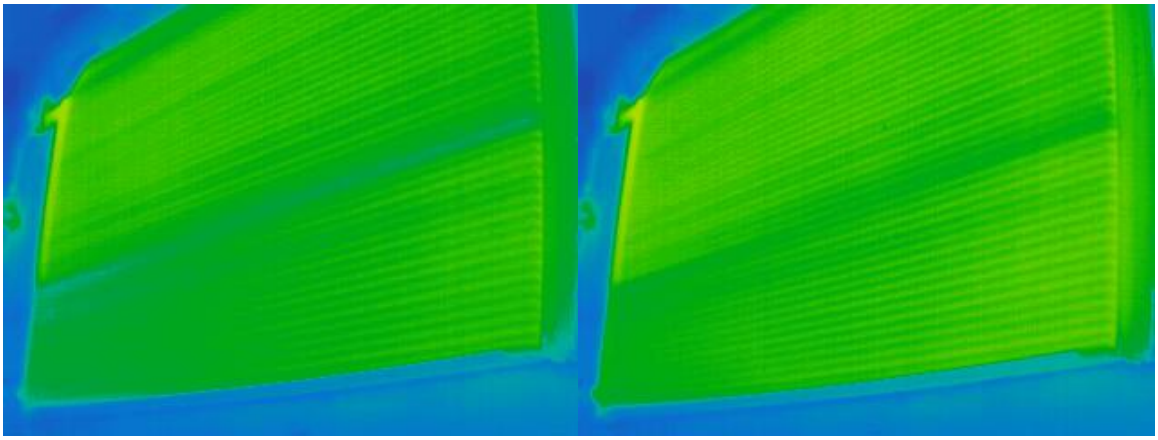

(e) 184 s (f) 185 s

Figure 6.58: Sequence of condenser infrared images during start-up for I35-wet condition

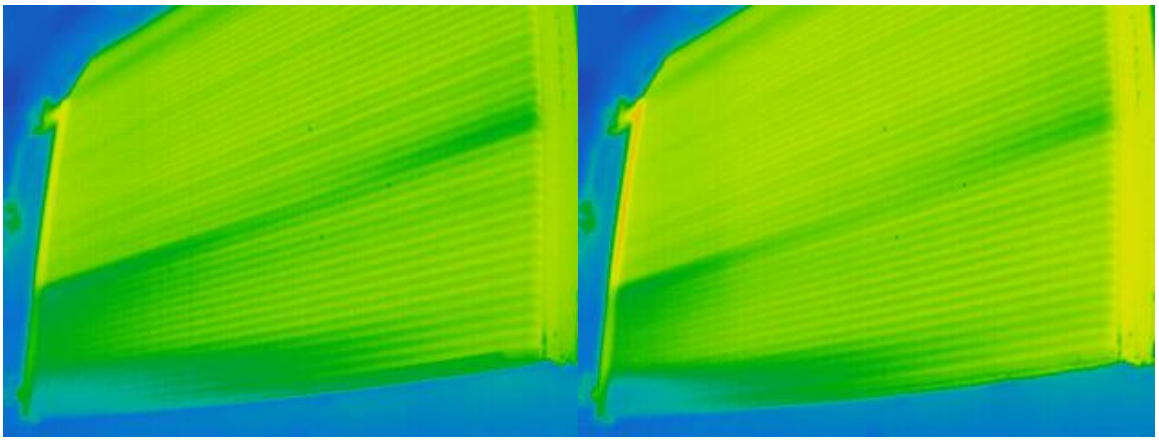

(g) 190 s (h) 200 s

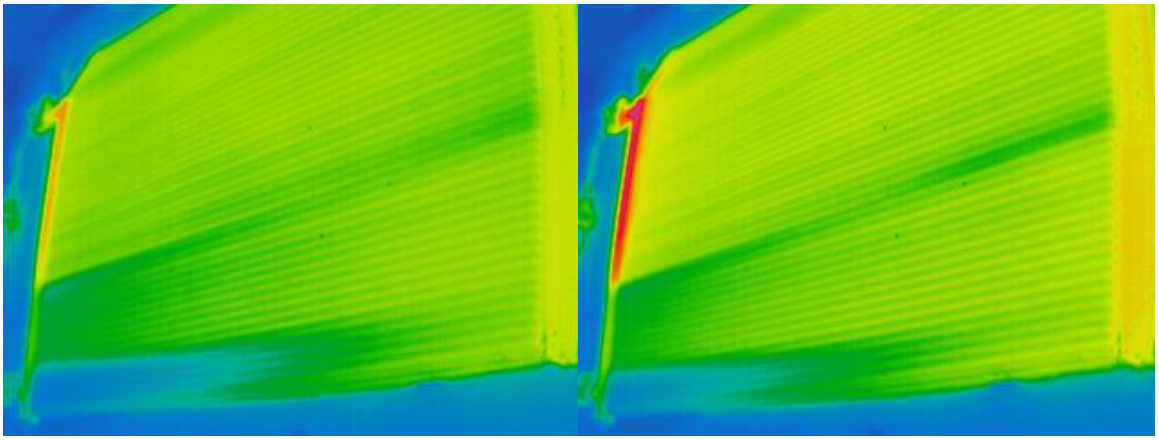

(i) 220 s (j) 300 s

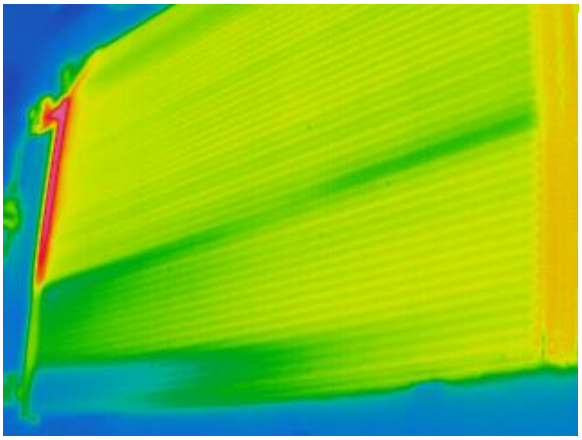

(k) 480 s

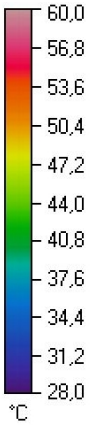

(l) Temperature scale

Figure 6.58: Sequence of condenser infrared images during start-up for I35-wet condition (cont.)

6.5 Lubricant Migration

This section discusses the experimental data of the lubricant mass migration presented in Chapter 5. The lubricant mass in the sections of the experimental breadboard system was measured during the same stop-start scenario as the refrigerant mass for the I35-wet operating condition. The lubricant masses in the sections were determined using the Quick Closing Valve Technique and the three different techniques described in Chapter 4. After the valves are closed, the refrigerant mass was determined first, followed by the lubricant mass. Therefore, the refrigerant mass distribution and lubricant mass distribution were taken for the same closing valve event. To analyze the experimental results—and gain a better understanding of the physics of refrigerant mass migration—additional measurements and techniques—such as temperature, pressure, mass flow rate, high speed and real time videography—are included in the discussion. Since the lubricant mass migration is measured for the same stop-start scenario as the refrigerant mass migration, references are made to the figures presented in Section 6.4.2—compressor stop period—and Section 6.4.4—start-up.

The section is organized into two parts. The first part discusses the lubricant migration during the compressor stop period, and the second part discusses the lubricant migration during the start-up. It should be noted that it is one stop-start event, and therefore the term "stop period" will be used instead of "off-cycle". The lubricant distribution at the end of the stop period is the initial distribution for the start-up. Because of this relation, the reader should read and consider both sections and not treat them as individual unrelated sections.

6.5.1 Lubricant Migration During the Stop-Period

The lubricant mass in the compressor was measured by the Remove and Weigh Technique and therefore is the lubricant mass in the compressor itself, not the compressor

section. The refrigerant mass measurement was completed for the entire compressor section which includes—besides the compressor—the suction and discharge tubes. The lubricant mass in the discharge tube was measured separately using the Mix and Sample Technique. The suction tube—tube #12 in Figure 2.3—between the ball valve separating the compressor section and accumulator section, was flushed as part of the accumulator section. The rational for this decision was that during shakedown experiments only small amounts of lubricant—less than one gram—were measured in the suction tube. The reason for a low amount of lubricant mass was most likely caused by the tube orientation. As shown in Figure 2.4, the suction tube—which is partly a flexible hose—bends downwards to the compressor allowing any lubricant to be drained into the compressor.

The lubricant mass migration during the compressor stop period for the I35-wet operating condition is shown in Figure 6.59. Since the accumulator section holds more

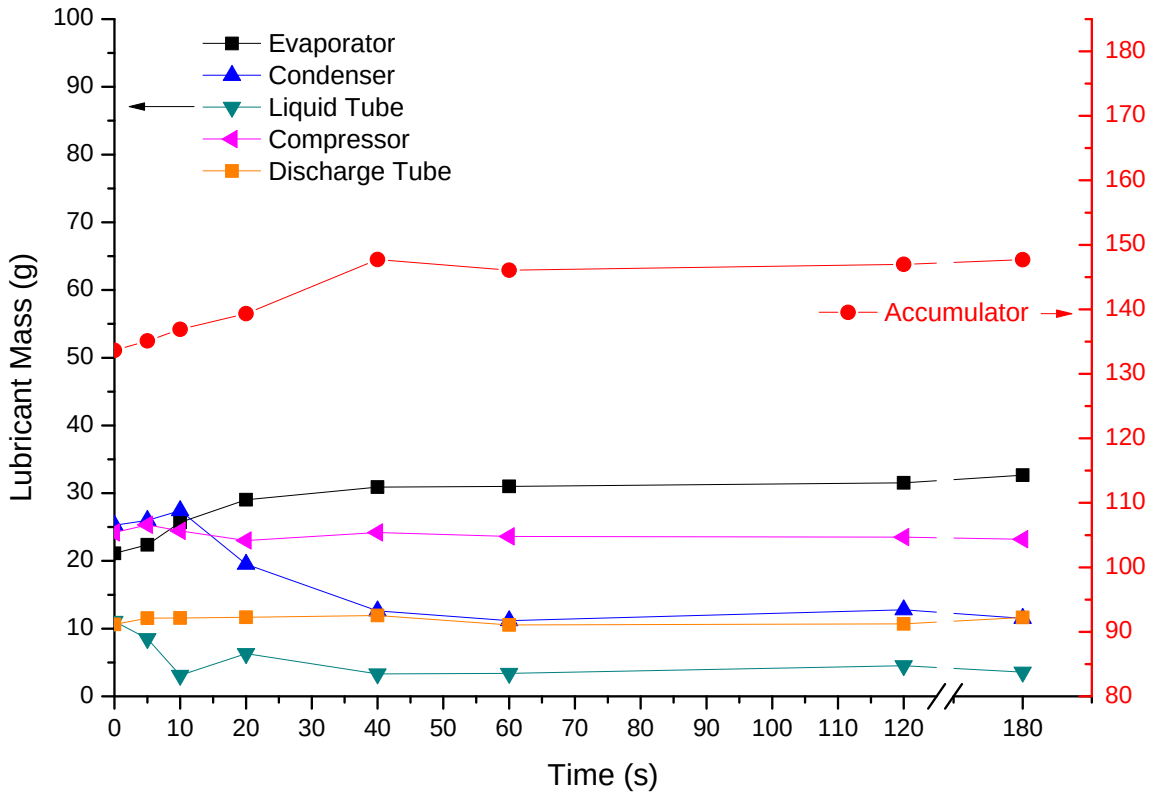

Figure 6.59: Stop period lubricant mass migration for I35-wet condition

than 50 percent of the total lubricant mass in the system at steady state operation, a second ordinate is used. The relative scaling of the seconds ordinate is identical to the first ordinate. Measurements are denoted by markers, and lines represent trends. Error bars are omitted to maintain readability of the graph.

During the first 10 seconds the lubricant in the condenser section increases by 2.1 g. The evaporator section has an increase of 4.6 g during the same time period, as does the accumulator by 3.3 g. The amount of lubricant in the compressor and the discharge tube changes by less than 1 g. The liquid tube is the only section showing a decrease of 8 g during the first 10 seconds. The migration of refrigerant mass and lubricant mass are correlated. Each section which has an increase in refrigerant mass also has an increase in lubricant mass. Therefore, the same conclusion as for the refrigerant mass migration can be made for the lubricant migration—during the first 10 seconds lubricant mass drains from the liquid tube into both, the condenser section and evaporator section. After 10 seconds the condenser section lubricant mass decreases—as does its refrigerant mass. Since the lubricant mass in the discharge tube and compressor section does not change, the lubricant must leave the condenser via the liquid tube. The result is a temporary increase in the lubricant mass in the liquid tube—as measured at 20 s—and at the same time an increase in refrigerant mass is measured. In both, the evaporator and accumulator sections, lubricant mass increases during the first 40 s of the stop period. After 60 s the lubricant migration ends. A total of 22 g of lubricant mass migrated from the high pressure sections—condenser and liquid tube—to the low pressure sections—evaporator and accumulator. Overall, the amount of lubricant mass migrating is a function of the lubricant concentration in the liquid refrigerant-lubricant mixture and hence the observed correlation between the migration of refrigerant mass and lubricant mass.

The infrared pictures of the condenser during the stop period—Figure 6.42—indicated that refrigerant evaporates inside the bottom header and minichannels be-

tween 40 s and 120 s. The presence of liquid refrigerant-lubricant mixture below the level of the outlet tube of the condenser after 40 s means the liquid is not drawn out of the condenser during the first 40 s. The evaporating refrigerant mass leaves the lubricant behind, explaining why the lubricant mass in the condenser remains above 10 g.

The comparison between the refrigerant mass migration and lubricant migration leads to the following conclusions regarding the physical mechanism of lubricant migration during the compressor stop period. Lubricant mass migrates during the primary refrigerant mass migration, but not during the secondary refrigerant migration. The primary refrigerant migration is caused by the diminishing pressure difference across the expansion device. During the primary refrigerant migration refrigerant—in both vapor phase and liquid phase—migrates. The secondary refrigerant migration—caused by a pressure gradient as a result of thermal nonequilibrium within the system—leads only to vapor phase refrigerant mass migration. Therefore, lubricant mass migrates when liquid phase refrigerant migrates. When vapor phase refrigerant migrates during the stop period, lubricant mass does not. The visualization of the sight glass supports this conclusion. The snapshots of the sight glass—Figure 6.37—show that during the first 60 s liquid is visible. The video shows movement of liquid out of the sight glass during the first 40 seconds. After 40 seconds foam—on top of the visible liquid layer—is caused by the release of refrigerant mass from the lubricant-refrigerant mixture. The released vapor phase refrigerant migrates—visible by the decreasing liquid layer and confirmed by the refrigerant mass measurements—leaving the lubricant behind.

Lubricant mass did not migrate during the secondary refrigerant mass migration for the investigated I35-wet condition. The investigation of the I35-dry refrigerant mass migration, however, shows a possible mechanism by which lubricant mass could be migrating during the secondary refrigerant mass migration. The visualization of

the accumulator section revealed that liquid—a mixture of refrigerant and lubricant—can leave the accumulator. A liquid plug inside the U-tube in combination with a pressure difference causes the liquid refrigerant-lubricant mixture to be drained into the outlet tube of the accumulator. As Figure 6.31 shows, the liquid in the outlet tube increases after 60 s—during the secondary refrigerant migration. Therefore, whenever a liquid plug is formed and a large enough pressure difference occurs, a potential for lubricant migration exists. Lubricant migration can also be caused by gravity. The visualization of the sight glass and accumulator section show that after the compressor is stopped, liquid will pool—as a result of gravity—in convexities. The accumulator is an example of a large convexity, as well as the headers of the heat exchangers. The orientation of tubes and headers will dictate to where the lubricant will migrate.

Here a three minute compressor stop period is investigated but another lubricant migration can occur for longer compressor stop periods. The infrared pictures of the condenser during the stop period—Figure 6.42—show that liquid is pooling inside the bottom header and minichannels, below the level of the outlet tube. It is possible that caused by temperature inequilibrium refrigerant vapor condenses inside the condenser until the liquid level reaches above the exit tube level. The result would be—depending on the orientation of the tube and relative heights of the components—that liquid can drain out of the condenser as a result of gravity. This would cause a lubricant migration even after the compressor is, e. g., turned off for hours. Another possibility of an increase in liquid level in a convexity is the diffusion of refrigerant vapor into the lubricant. This is essentially the reversion of the process observed in the sight glass between 60 s and 180 s—Figure 6.37. The diffusion of refrigerant vapor increases the liquid level of the refrigerant-lubricant mixture until it reaches a level which allows the liquid mixture to be drained out. Figure 4.7 shows that even if there is large difference between the vapor-liquid equilibrium pressure this process

is of the orders of hours.

6.5.2 Lubricant Migration During the Start-Up

The distribution of the lubricant after three minutes of compressor stop time and the difference compared to the steady state lubricant mass distribution are shown in Table 6.13. The differences shown in Table 6.13 do not add up to 0, but to 4.4 g since

Table 6.13: Lubricant mass distribution before compressor start and difference to steady state distribution

Discharge Tube	Evaporator	Accumulator	Condenser	Liquid Tube	Compressor
g	g	g	g	g	g
11.6	32.7	147.7	11.5	3.6	23.2
+1.0	+11.6	+14.1	-13.8	-7.5	-1.0

the amount of lubricant mass in the system at steady state was 225.9 g compared to 230.3 g after three minutes of compressor stop time. The increase in lubricant in the accumulator section is 14.1 g, but the increase in refrigerant mass is 230 g. As a consequence, the concentration of lubricant in the liquid refrigerant-lubricant mixture is reduced from 60 percent at steady state, to 33 percent before the start-up. The concentration of lubricant in the liquid refrigerant-lubricant mixture in the evaporator section is 6 percent and is therefore more diluted than in the accumulator. Based on the refrigerant mass migration results, 434 g of refrigerant leaves the evaporator during the first 5 seconds of the start-up. Assuming all this refrigerant mass leaving is a liquid refrigerant-lubricant mixture having a lubricant concentration of 6 percent—26 g of lubricant should be leaving the evaporator. The lubricant mass measurements between start-up and 5 seconds after start-up confirm that the evaporator section lubricant mass is reduced by 26 g.

The lubricant mass migration during the start-up is shown in Figure 6.60. Since

the changes in the lubricant mass during the first 25 seconds are dynamic, an inset graph is shown for this time period. Actual data points are denoted by markers, and lines connect data points. During the first 5 seconds, the lubricant mass increases in

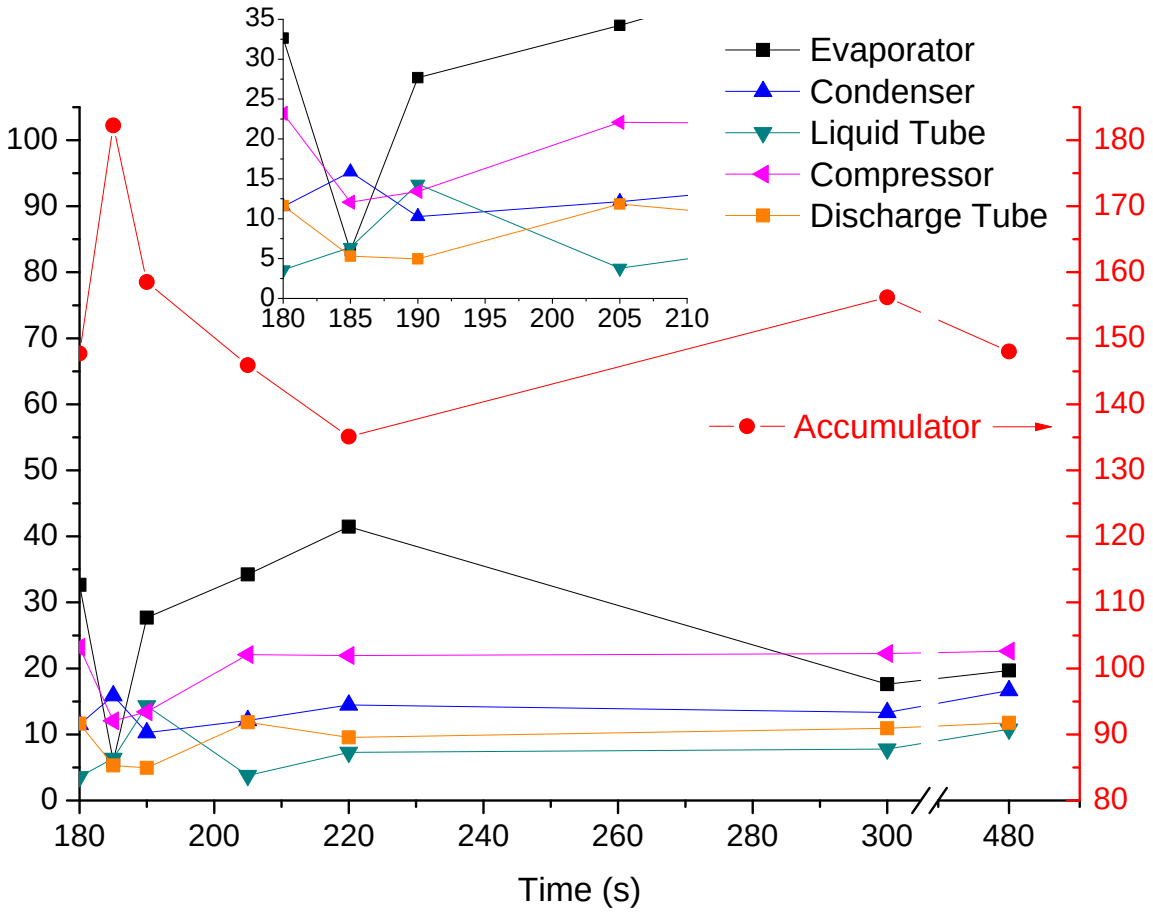

Figure 6.60: Start-up lubricant mass migration for I35-wet condition

the accumulator, the condenser and liquid tube sections. These sections also have an increase in refrigerant mass during the first 5 seconds. The evaporator section has a decrease in lubricant mass, which also corresponds to a decrease in refrigerant mass. The compressor section has an opposite trend—the refrigerant mass increases during the first 5 seconds; however, the lubricant mass decreases by 11.1 g—the amount of lubricant is reduced by half. The lubricant mass is also reduced by half in the discharge tube. For both components, the lubricant mass starts to increase again after 190 s and reaches a steady state value after 205 s. The reduced lubricant mass

in the compressor and discharge tube coincides with the increased refrigerant mass flow rate between 180 s and 190 s.

Between 183 s and 190 s, the compressor exit temperature equals its saturation temperature. The video snapshots of the accumulator outlet tube show fast moving foam during the first 5 seconds. Therefore, liquid leaving the accumulator and entering the compressor during the first 5 seconds flushes out half of the lubricant from the compressor and discharge tube. After less foam is visibly entrained in accumulator outlet tube and the refrigerant mass flow rate is around 50 g/s at 190 s, the compressor and discharge tube are "refilled" with lubricant mass. During the same time frame, the condenser is also "refilled". As a result of this "refilling process", more lubricant mass leaves than enters the liquid tube section and explains the decrease in lubricant mass by 10.5 g. The observed reduction in lubricant mass during the first 25 seconds of the start-up in the compressor is an important finding for compressor designers since even a short-term reduction in lubrication could potentially cause compressor damage.

Between 180 s and 185 s, the lubricant mass in the condenser section increases by 4.4 g, but then decreases by 5.6 g between 185 s and 190 s. The decrease occurs after fast moving foam is observed in the sight glass at 185 s—Figure 6.57—and an increase in lubricant mass in the liquid tube is observed between 185 s and 190 s. The largest increase in lubricant mass between 185 s and 190 s is observed in the evaporator—21.7 g. During the same time frame the accumulator lubricant mass is reduced by 27.7 g. Based on the observation that fast moving foam occurs in the sight glass after 185 s, it can be concluded that it takes at least 5 seconds before lubricant from the accumulator can reach the evaporator.

After 185 s, the lubricant mass in the evaporator increases and reaches a peak at 220 s, at which time the evaporator holds 41.5 g—twice as much as at steady state. To answer the question of what causes the accumulation of lubricant in the evaporator,

Figure 6.55—showing the refrigerant and air inlet temperatures—and Figure 6.52—showing snapshots of the accumulator inlet tube—are revisited. Figure 6.55 shows an apparent superheat of 14°C at 220 s at the evaporator exit—T_{reo}. Assuming only refrigerant vapor leaves the evaporator, lubricant mass has to accumulate in the evaporator. If this assumption were correct, the lubricant mass should increase until the apparent superheat disappears—which is not the case, the lubricant mass starts to decrease before the apparent superheat disappears. The accumulator inlet tube images offer an explanation for this alleged contradiction. The video snapshots of the accumulator inlet tube show a thin liquid film between 185 s and 218 s. The film is visible as a result of slow moving ripples. The estimated speed of the ripples from the video is less than 5 mm/s and therefore only minuscule amounts of lubricant leave the evaporator. The slow moving thin film confirms the assumption that—neglecting the exiguous amounts of liquid refrigerant in the film—only superheated refrigerant vapor leaves the evaporator. At 218 s, however, a visible thicker films enters the inlet tube from the evaporator side, as shown in Figure 6.52f. The estimated velocity of the film is 200 mm/s—40 times faster than the velocity of the thin liquid film. After the appearance of the thicker film, the lubricant mass starts to decrease in the evaporator. The film slowly disappears over the next 80 seconds, as does the apparent superheat. Therefore, a possible explanation for the lubricant migration observed in the evaporator is as follows. After 26.7 g of lubricant is flushed out of the evaporator section during the first 5 seconds, lubricant starts to enter the evaporator from the expansion device. The initially warm evaporator surface temperature causes the entering refrigerant two phase mixture to evaporate immediately and the resulting vapor is superheated. Since only a small amount of lubricant in a thin film driven by the superheated vapor can leave the evaporator, lubricant mass starts to accumulate in the evaporator. After 218 s, the increase in refrigerant mass inside the evaporator in combination with the heat transfer rate forms a thicker—presumed lubricant rich—

film which leaves the evaporator. The temperature measurement—which was taken using an immersed thermocouple in the center of the tube—shows that the refrigerant vapor leaving after 218 s is still superheated. After 300 s the evaporator reaches close to its steady state balance and the superheated vapor as well as the observed liquid film disappear. An essential conclusion from this observation is that the presence of apparent superheated vapor cannot be used a sole indicator for lubricant mass accumulation in the evaporator.

The observed apparent superheat and thin film between 185 s and 220 s have an influence on the migration of lubricant from the accumulator section. Between 185 s and 190 s, constant foam entrainment is observed in the accumulator. Between 190 s and 220 s, foam repeatedly reaches to the top of the accumulator. Therefore, lubricant can leave the accumulator through the top of the U-tube and through the hole at the bottom of the U-tube, while almost no lubricant enters the accumulator during this time. As a result, 47.1 g of lubricant leaves the accumulator between 185 s and 220 s. After the evaporator releases more lubricant starting at 218 s—caused by the appearance of the thicker liquid film—the lubricant mass in the accumulator starts to increase. After 480 s, the compressor, discharge tube, liquid tube and evaporator sections are within 2 g of their steady state lubricant mass distribution. The accumulator and condenser sections are within 15 g and 9 g, respectively, of their steady state distribution. Considering all uncertainties—refrigerant and lubricant mass in the system, valve closing offsets, repeatability of conditions for stop-start event—it is assumed that the lubricant migration has ended after 480 s.

6.6 Strategies to Improve Start-Up Energy Efficiency

As concluded in Section 6.1, refrigerant mass migrates from the high pressure components—condenser, liquid tube, high pressure receiver—to the low pressure components—evaporator, accumulator—during off-cycle or shut-down. During on-cycle or start-up, refrigerant mass must be transferred from the low pressure components to the high pressure components. The initial refrigerant mass distribution at the beginning of the on-cycle is identical to the mass distribution at the end of the off-cycle. Therefore, the off-cycle mass migration has a direct influence on the on-cycle performance since compressor energy is necessary to redistribute the refrigerant mass.

The results of the refrigerant mass migration for the I35-dry condition show that 482 g of refrigerant must be returned from the low pressure components to the high pressure components during start-up. A simplified calculation illustrates how much compressor energy is necessary for the redistribution of refrigerant mass. Neglecting the development of the pressures during start-up, and assuming the measured steady state conditions—330 kPa at the compressor inlet and 1350 kPa, 63°C at the compressor outlet—the energy necessary to compress 482 g of saturated R134a vapor from 330 kPa to the compressor outlet state is 18.2 kJ. If the refrigerant mass present at 330 kPa is a saturated liquid, the necessary energy is 112.6 kJ—six times higher than if the refrigerant mass were in a saturated vapor state. Therefore, using compressor energy to change refrigerant mass from liquid phase to vapor phase should be avoided.

As the analysis of the investigated start-up cases show, the entrainment of liquid phase refrigerant into the accumulator exit tube—and henceforth the compressor inlet—is not completely avoidable. The necessary energy to change the phase from liquid to vapor of the liquid refrigerant mass in the accumulator—to be redistributed

to the high pressure components—should ideally be from the energy transferred by heat to the evaporator. Superheated vapor from the evaporator entering the accumulator causes liquid refrigerant in the accumulator to be evaporated. The additional vapor leaves the accumulator and consequently more refrigerant mass leaves the accumulator than enters it until a balanced refrigerant mass distribution is achieved.

One option to reduce the energy consumption of the compressor during the on-cycle is to avoid the refrigerant migration during the off-cycle. Wang and Wu [77] prevented the charge migration of an air conditioner—which used a sealed reciprocating compressor and capillary tube—during the off-cycle by closing a magnetic cut-off valve. They concluded that "if the refrigerant is prevented from migrating during the shut-down cycle, the peak value of power input will reduce by 9.4 percent". Performing an identical experiment—keeping the valve upstream of the expansion device closed during the compressor stop period—showed a reduction of the peak value of the compressor power by 9.8 percent for the I35-dry condition and 5.4 percent for the I35-wet condition. The higher difference for the I35-dry condition is a result of the presence of liquid in the accumulator outlet tube before start-up. Including the result from Wang and Wu [77], it can be concluded that preventing refrigerant migration during the off-cycle reduces the compressor power peak at start-up.

Although the peak in compressor power during the first seconds is reduced, the question is if the development of the cooling capacity is affected—positively or negatively—by avoiding refrigerant mass migration during the off-cycle. Figure 6.61 shows a comparison of the compressor power and cooling capacity during start-up for two cases—baseline and no-migration. For the baseline case, refrigerant mass was free to migrate during the three minutes of compressor stop time. For the no-migration case, the valve directly upstream of the expansion device was closed during the three minutes of compressor stop time and was opened at the same time the compressor was turned on again. In Figure 6.61 markers are individual data points—data was taken

every 1.5 seconds. The initial peak in compressor power is reduced by 9.8 percent

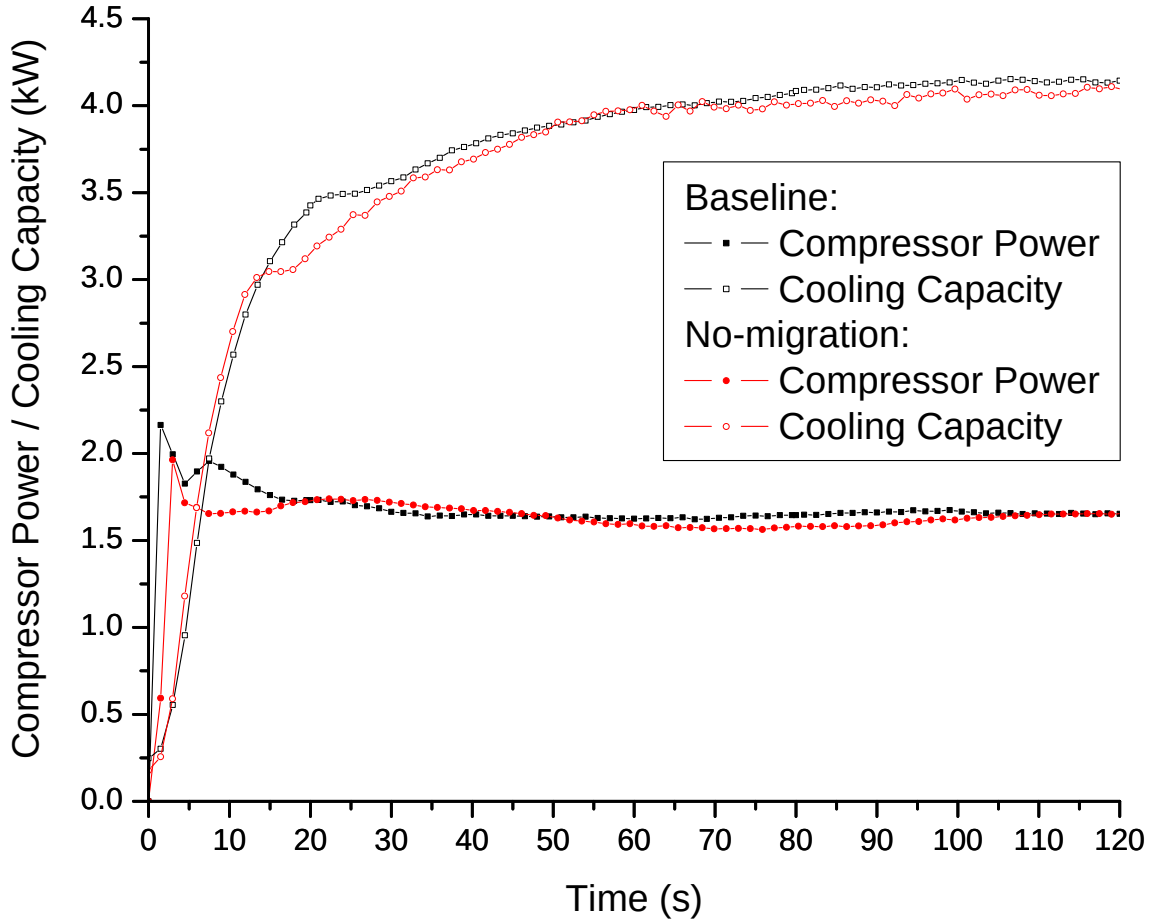

Figure 6.61: Comparison of start-up compressor power and cooling capacity for I35-dry condition with and without refrigerant mass migration during the stop period

as already mentioned. Between 0 s and 15 s the compressor power consumption for the no-migration case is below the baseline case, while the cooling capacities are identical. Between 15 s and 30 s the compressor power consumption is the same for both cases but the cooling capacity is lower for the no-migration case. To objectively compare the two different cases, an energy evaluation was performed. Of interest is the energy spent to drive the compressor, W, compared to the energy removed from the evaporator air stream by heat, Q. Energy spent to move the air across the heat exchangers was neglected since it is the same for both cases. From Figure 6.61,

it can be concluded that after 100 s the compressor power and cooling capacities are identical for both cases, within the measurement uncertainties. Therefore, the energies are calculated by integrating the energy rates of the compressor, $\dot{W}$, and evaporator, $\dot{Q}$, between 0 s and 100 s as shown in Equations (6.29) and (6.30).

$$W = \int_{0s}^{100s} \dot{W}\, dt \tag{6.29}$$

$$Q = \int_{0s}^{100s} \dot{Q}\, dt \tag{6.30}$$

The results show that the compressor energy spent for the no-migration case during the first 100 s of start-up was 163.5 kJ—4.6 kJ less than for the baseline case. The energy removed from the evaporator air stream was 350.4 kJ for the no-migration case—7.2 kJ more than for the baseline case. Overall, the no-migration case leads to a better start-up performance because less compressor energy is spent while more energy is removed from the air stream for the first 100 s.

Avoiding refrigerant migration by closing a valve during the off-cycle might not be an option for some systems. The additional cost of installing a valve and its controller, and the possibility of a failure—the valve does not open at start-up—might be a concern to system designers. Therefore, another option was experimentally investigated—ramping the compressor speed during start-up. The intention is to start with a slower compressor speed since—as described in Section 6.4.3—the refrigerant mass flow rate exceeded 70 g/s during the first 10 seconds of the start-up as a result of liquid phase refrigerant entering the compressor. Increasing the compressor speed at a slower rate might reduce the entrainment of liquid refrigerant into the compressor during start-up. For the baseline and no-migration cases mentioned earlier, the compressor speed reaches 900 rpm within one second. Three additional experiments were conducted under the I35-dry operation condition using an identical

compressor stop time of three minutes. For each of these experiments, the compressor speed was increased linearly to 900 rpm for 10 s, 20 s and 30 s. The compressor power and cooling capacity results for the three compressor ramp cases compared to the baseline and no-migration cases are shown in Figure 6.62.

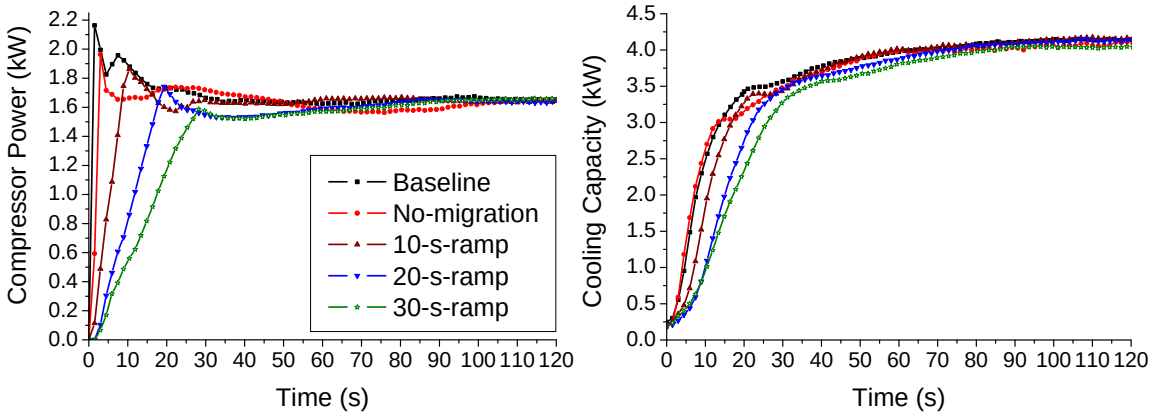

(a) Compressor Power (b) Cooling Capacity

Figure 6.62: Comparison of start-up compressor power and cooling capacity for I35-dry condition—compressor speed ramps

The peak in compressor power is reduced for longer compressor speed ramp times. For the 30 s compressor speed ramp case, a peak above the steady state value of 1.65 kW was no longer observed. As a result of the compressor speed ramping, the compressor power development is delayed accordingly. The development of the cooling capacities is, however, affected—the slower the compressor speed increases, the slower the cooling capacity development. However, after 100 s all cases have reached the steady state cooling capacity. To objectively compare the five cases, the compressor power and cooling capacity for each case was integrated from 0 s to 100 s using Equations (6.29) and (6.30). The results are presented in Table 6.14. The compressor energy savings increase with increasing compressor speed ramp time. For the 30-s-ramp case the energy spent is reduced by 32.3 kJ or 19.2 percent compared to the baseline case. The energy removed from the air stream by heat, Q, is reduced by 26.7 kJ or 7.8 percent, however. Calculating the ratio of energy input to the

Table 6.14: Start-up energy comparison from 0 s to 100 s

	W	Q	Q/W
	kJ	kJ	-
Baseline	168.1	343.2	2.04
No-migration	163.5	350.4	2.14
10-s-ramp	157.6	345.1	2.19
20-s-ramp	144.5	328.1	2.27
30-s-ramp	135.8	316.5	2.33

compressor and energy removed from the air stream—an energy coefficient for the first 100 s of the start-up—shows that the ratio increases with an increase in compressor speed ramp time. Based on this ratio, the 30-s-ramp case has the best energy efficient start-up—the reason can be seen in Figure 6.63.

For the baseline case the compressor power exceeds the cooling capacity during the first 7.5 s. The consequence is that more energy is spent at the compressor than is removed from the air stream during this time—denoted by the hatched area in Figure 6.63. For the 30-s-ramp case, the compressor power stays below the cooling capacity and therefore has a positive energy balance—more energy is extracted from the air stream than is inputted into the compressor.

Refrigerant charge migration prevention during off-cycle by using an additional valve reduces the compressor power peak at start-up for the system investigated and improves the energy efficiency of the start-up. It is important to note that the strategy is intended to increase the start-up performance—but the implementation is during the off-cycle. The measured improvement, however, was not as high as expected. As a result of the sudden opening of the valve, a peak in compressor power is still present. A gradual opening of the valve might provide a better start-up performance, and therefore future research in this direction is needed. If a closed valve during off-cycle is not an option, ramping the compressor speed during start-up should be

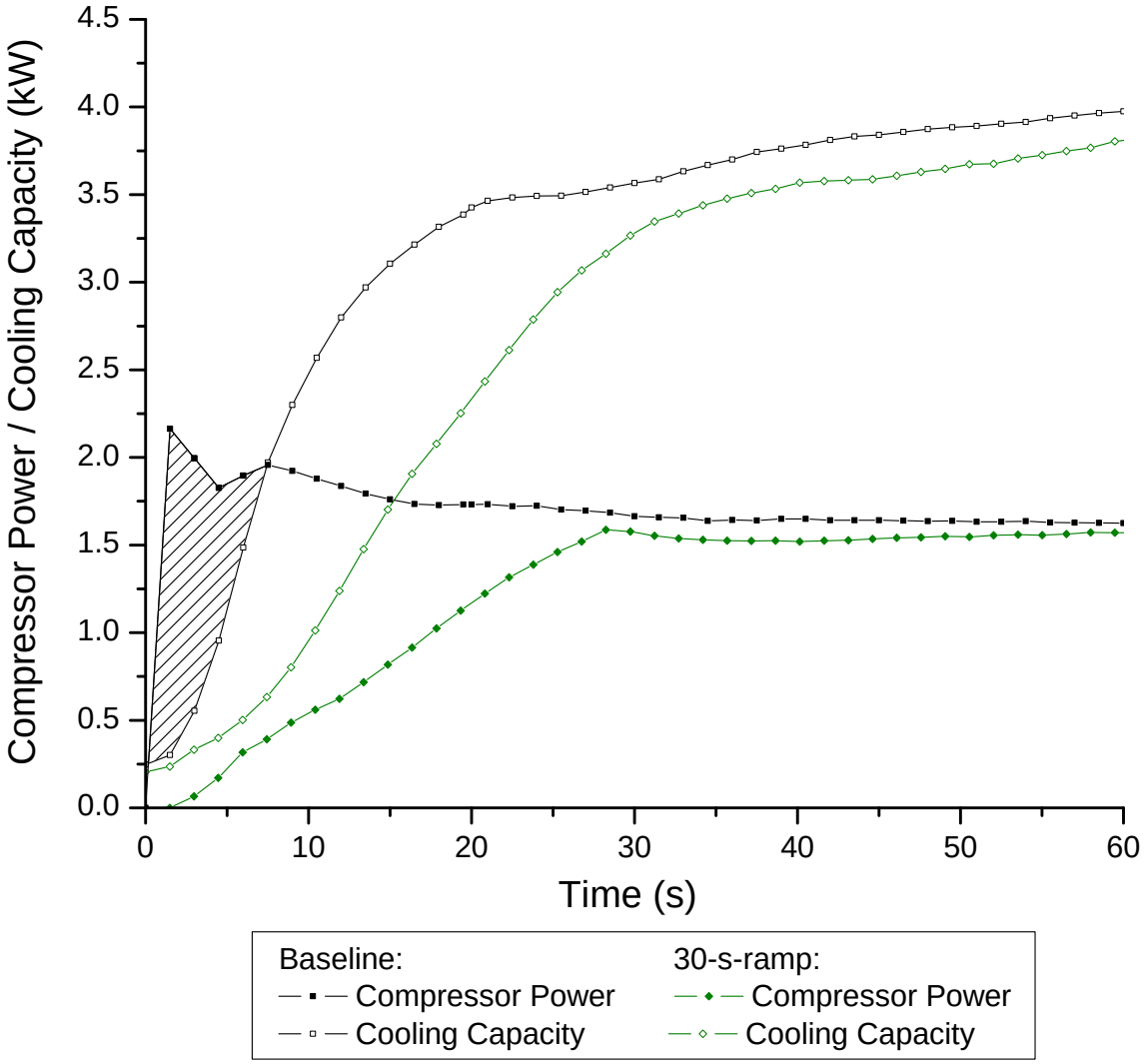

Figure 6.63: Comparison of start-up compressor power and cooling capacity for I35-dry condition—baseline vs. 30-s-ramp

considered. Ramping the compressor speed leads to a delayed development of the cooling capacity, but to a more energy efficient start-up. If a delay in the cooling capacity development is tolerable, ramping the compressor speed is an alternative to preventing refrigerant charge migration during off-cycle. Overall, the most beneficial start-up strategy may be a combination of both; refrigerant charge migration prevention and—not necessarily linearly—compressor speed ramping.

Chapter 7

Conclusions and Recommendations

The refrigerant and lubricant migration of an R134a automotive A/C system—utilizing a fixed orifice tube, minichannel condenser, plate and fin evaporator, U-tube type accumulator and fixed displacement compressor—was measured. Experimental procedures were developed to measure the refrigerant and lubricant migration through the major components of the system during steady-state and stop-start operation. Analyses of the experimental results provide insight into the mechanisms of refrigerant and lubricant distribution and migration. The conclusions of these studies and recommendations for future work are described in the following sections.

7.1 Summary and Conclusions

The experimental technique used to measure the refrigerant mass migration is the Quick-Closing Valve Technique (QCVT) combined with the Remove and Weigh Technique (RWT) using liquid nitrogen as the condensing agent. The following conclusions are made:

1. The combination of both techniques—QCVT and RWT—enables the measurement of the refrigerant mass distribution at any given time. The lubricant mass distribution can also be measured using these techniques in conjunction with supplementary procedures. Therefore, the QCVT—in combination with the RWT—are recommended for refrigerant and lubricant migration measurements.

2. The total refrigerant mass in the system is determined with an uncertainty of ±4.0 grams.

3. The valves are closed manually—a light indicator is used to signal when to close the valves. As a result, the uncertainty regarding the refrigerant mass in a single section is a function of the refrigerant mass flow rate and the reaction time of the persons closing the valves. For the refrigerant mass flow rate at steady state operation the uncertainty was determined to be less than ±10 grams.

4. The determination of the refrigerant mass distribution using the QCVT and RWT is time consuming. For the investigated breadboard system—divided into five sections—it takes ca. 40 hours to complete one set of data.

The lubricant-refrigerant combination used was R134a and a polyalkylene glycol (PAG) oil with an ISO viscosity grade of 46 mm^2/s—a miscible combination over a wide range of temperatures. The determination of the lubricant mass distribution was achieved by employing three different techniques—Remove and Weigh, Mix and Sampling, and Flushing. To employ the Mix and Sampling Technique a device—called the Mix and Sampling Device—was built. The following conclusions are made:

1. Both, the Mix and Sampling Technique and Flushing Technique require separating the refrigerant and lubricant. A method to separate the refrigerant and lubricant, which does not require the use of an additional solvent, was developed and allows reusing the lubricant after separation. This method has an accuracy of 0.04 grams of refrigerant left in the lubricant after separation.

2. The mix and sample technique was used to determine the lubricant mass inside the heat exchangers, and the liquid and discharge tube sections. Verification experiments demonstrated the Mix and Sampling Device—short circuited—can determine the lubricant mass within an uncertainty of 0.1 grams. Although

the complex geometry of the heat exchangers prevents a complete mixing of lubricant and refrigerant—the mechanism the method relies on—the uncertainty regarding the lubricant mass inside the heat exchangers was less than 1 gram.

3. The Remove and Weigh Technique provides the most accurate determination of lubricant mass if two conditions are met—the tare weight is known precisely and all refrigerant mass is removed from the lubricant. A method was developed to remove the refrigerant mass from the lubricant mass in the compressor before applying the Remove and Weigh Technique. It was demonstrated that the application of this method leaves less than 0.04 grams of refrigerant mass in the compressor. The tare weight of the compressor has an uncertainty of 1 gram.

4. The flushing technique, applied at the accumulator section, has the largest uncertainty—1.43±0.61 grams, or 1.97±1.16 grams if the refrigerant-lubricant mixture is not fully mixed.

5. The total amount of lubricant within the system—using the three measurement techniques—has a deviation of -1.03±1.57 grams compared to the known filled in amount of lubricant in the system—which has an uncertainty of ±0.06 grams. Therefore, the total amount of lubricant mass in the system can be determined to within two percent when applying the three techniques.

Experiments were conducted at steady state operating conditions—using different amounts of refrigeration mass inside the system—and the refrigerant mass and lubricant mass distributions were measured. The relationship between refrigerant mass and lubricant mass hold-up in the accumulator was analyzed. A condenser model was developed using published correlations to evaluate the difference between refrigerant mass prediction and measurements. The following conclusions are made:

1. The optimum amount of refrigerant mass—1000 grams—for the design condi-

tion was found when the liquid tube was filled with liquid phase refrigerant. Any added refrigerant mass beyond the optimum charge is stored in the accumulator.

2. An evaporator refrigerant exit temperature above its saturation temperature—apparent superheat—does not result in an "dry" accumulator as a result of the lubricant refrigerant miscibility. If the apparent superheat is taken as actual superheat, and the refrigerant mass in the accumulator is calculated using only refrigerant properties, an underestimation of 159 grams would result at the design condition for a total system charge of 1000 grams.

3. Whether the refrigerant-lubricant mixture inside the accumulator can be treated as a mixture in equilibrium at steady state operating conditions—and therefore vapor-liquid equilibrium (VLE) correlations can be incorporated into accumulator model calculations to account for the affect of lubricant on the refrigerant charge hold-up inside the accumulator—can not be conclusively determined from the measurements. The inlet and exit temperature and pressure measurements around the accumulator are not sufficient in combination with a VLE correlation to determine the concentration of R134a in the liquid refrigerant-lubricant mixture inside the accumulator under steady state operating conditions.

4. The lubricant distribution at steady state operating condition showed that 55 percent of the lubricant mass is found in the accumulator, 11 percent is found in the evaporator, condenser and compressor, and six percent in the liquid and discharge tube.

5. An increase in refrigerant mass above 1000 grams—while keeping the amount of lubricant constant—resulted in an increase in lubricant hold-up in the accumu-

lator and a decrease of lubricant in all other sections—including the compressor. The amount of lubricant in circulation is reduced from 4.5 percent to 3.4 percent if the refrigerant mass in the system is increased from 1000 grams to 1500 grams.

6. The condenser model investigation showed that the overall heat transfer predictions are within 10 percent of the experimental data. Including a void fraction correlation based on a probabilistic flow map increased the prediction of the refrigerant mass inventory by three percent to seven percent compared to using a homogeneous assumption. The model underpredicts the measured refrigerant mass by 20 percent to 40 percent. An infrared picture analysis indicated that the lower minichannels have significantly reduced mass flow rates, and are completely filled with liquid refrigerant. Including this observation increases the model prediction of the refrigerant mass to within 20 percent of the measurements.

A nondimensional approach was presented to scale the transient cooling capacity during stop-start operation using the steady state cooling capacity. This approach provides a better comparison of the dynamic development of the cooling capacity for different systems during stop-start.

1. A comprehensive curve fit was derived which represents the transient cooling capacity during on-off cycling and was validated for R134a at operating conditions with and without dehumidification. The limitations and conditions for applying this curve fit to other system have been discussed. The comprehensive curve fit is not restricted to refrigeration system using R134a as a refrigerant.

2. Experiments at different ambient temperatures did not influence the dynamics of the cooling capacity during stop-start operation.

3. The presence of water condensate on the evaporator coil did change the dy-

namics of the cooling capacity during the stop-start operation. An evaporative cooling effect was observed, which reduced the decrease in cooling capacity during the compressor stop time compared to the case with a dry evaporator coil. The presence of water condensate has a less pronounced effect on the development of the cooling capacities during start-up. Based on the scaled cooling capacity approach, the start-up development is faster—for water condensate present on the evaporator—but only during the first ten seconds. After ten seconds the difference between both cases is less than five percent and is identical after 90 seconds.

Two refrigerant mass migration results are presented for a transient event, during which only the compressor is stopped for three minutes and then started again. The first results were taken at the design operating condition with dry air—no dehumidification at the evaporator and referred to as the dry case—and the breadboard system using the original accumulator. The second results were taken at the design operating condition containing moist air—dehumidification occured at the evaporator and referred to as the wet case—and the breadboard system using a transparent accumulator section. The lubricant migration was also measured for the second case. The presented results for the second case are unique since the refrigerant and lubricant migration were measured simultaneously. The combination of measurement results—infrared photography and high speed and real time videography—provide unprecedented insight into the mechanisms of refrigerant and lubricant migration during stop-start operation.

From the analyses the following conclusions are made regarding the *refrigerant mass migration during the stop period*:

1. All experimental data available in the open literature—including this work—show consistently that refrigerant mass migrates from the high pressure compo-

nents—condenser, liquid tube, high pressure receiver (filter/drier)—to the low pressure components during off-cycle or shut-down. The dynamic of this migration can be categorized into two parts. A primary refrigerant mass migration—lasting 20 seconds to 3 minutes depending on the system—during which the majority of refrigerant mass migrates followed by a secondary migration.

2. The physical mechanisms of the primary and secondary refrigerant mass migration were identified. The primary refrigerant mass migration is caused by, and follows, the diminishing pressure difference across the expansion device. The secondary refrigerant migration is caused by a pressure gradient as a result of thermal nonequilibrium within the system and causes only vapor phase refrigerant migration.

3. The U-tube of the accumulator fills with liquid during the stop period forming a liquid plug. For the investigated accumulator a pressure difference of 1.5 kPa was enough to raise the liquid level inside the U-tube and liquid refrigerant and lubricant drained into the suction tube.

4. During the first ten seconds of the compressor stop period, more refrigerant mass left the liquid tube—located between condenser and expansion device—than passed through the expansion device. Consequently, an increase in refrigerant mass was measured in the condenser. A hypothesis was formulated to explain this unprecedented phenomenon—observed for both refrigerant mass migration results. As soon as the compressor is turned off, the mass flow rate to the condenser ceases. The condensation of refrigerant vapor in the condenser, however, does not stop immediately. Without supply of refrigerant vapor from the compressor, the condensation of the refrigerant vapor inside the condenser leads to a reduction in pressure. This reduction in pressure is assumed to be quicker during the first five to ten seconds—compared to the reduction in pres-

sure caused by the pressure equilibration across the expansion device—as a result of vapor condensation in the formerly superheated vapor zone and the accompanying sharp change in density. The resulting pressure gradient forces refrigerant and lubricant mass back into the condenser.

5. The videos of the liquid tube section sight glass showed that liquid was pooling below the tube entrance/exit after the initial flow ceased. This observation demonstrates that it is possible for liquid—refrigerant and lubricant—to accumulate in convexities during the stop period. During the secondary mass migration, the liquid refrigerant in the sight glass gradually evaporated. The infrared images of the condenser showed that—as result of liquid being pooled by gravity in the lower minichannels—refrigerant evaporates in the lower minichannels during the secondary mass migration.

6. The compressor section had the least refrigerant mass migration by an order of magnitude—tenths of grams compared to hundredths of grams in the other sections.

Comparing the results of the refrigerant mass migration for the two cases—with and without dehumidification at the evaporator—gives the following conclusions regarding the *effect of the presence of water condensate on the evaporator on the refrigerant mass migration during the stop period*:

1. The reversion of the latent heat transfer—which occurred at 37 seconds into the stop period—and the ensuing evaporative cooling effect, affects the refrigerant mass migration significantly.

2. The amount of refrigerant mass migrating from the high pressure components to the low pressure components during the primary refrigerant mass migration is higher—580 grams compared to 360 grams. The amount of refrigerant

mass migrating during the secondary migration is lower—26 grams compared to 125 grams. Overall, 121 grams more refrigerant mass migrates from the high pressure components to the low pressure components during the 180 s compressor stop period.

3. The refrigerant mass migration to the evaporator is significantly increased—576 grams of refrigerant mass was found in the evaporator after the primary refrigerant mass migration compared to 291 grams for the dry case. During the secondary mass migration the refrigerant mass in the evaporator decreased by 20 grams compared to 40 grams for the dry case.

4. The temperature of the liquid inside the accumulator stays below the saturation temperature throughout the stop period—a constant difference of 7°C was measured after the primary refrigerant mass migration ceased. The temperature difference and the accumulator videos—no boiling is observed during the 180 s compressor stop period—indicate that the liquid in the accumulator is in a subcooled state.

5. Liquid was observed in the outlet tube of the accumulator after 20 seconds into the compressor stop period—at the same time as for the dry case. The evaporative cooling effect caused a pressure difference of less than 1.5 kPa after 45 seconds and liquid was drawn back from the exit tube into the accumulator.

6. The apparent equilibration pressure was reached at the same time as for the dry case, i.e., the primary mass migration ended at the same time, but is lower by 100 kPa.

The following conclusions were made regarding the *refrigerant mass migration during the start-up*:

1. The start-up refrigerant mass migration is caused by an imbalance of the refrigerant mass flow rates across the compressor and expansion device. Until the steady state refrigerant mass distribution is reached the refrigerant mass flow rate across the compressor is higher than through the expansion device.

2. The higher compressor refrigerant mass flow rate—during the first ten seconds exceeding 70 g/s—is a result of the entrainment of foam into the U-tube of the accumulator. A peak in compressor power is observed during the first five seconds—liquid present at the accumulator outlet tube before start-up lead to a higher peak.

3. No liquid phase refrigerant reaches the expansion device for the first three to five seconds. As a result of vapor phase refrigerant at the expansion device inlet the refrigerant mass flow through the expansion device is not high enough to compensate the refrigerant mass leaving the evaporator—the refrigerant mass in the evaporator is depleted during the first five seconds. The ensuing decrease in apparent superheated vapor at the evaporator coincided with an increase in refrigerant mass. As a result of the longer period of apparent superheated vapor for the wet case the refilling of the evaporator took 30 seconds compared to 10 seconds for the dry case.

4. The entrainment of foam into the U-tube accelerates the refrigerant mass redistribution during start-up. The refrigerant mass flow rate—for the dry case—reached its steady state value after 40 seconds—as did the compressor power—which coincided with the disappearance of foam in the accumulator. After 40 seconds, 95 percent of the steady state refrigerant mass distribution was reached in all components for the dry case.

5. When the entrainment of foam into the U-tube of the accumulator ceases before

the steady state refrigerant mass distribution is reached—as observed for the wet case after 40 seconds—the remaining refrigerant mass migration is significantly slower—on average 0.5 g/s of refrigerant mass left the accumulator in four minutes. The refrigerant mass leaving the accumulator after 40 seconds is stored in the liquid tube since the heat exchangers already reached their steady state refrigerant mass hold-up capacities. The steady state refrigerant mass distribution was measured after five minutes for the wet case.

6. The condenser reached its steady state refrigerant mass distribution to within 10 percent after 10 seconds and the infrared pictures indicated that the lower seven minichannels—below and above the outlet tube—are filled with liquid as soon as 10 seconds after start-up.

The lubricant mass distributions were measured during stop-start operation at the design operating condition with moist air and the breadboard system using a transparent accumulator section. The presented results are unique since the refrigerant and lubricant migration were measured simultaneously. The following conclusions were made regarding the *migration of lubricant during stop-start operation*:

1. During the compressor stop period, lubricant migration was proportional—depending on the local concentration of lubricant in the liquid refrigerant lubricant mixture—to the refrigerant mass during the primary refrigerant mass migration. Lubricant did not migrate during the secondary refrigerant mass migration—refrigerant mass migrating in the vapor phase did not cause a lubricant mass migration. Distinguishing between refrigerant mass migration in the liquid phase or vapor phase during off-cycle is important because it affects the lubricant migration.

2. Although not observed for the experimental system, lubricant mass migration could occur during the secondary refrigerant mass migration. The diffusion

of refrigerant vapor could increase the liquid level of a refrigerant-lubricant mixture in a convexity until it reached a level such that the liquid mixture is drained out by gravity. A liquid plug—being moved as a result of the pressure difference–can cause lubricant migration. In both cases, the orientation of tubes and headers would dictate the direction of the lubricant migration.

3. The lubricant mass migration during the start-up is not proportional to the refrigerant mass migration.

4. The absolute higher magnitude of refrigerant mass migration compared to the lubricant mass migration during the compressor stop period resulted in a decreased concentration of lubricant in the liquid refrigerant-lubricant mixture in the low pressure components. The lubricant mass in the compressor and discharge tube was reduced by half during the first five seconds. The lubricant mass in the compressor stayed below the steady state lubricant hold-up capacity during the first 25 seconds of the start-up.

5. It took at least five seconds before lubricant mass migrated into the evaporator. As a result the lubricant mass was reduced from 32 grams to 6 grams in the evaporator. After five seconds, lubricant accumulated in the evaporator as long as only refrigerant mass in the vapor phase left the evaporator. The presence of apparent superheated vapor—based on immersed thermocouple and pressure measurements—is insufficient to determine that only refrigerant in the vapor phase left the evaporator. Videos confirmed the lubricant mass measurements—a presumed lubricant rich liquid film was observed in the evaporator outlet tube even when apparent superheat was measured—resulting in a decrease of lubricant mass in the evaporator.

6. Lubricant can leave the accumulator by two mechanisms during the start-up—

foam entrainment at the top of the U-tube, and liquid entrainment through the hole at the bottom of the U-tube. Foam entrainment leads to a faster lubricant mass migration out of the accumulator than liquid entrainment through the hole at the bottom of the U-tube.

The off-cycle refrigerant mass migration has a direct influence on the on-cycle performance since compressor energy is necessary to redistribute the refrigerant mass. Experiments with different strategies were conducted to *improve the start-up energy efficiency*:

1. Using compressor work to change refrigerant mass from a liquid to a vapor phase should be avoided. Energy to change the phase of refrigerant mass in the accumulator—which needs to be redistributed to the high pressure components—should ideally be from the energy transferred by heat to the evaporator.

2. Refrigerant mass migration prevented by closing a valve upstream of the expansion valve reduced the compressor power peak at start-up for the system investigated and improved the energy efficiency of the start-up. However, as a result of the sudden opening of the valve a peak in compressor power was still present. A gradual opening of the valve may provide better start-up performance.

3. Ramping the compressor speed linearly led to a delayed development of the cooling capacity, but to a more energy efficient start-up. The compressor power stayed below the cooling capacity, resulting in a positive energy balance—more energy is extracted from the air stream than is inputted into the compressor—during the start-up when the compressor speed was increased linearly over 30 seconds.

4. The most beneficial start-up strategy might be a combination of both refriger-

ant charge migration prevention and—but not necessarily linearly—compressor speed ramping.

7.2 Recommendations and Future Work

Experimental data regarding the refrigerant mass migration during transient operation is scarce, not because refrigerant mass migration is well understood, but because experiments to measure the refrigerant mass migration directly are time expensive—using the Quick Closing Valve and Remove and Weigh Technique with liquid nitrogen as a chilling agent required 40 hours to measure one set of data. The uncertainty regarding the mass in each section was a function of the reaction time since the ball valves were closed manually. The use of automated ball valves is recommended to further decrease the measurement uncertainty. Additional recommendations and general guidelines when using the Quick Closing Valve and Remove and Weigh Technique are given in Section 3.5.

The lubricant distribution measurement was accomplished by using different techniques which are—in the order of complexity—Remove and Weigh, Flushing, and Mix and Sample. Application of these techniques added additional experimental time—one set of data required a week to complete. The techniques were optimized for the investigated system to give accurate measurements while keeping the experimental time manageable. For the Flushing technique, e.g., the measurement uncertainty could be improved by increasing the number of flushing runs but this would also increase the experimental time. The Mix and Sample technique is the most flexible but complex technique. Recommendations and general guidelines to extend the Mix and Sample Technique to different systems are given in Section 4.5.3.

The migration of refrigerant mass from the high pressure components—condenser, liquid tube, high pressure receiver, high pressure side of an internal heat exchanger—

to the low pressure components—evaporator, accumulator, suction tube, low pressure side of an internal heat exchanger—during off-cycle or shut-down has to be reversed during the on-cycle or start-up. The experimental investigation presented showed more energy efficient start-up performance is achieved by avoiding the migration of refrigerant mass during off-cycle and ramping the compressor speed during start-up. Future research should be directed to investigate the efficient use of energy to achieve the refrigerant mass redistribution which could include, using control strategies, pumping the liquid refrigerant during the off-cycle back to the high pressure components, or investigating new designs of components.

The visualization of the transparent accumulator revealed the entrainment of liquid into the suction line during off-cycle. An anti-siphon hole—a small hole at the top of the U-tube—allows pressure equilibration between the inside of the accumulator and suction tube during off-cycle, and as a result liquid entrainment into the suction tube can be prevented. However, the U-tube would be still filled with liquid at the internal liquid level of the accumulator which could still result in a liquid slug during start-up. Future research should be directed to investigate design changes to the accumulator. These could include a valve inside the accumulator to prevent the filling of the U-tube with liquid during off-cycle, a controlled liquid bypass instead of a U-tube, or an ejector for the entrainment of liquid into the vapor stream. Providing an adequate lubricant return to the compressor at all times—including the first seconds of a start-up—must be considered as well.

Many physical phenomena exist—two-phase flow development during start-up, liquid-vapor separation in the heat exchanger headers, changes in lubricant-refrigerant thermophysical properties—which are not well understood. The simulation of refrigerant mass movement during transient scenarios, especially cycling (stop-start), is therefore extremely challenging. Experimental studies are essential to provide a basis to validate computer simulations. Furthermore, experimental studies identify the

relevant physical mechanisms. A simplified engineering model can be derived by neglecting less relevant physical mechanisms which provides a close representation of the actual system behavior. A collaboration with Li and Alleyne [78]—who developed a dynamic model of a vapor compression cycle for shut-down and start-up operations [79]—demonstrates the importance of experimental research and analysis on modeling development. As an example, Figure 7.1 shows a comparison between the simulation prediction and the experimental data of refrigerant mass migration in the liquid tube during stop-start operation.

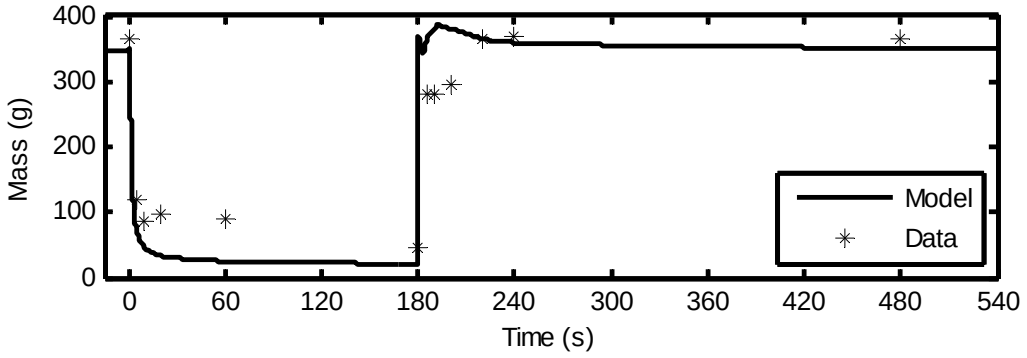

(a) Liquid tube modeled using one zone model

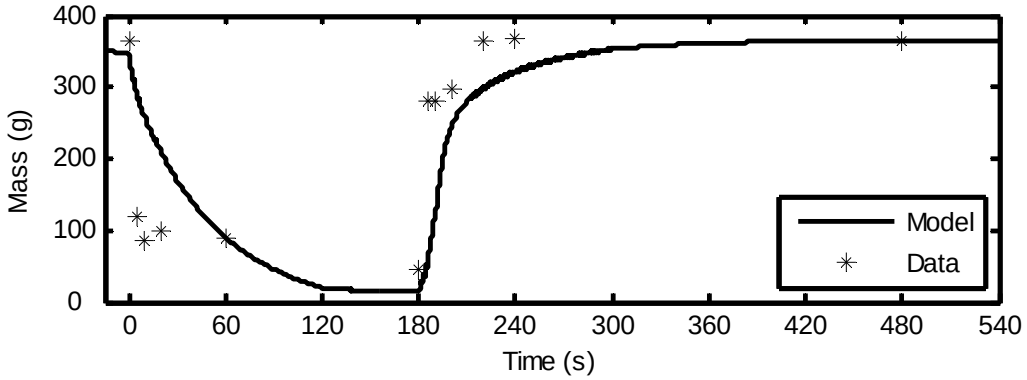

(b) Liquid tube modeled using two zone model

Figure 7.1: Comparison of refrigerant mass migration in liquid tube—experimental results vs. model prediction

Originally the liquid tube was modeled as a one zone model allowing the refrigerant

phase to be either liquid or vapor. However, the experimental measurements and the visualization of the liquid tube showed that during start-up the liquid tube is not instantaneously filled with liquid phase refrigerant—liquid and vapor phase are both present for a certain time. Changing the model from a one zone to a two zone model—allowing for two phases to be present—improved the model prediction during the start-up, shown in Figure 7.1b.

Not only can deviations be quantified by comparing experimental results and model results, but also the physical causes of the deviations can be identified. The deviation during the beginning of the compressor stop-period—between 0 and 60 s in Figure 7.1b—results because the model does not account for the reversal in refrigerant flow back to the condenser during the first 10 seconds. The model prediction in Figure 7.1a might seem better for the compressor stop period, but the actual physics are not captured. Future experimental work has to integrate mass measurements and visualization techniques to further enhance the understanding of the physical mechanisms of the refrigerant mass and lubricant mass migration during transient operation. Dynamic models need to be able to predict the refrigerant mass—and eventually the lubricant mass—migration to be useful in predicting transient energy consumption. Dynamic models matching only transient pressure and temperature developments are not sufficient to faithfully represent real systems.

Appendix A

Specifications of System Components

This appendix contains additional information about the system components. Information regarding the internal volumes of the heat exchangers, dimensions and flow orientations, as well as the geometry of the fixed orifice tube and specifications of the compressor are presented.

Condenser

Figure A.1 shows a picture of the condenser and its header arrangement. The direction of the air flow is into the page. The condenser was installed in a vertical upright position in the wind tunnel, and therefore the gravity in Figure A.1 acts downward. The air velocities at steady state operation—I35-wet condition—were measured using a hot wire anemometer. The condenser face area was divided into 35 quadrants and the average air velocity in meter per seconds was determined. The quadrants and corresponding air velocities are shown in Figure A.2. The main dimensions and volumes of the condenser are presented in Table A.1.

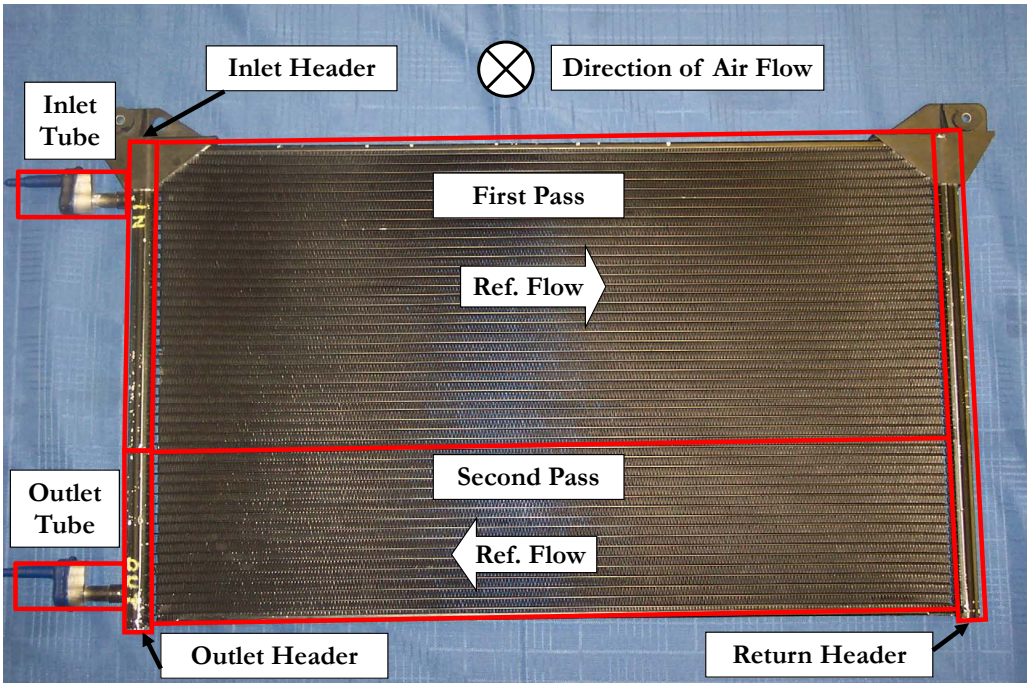

Figure A.1: Condenser

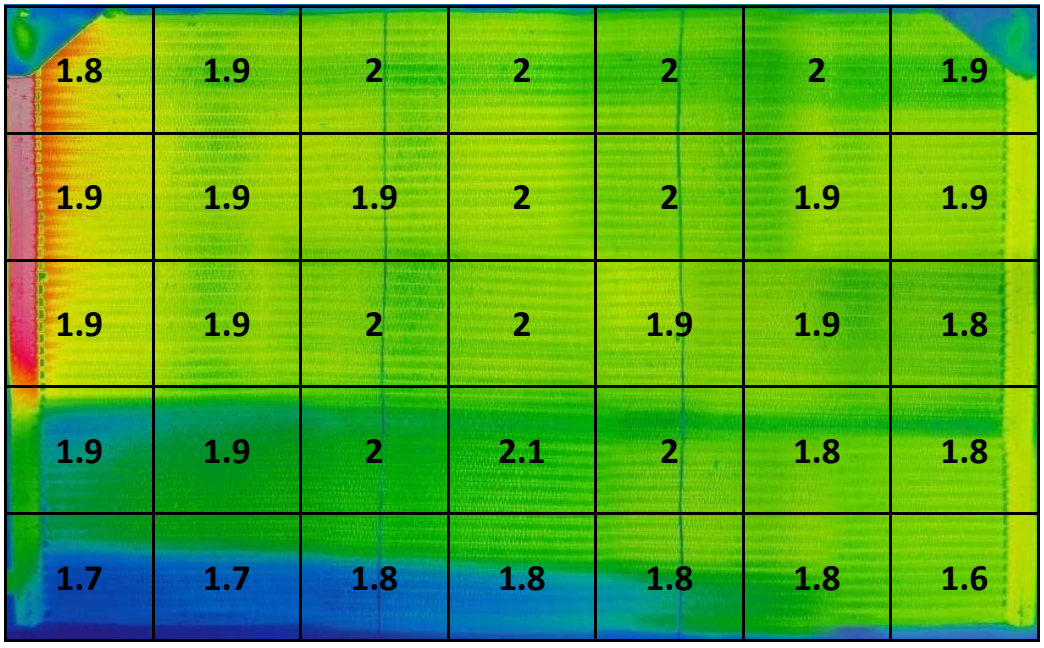

Figure A.2: Infrared picture of condenser with air velocity measurements in m/s

Table A.1: Specifications–condenser

Description	Brazed microchannel, 2 pass, 1 slab, cross-counterflow	
Face area (width x height)	cm^2 (cm)	3129 (71.8 x 43.58)
Core depth	cm	1.8
Number of tubes		48 (1st pass: 31, 2nd pass: 17)
Height of one tube	cm	0.13
Tube internal volume per pass	cm^3	1st pass: 201.6 2nd pass: 110.5
Inlet header volume	cm^3	63.7
Return header volume	cm^3	99.2
Outlet header volume	cm^3	34.9
Inlet tube volume[1]	cm^3	73.0
Outlet tube volume[1]	cm^3	20.0
Total Volume	cm^3	602.9
Heat transfer area air side	m^2	8.43
Number of louvered fins per 0.1 m		70

[1] From section ball valve to header

Evaporator

Figure A.3 shows a picture of the evaporator, its header arrangement and the direction of the air flow—out of the page. The evaporator was installed in a vertical upright position inside the HVAC module. The gravity acts downward, and therefore is at a 90°angle to the air flow direction. Table A.2 presents the main dimensions and volumes of the evaporator.

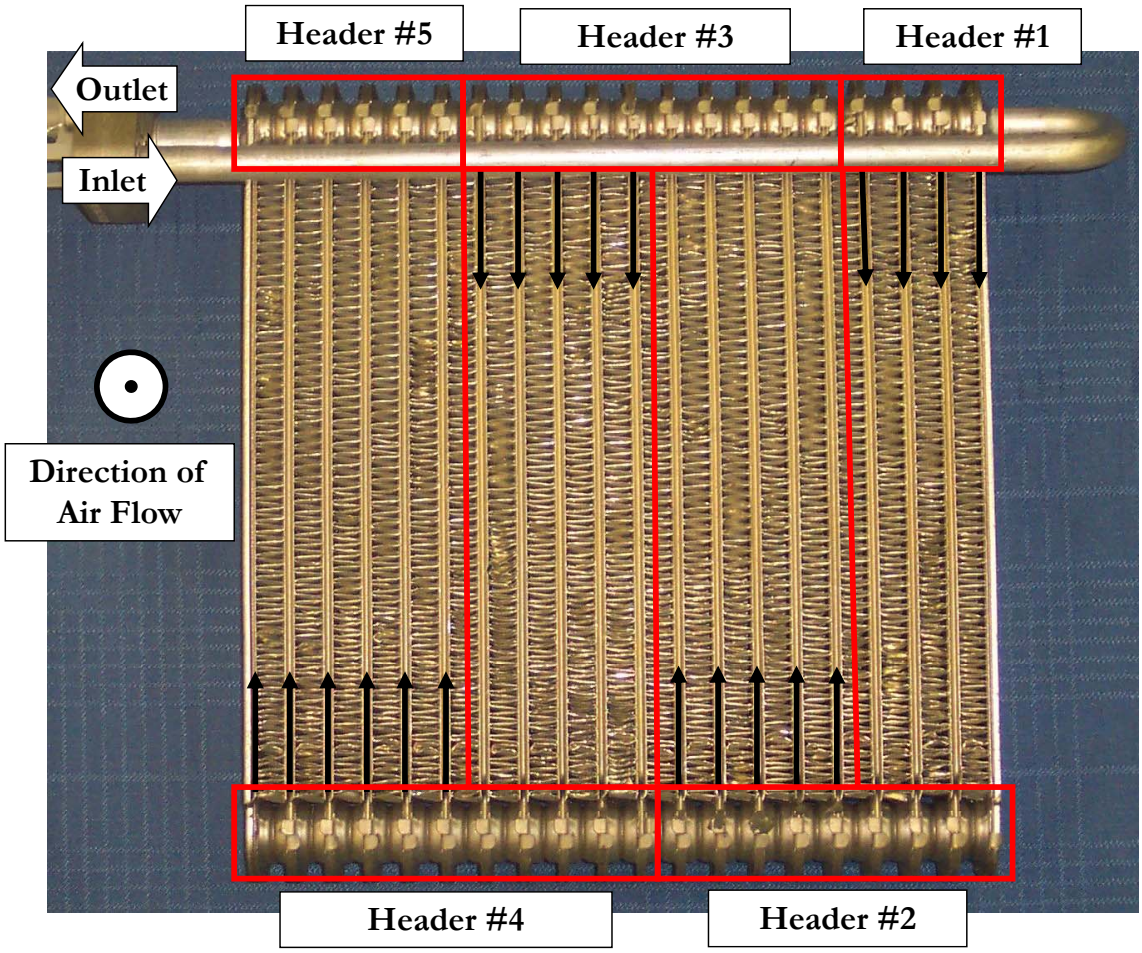

Figure A.3: Evaporator

Table A.2: Specifications–evaporator

Description	Plate and fin; pass arrangement: 3.5, 5, 5, 5.5 (end plates are half tubes with refrigerant flowing through them)	
Face area (width x height)	cm^2 (cm)	582 (25.46 x 22.86)
Core depth	cm	7.3 cm
Number of plates		18 and two half tubes at the ends
Height of one plate	cm	0.326
Internal volume of one plate	cm^3	21.2
Internal volume per pass	cm^3	1st pass: 74.2 2nd pass: 106.0 3rd pass: 106.0 4th pass: 116.6
Volume of Headers	cm^3	Header #1: 39.1 Header #2: 94.9 Header #3: 111.7 Header #4: 122.8 Header #5: 61.4
Inlet pipe volume, outlet pipe volume	cm^3	35.3 , 12.9
Total Volume	cm^3	881
Heat transfer area air side	m^2	4.53
Number of louvered fins per 0.1 m		51.18

Expansion Device

The fixed orifice tube assembly used in the breadboard system for all experiments is shown in Figure A.4. Fixed orifice tube expansion devices have a brass orifice tube surrounded by a plastic housing, and inlet and exit meshed screens to protect the orifice tube from particles. The orifice tube used has an internal diameter of 1.823 mm and a length of 76.2 mm. A schematic is shown in Figure A.5.

Figure A.4: Fixed orifice tube

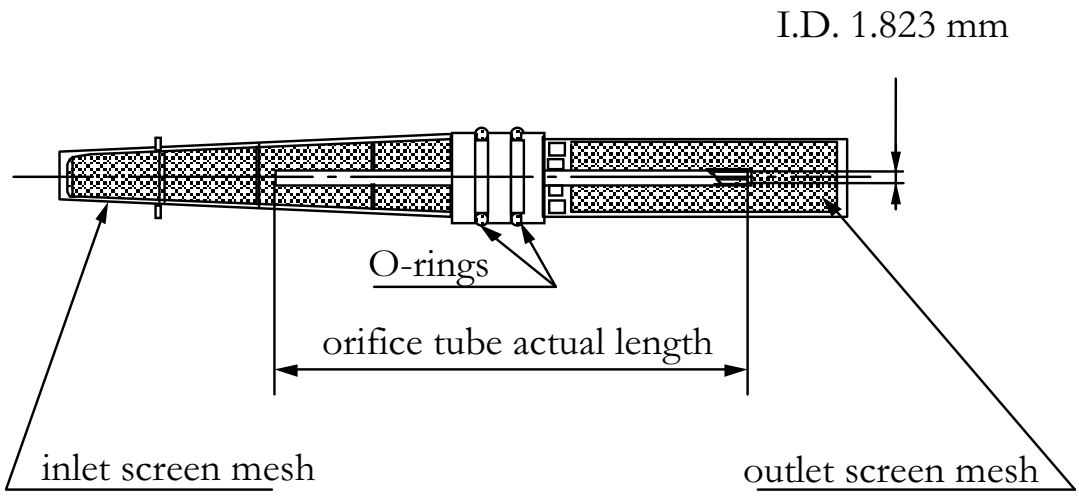

Figure A.5: Fixed orifice tube schematic

Compressor

The compressor used for all experiments was a piston-cylinder type compressor having an open shaft and a fixed displacement. The specifications are shown in Table A.3.

Table A.3: Specifications–compressor

Type	Open shaft reciprocating fixed displacement	
Number of cylinders		10
Stroke	mm	26.7
Diameter of bore	mm	32
Displacement	cm^3/REV	214.7

Appendix B

EES Codes

This appendix contains a selection of EES [31] codes. Line breaks are denoted by a "&" sign, which is also used in EES, and therefore the source code can be directly copied into the EES equation environment.

B.1 Program to Calculate Transient Cooling Capacities

The following EES code was used to calculate the heat transfer rate between air and refrigerant for the evaporator at each time step. The solution, e. g., of the heat transfer rate, can then be plotted for each time step to show the transient progression. The input variables—declared in a parametric table in the original EES program—are listed in Table B.1. The code is used to calculate the heat transfer rates for both the wet and dry condition, whereas for the dry condition the latent heat transfer is equal to zero since no water vapor will condense on the evaporator surface.

```
Procedure AirFlowRate (CDguess, D, Tn, Pn, DPn, Wn : Ma_wet, Ma_dry, &
 Q_m3, Vel, Vn, Re, CDold)

  An=pi*D^2/4                                        {nozzle throat area (m^2)}
  Vn=VOLUME(AirH2O,T=Tn,P=Pn,w=Wn)      {specific volume of air at nozzle &
   (m^3/kg)}
  CDnew=CDguess
 repeat                        {iterate to find proper discharge coefficient}
  CDold=CDnew
  Q_m3=CDold*An*(2*DPn*Vn)^0.5                    {volume flow rate (m^3/s)}
  Vel=Q_m3/An                                 {velocity at nozzle throat (m/s)}
```

```
  Ma_wet=Q_m3/Vn                                {wet air mass flow rate (kg/s)}
  Ma_dry=Ma_wet/(1+Wn)                          {dry air mass flow rate (kg/s)}
  rho=DENSITY(AirH2O,T=Tn,P=Pn,w=Wn)      {air density at nozzle, (kg/m^3)}
  mu=VISCOSITY(AirH2O,T=Tn,P=Pn,w=Wn) {air viscosity at nozzle, (kg/m-sec)}
  Re=rho*Vel*D/mu
  CDnew=0.9986-7.006/Re^.5+134.6/Re     {discharge coefficient correlation}
 until (abs(CDold-CDnew)<.001)

END

{Humidity ratio at nozzle throat, evaporator exit}
omega_2=HUMRAT(AirH2O,T=Taen,P=(Patm-DPae*CONVERT(Pa,kPa)),D=Tdeo)
{Humidity ratio of air entering evaporator}
omega_1=HumRat(AirH2O,T=Taei,D=Tdei,P=Patm)

{Air flow rates through nozzles - two nozzles, same diameter}
D_n=2.5*CONVERT(in,m)                                  {nozzle diameter [m]}
{Air flow rate parameters}
Pen=Patm-DPen*CONVERT(Pa,kPa)           {air pressure at nozzle exit (kPa)}
CDe=0.975                               {discharge coefficient guess value}
Call AirFlowRate(CDe, D_n, Taen, Pen, DPen, omega_2 : ma_wet_1, ma_dry_1, &
 AFR_m3_1e1,  Vel_1e1, Vn_1e1, Re_1e1, CD1e1)

{Air flow rates}
m_dot_a=ma_dry_1*2                    {total dry air mass flow rate (kg/s)}
m_dot_a+m_dot_v2=ma_wet_1*2      {wet air mass flow rate after evaporator &
 (kg/s)}
m_dot_v1=m_dot_a*omega_1     {water vapor mass flow rate evaporator inlet &
 (kg/s)}
m_dot_w=m_dot_a*(omega_1-omega_2)              {water condensate flow rate}

{Calculation of enthalpy values}
h_a1=ENTHALPY(Air,T=Taei)       {evaporator inlet dry air enthalpy (kJ/kg)}
h_a2=ENTHALPY(Air,T=Taeo)                  {dry nozzle air enthalpy (kJ/kg)}
h_v1=ENTHALPY(Steam_NBS,T=Taei,x=1)         {evaporator water vapor inlet &
 enthalpy (kJ/kg)}
h_v2=ENTHALPY(Steam_NBS,T=Taeo,x=1)   {water vapor nozzle enthalpy (kJ/kg)}
h_w=Enthalpy(Water,T=Taen,P=Patm)    {enthalpy of water condensate (kJ/kg)}

{Rates of heat transfer, expressed positive if heat is transferred from &
 the air to the refrigerant}
{Total heat transfer rate (kW)}
Q_dot=(m_dot_a*h_a1+m_dot_v1*h_v1)-m_dot_w*h_w-(m_dot_a*h_a2+m_dot_v2*h_v2)
{Sensible heat transfer rate (kW)}
Q_dot_sensible=m_dot_a*(h_a1-h_a2)+(m_dot_v2)*(h_v1-h_v2)
{Latent heat transfer rate (kW)}
Q_dot_latent=(m_dot_v1-m_dot_v2)*(h_v1-h_w)
```

Table B.1: Input variables

Variable	Unit	Description
Time	s	Optional time index to plot variables versus time
DPae	Pa	Air side pressure drop across evaporator
DPen	Pa	Air pressure drop across flow nozzles
Patm	kPa	Pressure inside climate chamber
Tdeo	°C	Dew point temperature downstream of evaporator
Tdei	°C	Dew point temperature upstream of evaporator
Taei	°C	Air dry bulb temperature upstream of evaporator
Taeo	°C	Air dry bulb temperature downstream of evaporator
Taen	°C	Average air dry bulb temperature at nozzles throat

B.2 Condenser Model

The EES code for the condenser model presented in Section 6.2.4 is shown in this section. The input variables not declared in the code are declared in a parametric table, and are listed in Table B.2. The time fractions were taken from Jassim and Newell [69] and are listed in a Lookup-Table called "Time fraction constants". The values are shown in Table B.3.

Table B.2: Input variables for condenser model

Variable	Unit	Description
mc	kg/s	Air mass flow rate
m_dot_total	kg/s	Refrigerant mass flow rate
Prci	kPa	Refrigerant pressure condenser inlet
Prco	kPa	Refrigerant pressure condenser outlet
T_air_in	°C	Air inlet temperature
Trci	°C	Refrigerant inlet temperature
Trco	°C	Refrigerant exit temperature from experiment (used to compare experimental result to model result)

Table B.3: Lookup-Table used in EES code for timefractions

Mass Flux	a	b	c	d	g
50	25.23	0.66	0.01	25.23	2.97
100	36.99	3.27	0.27	36.99	12.81
200	50.92	31.82	0.62	50.92	37.75
300	55.68	60.17	1.00	55.68	51.21

```
{---Begin Procedures---}
PROCEDURE AIRHT_LOUVERED_KB_MCHX(Ta,mc,A_air_CS, SfinoverSair,ThetaLo,Lp, &
 Fp,Lh,Finth,Tp, Fd,Fh,k_FIN: hairMC,etaa)
{Air side heat transfer coefficient calculation, Kim and Bullard 2000}
  muair=VISCOSITY(Air,T=Ta)                                    {Air visicosity}
  Rhoair=DENSITY(Air,T=Ta,P=101.3)                               {Air density}
  Gair=mc/A_air_CS                                              {Air mass flux}
  Re_Lp=Gair*Lp/muair                                          {Reynolds number}
  j_kb=(Re_Lp)^(-0.487)*(ThetaLo/90)^(0.257)*(Fp/Lp)^(-0.13)&
   *(Fh/Lp)^(-0.29)*(Fd/Lp)^(-0.235)*(Lh/Lp)^(0.68)*(Tp/Lp)^(-0.279)&
   *(Finth/Lp)^(-0.05)
  Kair=CONDUCTIVITY(Air,T=Ta)              {Air thermal conductivity W/m-K}
  cpair=SPECHEAT(Air,T=Ta)*CONVERT(kJ/kg*K,J/kg*K)      {Air specific heat}
  Prair=muair*cpair/(kair)                                      {Prandtl number}
  st=j_kb*Prair^(-2/3)                                          {Stanton number}
  hairMC=Gair*CPair*st                         {Air heat thansfer coefficient}
  ML=(2*hairMC/(K_fin*Finth))^0.5*Fh/2
  etaf=tanh(ML)/ML                                              {Fin efficiency}
  etaa=1-SfinoverSair*(1-etaf)                {Air side surface efficiency}
end

PROCEDURE timefraction(G_m,x:F_liq,F_int,F_vap,F_ann)
{Calculation of time fractions for flow regime based void fraction, &
 Jassim and Newell 2006}
  a=INTERPOLATE('Time fraction constants','Mass Flux','a','Mass Flux'=G_m)
  b=INTERPOLATE('Time fraction constants','Mass Flux','b','Mass Flux'=G_m)
  c=INTERPOLATE('Time fraction constants','Mass Flux','c','Mass Flux'=G_m)
  d=INTERPOLATE('Time fraction constants','Mass Flux','d','Mass Flux'=G_m)
  g=INTERPOLATE('Time fraction constants','Mass Flux','g','Mass Flux'=G_m)
  IF (x<0) THEN
    F_vap:=0
    F_liq:=1
    F_int:=0
    F_ann:=0
  ELSE
    IF (x>1) THEN
```

```
      F_vap:=1
      F_liq:=0
      F_int:=0
      F_ann:=0
    ELSE
        F_vap:=x^g
        F_liq:=(1-x)^a
        F_int:=((1-x)^((b*x)^c))-(1-x)^d
        F_ann:=1-F_liq-F_int-F_vap
    ENDIF
  ENDIF
END

PROCEDURE voidfraction(rho_vap,rho_liq,x,F_liq,F_int,F_vap,F_ann,mu_liq, &
 mu_vap,d_h,G,sigma,dz:alpha,dP)
{Calculation of void fractions and pressure drops based on probabilistic &
 flow map, Jassim and Newell 2006}
   IF (x<0) THEN
     alpha:=0
     Re_h=G*D_h/mu_liq
     IF (Re_h<2300) THEN
          f_D=64/Re_h
     ELSE
          f_D=0.3164/(Re_h^(0.25))
     ENDIF
     dP=(f_D*(1/D_h)*G^2/(2*rho_liq))*dz
   ELSE
   IF (x>1) THEN
     alpha:=1
     Re_h=G*D_h/mu_vap
     IF (Re_h<2300) THEN
       f_D=64/Re_h
     ELSE
       f_D=0.3164/(Re_h^(0.25))
   ENDIF
    dP=(f_D*(1/D_h)*G^2/(2*rho_vap))*dz
   ELSE
     {Lockhart-Martinelli parameter}
   X_tt=((1-x)/x)^0.875*(rho_vap/rho_liq)^0.5*(mu_liq/mu_vap)^0.125
   We_v=((x*G)^2/rho_vap)/(sigma/d_h)
   alpha_ann=(1+(X_tt+1/We_v^(1.3))*(rho_liq/rho_vap)^0.9)^(-0.06)
   alpha_int=((0.833+0.167*x)*x*(1/rho_vap))/((1-x)*(1/rho_liq)&
    +x*(1/rho_vap))
   alpha=F_ann*alpha_ann+F_int*alpha_int+F_liq*0+F_vap*1
     {Intermittent flow pressure drop}
     rho_2ph=((x/rho_vap)+(1-x)/rho_liq)^(-1)
     KE_Avg=G^2/(2*rho_2ph)
```

```
      dP_int=0.045*(1/D_h)*KE_Avg*dz
      {Vapor only}
      Re_vo=G*D_h/mu_vap
      IF (Re_vo<2300) THEN
        f_vo=64/Re_vo
      ELSE
        f_vo=0.3164/(Re_vo^(0.25))
      ENDIF
      dP_vap=(f_vo*(1/D_h)*G^2/(2*rho_vap))*dz
      {Liquid only}
      Re_lo=G*D_h/mu_liq
      IF (Re_lo<2300) THEN
        f_lo=64/Re_lo
      ELSE
        f_lo=0.3164/(Re_lo^(0.25))
      ENDIF
       dP_liq=(f_lo*(1/D_h)*G^2/(2*rho_liq))*dz
       {Annular flow pressure drop}
       X_ann=((X_tt+1/We_v^(1.3))*(rho_liq/rho_vap)^(0.9))
       phi_vo=exp(-0.046*X_ann)+0.22*(exp(-0.002*X_ann)-exp(-7*X_ann))
       dP_ann=phi_vo^2*(f_vo*(1/D_h)*G^2/(rho_vap))*dz
       {Total pressure drop}
       dP=(F_liq*dP_liq+F_int*dP_liq+F_vap*dP_vap+F_ann*dP_ann)
     ENDIF
  ENDIF
END

PROCEDURE mass_vf(x,rho,rho_vap,rho_liq,V,alpha:m,V_vap,V_liq)
{Calculation of vapor and liquid refrigerant masses based on void fraction}
  IF (x<0) THEN
    m=rho*V
    V_liq=V
    V_vap=0
  ELSE
    IF  (x>1) THEN
      m=rho*V
      V_vap=V
      V_liq=0
    ELSE
      V_vap=alpha*V
      V_liq=V-V_vap
      m=rho_vap*V_vap+rho_liq*V_liq
    ENDIF
  ENDIF
END

PROCEDURE REFSIDE_HT(D_h,m_dot_ref,T_ref,P_ref,h_ref,G,T_air,dT: &
```

```
 ht_ref,Re_D,x,rho_l,rho_v,mu_l,mu_v,sigma,X_tt,J_TG,J_G)
{Saturated liquid properties}
  h_liq=Enthalpy(R134a,T=T_ref,x=0)                                  {Enthalpy}
  rho_l=Density(R134a,T=T_ref,x=0)                                    {Density}
  mu_l=Viscosity(R134a,T=T_ref,x=0)                                  {Viscosity}
  k_l=Conductivity(R134a,T=T_ref,x=0)                              {Conductivity}
  cp_l=Cp(R134a,T=T_ref,x=0)*CONVERT(kJ/kg*K,J/kg*K)              {Specific heat}
  Pr_l=mu_l*cp_l/(k_l)                                            {Prandtl number}
{Saturated vapor properties}
  h_vap=Enthalpy(R134a,T=T_ref,x=1)                                  {Enthalpy}
  rho_v=Density(R134a,T=T_ref,x=1)                                    {Density}
  mu_v=Viscosity(R134a,T=T_ref,x=1)                                  {Viscosity}
  sigma=SurfaceTension(R134a,T=T_ref)                          {Surface tension}
  x=Quality(R134a,h=h_ref,T=T_ref)
  IF (h_ref>h_liq) AND (h_ref<h_vap) THEN
    X_tt=((1-x)/x)^0.9*(rho_v/rho_l)^0.5*(mu_l/mu_v)^0.1
    Re_l=G*D_h/mu_l
    IF (h_ref>h_liq) AND (h_ref<h_vap) THEN
    {Condensation model, Cavallini 2006}
      J_G=x*G/(g#*D_h*rho_v*(rho_l-rho_v))^(0.5)
      C_T=2.6
      J_TG=((7.5/(4.3*X_tt^(1.111)+1))^(-3)+C_T^(-3))^(-1/3)
      h_LO=0.023*(k_l/D_h)*Re_l^(0.8)*Pr_l^(0.4)
      IF (J_G>J_TG) THEN
      {dT independent}
        ht_ref=(h_LO*(1+1.128*x^(0.8170)*(rho_l/rho_v)^(0.3685)&
         *(mu_l/mu_v)^(0.2363)*(1-(mu_v/mu_l))^2.144*Pr_l^(-0.1)))
      ELSE
      {dT dependent}
        ht_ann=h_LO*(1+1.128*x^(0.8170)*(rho_l/rho_v)^(0.3685)&
         *(mu_l/mu_v)^(0.2363)*(1-(mu_v/mu_l))^2.144*Pr_l^(-0.1))
        ht_strat=0.725*(1+0.741*((1-x)/x)^(0.3321))^(-1)&
         *(k_l^3*rho_l*(rho_l-rho_v)*g#*(h_vap-h_liq)&
         *1000/(mu_l*D_h*dT))^(0.25)+(1-x^0.087)*h_LO
        ht_ref=((ht_ann*(J_TG/J_G)^0.8-ht_strat)&
         *(J_G/J_TG)+ht_strat)
      ENDIF
    ENDIF
      Re_D=0
    ELSE
    {Single Phase heat transfer coefficient calculation}
      mu=Viscosity(R134a,T=T_ref,P=P_ref)                              {Viscosity}
      k=Conductivity(R134a,T=T_ref,P=P_ref)                          {Conductivity}
      cp=Cp(R134a,T=T_ref,P=P_ref)*CONVERT(kJ/kg*K,J/kg*K)          {Specific heat}
      Re_D=(4*m_dot_ref)/(PI*D_h*mu)                               {Reynolds number}
      Pr=mu*cp/(k)                                                  {Prandtl number}
      e=4.3E-7     {surface roughness extruded minichannel, Cavallini 2009}
```

```
      {friction factor, Churchill 1977}
      A=(-2.457*ln((7/Re_D)^(0.9)+(e/D_h)/3.7))^16
      B=(37530/Re_D)^16
      f=8*((8/Re_D)^12+(A+B)^(-3/2))^(1/12)
      {Gnielinski, 1976}
      Nusselt_D=((f/8)*(Re_D-1000)*Pr)/(1+12.7*(f/8)^(0.5)*(Pr^(2/3)-1))
      ht_ref=(Nusselt_D*k/D_h)
      F_int_liq=0
      F_strat=0
      F_ann=0
      X_tt=0
      J_TG=0
      J_G=0
  ENDIF
END

PROCEDURE epsilon_NTU(x,NTU,C_air,m_dot_ref,T_ref,h_ref:epsilon,C_ref)
{Saturated properties}
  h_vap=Enthalpy(R134a,T=T_ref,x=1)                              {Enthalpy}
  h_liq=Enthalpy(R134a,T=T_ref,x=0)                              {Enthalpy}
  IF (h_ref>h_liq) AND (h_ref<h_vap) THEN
    C_ref=0
    epsilon=1-exp(-NTU)
  ELSE
    cp_ref=Cp(R134a,T=T_ref,h=h_ref)*CONVERT(kJ/kg*K,J/kg*K)
    C_ref=cp_ref*m_dot_ref
    C=C_air/C_ref
    epsilon=1-exp((1/C)*NTU^(0.22)*(exp(-C*NTU^(0.78))-1))
  ENDIF
END

PROCEDURE subcool(T_ref,h_ref,P_ref:DT_subcool)
"Saturated properties"
  h_vap=Enthalpy(R134a,T=T_ref,x=1)                              {Enthalpy}
  h_liq=Enthalpy(R134a,T=T_ref,x=0)                              {Enthalpy}
  T_sat=Temperature(R134a,P=P_ref,x=0)
  IF (h_ref>h_liq) AND (h_ref<h_vap) THEN
    DT_subcool=0
  ELSE
    DT_subcool=T_sat-T_ref
  ENDIF
END
{---End of Procedures---}

{---Start Main Program---}

DP=(Prci-Prco)/2          {Actual pressure drop based on experimental data}
```

```
{Geometrical parameters of condenser}
ThetaLo=28                                              {Louver angle (degree)}
Lp=0.0014                                                    {Louver pitch (m)}
Fp=0.001429                                                     {Fin pitch (m)}
Lh=Fh                                                        {Louver length (m)}
Finth=0.0001                                                 {Fin thickness (m)}
Tp=0.008835                                          {Tube to tube distance (m)}
Fd=0.018                                                    {Flow/Fin depth (m)}
D_m=0.0013                                              {Channel thickness (m)}
L_tube=0.718                                          {Length of one microchannel}
Fh=(PI*Fp)/2+Tp-Fp                                             {Fin length (m)}
N_fins=L_tube/Fp                                      {Number of fins per channel}
k_FIN=k_('Aluminum', T_air_in)                               {Conductivity fin}
V_face=(mc/DENSITY(Air,T=T_air_in,P=101.3))/A_CS                {Face Velocity}
{Calculating air side areas}
A_channel_CS=D_m*L_tube*(n_tubes_1st_pass+n_tubes_2nd_pass)
A_fin_CS=Fh*Finth*(2*L_tube*N_fins)*(n_tubes_1st_pass+n_tubes_2nd_pass)
A_fin_S=(Fh*Tp*(2*L_tube*N_fins)*(n_tubes_1st_pass+n_tubes_2nd_pass))*2
A_tubes_S=L_tube*2*Fd*(n_tubes_1st_pass+n_tubes_2nd_pass)*2
A_CS=L_tube*Tp*(n_tubes_1st_pass+n_tubes_2nd_pass)
A_tubes_S_mc=(A_tubes_S)/(2*N*(n_tubes_1st_pass+n_tubes_2nd_pass))
A_air_total=A_fin_S+A_tubes_S                      {Total air side surface area}
A_air_CS=A_CS-(A_channel_CS+A_fin_CS)                {Air cross sectional area}
{Ratio of Fin surface area divided by total air side surface area}
SfinoverSair=A_fin_S/(A_fin_S+A_tubes_S)

{Calculating air side heat transfer coefficient}
cp_air=Cp(Air,T=T_air_in)*CONVERT(kJ/kg*K,J/kg*K)
C_air=m_dot_air*cp_air
CALL AIRHT_LOUVERED_KB_MCHX(T_air_in,mc,A_air_CS,SfinoverSair,ThetaLo,Lp, &
 Fp,Lh,Finth,Tp, Fd,Fh,k_FIN: hairMC,etaa)

{Calculating the average heat transfer rate per unit length (W/m)}
Total_length=n_tubes_1st_pass*L_tube+n_tubes_2nd_pass*L_tube
Q_meter=Q_dot_cond/Total_length

{1st pass - Calculating parameters based on total volume}
V_1st_pass=201.6*CONVERT(cm^3,m^3)      {Total internal volume of 1st pass}
n_tubes_1st_pass=31                   {Number of microchannels in 1st pass}
{Refrigerant mass flow rate per microchannel}
m_dot_1st_pass_mc=m_dot_total/n_tubes_1st_pass
{Refrigerant mass flow rate per port}
m_dot_port_1st_pass=m_dot_1st_pass_mc/n_ports_mc
V_1st_pass_mc=V_1st_pass/n_tubes_1st_pass      {Volume of one microchannel}
{Internal flow cross sectional area of one microchannel}
A_cs_1st_pass_mc=(PI*(d_1st_h_mc)^2/4)
{Calculating hyraulic diameter, d_1st_h_mc, of one microchannel}
```

```
V_1st_pass_mc=(PI*(d_1st_h_mc)^2/4)*L_tube
{Calculating mass flux G for 1st pass}
A_cs_1st_pass=(PI*(d_1st_h)^2/4)
V_1st_pass=(PI*(d_1st_h)^2/4)*L_tube
G_1st_pass=m_dot_total/A_cs_1st_pass

{2nd pass - Calculating parameters based on total volume}
V_2nd_pass=110.5*CONVERT(cm^3,m^3)      {Total internal volume of 2nd pass}
n_tubes_2nd_pass=17                   {Number of microchannels in 2nd pass}
{Refrigerant mass flow rate per microchannel}
m_dot_2nd_pass_mc=m_dot_total/n_tubes_2nd_pass
{Refrigerant mass flow rate per port}
m_dot_port_2nd_pass=m_dot_2nd_pass_mc/n_ports_mc
V_2nd_pass_mc=V_2nd_pass/n_tubes_2nd_pass      {Volume of one microchannel}
{Internal flow cross sectional area of one microchannel}
A_cs_2nd_pass_mc=(PI*(d_2nd_h_mc)^2/4)
{Calculating hyraulic diameter, d_2nd_h_mc, of one microchannel}
V_2nd_pass_mc=(PI*(d_2nd_h_mc)^2/4)*L_tube
{Calculating mass flux G for 2nd pass}
A_cs_2nd_pass=(PI*(d_2nd_h)^2/4)
V_2nd_pass=(PI*(d_2nd_h)^2/4)*L_tube
G_2nd_pass=m_dot_total/A_cs_2nd_pass
{Mass Flux if flow is only thru unfilled minichannels}
{G_2nd_pass=(m_dot_total/(n_tubes_2nd_pass-n_mc))/A_cs_2nd_pass_mc}

{Calculating diameter and wall thickness of one microchannel}
n_ports_mc=12                         {Number of ports in one microchannel}
V_1st_pass_mc=n_ports_mc*(PI*(d_port)^2/4)*L_tube
L_wall_mc=(D_m-d_port)/2

{Calculating variables for finite elements}
N=135                                          {Number of finite elements}
{Using same number of finite elements for both passes (if changed &
several equations need to be rewritten!!!)}
M=N

{mass flow rate air in one element}
m_dot_air=(mc/(n_tubes_1st_pass+n_tubes_2nd_pass))/N
{Airside surface area per element}
A_air=((A_fin_S+A_tubes_S)/(n_tubes_1st_pass+n_tubes_2nd_pass))/N
{Refrigerant side surface area per element}
A_ref=n_ports_mc*(PI*d_port*L_tube)/N
{Outside surface area of minichannel, one element}
A_mc_outside=D_m*(L_tube/N)*2+Fd*(L_tube/N)*2
{Inlet conditions first pass}
h_out_1st_pass[0]=hrci
T_ref_in_1st_pass[0]=Trci
```

```
L_1st_pass[0]=0
P_1st_pass[0]=Prci
dT_1st_pass_ref[0]=0
dP_1st_pass[0]=0

{First pass finite element calculations}
Duplicate j=1,N
  P_1st_pass[j]= P_1st_pass[j-1]-dP_1st_pass[j-1]/1000 {DP/N}
  L_1st_pass[j]=L_1st_pass[j-1]+L_tube/N
  k_wall_1st_pass[j]=k_('Aluminum', (T_wall_inside_1st_pass[j]))
  1/UA_1st_pass[j]=1/(etaa* hairMC*A_air)+1/(h_ref_1st_pass[j]*A_ref) &
   +L_wall_mc/(k_wall_1st_pass[j]*A_ref)
  NTU_1st_pass[j]=UA_1st_pass[j]/C_air
  CALL epsilon_NTU(x_1st_pass[j], NTU_1st_pass[j],C_air, &
   m_dot_1st_pass_mc,T_ref_in_1st_pass[j],h_in_1st_pass[j]: &
   epsilon_1st_pass[j],C_ref_1st_pass[j])
  epsilon_1st_pass[j]=q_1st_pass[j]/q_max_1st_pass[j]
  q_max_1st_pass[j]=C_air*(T_ref_in_1st_pass[j-1]-T_air_in)
  q_1st_pass[j]=C_air*(T_air_out_1st_pass[j]-T_air_in)
  q_1st_pass[j]=m_dot_1st_pass_mc*Delta_h_1st_pass[j]*CONVERT(kW,W)
  h_in_1st_pass[j]=h_out_1st_pass[j-1]
  h_out_1st_pass[j]=h_in_1st_pass[j]-Delta_h_1st_pass[j]
  T_ref_in_1st_pass[j]=Temperature(R134a,P=P_1st_pass[j], &
   h=h_in_1st_pass[j])
  dT_1st_pass_air[j]= (q_1st_pass[j])/(etaa* hairMC*A_air)
  dT_1st_pass_ref[j]= (q_1st_pass[j])/(h_ref_1st_pass[j]*A_ref)
  T_wall_inside_1st_pass[j]=T_ref_in_1st_pass[j]-dT_1st_pass_ref[j]
  q_1st_pass[j]= k_wall_1st_pass[j]*A_mc_outside &
   *(T_wall_inside_1st_pass[j]-T_wall_outside_1st_pass[j])/L_wall_mc
  CALL REFSIDE_HT(d_port,m_dot_port_1st_pass,T_ref_in_1st_pass[j], &
   P_1st_pass[j], h_in_1st_pass[j],G_1st_pass,T_air_in,dT_1st_pass_ref[j]:&
   h_ref_1st_pass[j],Re_D[j],x_1st_pass[j],rho_liq_1st_pass[j], &
   rho_vap_1st_pass[j],mu_liq_1st_pass[j], mu_vap_1st_pass[j], &
   sigma_1st_pass[j],X_tt_1st_pass[j],J_TG_1st_pass[j],J_G_1st_pass[j])
  {Calculating timefractions for flow regime, Jassim and Newell 2006}
CALL timefraction(G_1st_pass,x_1st_pass[j]:F_liq_1st_pass[j], &
 F_int_1st_pass[j],F_vap_1st_pass[j],F_ann_vf_1st_pass[j])
  {Calculating void fraction, Jassim and Newell 2006}
  rho_1st_pass[j]=DENSITY(R134a, P=P_1st_pass[j],h=h_in_1st_pass[j])
CALL voidfraction(rho_vap_1st_pass[j],rho_liq_1st_pass[j],x_1st_pass[j], &
  F_liq_1st_pass[j],F_int_1st_pass[j],F_vap_1st_pass[j], &
  F_ann_vf_1st_pass[j],mu_liq_1st_pass[j],mu_vap_1st_pass[j],d_port, &
  G_1st_pass,sigma_1st_pass[j],L_tube/N:alpha_1st_pass[j],dP_1st_pass[j])
  {Calculation of refrigerant mass based on void fraction}
  V_1st_pass[j]=V_1st_pass_mc/N
  CALL mass_vf(x_1st_pass[j],rho_1st_pass[j],rho_vap_1st_pass[j], &
   rho_liq_1st_pass[j],V_1st_pass[j],alpha_1st_pass[j]: &
```

```
   mass_1st_vf[j],V_vap[j],V_liq[j])
  {Calculation of mass based on density}
  rho_1st_pass[j]=mass_1st_pass[j]/V_1st_pass[j]
END

{Overall heat transfer rate of 1st pass}
Q_dot_1st_pass=SUM( q_1st_pass[i], i=1,N)*n_tubes_1st_pass
{Sum of masses in 1st pass}
Mass_1st_pass_vf=SUM( mass_1st_vf[i], i=1,N)*n_tubes_1st_pass
Mass_1st_pass=SUM( mass_1st_pass[i], i=1,N)*n_tubes_1st_pass
{Pressure drop of 1st pass}
dP_total_1st_pass=SUM( dP_1st_pass[i], i=1,N)/1000

{Inlet conditions second pass}
h_out_2nd_pass[0]=h_out_1st_pass[N]
T_ref_in_2nd_pass[0]=T_ref_in_1st_pass[N]
L_2nd_pass[0]=L_1st_pass[N]
P_2nd_pass[0]=P_1st_pass[N]
P_2nd_pass[M+1]=Prco
dP_2nd_pass[0]=0
T_wall_inside_2nd_pass[0]=35

{Second pass finite element calculations}
Duplicate k=1,M
  P_2nd_pass[k]= P_2nd_pass[k-1]-dP_2nd_pass[k-1]/1000
  L_2nd_pass[k]=L_2nd_pass[k-1]+L_tube/M
  k_wall_2nd_pass[k]=k_('Aluminum', (T_wall_inside_2nd_pass[k]))
  1/UA_2nd_pass[k]=1/(etaa* hairMC*A_air)+1/(h_ref_2nd_pass[k]*A_ref) &
   +L_wall_mc/(k_wall_2nd_pass[k]*A_ref)
  NTU_2nd_pass[k]=UA_2nd_pass[k]/C_air
  CALL epsilon_NTU(x_2nd_pass[k], NTU_2nd_pass[k],C_air,m_dot_2nd_pass_mc,&
   T_ref_in_2nd_pass[k], h_in_2nd_pass[k]: epsilon_2nd_pass[k], &
   C_ref_2nd_pass[k])
  epsilon_2nd_pass[k]=q_2nd_pass[k]/q_max_2nd_pass[k]
  q_max_2nd_pass[k]=C_air*(T_ref_in_2nd_pass[k-1]-T_air_in)
  q_2nd_pass[k]=C_air*(T_air_out_2nd_pass[k]-T_air_in)
  q_2nd_pass[k]=m_dot_2nd_pass_mc*Delta_h_2nd_pass[k]*CONVERT(kW,W)
  h_in_2nd_pass[k]=h_out_2nd_pass[k-1]
  h_out_2nd_pass[k]=h_in_2nd_pass[k]-Delta_h_2nd_pass[k]
  T_ref_in_2nd_pass[k]=Temperature(R134a,P= P_2nd_pass[k], &
   h=h_in_2nd_pass[k])
  dT_2nd_pass_air[k]= (q_2nd_pass[k])/(etaa* hairMC*A_air)
  dT_2nd_pass_ref[k]= (q_2nd_pass[k])/(h_ref_2nd_pass[k]*A_ref)
  T_wall_inside_2nd_pass[k]=T_ref_in_2nd_pass[k]-dT_2nd_pass_ref[k]
  q_2nd_pass[k]= k_wall_2nd_pass[k]*A_mc_outside &
   *(T_wall_inside_2nd_pass[k]-T_wall_outside_2nd_pass[k])/L_wall_mc
  CALL REFSIDE_HT(d_port,m_dot_port_2nd_pass,T_ref_in_2nd_pass[k], &
```

```
   P_2nd_pass[k], h_in_2nd_pass[k],G_2nd_pass,T_air_in,dT_2nd_pass_ref[k]:&
   h_ref_2nd_pass[k],Re_D_2nd_pass[k],x_2nd_pass[k],rho_liq_2nd_pass[k], &
   rho_vap_2nd_pass[k],mu_liq_2nd_pass[k], mu_vap_2nd_pass[k], &
   sigma_2nd_pass[k],X_tt_2nd_pass[k],J_TG_2nd_pass[k],J_G_2nd_pass[k])
  {Calculating timefractions for flow regime, Jassim and Newell 2006}
CALL timefraction(G_2nd_pass,x_2nd_pass[k]:F_liq_2nd_pass[k], &
 F_int_2nd_pass[k],F_vap_2nd_pass[k],F_ann_vf_2nd_pass[k])
  {Calculating void fraction, Jassim and Newell 2006}
  rho_2nd_pass[k]=DENSITY(R134a, P= P_2nd_pass[k],h=h_in_2nd_pass[k])
CALL voidfraction(rho_vap_2nd_pass[k],rho_liq_2nd_pass[k],x_2nd_pass[k], &
 F_liq_2nd_pass[k],F_int_2nd_pass[k],F_vap_2nd_pass[k], &
 F_ann_vf_2nd_pass[k],mu_liq_2nd_pass[k],mu_vap_2nd_pass[k],d_port, &
 G_2nd_pass,sigma_2nd_pass[k],L_tube/M:alpha_2nd_pass[k],dP_2nd_pass[k])
  {Calculation of refrigerant mass based on void fraction}
  V_2nd_pass[k]=V_2nd_pass_mc/M
  CALL mass_vf(x_2nd_pass[k],rho_2nd_pass[k],rho_vap_2nd_pass[k], &
   rho_liq_2nd_pass[k],V_2nd_pass[k],alpha_2nd_pass[k]:mass_2nd_vf[k], &
   V_vap_2nd_pass[k],V_liq_2nd_pass[k])
 {Calculation of mass based on density}
 rho_2nd_pass[k]=mass_2nd_pass[k]/V_2nd_pass[k]
END

{Calculating subcool condition at condenser outlet}
CALL subcool(T_ref_in_2nd_pass[M],h_out_2nd_pass[M],P_2nd_pass[M]: &
 DT_subcool)

{Overall heat transfer rate of 2nd pass}
Q_dot_2nd_pass=SUM( q_2nd_pass[i], i=1,M)*n_tubes_2nd_pass
{Sum of masses in 2nd pass}
Mass_2nd_pass_vf=SUM( mass_2nd_vf[i], i=1,M)*n_tubes_2nd_pass
Mass_2nd_pass=SUM( mass_2nd_pass[i], i=1,M)*n_tubes_2nd_pass

{Pressure drop of 2nd pass}
dP_total_2nd_pass=SUM( dP_2nd_pass[i], i=1,M)/1000

{Overall heat transfer rate of condenser based on model}
Q_dot_overall=Q_dot_1st_pass+Q_dot_2nd_pass

{Overall heat transfer rate of condenser based on experiment}
hrci=ENTHALPY(R134a,P=Prci,T=Trci)
hrco=ENTHALPY(R134a,P=Prco,T=Trco)
Q_dot_cond=m_dot_total*(hrci-hrco)*CONVERT(kW,W)

{Refrigerant mass in inlet tube}
V_inlet_tube=73*CONVERT(cm^3,m^3)
rho_inlet_tube=Mass_inlet_tube/V_inlet_tube
rho_inlet_tube=DENSITY(R134a, P=Prci,h=hrci)
```

```
{Refrigerant mass in inlet header}
V_inlet_header=63.7*CONVERT(cm^3,m^3)
rho_inlet_header=Mass_inlet_header/V_inlet_header
rho_inlet_header=DENSITY(R134a, P=Prci,h=hrci)

{Refrigerant mass in return header}
V_return_header=99.2*CONVERT(cm^3,m^3)
rho_return_header=Mass_return_header/V_return_header
rho_return_header=DENSITY(R134a, P=P_2nd_pass[0],h=h_out_1st_pass[N])

{Refrigerant mass in outlet header}
V_outlet_header=34.9*CONVERT(cm^3,m^3)
rho_outlet_header=Mass_outlet_header/V_outlet_header
rho_outlet_header=DENSITY(R134a, P=Prco,h=h_out_2nd_pass[M])

{Refrigerant mass in outlet tube mass}
V_outlet_tube=20*CONVERT(cm^3,m^3)
rho_outlet_tube=Mass_outlet_tube/V_outlet_tube
rho_outlet_tube=DENSITY(R134a, P=Prco,h=h_out_2nd_pass[M])

{Refrigerant mass in condenser accounting for void fraction in  &
 microchannels}
Mass_total_vf=Mass_1st_pass_vf+Mass_2nd_pass_vf+Mass_outlet_header &
 +Mass_return_header+Mass_inlet_header+Mass_inlet_tube+Mass_outlet_tube
{Refrigerant mass in condenser neglecting void fraction in microchannels}
Mass_total=Mass_1st_pass+Mass_2nd_pass+Mass_outlet_header &
 +Mass_return_header+Mass_inlet_header+Mass_inlet_tube+Mass_outlet_tube

{Calculation of outlet properties}
Trco_model=T_ref_in_2nd_pass[M]
Prco_model=Prci-dP_total_1st_pass-dP_total_2nd_pass
x_out_model=x_2nd_pass[M]

{Calculation of additional refrigerant mass based on the assumption that &
 lower microchannels are filled with liquid}
{The density is set to the saturation density based on the outlet pressure}
rho_sat=DENSITY(R134a, P=Prco,x=0)
rho_sat=mass_2nd_pass_mc/V_2nd_pass_mc

n_mc=7                    {Number of mc's assumed to be filled with liquid}
mass_add_mc=n_mc*mass_2nd_pass_mc-n_mc*mass_2nd_pass_channel
{Mass in one mc based on model}
mass_2nd_pass_channel=Mass_2nd_pass_vf/n_tubes_2nd_pass

height_return_header=0.4358 [m]
V_return_header=(PI*(D_h_rh^2)/4)*height_return_header
```

```
{Height of return header filled with liquid}
height_liq=n_mc*Tp
{Volume of return header filled with liquid}
V_return_header_liq=(PI*(D_h_rh^2)/4)*height_liq
{Mass of liquid ref in return header}
rho_outlet_tube=mass_return_header_liq/V_return_header_liq
{Mass in part of return header based on two phase condition from model}
rho_return_header=mass_return_header_2phase/V_return_header_liq
mass_return_header_add=mass_return_header_liq-mass_return_header_2phase

{Additional mass based on assumption that n_mc microchannels are filled &
 with liquid, including part of return header filled with liquid ref.}
Mass_total_separation=Mass_total_vf+mass_return_header_add+mass_add_mc

{---End Program---}
```

References

[1] M. Youbi-Idrissi. The effect of oil in refrigeration: Current research issues and critical review of thermodynamic aspects. *International Journal of Refrigeration*, 31(2):165–179, 2008.

[2] P. J. Rubas and C. W. Bullard. Factors contributing to refrigerator cycling losses. *International Journal of Refrigeration*, 18(3):168–176, 1995.

[3] G. F. Hewitt. *Measurement of Two Phase Flow Parameters*. Academic Press Inc., 1978.

[4] E. Björk. A simple technique for refrigerant mass measurement. *Applied Thermal Engineering*, 25(8-9):1115–1125, 2005.

[5] T. V. Moore and H. D. Wilde Jr. Experimental measurement of slippage in flow through vertical pipes. *Transactions of the American Institute of Mining, Metallurgical and Petroleum Engineers*, 92:296–319, 1931.

[6] R. W. Lockhart and R. C. Martinelli. Proposed correlation of data for isothermal two-phase, two-component flow in pipes. *Chemical engineering progress symposium series*, 45:39–48, 1949.

[7] A. Colombo, A. Hassid, and A. Premoli. Steam-water mixture density measurements in heated channels at high pressure by means of a quick-closing valve method. *Energia Nucleare*, 15(2):119–128, 1968.

[8] N. Tanaka, M. Ikeuchi, and G. Yamanaka. Experimental study on the dynamic characteristics of a heat pump. *ASHRAE Transactions*, 88(2):323–331, 1982.

[9] W. J. Mulroy and D. A. Didion. Refrigerant migration in a split-unit air conditioner. *ASHRAE Transactions*, 91(1A):193–206, 1985.

[10] M. R. Hoehne and P. S. Hrnjak. Charge minimization in systems and components using hydrocarbons as a refrigerant. Technical Report ACRC TR-224, University of Illinois at Urbana-Champaign, 2004.

[11] M. Lallemand L. Machado, P. Haberschill. Refrigerant mass inside an evaporator in a steady or non-steady state. *International Journal of Refrigeration*, 21(6):430–439, 1998.

[12] L. Margat. Étude thermodynamique de la charge en fluide diphasique dans un canal corrugué brasé. Université de Provence Aix-Marseille, 1997.

[13] D. C. Zietlow and C. O. Pedersen. Refrigerant inventory of R-134a in a small-channel cross-flow condenser. *ASHRAE Transactions*, 104(2):531–539, 1998.

[14] S. Marinhas, H. Macchi-Tejeda, D. Leducq, and T. Serghini. Evaluation de la charge en fluide frigorigène dans un condenseur à mini-canaux. Congrès de la Société Française de Thermique, Presqu'île de Giens, 2004.

[15] K. M. Traeger and P. S. Hrnjak. Charge minimization of microchannel heat exchangers. Technical Report ACRC TR-251, University of Illinois at Urbana-Champaign, 2005.

[16] W. A. Miller. The laboratory evaluation of the heating mode part-load operation of an air-to-air heat pump. *ASHRAE Transactions*, 91(2B):524–536, 1985.

[17] M. I. Belth, T. E. Grzymala, and D. R. Tree. Transient mass-flow rate of a residential air-to-air heat-pump. *International Journal of Refrigeration*, 11(5):298–304, 1988.

[18] L. J. M. Kuijpers and J. de Wit. Experimental verification of liquid hold-up predictions in small refrigeration heat exchangers. *Proc. 17th Int. Cong. Refrig.*, pages 307–315, 1987.

[19] M. I. Belth and D. R. Tree. Design and preliminary analysis for measuring transient mass rate of flow in unitary heat pumps. *ASHRAE Transactions*, 92(1B):843–853, 1986.

[20] W. E. Murphy. Transient response of air conditioners - a qualitative interpretation through a sample case. *ASHRAE Transactions*, 90(1B):997–1008, 1984.

[21] M. H. Kim and C. W. Bullard. Dynamic characteristics of a R-410A split air-conditioning system. *International Journal of Refrigeration*, 24(7):652–659, 2001.

[22] S. Kocaturk, Y. Guldali, and A. Egrican. Experimental investigation of the paramters influencing refrigerant migration in a refrigeration system. In *Proceedings of IMECE2007*, volume 8, pages 1409–1419, 2008.

[23] C. D. Collins and N. R. Miller. Experimental study of mobile air conditioning system behavior. Technical Report ACRC TR-102, University of Illinois at Urbana-Champaign, 1996.

[24] V. P. Sheth and T. A. Newell. Refrigerant and oil migration and retention in air conditioning and refrigeration systems. Technical Report ACRC TR-224, University of Illinois at Urbana-Champaign, 2005.

[25] E. Björk and B. Palm. Refrigerant mass charge distribution in a domestic refrigerator. Part I: Transient conditions. *Applied Thermal Engineering*, 26(8-9):829–837, 2006.

[26] E. Björk and B. Palm. Refrigerant mass charge distribution in a domestic refrigerator. Part II: Steady state conditions. *Applied Thermal Engineering*, 26(8-9):866–871, 2006.

[27] ASHRAE. *2010 ASHRAE Handbook Refrigeration*. ASHRAE, 2010.

[28] C. J. Seeton and P. S. Hrnjak. CO_2-lubricant two-phase flow patterns in small horizontal wetted wall channels: The effects of refrigerant/lubricant thermophysical properties. Technical Report ACRC TR-269, University of Illinois at Urbana-Champaign, 2009.

[29] J. A. Crompton, T. A. Newell, and J. C. Chato. Experimental measurement and modeling of oil holdup. Technical Report ACRC TR-226, University of Illinois at Urbana-Champaign, 2004.

[30] L. Cremaschi. Experimental investigation of oil retention in air conditioning systems. *International Journal of Refrigeration*, 28(7):1018–1028, 2005.

[31] S. A. Klein. EES - Engineering Equation Solver.

[32] B.N. Taylor and Kuyatt C.E. Guidelines for evaluating and expressing the uncertainty of NIST measurement results. *NIST Technical Note 1297, Physics Laboratory, National Institute of Standards and Technology, Gaithersburg, MD*, 1994.

[33] ASME. Test uncertainty - ASME PTC 19.1-1998. *American Society of Mechanical Engineers, New York, NY*, 1998.

[34] ISO. *Guide to the Expression of Uncertainty in Measurement*. International Organization for Standardization, Geneva, Switzerland, 1993.

[35] DIN EN 60534-2-1. Industrial-process control valves - Part 2-1: Flow capacity - sizing equations for fluid flow under installed conditions. 1998.

[36] Section 608 of the Clean Air Act 1990. Regulation 40 CFR Part 82, Subpart F.

[37] S. Gupta. Simple visual reaction time, personality and strength of the nervous system: A signal-detection theory approach. *Personality and Individual Differences*, 6(4):461–469, 1985.

[38] ANSI/ASHRAE 41.4-1996. Standard method for measurement of proportion of lubricant in liquid refrigerant. *American Society of Heating, Refrigerating and Air-Conditioning Engineers, Inc., Atlanta, GA*, 1996.

[39] Society of Automotive Engineers. HFC-134a (R-134a) recovery/recycle/recharging equipment for mobile air-conditioning systems. *Standard J2788*, 2010.

[40] N. E. Carpenter. Retrofitting HFC134a into existing CFC12 systems. *International Journal of Refrigeration*, 15(6):332, 1992.

[41] Skip Symonds. Coil care. *Refrigeration service and contracting*, 66(12):22, 1998.

[42] T. R. Gessner. Modeling absorption of pure refrigerants and refrigerant mixtures in lubricant oil. *International Journal of Refrigeration*, 29(5):773, 2006.

[43] S. Peuker and P. S. Hrnjak. Transient refrigerant and oil migration of an R134a automotive A/C system. *SAE Int. J. Passeng. Cars - Mech.Syst.*, 2(1):714–724, 2009.

[44] Y. A. Çengel and M. A. Boles. *Thermodynamics: An Engineering Approach, Fourth Edition*. McGraw-Hill, 2003.

[45] J. R. Thome. Comprehensive thermodynamic approach to modeling refrigrant-lubricant oil mixtures. *HVAC&R Research*, 1(2):110–126, 1995.

[46] W. L. Martz, C. M. Burton, and A. M. Jacobi. Local composition modelling of the thermodynamic properties of refrigerant and oil mixtures. *International Journal of Refrigeration*, 19(1):25, 1996.

[47] G. M. Wilson. A new expression for excess free energy of mixing. *Journal of The American Chemical Society*, 86(2):127–130, 1964.

[48] T. Takeshi and K. Tsuboka. Modified wilson equation for vapor-liquid and liquid-liquid equilibria. *J Chem Eng Jap*, 8(3):181–187, 1975.

[49] W. Wang and K. Chao. The complete local concentration model activity-coefficients. *Chemical engineering science*, 38(9):1483–1492, 1983.

[50] J. Heil and J. M. Prausnitz. Phase equilibria in polymer solutions. *American Institute of Chemical Engineers.AIChE Journal*, 12(4):678, 1966.

[51] H. Renon and J. M. Prausnitz. Local compositions in thermodynamic excess functions for liquid mixtures. *American Institute of Chemical Engineers.AIChE Journal*, 14(1):135, 1968.

[52] D. P. Tassios. *Applied Chemical Engineering Thermodynamics*. Springer, 1993.

[53] J. J. Grebner and R. R. Crawford. The effects of oil on the thermodynamic properties of dichlorodifluoromethane (R-12) and tetrafluoroethane (R-134a). Technical Report ACRC TR-13, University of Illinois at Urbana-Champaign, 1992.

[54] Y. Takaishi and K. Oguchi. Measurements of vapor pressures of R-22/oil solutions. In *Proceedings of the XVIIIth International Congress of Refrigeration*, volume B, pages 217–222, Vienna, Austria, 1987.

[55] S. G. Kandlikar. A roadmap for implementing minichannels in refrigeration and air-conditioning systems - current status and future directions. *Heat Transfer Engineering*, 28(12):973–985, 2007.

[56] F. D. Incropera and D. P. DeWitt. *Fundamentals of Heat and Mass Transfer, Fifth Edition*. Wiley, 2002.

[57] R. D. Ellison. A computer model for air-cooled refrigerant condensers with specified refrigerant circuiting. *ASHRAE Transactions*, 87(1):1106–1124, 1981.

[58] F. Ragazzi and C. O. Pedersen. Modular-based computer simulation of an air-cooled condenser. Technical Report ACRC TR-7, University of Illinois at Urbana-Champaign, 1991.

[59] A. Vardhan. A new procedure for performance prediction of air conditioning coils. *International Journal of Refrigeration*, 21(1):77–83, 1998.

[60] T. M. Harms. The impact of modeling complexity and two-phase flow parameters on the accuracy of system modeling for unitary air conditioners. *HVAC&R Research*, 10(1):5–20, 2004.

[61] L. L Shao, L. Yang, C. L Zhang, and B. Gu. Numerical modeling of serpentine microchannel condensers. *International Journal of Refrigeration*, 32(6):1162–1172, 2009.

[62] M. H Kim and C. W. Bullard. Air-side thermal hydraulic performance of multi-louvered fin aluminum heat exchangers. *International Journal of Refrigeration*, 25(3):390–400, 2002.

[63] V. Gnielinski. New equations for heat and mass transfer in turbulent pipe and channel flow. *International Chemical Engineering*, 16:359–368, 1976.

[64] S. Churchill. Friction-factor equation spans all fluid-flow regimes. *Chemical Engineering*, 84(24):91–92, 1977.

[65] A. Cavallini, D. Del Col, L. Doretti, M. Matkovic, L. Rossetto, C. Zilio, and G. Censi. Condensation in horizontal smooth tubes: A new heat transfer model for heat exchanger design. *Heat Transfer Engineering*, 27(8):31–38, 2006.

[66] M. Matkovic, A. Cavallini, D. Del Col, and L. Rossetto. Experimental study on condensation heat transfer inside a single circular minichannel. *International Journal of Heat and Mass Transfer*, 52(9-10):2311–2323, 2009.

[67] C. K. Rice. Effect of void fraction correlation and heat flux assumption on refrigerant charge inventory predictions. *ASHRAE Transactions*, 93(pt 1):341–367, 1987.

[68] M. A. Woldesemayat and A. J. Ghajar. Comparison of void fraction correlations for different flow patterns in horizontal and upward inclined pipes. *International Journal of Multiphase Flow*, 33(4):347–370, 2007.

[69] E. W. Jassim and T. A. Newell. Prediction of two-phase pressure drop and void fraction in microchannels using probabilistic flow regime mapping. *International Journal of Heat and Mass Transfer*, 49(15-16):2446–2457, 2006.

[70] V. G. Nino, E. W. Jassim, P. S. Hrnjak, and T. A. Newell. Flow-regime-based model for pressure drop predictions in microchannels. *HVAC&R Research*, 12(1):17–34, 2006.

[71] A. A. Armand. The resistance during the movement of a two-phase system in horizontal pipes. *Izv.Vses.Teplotekh.Inst.*, 1:16–23, 1946.

[72] V. G. Nino. Characterization of two-phase flow in microchannels, 2002.

[73] W. E. Murphy and V. W. Goldschmidt. The degradation coefficient of a field tested self-contained 3-ton air-conditioner. *ASHRAE Transactions*, 85(2):396–405, 1979.

[74] S. Peuker and P. S. Hrnjak. Refrigerant mass and oil migration during start-up transient. 12th International Refrigeration and Air Conditioning Conference at Purdue, West Lafayette, IN, USA, 2008.

[75] W. F. Stoecker and J. W. Jones. *Refrigeration and Air Conditioning, Second Edition*. McGraw-Hill, 1982.

[76] G. M. Singh, P. S. Hrnjak, and C. W. Bullard. Flow of refrigerant 134a through orifice tubes. *HVAC&R Research*, 7(3):245–262, 2001.

[77] J. Wang and Y. Z. Wu. Start-up and shut-down operation in a reciprocating-compressor refrigeration system with capillary tubes. *International Journal of Refrigeration*, 13(3):187–190, 1990.

[78] B. Li, S. Peuker, A. Alleyne, and P. S. Hrnjak. Refrigerant migration modeling during shut-down and start-up cycling transients. 13th International Refrigeration and Air Conditioning Conference at Purdue, West Lafayette, IN, USA, 2010.

[79] B. Li and A. Alleyne. A dynamic model of a vapor compression cycle with shut-down and start-up operations. *International Journal of Refrigeration*, 33(3):538–552, 2010.